5-17-2012 12:00 AM

Heme Binding and Transfer in the Isd Heme Scavenging Pathway of Staphylococcus aureus

Michael T. Tiedemann
The University of Western Ontario

Supervisor
Dr. Martin J. Stillman
The University of Western Ontario

Graduate Program in Chemistry
A thesis submitted in partial fulfillment of the requirements for the degree in Doctor of Philosophy

Heme Binding and Transfer in the Isd Heme Scavenging Pathway of *Staphylococcus aureus*

(Spine title: Heme Binding and Transfer in *Staphyloccus aureus*)

(Thesis format: Integrated-Article)

By

Michael Thomas Tiedemann

Graduate Program in Chemistry

Submitted in partial fulfillment of the requirements for the degree of

Doctor of Philosophy

The School of Graduate and Postdoctoral Studies

The University *of* Western Ontario

London, Ontario, Canada

April, 2012

The School of Graduate and Postdoctoral Studies

The University *of* Western Ontario

CERTIFICATE OF EXAMINATION

Supervisor

Dr. Martin Stillman

Examiners

Dr. John F. Corrigan

Dr. Len G. Luyt

Dr. Gilles A. Lajoie

Dr. Rebecca A. Jockusch

The thesis by

Michael Thomas Tiedemann

entitled:

Heme Binding and Transfer in the Isd Heme Scavenging Pathway of *Staphylococcus aureus*

is accepted in partial fulfillment of the requirements for the degree of

Doctor of Philosophy

Date_____

Chair of the Thesis Examination Board

ABSTRACT

The antibiotic resistant bacterium *Staphylococcus aureus* is a significant problem in hospitals and communities worldwide. Survival of the bacterium in the host is reliant on iron scavenging. *Staphylococcus aureus* has adopted specialized mechanisms for scavenging iron from the host. The cell wall and membrane-associated iron regulated surface determinant (Isd) proteins allow *Staphylococcus aureus* to scavenge iron from the heme in hemoglobin. There are nine Isd proteins (IsdH, IsdB, IsdA, IsdC, IsdE, IsdD, IsdF, IsdG and IsdI) located at different depths in the cell wall and membrane. Magnetic circular dichroism (MCD) spectroscopy and electrospray ionization mass spectrometry (ESI-MS) have been used to determine the direction, mechanistic details and heme binding ligands of the Isd heme transfer system. Ferric heme extracted from metHb by IsdB and has been demonstrated to transfer in a unidirectional fashion with the heme transferring along the pathway in the sequence (proximal amino acid) IsdB-N2 (Tyr) $\rightarrow$ IsdA-N (Tyr) $\rightarrow$ IsdC-N (Tyr) $\rightarrow$ IsdE (His) or, alternatively, when initiating from IsdH-N3 (Tyr) the transfer sequence is $\rightarrow$ IsdA-N (Tyr) $\rightarrow$ IsdC-N (Tyr) $\rightarrow$ IsdE (His). Heme transfer through the cell wall must occur through IsdC indicating that IsdC acts as the central conduit of the Isd system. MCD and ESI-MS data show that disruption of unidirectional heme transfer occurs with heme analogs and protein mutational studies. Finally, kinetic analysis provides rate constants for the major unidirectional reaction steps.

Keywords: *Staphylcoccus aureus*, iron-regulated surface determinant, heme transfer pathway, heme binding proteins, heme transfer kinetics, heme analogs, protein mutants, MCD spectroscopy, ESI-mass spectrometry.

CO-AUTHORSHIP STATEMENT

The following thesis contains material from previously published manuscripts. Martin Stillman is coauthor on all the published papers and was responsible for supervising Michael T. Tiedemann during his studies. For any chapters for which a version has been published, Michael T. Tiedemann wrote the first draft of the paper and Martin Stillman had a major role in the editing and revisions of the published manuscripts.

Prof. David Heinrichs is a long-term collaborator on the project. His lab prepared all protein constructs and growing methodologies for each Isd protein. Michael T. Tiedemann was responsible to grow and purify proteins for his experimental work. For the Heinrich's lab contribution of new protein constructs, authorship was guaranteed on their first paper.

For Chapter 3, Michael T. Tiedemann was responsible for all the data, prepared all the figures and helped rewrite the manuscript for publication. First authorship was granted to a collaborator group member due to an agreement to switch first authors on paper publishing.

Michael T. Tiedemann was responsible for all experimental considerations, training of personnel, preparing of the figures, writing of the manuscript for Chapter 8 and was present during the experiments. Tyler B. J. Pinter (member of Prof. Stillman's Group, UWO) performed all ESI-MS measurements for this chapter under my supervision.

ACKNOWLEDGEMENTS

First and foremost I would like to thank my family and Jess who although had no idea what I was talking about every time I mentioned my thesis, still listened and always gave me words of encouragement.

Thanks to my collaborator David Heinrichs (UWO, London, ON) and his research lab for the Isd protein constructs and their patience in teaching me protein growth and purification techniques. In particular, I would like to thank Johnson Cheung and Naomi Muroi for all their support and answering my many questions.

A special thanks to past and current Stillman members for being such great friends and labmates: Especially, Duncan "The Hammer" Sutherland, who through undergrad and graduate school always was there in the thick of things. Tyler Pinter, for a successful fourth year thesis that lead to a paper. I will never forget the last minute "Isd super week of experiments."

Many thanks to the the Electronic Shop (John Vanstone, Warren Lindsay, Barakat Minsk and Jon Aukema) for fixing the antiquated machines that probably should have died 10 years ago in our lab. I was always amazed that you could fix the strangest of problems. I would also like to thank the Chemstore (MaryLou Hart, Sherry McPhee and Don Yakobchuk) for answering all my questions about what I could buy and ordering "obscure" items that were essential in my thesis. My deepest appreciation to Doug Hairsine for his training, advice and help on the ESI-MS. Without your technical skill I would wonder if I would even be able to get protein signal.

Last but not least I would like to thank Martin Stillman for his guidance over these years. Thank you for letting me roam free and try experiments that "never should have worked".

TABLE OF CONTENTS

LIST OF FIGURES

LIST OF TABLES

LIST OF ABBREVIATIONS AND DEFINITIONS

ABC	ATP binding cassette
apo-	heme-free protein
CD	circular dichroism
DNA	deoxyribonucleic acid
ε	molar absorptivity or molar extinction coefficient
E. coli	*Escherichia coli*
EI	electron impact
ESI	electrospray ionization
holo-	heme bound protein
in vitro	in an aqueous environment in a test tube
in vivo	in a biological or cellular environment
Isd	iron regulated surface determinant
k	rate constant
m/z	mass-to-charge ratio
MCD	magnetic circular dicroism
MM3	molecular mechanics
MRSA	methicillin resistant *Staphyloccocus aureus*
MS	mass spectrometry
NEAT	near transporter domain
pET	plasmid for expression by T7 RNA polymerase
PBS	phosphate buffer solution
PPIX	protoporphyrin IX
TOF	time-of-flight
VRSA	vancomycin resistant *Staphylococcus aureus*
S. aureus	*Staphyloccocus aureus*
ZINDO	Zerner's intermediate neglect of differential overlap

Chapter 1. Introduction

1.1 *Staphylococcus aureus*

Staphylococcus aureus (*S. aureus*), also known as "golden staph" due to its colour when grown on a laboratory plate, Figure 1-1, is an invasive Gram-positive coccoid bacterium that innocuously colonizes the anterior nares of approximately 30% of the human population [1, 2].

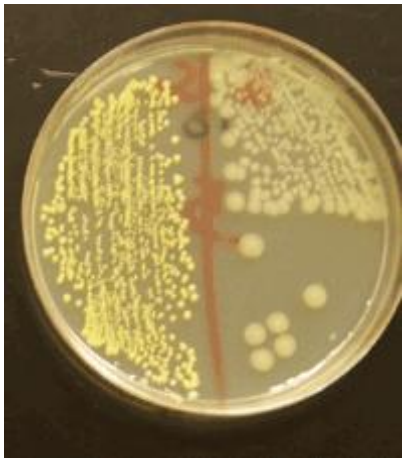

Figure 1-1 *Staphylococcus aureus*, "golden staph", left side and E.coli on right for comparison, grown on a trypticase soy agar plate. Reprinted with permission from [3]. Copyright 2007 American Society of Clinical Pathology.

In hospitals, *S. aureus* is one of the most commonly acquired bacterial infections. About 20% of nosocomial bloodstream infections are caused by *S. aureus* making it a leading cause of nosocomial infections [4]. *S. aureus* causes more severe infections when it gains access to deeper tissues and the bloodstream after penetrating the skin surface or mucosal barriers. Breaching this initial state of colonization, *S. aureus* causes a range of potentially lethal diseases such as pneumonia, meningitis, toxic shock syndrome (TSS), endocarditis, septicemia and death [5, 6]. The disease severity and outcome is dependent on the infection site and immune status of the host.

To complicate this crippling bacterial infection, the emergence of resistant *S. aureus* has taken place over several decades. The first reported cases of penicillin resistant *S. aureus* was reported around 1944 [7, 8]. More potent antibiotic-resistant *S. aureus* started emerging more recently. Methicillin was first released in North America in 1961 to combat drug resistant bacterial strains and reports of methicillin-resistant *S. aureus* (MRSA) have appeared as early as 1968 [9].

Vancomycin is often referred to as a last resort drug but resistance was first reported in 2002 [10]. Now, vancomycin-resistant *S. aureus* (VRSA) infection cases are observed more frequently in health care facilities [5, 11]. Strict control over the use of vancomycin and other MRSA effective antibiotics has now been implemented, only being used in severe cases where other less-toxic antibiotics are ineffective. Furthermore, MRSA, initially limited to hospitals, has since spread to the community [12]. This clinical challenge is compounded each year in the United States since MRSA strains alone cause an estimated 94,360 invasive infections, resulting in ~19,000 deaths [13], which is more deaths than HIV [14]. In Canada, the death toll is lower compared to the United States, ~2000 deaths in 2006 [15]. However, MRSA still represents a significant financial burden with annual costs for treatment and control in Canadian hospitals estimated to be ~$130 million [16]. These facts highlight the need for further study of the bacteria and search for novel targets and identification of new antimicrobials to treat this infectious threat [17, 18].

The invasive and pathogenic success of *S. aureus* is due to the bacteria's ability to survive within many different hostile host environments and systems. The *S. aureus* bacterial surface is coated by a capsule and the thick cell wall is laden with other protective components to impede immune recognition [19]. Numerous surface adhesions allow *S. aureus* to adhere to almost any surface in the human body extending the bacteria's efficiency in infecting almost any system of the human body [20, 21]. *S. aureus* secretes numerous proteases, lytic toxins and lipases that exacerbate tissue and immune damage in order to avoid the host's immune system [22]. However, in order to facilitate such an anti-immune response and flourish in a host system, a steady supply of nutrients must be garnered from host tissues for growth. *S. aureus* achieves this through tissue damage and high affinity uptake systems. Iron is likely one of the most important limiting nutrients and as a result, *S. aureus* expends significant resources to acquire iron.

1.2 Iron in the human host

Iron is the fourth most abundant metal in the earth's crust and is an essential component of nearly every living biological system [23] due to the ability to undergo changes in oxidation state (Fe^{3+} (ferric) and Fe^{2+} (ferrous)), hence, iron is an important biological catalyst [24]. Iron plays a major role in vital processes such as energy production, detoxification, nucleotide biosynthesis and oxygen transport and storage [25, 26]. Free iron is insoluble at physiological pH

[$K_{sp}(Fe(III))=10^{-39}$ M] [27] and can cause oxidative damage via the Fenton reaction (Fe^{2+} + $H_2O_2 \longrightarrow Fe^{3+} + OH^- + OH^{\cdot}$) in vertebrate tissues where H_2O_2 is a byproduct of the body's protective reaction to free reactive oxygen species. In order to prevent host damage free iron is quickly removed or sequestered into high-affinity iron-binding proteins such as transferrin, lacotoferrin and the iron storage protein ferritin, or by incorporation into a protoporphyrin ring as heme in hemoproteins [23, 25]. The human body contains ~4g of iron and free iron concentrations are maintained at orders of magnitude below (approximately 10^{-18} M [28]) those required to support bacterial growth, making it difficult for bacteria to obtain iron [29, 30]. Due to host sequestration of free iron, free iron is not typically available and as a result invasive organisms have developed high affinity systems to acquire and store iron [31].

Table 1-1 shows the major iron sources in the human body. Interestingly, the most abundant potential iron source for bacteria is heme-b (Fe-PPIX). Approximately 75% of the intracellular iron pools are heme-iron, predominantly found in the oxygen transporter, hemoglobin (Hb) and myoglobin including other heme-iron enzymes [30]. Heme is a prosthetic group in many proteins and enzymes where it plays key and significant roles in many fundamental biological processes including O_2 storage and transport (myoglobin and hemoglobin), respiration and electron transfer (cytochromes), activation of the O-O bond (P450 enzymes and peroxidase), and signal transduction and gas sensing (CooA, nitric oxide synthase (NOS)) [25].

Table 1-1 List of the major iron containing molecules in humans and their percentage of the total iron pool [27]

Iron containing molecules	% of total human iron pool
Heme (hemoglobin)	~70%
Heme (myoglobin)	~5%
Ferritin	~25%
Transferrin	<1%
Heme enzymes	<1%
Other heme/iron containing molecules	<1%

This lipophilic molecule with low molecular weight (616.48 Da), Figure 1-2, can easily percolate into membranes and thus impair lipid bilayers and organelles. Damage results in destabilization of the cytoskeleton of cells and furthermore, heme catalyzes the formation of reactive oxygen species [25]. Therefore, like free iron, free heme is poorly tolerated by cells and heme is rapidly bound by molecules such as hemopexin, albumin and hemoglobin. Ultimately, both heme-hemopexin and albumin are recycled in the liver [32].

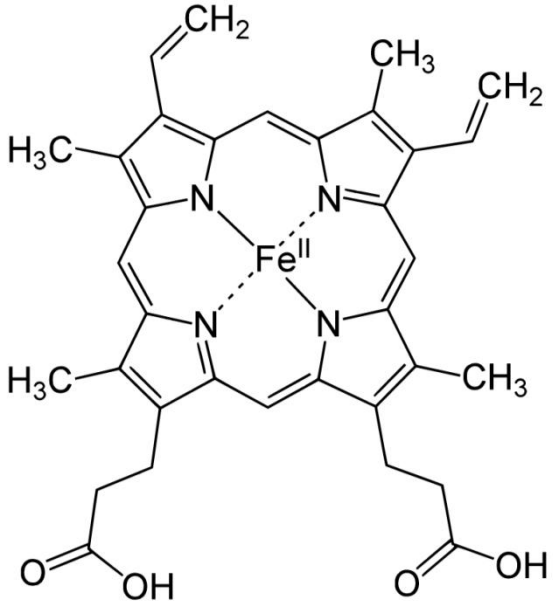

Figure 1-2 Structure of ferrous (Fe(II)) heme-b. Free heme is sequestered in the human body and bound by axial amino acid ligands from proteins typically forming octahedral like complexes.

1.3 Iron uptake in Gram-positive bacteria

The body's response to sequester and reduce extracellular iron levels and free heme may be a potentially effective strategy however, pathogenic bacteria have evolved specialized mechanisms for acquiring iron from the host. Numerous iron acquisition systems target a number of iron containing molecules. Iron uptake in Gram-positive bacteria is not as well understood as their Gram-negative counterparts despite the fact that many of these systems comprise of fewer components. This is mainly due to a larger research focus on Gram-negative bacteria in the past [25].

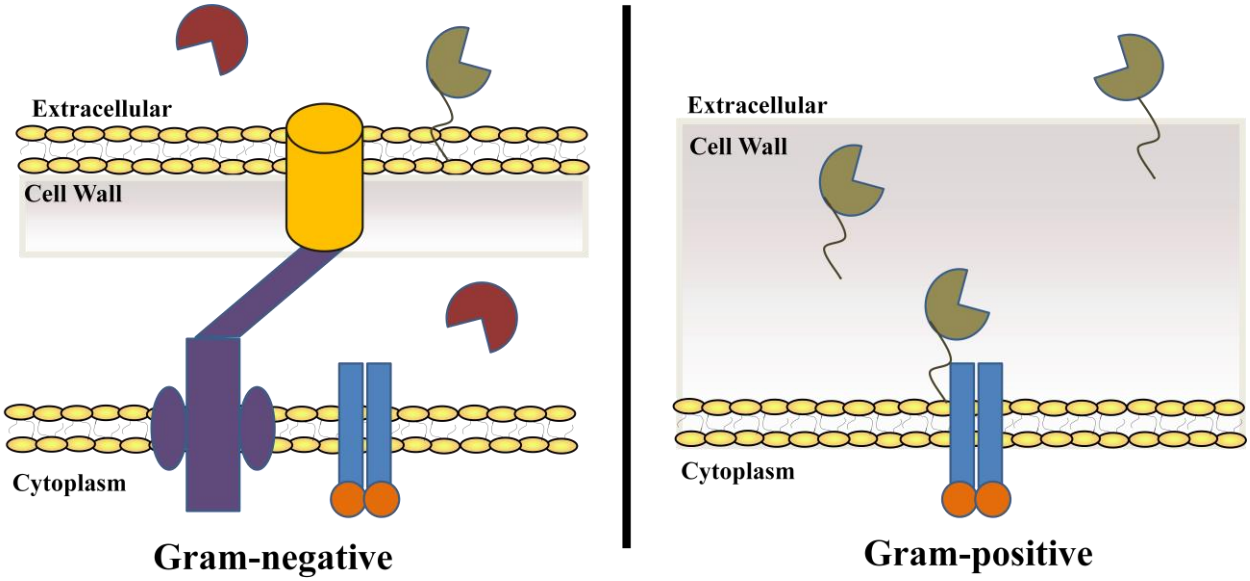

Figure 1-3 Cartoon schematic showing the difference Gram-negative (left) and Gram-positive (right) bacteria. All similar structures are similarly coloured. Gram-negative bacteria typically secrete iron-chelator molecules (red) and due to the extra cell wall, receive complexes in outer membrane receptors (yellow) using energy derived from the TonB-ExbB-ExbD complex (purple). Gram-positive bacteria receive iron-chelator molecules at the cytoplasmic membrane. Other protein receptors (brown), which are not exclusive to only one system, are bound to the cell wall typically through anchors to either the outer membrane or the cell wall. Both bacteria contain permeases (blue), which facilitate membrane transport and are driven by ATP produced from ATPase (orange).

Figure 1-3 shows the main differences between Gram-positive and Gram-negative bacteria. Gram-positive bacteria have a thicker cell wall, typically 15-80 nm thick [33] which is composed of murein sacculus, attached polysaccardides, teichoic acid and cell wall proteins [34]. Gram-positive bacteria characteristically have more complex cell wall structures and due to the

lack of an outer cell membrane the cell-wall proteins are typically tethered which anchors them into the cell wall instead of having free transport components like in Gram-negative bacteria [35]. The Ton system that is found in Gram-negative bacteria is not found in Gram-positive bacteria [25]. However, surprising similarities have been found between Gram-positive bacteria where many of them contain ATP binding cassette (ABC)-transporters, powered by ATP that facilitate heme transfer across the cell wall [25]. Interestingly, a ferric hydroxamate uptake (Fhu) system was discovered in *S. aureus* with similarities to the *E. coli* system which shows the promiscuity of these iron systems in bacteria [36, 37].

1.4 *Staphylococcus aureus* iron uptake systems

1.4.1 Siderophores in Staphylococcus aureus

S. aureus responds to the iron-restricted environment of the host with an array of iron-uptake and acquisition systems. It has been shown that *S. aureus* is able to grow using heme, hemoglobin, hemoglobin-haptoglobin, transferrin, ferric iron or ferrous iron as the sole iron source [38-40]. An example of iron uptake is through the use of siderophores, low molecular weight iron binding molecules (usually 400-1000 Da) that are secreted by bacteria into their extra-cellular environments. Typically, siderophores have a high affinity for iron and are found in numerous bacterial systems. Siderophores secreted by bacteria are able to remove iron from transferrin and *S. aureus* is no exception with two structurally characterized polycarboxylate-type siderophores, Staphyloferrin A and Staphyloferrin B, Figure 1-4, have been shown to be produced by *S. aureus* [41, 42]. Siderophores are transported through the cell wall in a cartoon schematic found in Figure 1-5. Siderophores are bound by substrate binding proteins which are anchored to the cell wall (brown) at the cell wall to cytoplasm interface where HtsA binds Staphyloferrin A and SirB binds Staphyloferrin B. The heterodimeric permeases (HtsBC and SirBC (blue)) allow release and passage of siderophores through the cell membrane and into the cytoplasm. The permeases receive ATP from FhuC (orange), a functional ATPase for both importers.

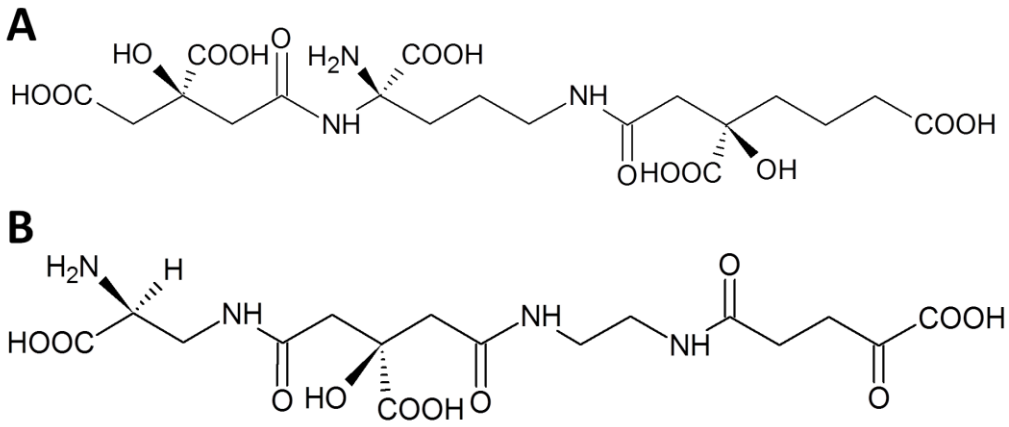

Figure 1-4 Structure of A) Staphyloferrin A and B) Staphyloferrin B [41, 42]

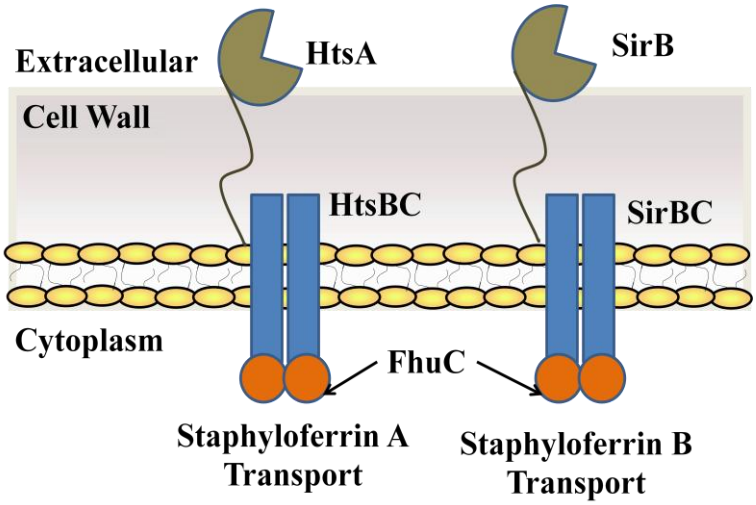

Figure 1-5 Left) Staphyloferrin A transport and Right) Staphyloferrin B transport in *Staphyloccus aureus.* These systems comprise of 3 main components which facilitate siderophore-iron complexes through the cell wall: Siderophore binding protein (HtsA or SirB), permease (HtsBC or SirBC) and ATP generator (FhuC) [41, 42].

1.4.2 Isd heme transport system in Staphylococcus aureus

Since the majority of iron is sequestered and bound as heme-iron, *S. aureus* has also evolved mechanisms to exploit and scavenge heme as an iron source. The iron-regulated surface determinant (*isd*) gene cluster was first identified in 2002 [40, 43, 44], and then in 2003, Mazmanian *et al.* [38] reported that when grown in iron-limiting medium, *S. aureus* expresses genes that are involved in iron acquisition. Mazmanian *et al.* were the first to propose that the Isd series of protein comprise of a heme transfer pathway across the cell wall and through the

cell membrane. The Isd system is so named because it is based on the iron regulation of all genes in the cluster, and the observation that four of the protein products of the system (IsdA, IsdB, IsdC and IsdH) are cell wall anchored. The genetic Isd system is encoded by five transcriptional units (*isdA, isdB, isdCDEFsrtBisdG, isdH* and *isdI*) [45, 46]. These genes encode cell wall anchored proteins (IsdA, IsdB, IsdC and IsdH), a membrane transporter (IsdDEF), a sortase (SrtB), and two cytoplasmic proteins (IsdG and IsdI). Overall, the Isd system is composed of and consists of nine iron-regulated proteins named IsdA, IsdB, IsdC, and IsdH, which are cell-wall anchored surface proteins; IsdDEF, which together constitute a membrane-localized ABC transporter; and finally, IsdG and IsdI, which encode heme-degrading enzymes in the cytoplasm [47, 48]. This system has been proposed [40, 43, 44] and shown [38] to pass heme through the gram-positive cell wall and cell membrane into the cytoplasm where heme is deconstructed and free iron is released. These nine proteins mediate the delivery of heme from the host's plasma into the *S. aureus* cytoplasm [49]. Surface proteins are often covalently anchored to the cell wall by the action of sortase enzymes due to the fact that Gram-positive bacteria lack an outer membrane. Sortase enzymes cleave a specific amino acid sequence at the end of the C terminal protein to attach the surface proteins to the cell wall. IsdC is achored by sortase B (SrtB) while the rest of the surface receptors are anchored by sortase A (SrtA) [38]. Studies have shown that IsdB and IsdH are exposed to the surface environment of the cell, while IsdA is only partially exposed. IsdC is buried within the cell wall and since it is attached with a sortase B anchor rather than the rest of the proteins, it is speculated that IsdC is attached to a unique portion of the cell wall compared with other protein components of the Isd system [38, 45, 46]. Interestingly, genetic inactivation of IsdA, IsdF or either SrtA or SrtB led to a decreased association of heme with *S. aureus* cells [38]. Other studies have shown similar results where inactivating IsdA, IsdG or IsdI impaired growth in iron-chelated minimal media with heme as the sole iron source [50, 51]. Furthermore, inactivation of IsdH and IsdB also led to decreased growth on hemoglobin as a sole iron source [52].

In *S. aureus*, all the cell wall anchored Isd proteins, IsdA, IsdB, IsdC and IsdH each contain one to three copies of a conserved near transporter (NEAT) domain. The NEAT domain is found in most pathogenic bacteria. The domain has been found to be related to iron transport. NEAT domains are composed of about 125 amino acids and are mostly composed of beta sheets [53]. A cartoon schematic representation of the cell wall anchored Isd proteins, Figure 1-6, shows the

NEAT domain structure of the proteins as well as the C-terminal tags which anchor the proteins to the cell wall. IsdA and IsdC each contain one NEAT domain which has been shown to bind heme [50, 54, 55]. IsdB contains two NEAT domains of which only IsdB-NEAT domain 2 binds heme. IsdH contains three NEAT domains of which only IsdH-NEAT domain 3 binds heme.

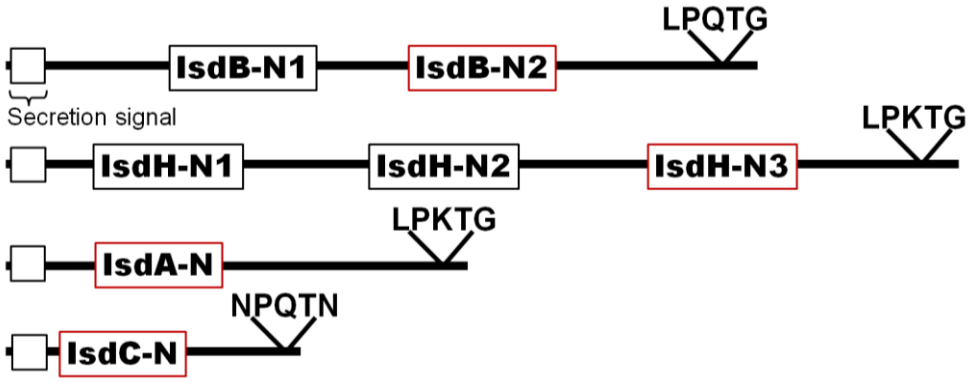

Figure 1-6 Schematic showing the cell wall anchored Isd proteins. Heme binding NEAT domains are colored red.

Early research on the Isd system from *S. aureus* focused on characterization of the heme binding characteristics of the Isd proteins and mechanism of heme transfer and extraction from iron sources. A schematic of known information when starting this thesis is summarized in Figure 1-7. Early mechanistic research had found that heme acquisition proteins, IsdB and IsdH captured heme from Hb released from erythrocytes by hemolysins [52, 56]. IsdH binds haptoglobin (a serum glycoprotein that protects the host from free hemoglobin) and the haptoglobin-hemoglobin complex [39, 57]. IsdA is proposed to function as a heme scavenging protein and a "heme reservoir" for IsdH and IsdB [55, 58]. IsdC, which is located in the cell wall, acts as the central conduit of heme transfer in the Isd system [50, 59, 60]. The membrane bound complex IsdDEF complex pumps heme across the membrane [49]. Heme is finally deconstructed by IsdG monooxygenase or its paralog, IsdI [48, 49]. The proteins IsdA, IsdB, IsdC and IsdH each contain at least one NEAT domain that adopts a beta sandwich structure to bind one ferric heme into a groove with heme-iron coordination via Tyr. IsdA can bind ferrous heme through a histidine binding motif while IsdC is not able to bind ferrous heme [50, 55, 58, 59, 61-63]. IsdE, a lipoprotein, which does not contain any NEAT domains, binds heme into a shallow groove between two lobes of the protein using His to coordinate to the ferric heme-iron. Ferrous heme is bound by histidine and methionine amino acid binding ligands [64, 65]. Current

studies on the Isd system in *S. aureus* are focusing on the structural aspects of the heme and heme analog binding [49, 54], mechanistic details in terms of heme transfer/binding [56, 66, 67], and the heme degradation reaction [68, 69]. Some studies have started to look at different metal-substituted porphryins and their binding to the Isd system [49, 54, 69-71].

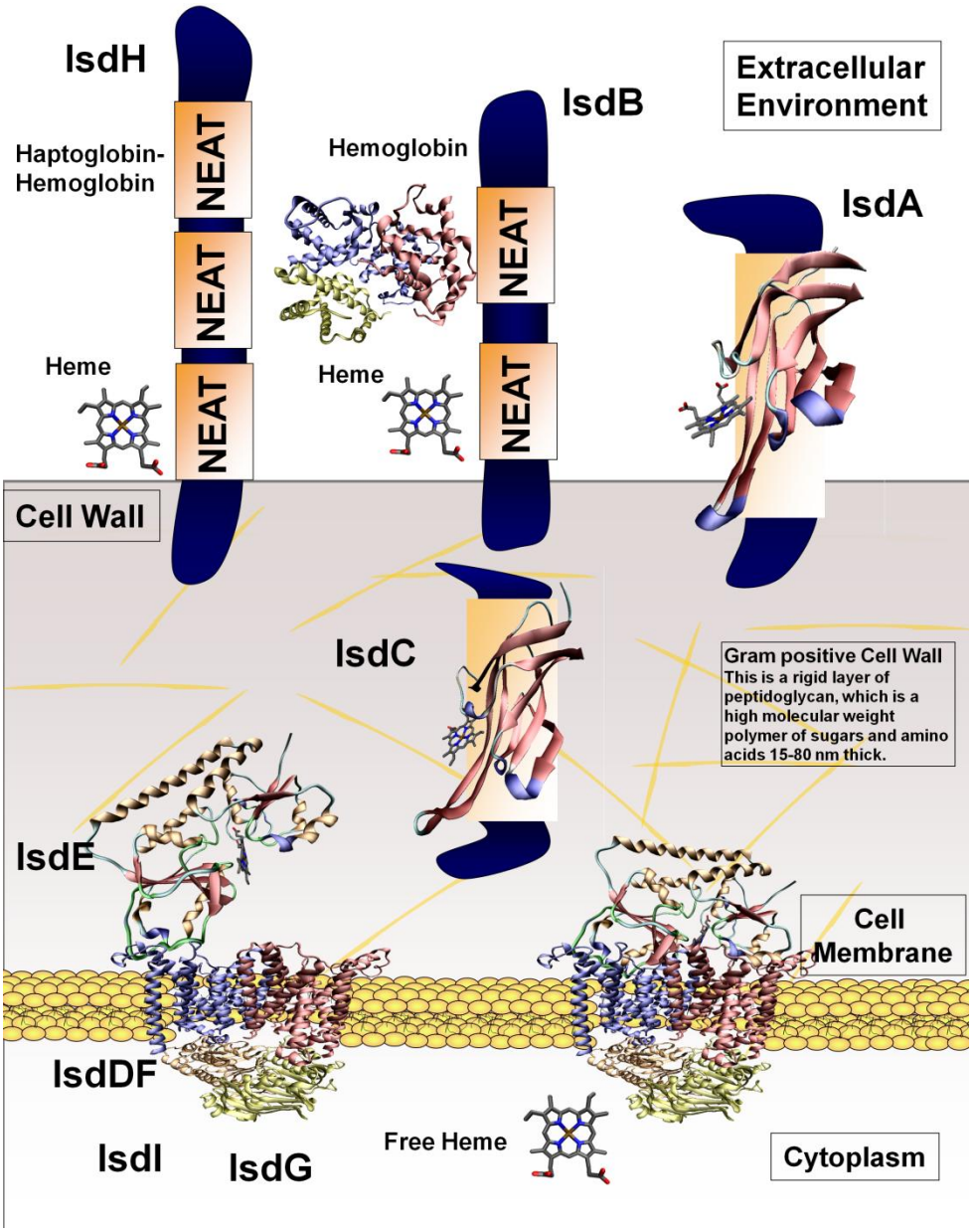

Figure 1-7 Proposed model for the Isd heme scavenging pathway in *Staphyloccocus aureus.* This scheme was adapted from the proposal by Mazmanian *et al*. [38]. Shown are the structures of the NEAT domains for IsdA and IsdC, and IsdE (using the deposited pdb files [2itf, 2o6p, 2q8q]). It is proposed that IsdH-N1 binds the haptoglobin-hemoglobin complex, and IsdH-N3 binds heme. IsdB-N1 binds hemoglobin, while IsdB-N2 binds heme. IsdC is believed to be a central conduit to the heme transfer mechanism and only binds heme in the NEAT domain. IsdE does not contain a NEAT domain since it is a lipoprotein involved in heme

passage through the ABC transporter comprised of IsdEF. IsdG and IsdI are responsible for degradation and release of free useable iron into the bacterial cell. Adapted from [72].

1.5 Scope of thesis

Heme uptake mechanisms of bacterial pathogens present an ideal path for targeted drug delivery because they accumulate heme via active transport and are maximally expressed in iron-limiting conditions in the host, which happens during infection [24]. However, mechanistic detail about heme and heme analog transfer through this pathway has not been studied. Furthermore, the heme binding characterization of the remaining Isd proteins, IsdB and IsdH has also not been explored as in depth as the other NEAT containing Isd proteins, IsdA and IsdC. The research in this thesis focuses on the characterization and mechanistic detail of heme and heme analog binding and transfer in the Isd system of *Staphylococcus aureus*.

This thesis consists of 9 chapters. The first chapters give an overview of *Staphyloccocus aureus* and the importance of iron to bacteria. Chapter 1 provides an introduction into the heme transfer Isd system in *S. aureus* with a summary of research on the system that was performed when starting this thesis. Chapter 2 explores the recombinant protein synthesis method used to produce the Isd proteins used in this thesis as well as an explanation of the techniques used which include UV-visible absorption spectroscopy, magnetic circular dichroism spectroscopy and electrospray-ionization mass spectrometry. An introduction to heme spectroscopy and heme proteins is also provided.

Chapter 3 consists of the first and complete experimental mapping of heme transfer *in vitro* of the Isd system. Protein-protein interactions are speculated to control the specific heme transfer reactions found. Chapter 4 explores the heme binding motif of the unexplored IsdB-NEAT domain 2 and IsdH-NEAT domain 3. The results found in this chapter lead to speculation that the heme binding motif plays a characteristic role in the selectivity of heme transfer found in the Isd system.

Chapter 5 explores the importance of the heme binding ligands of IsdE with regards to the selective transfer found in the Isd system. Importantly, the strong unidirectional nature of the system is controlled by the amino acids ligands in IsdE and without them, heme transfer does not

involve specific protein-protein interactions but is transformed into a associative/dissociative mechanism.

Chapter 6 describes the difference in rates of heme transfer found within the Isd system of *S. aureus*. This chapter also explores the importance of performing heme transfer kinetics using ESI-MS techniques with heme binding multi-protein systems where characterization by absorption spectroscopy is difficult and ambiguous due to the similar spectral properties of heme binding proteins.

Chapter 7 explores the start of the Isd pathway looking at interactions with IsdB with bovine hemoglobin as a model for human hemoglobin extraction. The importance of oxidation state as well as protein-protein interactions is explored.

Chapter 8 looks at heme analog transfer through the core three Isd proteins, IsdA, IsdC and IsdE. The correlation between central metal and ring structure is explored with insight into potentially interrupting and disrupting the Isd system in order to potentially kill the bacteria by blocking important resource pathways.

Chapter 9 draws together the results from each chapter and discusses them with respect to the structural properties, heme binding properties, heme transfer properties and mechanistic detail of the Isd proteins.

1.6 References

1. Haley, K. P.; Skaar, E. P., *Microbes and Infection* **2011,** 14, 217-227.
2. Kuehnert, M. J.; Kruszon-Moran, D.; Hill, H. A.; McQuillan, G.; McAllister, S. K.; Fosheim, G.; McDougal, L. K.; Chaitram, J.; Jensen, B.; Fridkin, S. K.; Killgore, G.; Tenover, F. C., *J. Infect. Dis.* **2006,** 193, 172-179.
3. Harrington, B. J.; Valigosky, M., *Lab. Med.* **2007,** 38, 165-168.
4. Wisplinghoff, H.; Bischoff, T.; Tallent, S. M.; Seifert, H.; Wenzel, R. P.; Edmond, M. B., *Clin. Infect. Dis.* **2004,** 39, 309-307.
5. McGowan, J. E.; Tenover, F. C., *Nature Rev.* **2004,** 2, (3), 251-259.
6. Gordon, R. J.; Lowy, F., *Clin. Infect. Dis.* **2008,** 46, (Suppl 5), S350-359.
7. Bullen, J.; Griffiths, E., Iron and Infecton: Molecular, Physiological, and Clinical Aspects, John Wiley and Sons: New York, 1999; Vol. 2, p 409-415.
8. Neu, H. C., *Science.* **1992,** 257, 1064-1073.
9. Barrett, F. F.; McGehee, R. F.; Finland, M., *N. Engl. J. Med.* **1968,** 279, 441-448.
10. Bamberger, D. M.; Boyd, S. E., *Am. Fam. Phys.* **2005,** 72, 2474-2481.
11. Chang, S.; Sievert, D. M.; Hageman, J. C.; Boulton, M. L.; Tenover, F. C.; Downes, F. P.; Shah, R.; Rudrik, J. T.; Pupp, G. R.; Brown, W. J.; Cardo, D.; Fridkin, S. K., *N. Engl. J. Med.* **2003,** 348, 1342-1347.
12. Herold, B. C.; Immergluck, L. C.; Maranan, M. C., *J. Am. Med. Ass.* **1998,** 279, 541-545.

13. Klevens, R. M.; Morrison, M. A.; Nadle, J.; Petit, S.; Gershman, K.; Ray, K.; Harrison, S.; Lynfield, L. H.; Dumyati, R.; Townes, J. M.; Craig, A. S.; Zell, E. R.; Fosheim, G. E.; McDougal, L. K.; Carey, R. B.; Fridkin, S. K., *J. Am. Med. Assoc.* **2007,** 298, 1763-1771.
14. CDC, *HIV/AIDS Surveill. Rep.* **2007,** 17.
15. (CNISP), *http://www.phacaspc.gc.ca/noissinp/projects/pdf/mrsa_report2006end.pdf* **2006**.
16. Goetghebeur, M.; Landry, P. A.; Han, D.; Vicente, C., *Can. J. Infect. Dis. Med. Microbiol.* **2007,** 18, 27-34.
17. Donovan, A.; Lima, C. A.; Pinkus, J. L.; Pinkus, G. S.; Zon, L. I.; Robine, S.; Andrews, N. C., *Cell. Metab. 1* **2005**, 191-200.
18. Garcia-Lara, J.; Masalha, M.; Foster, S. J., *Drug. Discov. Today* **2005,** 10, 643-651.
19. O'Riordan, K.; Lee, J. C., *Clin. Microbiol. Rev.* **2004,** 17, 218-234.
20. Clarke, S. R.; Foster, S. J., *Adv. Microb. Physiol.* **2006,** 51, 187-224.
21. Baba-Moussa, L.; Ahissou, H.; Azokpota, P.; Assogba, B.; Atindehou, M. M.; Anagonou, S.; Keller, D.; Sanni, A.; Prevost, G., *Afr. J. Biotech.* **2010,** 9, 604-611.
22. Foster, T. J., *Nat. Rev. Microbiol.* **2005,** 3, 948-958.
23. Wandersman, C.; Delepelaire, P., *Annu. Rev. Microbiol.* **2004,** 58, 611-647.
24. Stojiljkovic, I.; Evavold, B. D.; Kumar, V., *Exp. Opin. Invest. Drugs.* **2001,** 10, 309-320.
25. Tong, Y.; Guo, M., *Arch. Biochem. Biophys.* **2009,** 481, 1-15.
26. Bertini, I.; Gray, H. B.; Stiefel, E. I.; Valentine, J. S., Biological Inorganic Chemistry: Structure & Reactivity, University Science Books: Sausalito, California, 2007.
27. Papanikolaou, G.; Pantopoulos, K., *Tox. Appl. Pharm.* **2005,** 202, 199-211.
28. Bullen, J. J.; Rogers, H. J.; Griffiths, E., **1978,** 80, 1-35.
29. Weinberg, E. D., *Microbiol. Rev.* **1978,** 1, 45-66.
30. Stojiljkovic, I.; Perkins-Balding, D., *DNA Cell Biol.* **2002,** 21, 281-295.
31. Radtke, A. L.; O'Riordan, M. X., *Cell Microbiol.* **2006,** 8, 1720-1729.
32. Nielsen, M. J.; Moller, H. J.; Moestrup, S. K., *Antioxid. Redox. Signal.* **2010,** 12, 261-273.
33. Beveridge, T. J.; Matias, V. R., Ultrastructure of Gram-postive Cell Walls in Gram-Positive Pathogens, ASM Press: Washington, DC, 2006; Vol. 2nd Ed., 3-11.
34. Navarre, W. W.; Schneewind, O., *Microbiol. Mol. Biol. Rev.* **1999,** 63, 174-229.
35. Letoffe, S.; Heuck, G.; Delepelaire, P.; Lange, N.; Wandersman, C., *Proc. Natl. Acad. Sci. U.S.A.* **2009,** 106, 11719-11724.
36. Sebulsky, M. T.; Hohnstein, D.; Hunter, M. D.; Heinrichs, D. E., *J. Bacteriol.* **2000,** 182, 4394-4400.
37. Sebulsky, M. T.; Heinrichs, D. E., *J. Bacteriol.* **2001,** 183, 4494-5000.
38. Mazmanian, S. K.; Skaar, E. P.; Gaspar, A. H.; Humayun, M.; Gornicki, P.; Jelenska, J.; Joachmiak, A.; Missiakas, D. M.; Scheenwind, O., *Science* **2003,** 299, 906-909.
39. Dryla, A.; Gelbmann, D.; Gabain, A. v.; Nagy, E., *Mol. Microbiol.* **2003,** 49, 37-53.
40. Taylor, J. M.; Heinrichs, D. E., *Mol. Microbiol.* **2002,** 43, 1603-1614.
41. Cheung, J.; Beasley, F. C.; Liu, S.; Lajoie, G. A.; Heinrichs, D. E., *Mol. Microbiol.* **2009,** 74, 594-608.
42. Drechsel, H.; Winkelmann, G., *Biometals* **2005,** 18, 75-81.
43. Mazmanian, S. K.; Ton-That, H.; Su, K.; Scheenwind, O., *PNAS* **2002,** 99, 2293- 2298.

44. Morrissey, J. A.; Cockayne, A.; Hammacott, J.; Bishop, K.; Denman-Johnson, A.; Hill, P. J.; Williams, P., *Infect. Immun.* **2002,** 70, 2399-2298.
45. Skaar, E. P.; Schneewind, O., *Microbes Infect.* **2004,** 6, 390-397.
46. Skoog, D. A.; Holler, F. J.; Nieman, T. A., Principles of Instrumental Analysis, 5th Ed. ed.; Thomson Learning: Toronto, 1998.
47. Skaar, E. P.; Gaspar, A. H.; Scheenwind, O., *J. Biol. Chem* **2004,** 279, 436-443.
48. Reniere, M. L.; Skaar, E. P., *Mol. Microbiol.* **2008,** 69, 1304-1315.
49. Grigg, J. C.; Ukpabi, G.; Gaudin, C. F. M.; Murphy, M. E. P., *J. Inorg. Biochem.* **2010,** 104, 341-348.
50. Grigg, J. C.; Vermeiren, C. L.; Heinrichs, D. E.; Murphy, M. E., *Mol. Microbiol.* **2007,** 63, 139-149.
51. Reniere, M. L.; Torres, V. J.; Skaar, E. P., *Biometals* **2007,** 20, (3-4), 333-345.
52. Torres, V. J.; Pishchany, G.; Humayun, M.; Scheenwind, O.; Skaar, E. P., *J. Bacteriol.* **2006,** 188, 8421-8429.
53. Andrade, M. A.; Ciccarelli, F. D.; Perez-Iratxeta, C.; Bork, P., *Genome Biol.* **2002,** 3, 1-5.
54. Grigg, J. C.; Mao, C. X.; Murphy, M. E. P., *J. Mol. Biol.* **2011,** 413, 684-698.
55. Pluym, M.; Muryoi, N.; Heinrichs, D. E.; Stillman, M. J., *J. Inorg. Biochem.* **2008,** 102, 480-488.
56. Zhu, H.; Xie, G.; Liu, M.; Olson, J.; Fabian, M.; Dooley, D.; Lei, B., *J. Biol. Chem.* **2008,** 283, 18450-18460.
57. Watanabe, M.; Tanaka, Y.; Suenaga, A.; Kurodo, M.; Yao, M.; Watanabe, N.; Arisaka, F.; Ohta, T.; Tanaka, I.; Tsumoto, K., *J. Biol. Chem.* **2008,** 283, 28649-28659.
58. Vermeiren, C. L.; Pluym, M.; Mack, J.; Heinrichs, D. E.; Stillman, M. J., *Biochemistry* **2006,** 45, 12867-12875.
59. Muryoi, N.; Tiedemann, M. T.; Pluym, M.; Cheung, J.; Heinrichs, D. E.; Stillman, M. J., *J. Biol. Chem.* **2008,** 283, 28125-28136.
60. Villareal, V. A.; Pilpa, R. M.; Robson, S. A.; Fadeev, E. A.; Clubb, R. T., *J. Biol. Chem.* **2008,** 283, 31591-31600.
61. Tiedemann, M. T.; Muryoi, N.; Heinrichs, D. E.; Stillman, M. J., *J. Porphyrins Phthalocyanines.* **2009,** 13, 1006-1016.
62. Mack, J.; Yoshiaki, A.; Kobayashi, N.; Stillman, M. J., *J. Am. Chem. Soc.* **2005,** 127, 17697-17711.
63. Pilpa, R. M.; Robson, S. A.; Villareal, V. A.; Wong, M. L.; Phillips, M.; Clubb, R. T., *J. Biol. Chem.* **2009,** 284, 1166-1176.
64. Grigg, J. C.; Vermeiren, C. L.; Heinrichs, D. E.; Murphy, M. E., *J. Biol. Chem.* **2007,** 282, 28815-28822.
65. Pluym, M.; Vermeiren, C. L.; Mack, J.; Heinrichs, D. E.; Stillman, M. J., *Biochem.* **2007,** 46, 12777-12787.
66. Villareal, V. A.; Spirig, T.; Robson, S. A.; Liu, M.; Lei, B.; Clubb, R. T., *J. Am. Chem. Soc.* **2011,** 133, 1417-14179.
67. Robson, S. A.; Peterson, R.; Bouchard, L.-S.; Villareal, V. A.; Clubb, R. T., *J. Am. Chem. Soc.* **2010,** 132, 9522-9523.
68. Takayama, S. J.; Ukpabi, G.; Murphy, M. E. P.; Mauk, A. G., *PNAS.* **2011,** 108, 13071-13076.

69. Reniere, M. L.; Ukpabi, G. N.; Harry, S. R.; Stec, D. F.; Krull, R.; Wright, D. W.; Bachmann, B. O.; Murphy, M. E.; Skaar, E. P., *Mol. Microbiol.* **2010,** 75, 1529-1538.
70. Lee, W. C.; Reniere, M. L.; Skaar, E. P.; Murphy, M. E., *J. Biol. Chem* **2008,** 283, (45), 30957-30963.
71. Moriwaki, Y.; Caaveiro, J. M. M.; Tanaka, Y.; Tsutsumi, H.; Hamachi, I.; Tsumoto, K., *Biochem.* **2011,** 50, 7311-7320.
72. Tiedemann, M. T.; Muryoi, N.; Heinrichs, D. E.; Stillman, M. J., *Biochem. Soc. Trans* **2008,** 36, 1138-1143.

Chapter 2. Materials and Methods: Preparation, Purification and Characterization of Isd Proteins from *S. aureus*[1]

2.1 Introduction

Modern studies rely heavily on recombinant protein expression systems, where the protein of interest is grown and isolated from a non-natural source. For the Isd system, the protein of interest is grown and purified from a recombinant system using *Escherichia coli* (*E. coli*). The Isd protein gene was integrated into an expression plasmid that had been inserted into a host organism. Hence, the plasmid was induced to produce significant quantities of the protein. There are several advantages when compared to isolation from natural sources, including enhanced isolation techniques, purity, yield and efficiency. This is important since *Staphylococcus aureus* is a dangerous pathogenic bacteria and the Isd genes are only expressed during non-optimal, iron-limiting environments.

In this chapter, the recombinant protein preparation techniques are described for the production of the Isd proteins. A multitude of instrumental techniques was used to study the Isd heme transfer system including UV-visible absorption spectroscopy, magnetic circular dichroism (MCD) spectroscopy and electrospray ionization mass spectrometry (ESI-MS). A brief description of the instrumental techniques used to characterize the Isd proteins and their heme binding properties is also provided.

2.2 Chemical Inventory

Table 2-1: List of materials used

Chemical / Reagent	Supplier
Acetonitrile	Caledon
Agar-Agar	Fisher Scientific
Ammonium Hydroxide	EMD
Ampicillin	Bioshop
L-Arabinose	Fisher Scientific
2-Butanone	Alfa Aesar
Carbon Monoxide gas	Praxair
Co(III)-Protoporphyrin IX	Frontier Scientific

[1] A portion of this work has been published:
Tiedemann M. T., Stillman M. J., J. Porphyrins Phthalocyanines, **2011,** 15, 1134-1149.

Deionized (dI) water >16 MΩ•cm	Branstead Nanopure Infinity
N,N-Dimethylformamide	Caledon
Dimethylsulfoixde	Caledon
Ferrous Chloride	Sigma
Formic Acid	Caledon
Formic Acid (Ammonium Salt)	J. T. Baker
Hemin	Fluka
His-Trap HP 1mL Column	GE Healthcare
Hydrochloric Acid	Caledon
Imidazole	Fisher Scientific
Luria Bertani Broth Mix	Difco
Mn(III)- Protoporphyrin IX	Frontier Scientific
Myoglobin	Sigma
Nitric Acid	Fisher Scientific
Potassium Ferricyanide	Fisher Scientific
Protoporphyrin IX	Frontier Scientific
Protoporphyrin IX-Dimethylester	Frontier Scientific
Pyridine	Caledon
Sodium Chloride	Caledon
Sodium Cyanide	Fisher Scientific
Sodium Dithionite	Fisher Scientific
Sodium Phosphate	Caledon
Thrombin	GE Heathcare

2.3 Isd Proteins

The recombinant Isd proteins were kindly engineered in the laboratory of David Heinrichs at The University of Western Ontario (London, Ontario). DNA encoding residues 62-184 of IsdA (the NEAT domain of IsdA or IsdA-N), residues 144-462 of IsdB (IsdB-N1N2), residues 144-269 of IsdB (IsdB-N1), residues 337-462 of IsdB (IsdB-N2), residues 28-150 of IsdC (IsdC-N), residues 539-658 of IsdH (IsdH-N3) and residues 32-292 of IsdE were PCR amplified from *S. aureus* RN6390 chromosome and cloned into pET28(+) in such a way as to incorporate N-terminal 6X-His tags. DNA encoded His-tagged protein was digested out of pET28a(+) and cloned into pBAD30 [1], for ampicillin resistance, before being introduced into *E.coli* RP523, a *hemB* mutant, which cannot produce heme [2].

2.4 Protein Growth and Purification

2.4.1 Protein Expression and Growth

All solutions were prepared with deionized water with a resistivity greater than 16 MΩ•cm with a Nanopure Inifinity water system (Barnstead, Illinois, USA). All solutions were either made with autoclaved water (eg. growth cultures, heme, ampicillin, L-arabinose solutions) at 121 ^{o}C for 20 minutes with a Sterilmax Table Top Sterilizer (Thermo Scientific, Iowa, USA).

Figure 2-1 shows the detailed outline of the protocol used to synthesize and isolate Isd proteins. Production of each Isd protein follows the same protocol. Transformed cells stored in glycerol stocks in a -80 ^{o}C freezer were plated onto agar plates containing 10 mg/L ampicillin and 20 mg/L heme. The cells were allowed to grow at 37 ^{o}C overnight. Cells were then transferred to liquid cultures (2x50 mL LB-Luria) containing 10 mg/L ampicillin and 10 mg/L heme. Twenty hours after incubation (37 ^{o}C), the cells were collected by centrifugation, 5 000 rpm for 15 min at 4 ^{o}C with an Avanti J-series centrifuge (Beckman-Coulter, Canada) and a JLA-25.50 rotor. Cells were then resuspended in minimal LB-Luria media and added to liquid cultures (3x1 L LB-Luria) containing 10 mg/L ampicillin and 10 mg/L heme with an absorbance of the cell culture at 0.1 at 600 nm; the starting absorbance for optimal growth. After 20 hours (37 ^{o}C) cells were then collected by centrifugation, 5 000 rpm for 15 min at 4 ^{o}C with an Avanti J-series centrifuge and a JLA-16.250 rotor. Heme was washed away by gently swirling the cells in 10 mM PBS Buffer, pH 7.4. Cells were then resuspended in minimal LB-luria media and added to liquid cultures (3x2 L LB-Luria) containing 10 mg/L ampicillin and 0.2% L-arabinose at 30 ^{o}C to induce protein expression. 20 hours after induction, the cells were harvested by centrifugation at 5 000 rpm for 15 min at 4 °C with an Avanti J-series centrifuge and a JLA-9.1000 rotor. The supernatant was decanted and the cell pellet was resuspended in a solution of 10 mM PBS Buffer, pH 7.4. The cell pellet was then frozen at -80 ^{o}C.

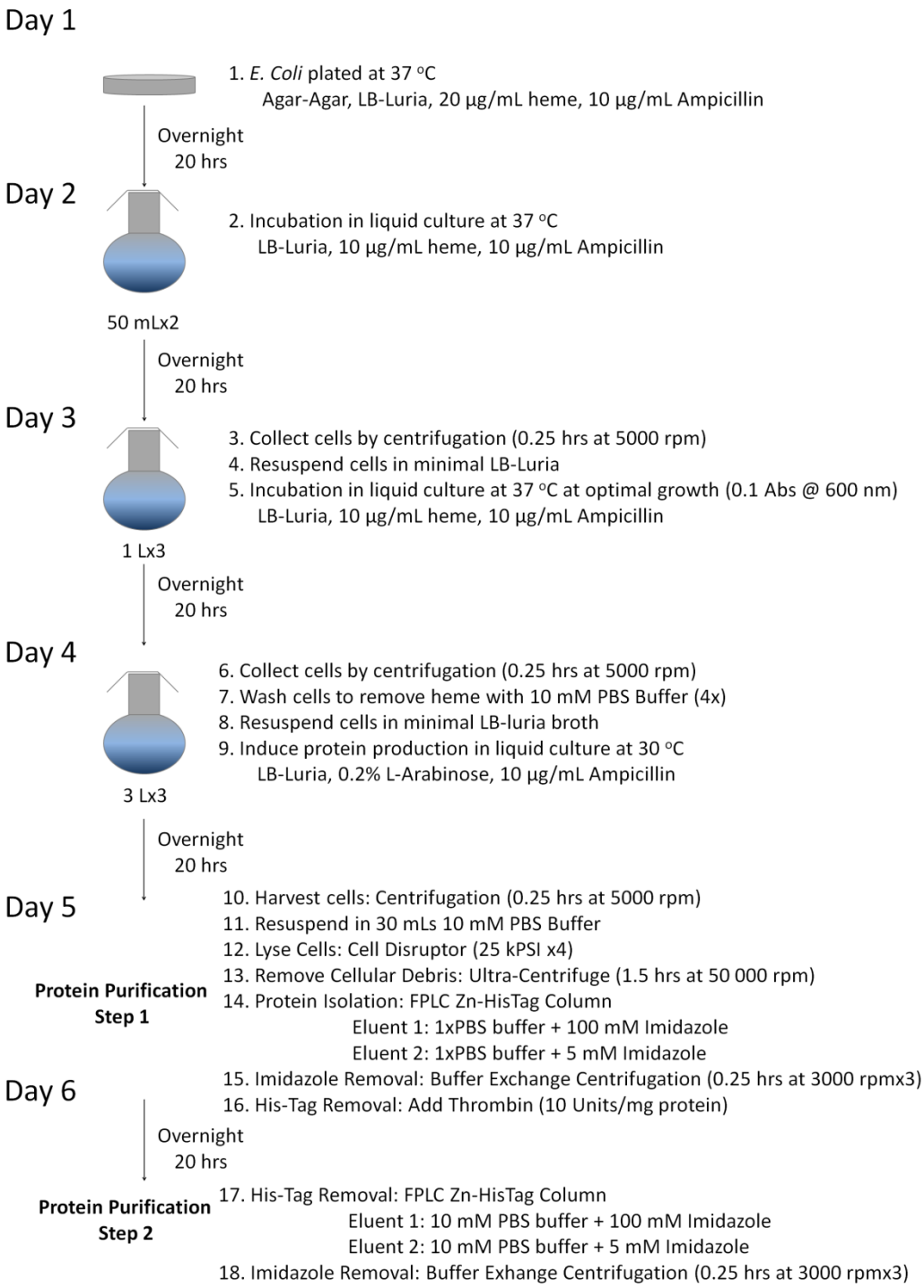

Figure 2-1 Protein preparation protocol for the synthesis of recombinant Isd proteins from *S. aureus*

2.4.2 Protein Purification

The cell pellet was then frozen at -80 ^{o}C, thawed, and lysed using the cell disruptor method (3 passes at 25 kPSI) (Constant Cell Disruption Systems, UK). The freeze-thaw cycle allows for easier lysing of the cells. Un-disrupted cellular debris was removed by centrifugation at 5 000 rpm for 15 min at 4 ^{o}C with an Avanti J-series centrifuge (Beckman-Coulter, Mississauga, ON, Canada) and a JLA-25.50 rotor. Disrupted cellular debris was removed by ultra-centrifugation at 50 000 rpm (150 000 x g) for 1.0 hr at 4 ^{o}C to remove insoluble materials.

Proteins were purified using a 1 ml HisTrap column (GE Healthcare) and an FPLC (ÄKTA, US) system with a binding buffer containing 10 mM sodium phosphate, pH 7.4, 500 mM NaCl. 5 mM imidazole and an elution buffer containing 10 mM sodium phosphate, pH 7.4, 500 mM NaCl, 100 mM imidazole. Proteins were then desalted by buffer exhchange to 10 mM PBS, pH 7.4, using Amicon Ultracel 10k centrifuge tubes (Millipore, USA) and a CS-6 swinging bucket centrifuge (Beckman, USA) for three 15 minute spins at 5k rpm. The 6xHis-tags were removed by incubation with thrombin (10 units/mg protein; GE Healthcare) at 4 ^{o}C for 20 hours and run through a HisTrap column for final purification.

2.4.3 Adding heme to apo-Isd proteins

For heme loading to apo-protein, hemin (Fluka) at pH 10 was added to the Isd protein in approximately 10x excess. Following incubation for 0.5 h, protein samples were separated using G-25 size-exclusion chromatography. The extent of heme binding was verified with mass spectrometry.

2.5 UV-visible absorption spectroscopy

2.5.1 Introduction to UV-visible absorption spectroscopy of heme protein

In absorption spectroscopy, the loss of light in an incident beam is measured as a function of the frequency (or wavelength) of the radiation. A simple UV-visible absorption setup is shown in Figure 2-2.

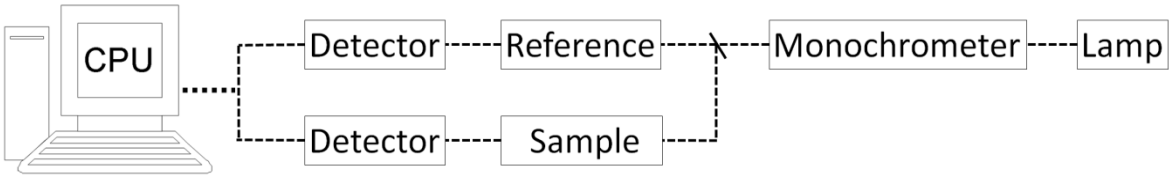

Figure 2-2 Simplified sketch of a UV-visible absorption spectrometer based on a dual beam approach.

The absorbance or optical density, A(λ), of a given sample is described by Beer's Law, Eq. 1:

$$A(\lambda)=\log(\frac{I_0}{I})=\varepsilon(\lambda)cl \quad (1)$$

with incident light intensity, I_0; light intensity after passing through the sample, I; extinction coefficient, ε(λ); concentration, c; and path length, l. With the concentration in [M] and the path length in cm, the unit of extinction coefficient ε is $M^{-1}cm^{-1}$. However, for heme binding proteins, this coefficient is often reported in $mM^{-1}cm^{-1}$.

In proteins, three different internal chromophores give rise to electronic absorptions bands: 1) the peptide bond linking the amino acids absorbs weakly at 220 nm, 2) the aromatic amino acids phenylalanine, tyrosine, tryptophan and histidine contribute with bands in the range of 230-300 nm, and 3) most importantly, many biological molecules show strong absorbance in the visible region of the spectrum as a result of the presence of metal ions and prosthetic groups with extended π-electron systems, such as heme, chlorophyll, carotinoid and flavin [3, 4]. These bands are sensitive to the surrounding polypeptide environment and reflect structural changes, oxidation states and the binding ligands, making UV-visible absorption spectroscopy an excellent tool for physical studies of protein function.

2.5.2 Calculating protein concentration

The 280 nm band is extremely useful for calculating protein concentration, especially in the absence of heme binding. However, there is too much error when using an estimated ε(280) value to determine protein concentrations for quantitative mass spectrometry experiments. By coupling UV-absorption spectroscopy and atomic absorption spectroscopy (AAS) of the heme bound holo-proteins (confirmed by ESI-MS), it was possible to measure the amount of bound heme present (each protein only binds one heme). Hence, the accuracy of AAS can be combined with UV-visible absorption spectroscopy to accurately calculate protein concentration and ε(280)

values. Summarized in the table below are the calculated molar extinction coefficients ε(280) by this technique. Note, for IsdB-N1 the ε(280) is estimated since this protein does not bind heme.

Table 2-2: Absorption ε(280) values of Isd proteins used in this thesis. *: IsdB-N1 ε(280) is estimated since this protein does not bind heme.

Isd Protein	Absorption ε(280) ($mM^{-1}cm^{-1}$)
IsdA-N	28.85
IsdB-N1	17.21*
IsdB-N2	15.93
IsdB-N1N2	38.26
IsdC-N	38.50
IsdH-N3	14.65
IsdE	20.07

2.5.3 Protoporphyrin IX and heme spectroscopy

In metalloporphyrins, such as heme, Figure 2-3, there are two major electronic bands and a strong vibronic band arising from $\pi \rightarrow \pi^*$ transitions of the conjugated 18π e^- system, Figure 2-4. At higher energy (typically observed between 380 and 430 nm) is the very intense B (or Soret) band. It represents an allowed transition with extinction coefficients on the order of 10^5 $M^{-1}cm^{-1}$. At lower energy (500 - 600 nm) is the Q_{00}, or α band, and the Q_{vib}, or β band, arising from the lowest porphyrin π–π* singlet transition and its vibronic envelope, respectively. They represent forbidden transitions and as such are typically weaker than the B band, possessing extinction coefficients on the order of 10^4 $M^{-1}cm^{-1}$ [5-7].

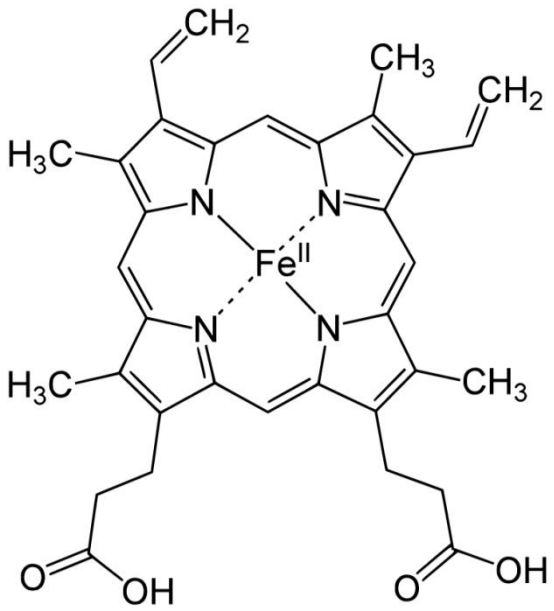

Figure 2-3 Structure of ferrous (Fe(II)) heme-b. Structurally, heme-b has pseudo-D_{4h} symmetry with a formula $C_{34}H_{32}FeN_4O_4$ and molecular mass of 616.48 g/mol.

Demetallation of a metalloporphyrin (for example forming protoporphryin IX (PPIX)), reduces the symmetry of the molecule from psuedo-D_{4h} (square) to D_{2h} (rectangular). As a result a splitting of the doubly degenerate Q bands is observed. The Q_{00} band splits into x and y components ($Q_{x,\ 00}$ and $Q_{y,\ 00}$) as does the Q_{vib} band ($Q_{x,\ vib}$ and $Q_{y,\ vib}$). The result is a visible region absorption spectrum consisting of four peaks, Figure 2-5 [8].

The three metalloporphyrin bands (B, Q_{00} and Q_{vib}) vary considerably in band maximum and relative intensity. These variations are characteristic of the oxidation and spin state of the central iron. Overlaid on the 3 bands are charge transfer transitions between the central metal and the ring, which occur in the same spectral region. Charge transfer transitions are particularly sensitive to the oxidation and spin state of the central iron and are observed at different characteristic wavelengths in the visible region for all but the diamagnetic low spin ferrous iron. The combination of $\pi-\pi^*$ and charge transfer transitions produces a very complex UV-visible absorption spectrum. In some instances this leads to a masking of important spectroscopic information. For this reason, magnetic circular dichroism (MCD) spectroscopy has often been utilized in the study of heme-containing proteins.

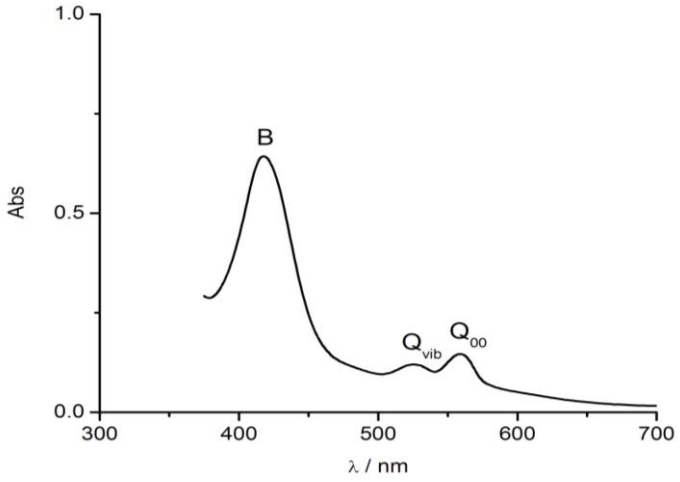

Figure 2-4 UV-visible absorption spectrum of ferrous heme with pyridine axial ligands. Shown is the B (Soret) band and the two Q bands (Q_{vib} and Q_{00}).

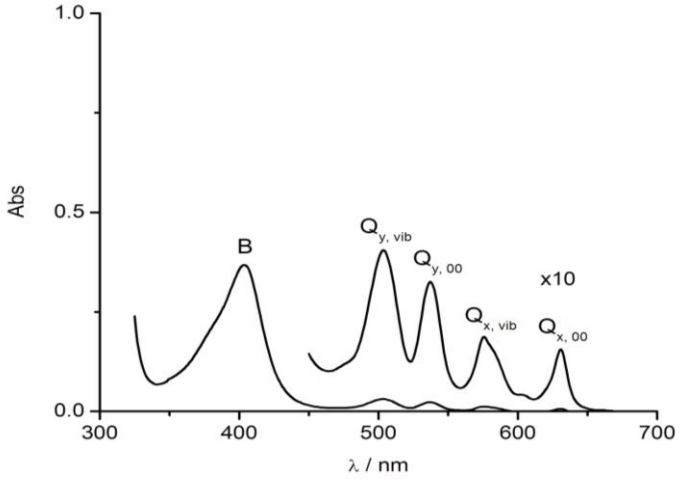

Figure 2-5 UV-visible absorption spectrum of PPIX-dimethyl ester in 2-butanone. Due to the decrease in symmetry from D_{4h} to D_{2h} from the loss of the central iron, the double degenerate orbitals split and now four Q bands ($Q_{y, vib}$, $Q_{x, vib}$, $Q_{y, 00}$, $Q_{x, 00}$) are now visible.

2.6 Magnetic circular dichroism (MCD) spectroscopy

2.6.1 Introduction to MCD spectroscopy

Magnetic circular dichroism (MCD) spectroscopy developed from magnetic optical rotary dispersion (MORD) spectroscopy, a measure of the variation in the optical rotation of a substance with a change in the wavelength of plane polarized light [9]. The change to MCD

spectroscopy was slow partly because it was easier to measure ORD and MORD spectra than CD and MCD spectra. However, the great value of the CD spectrum in structural analysis of both biomolecules and chiral inorganic complexes accelerated the switch as new instruments became available in the late 1960's [10]. The MCD spectrum also was easier to work with because of the direct connection of the MCD signal morphology and magnitude with readily computed state to state transition properties. This is because the group theory of the 1960's provided an interpretation of the sign and estimate of the relative magnitudes of particularly, transition metal complexes then being studied [11].

The instrumental difficulties in measuring CD spectra were greatly reduced with the development of the acousto-optic modulator that allowed measurement in all regions of the optical spectrum, through the use of different stress materials. As the Faraday Effect measured in the MCD experiment occurs for all optical transitions it has been applied with great success from the X-ray region using synchrotron radiation down in energy to the IR region. A number of designs of CD machines have been introduced and all will work with the magnet required for the MCD experiment.

Although the MCD experiment uses a CD machine, there is no connection between the phenomena of circular dichroism and of magnetic circular dichroism and both the MCD and CD spectral data of a sample are obtained simultaneously. For the MCD spectrum, the CD spectrum in the region of interest must be subtracted. Natural CD intensity requires a molecular environment where molecular structure features distribute electric charge in a spatial array that has helical "handedness." MCD intensity is due to interaction of the external field with electronic structure within the sample, no matter how it is distributed. This is a universal property of light absorption for all matter when placed in a magnetic field. A chiral molecular structure is not a requirement for MCD intensity [12].

The MCD spectra of many different porphyrinoids were measured from the very first days of MORD and MCD spectroscopy [13]. This is because the remarkably high value of the angular momentum in S_1 (commonly called the Q band) in the visible region meant that strong signals were obtained readily in all instruments. This characteristic and intense MCD spectrum of porphyrins allowed heme proteins to be studied. As a consequence, there is a rich and deep literature of MCD spectra from a very wide range of both synthetic and natural porphyrins [5, 6, 14-21].

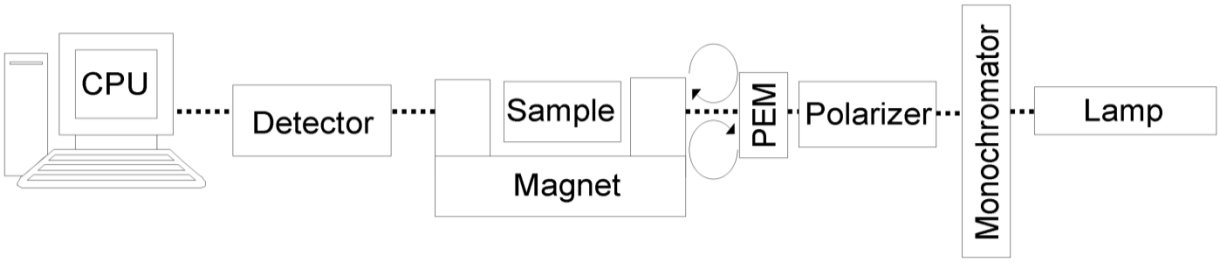

Figure 2-6 Simplified sketch of an MCD spectrometer based on a CD spectrometer using a traditional single beam approach. Reprinted with permission from [22]. Copyright 2011 World Scientific.

Figure 2-6 shows a simplified sketch of the instrument design used for MCD spectroscopy. When measuring MCD spectra it is required that the sample be placed in a strong magnet with field orientation of the magnet field vector (B) along the +z coordination direction, parallel to the light. Typical instruments can measure absorption as well as the MCD (or CD in the absence of the magnetic field) spectra simultaneously for a sample. However, other arrangements use a separate higher-powered spectrometer to measure absorbance in order to obtain better data. In the arrangement shown in Figure 2-6, a plane polarized, monochromatic light is passed through a photoelastic modulator (PEM) which converts the light to alternating left circular polarized (lcp) and right circular polarized (rcp) light. This polarized and monochromatic light will pass through a sample which is situated in the magnet and then to a detector which is normally a photomultiplier tube (PMT) for the UV-visible region [12]. Because of the use of highly polarized light for measurements, the cuvettes used must be strain free.

The measured intensity is $\Delta A_{l\text{-}r}$, where A is the absorbance of the lcp (-) or rcp (+). The $\Delta A_{l\text{-}r}$ for MCD spectrum results from a magnetic perturbation (the Zeeman effect) of the states involved in optical transitions responsible for light absorption. $\Delta A_{l\text{-}r}$ will be negative if A_r is greater than A_l. Typically older MCD data may be reported as ellipticity, Θ_M (deg T^{-1}) or molar ellipticities, $[\Theta]_M$ (deg dL $mol^{-1}dm^{-1}T^{-1}$). However, current studies use differential molar absorptivities $\Delta\varepsilon = \Delta A_{l\text{-}r}/(cl)$, where c is the sample molar concentration and l is the path length in centimeters. For MCD data, $\Delta\varepsilon$ is normalized for the magnetic field B in Tesla and written as: $\Delta\varepsilon_M$. Older MCD data are normalized to Gauss. It should be noted that the older units do not change the shape of the spectral features or affect the qualitative interpretation but when comparing quantitatively old data with new data, one must take care to ensure compatible units

of field and path length. The relations between Θ, $[\Theta]_M$, ΔA and $\Delta\varepsilon_M$ are shown by the following equations:

Equations 2-4: Conversion of measured MCD spectroscopy units:

$$\text{CD: } \Theta = 32.982 \cdot \Delta A_{l\text{-}r} \tag{2}$$

(Θ in deg; but note that many instruments the intensity is reported in mdeg (10^{-3}deg) units)

$$\text{MCD: } \Theta/B = 32.982 \cdot \Delta A_{(l\text{-}r)}/B \tag{3}$$

$$\text{MCD: } \frac{[\Theta]_M}{B/10^4 \text{Gauss}} = \frac{3298.2\Delta\varepsilon_M}{\text{B/Tesla}} \tag{4}$$

Analysis of MCD spectroscopic data reveals that the MCD bands lie at the same energy and have the same approximate band width as the corresponding absorption bands. It is important to note that in MCD spectroscopy band morphology assignment is straightforward if the band resolution is sufficient to separate other transitions by energies greater than their bandwidths; overlapping transitions and congestion lead to more complicated spectra. MCD spectra consist of 3 specific band morphologies (or terms), which come from the magnetically induced state splitting ($\mathcal{A}_1$ and $\mathcal{C}_0$) or coupling ($\mathcal{B}_0$) [5, 6, 23].

2.6.2 The major spectroscopic features: The Faraday $\mathcal{A}_1$, $\mathcal{B}_0$ and $\mathcal{C}_0$ terms

The MCD spectral intensity at any wavelength, ΔA_{l-r}, can be described in terms of the combined intensities of three components, each arising from different phenomena:

$$\Delta A_{l-r} = 152.5Bcl[\mathcal{A}_1(-df(\varepsilon) / d\varepsilon) + (\mathcal{B}_0 + \mathcal{C}_0 / kT)f(\varepsilon)] \tag{5}$$

where B is the field strength in Tesla, c is the concentration (mol L^{-1}) and l, the path length (cm). The normalized band shape f(ε) is usually a Gaussian−shaped curve and df(ε) is the derivative of this band envelope. The three Faraday terms, $\mathcal{A}_1$, $\mathcal{B}_0$ and $\mathcal{C}_0$ each arise from different transitions as shown Figure 2-7 [5, 6].

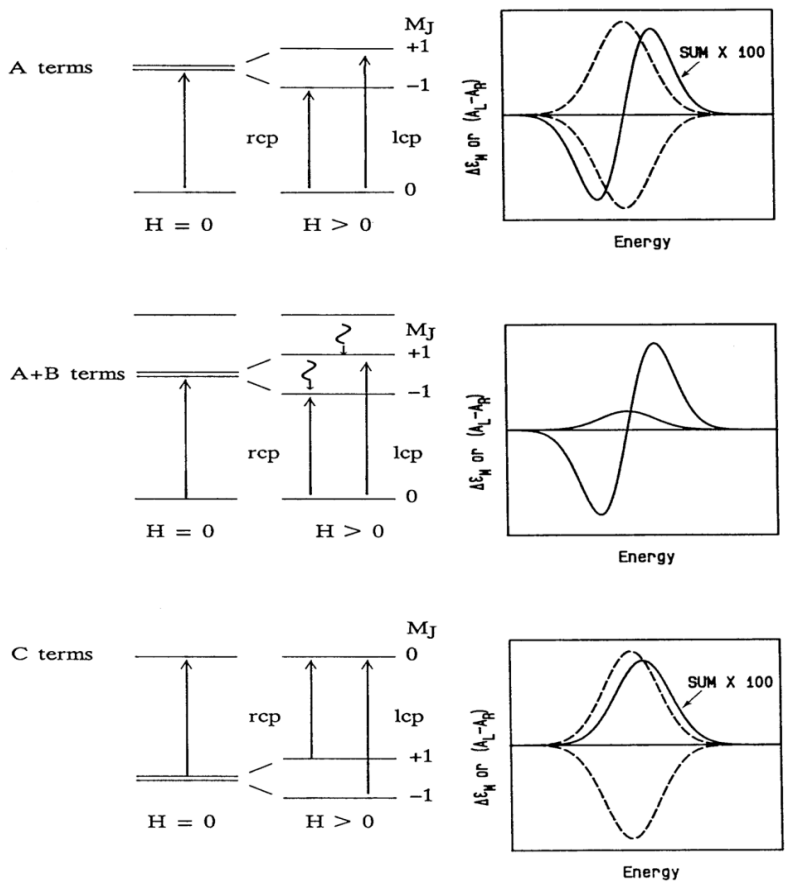

Figure 2-7 Three Faraday Terms ($\mathcal{A}_1$, $\mathcal{B}_0$ and $\mathcal{C}_0$) are the basis of the band envelope measured in MCD spectroscopy. All transitions occur from a ground state but the difference in the spectroscopic band envelopes arises from whether the ground state and/or excited state are degenerate, which is a result of the degree of symmetry in the measured complex.

Since $\mathcal{A}_1$ terms arise from the splitting of degenerate excited states, they are a common and a very useful feature in assigning the spectra of porphyrins and phthalocyanines. Indeed, many of the earliest published MCD spectral data were from the porphyrinoids simply because the $\mathcal{A}_1$ terms dominated the spectrum and were relatively easy to measure [7]. This will be the case for low spin ferrous heme [24]. With a non-degenerate ground state, $\mathcal{A}_1$ terms are temperature independent, as such are studied using room temperature experiments as the only advantage of low temperatures is to sharpen the band envelope.

From Figure 2-7, $\mathcal{A}_1$ and $\mathcal{C}_0$ terms can only be observed in the spectra of high symmetry complexes where the ground and/or excited states are orbitally degenerate. The

derivative−shaped Faraday $\mathcal{A}_1$ term is temperature independent and identifies degenerate excited states when the intensity cross-over point ($\Delta A = 0$) aligns with the absorption band maximum in the absence of strong $\mathcal{B}_0$ terms. This spectroscopic feature is the most useful assignment criterion from MCD spectra of porphyrinoids essentially providing polarized spectra from solutions rather than the previous requirement for a good quality crystal in MORD spectroscopy. In addition, for porphyrinoids the ratio $\mathcal{A}_1/\mathcal{D}_0$, $\mathcal{D}_0$ is the dipole moment, easily and directly provides the difference in the angular momentum between the ground and excited states which is related to the excited g-factor [9]. In this way we have an equivalent parameter to the ground state g-factor of paramagnetic species obtained directly from the EPR spectrum. Although an accurate estimation of the ratio $\mathcal{A}_1/\mathcal{D}_0$ requires good band fitting or integration via the Method of Moments, 'back of envelope' calculations based on the peak-trough magnitude and the absorptivity read from the absorption spectrum can give very good approximations [25]. Since, in general for aromatic organic compounds, the angular momentum of the HOMO is less than that of the LUMO, the equation for $\mathcal{A}_1$ will always return a positive value. For example, $\mathcal{A}_1$ terms observed in the spectrum of an aromatic compound are expected to be 'positive'. The negative lobe of the derivative shaped envelope is observed to the low energy side of the cross-over point.

The reduction in symmetry leads to differential splitting of the previously-degenerate ground and excited states. When the degenerate LUMO pair splits to a greater extent than the HOMO pair, then negative $\mathcal{A}_1$ terms may be measured. As a follow up, while the $\mathcal{D}_0$ magnitude might be very small (in the porphyrinoids we can expect close to zero) $\mathcal{A}_1/\mathcal{D}_0$ still retains the value of the nominally forbidden state. However, if there is appreciable geometry-induced splitting of both HOMO and LUMO molecular orbital pairs, $\mathcal{A}_1$ may actually approach zero. The relatively new reports of these spectroscopic signatures have great value in the interpretation of the optical data with respect to the geometry and electronic structure of specific porphyrinoids.

The Gaussian−shaped $\mathcal{C}_0$ term is highly temperature dependent and identifies an orbitally-degenerate ground state. Since the $\mathcal{C}_0$ term arises from a field-split degenerate ground state, its intensity changes dramatically with temperature. According to the Boltzman distribution, these levels are relatively equally occupied at room temperature. The overall result is that the split states cancel one another out, producing a weak signal. However upon reducing the temperature, using liquid nitrogen or liquid helium, the lower ground state becomes more highly populated, resulting in the temperature dependence of $\mathcal{C}_0$ terms. Variable temperature and variable field

experiments can therefore be used to identify and quantify $\mathcal{C}_0$ terms. The temperature range of <4.2 - 100 K is the most useful in terms of analysis because of the effect of 1/kT in the $\mathcal{C}_0$ term intensity above. The MCD spectra of heme proteins are dominated by $\mathcal{C}_0$ terms. However, because the excited states are also degenerate, the room temperature MCD spectra may exhibit $\mathcal{A}_1$-like spectra, pseudo $\mathcal{A}_1$ terms [9].

Complicating the spectral analysis is the appearance of the temperature independent Faraday $\mathcal{B}_0$ terms, which exhibit a Gaussian shape of either sign. For symmetric porphyrinoids the intensity of $\mathcal{B}_0$ terms is usually significantly less than either the $\mathcal{A}_1$ or $\mathcal{C}_0$ terms. $\mathcal{B}_0$ terms are observed for all transitions resulting, as can be seen from the equations above, from magnetically-induced mixing of states with appropriate symmetry [9]. The ΔE parameter between these excited states is important in determining the magnitude of the dominant $\mathcal{B}_0$ terms in the MCD spectra of porphyrinoids, as we shall see below. $\mathcal{B}_0$ terms arising from a mixing of excited states are predominant in molecules with low symmetry, such as D_{2h} (rectangular), the free bases of protoporphyrin IX or phthalocyanine. As we see above, the field induced mixing of the excited states will result in a preference to proportionally absorb more of either left or right handed circularly polarized light, depending on the nature of the mixed states. Like $\mathcal{A}_1$ terms, $\mathcal{B}_0$ terms are also temperature independent due to the non-degenerate ground state.

Another important feature of the MCD spectra of porphyrins and phthalocyanines (including, heme proteins) is the appearance of pseudo-$\mathcal{A}_1$ terms, which may be seen when two, oppositely-signed $\mathcal{B}_0$ or $\mathcal{C}_0$ terms exist closely in energy. Pseudo-$\mathcal{A}_1$ terms may be of either sign. For diamagnetic porphyrins $\mathcal{A}_1$-term like spectral envelopes are frequently measured where the symmetry of the ring is lower than D_{4h} and the degenerate excited states are split to some extent.

2.6.3 Connection between the optical spectra of porphyrinoids and MCD spectral properties

It has been noted that the porphyrin absorption spectrum is remarkably consistent: usually a strong absorption band near 400 nm and another weaker band near 600 nm. Closer observation however shows many differences between the spectra of the different porphyrinoids, particularly between symmetric porphyrins, peripherally substituted porphyrins and methylene-bridge substituted porphyrins. In addition, other major complications in the spectrum arise from

interactions with the central metal, primarily metal-ligand or ligand-metal charge transfer, and the vibronic bands associated with the formally-forbidden Q band.

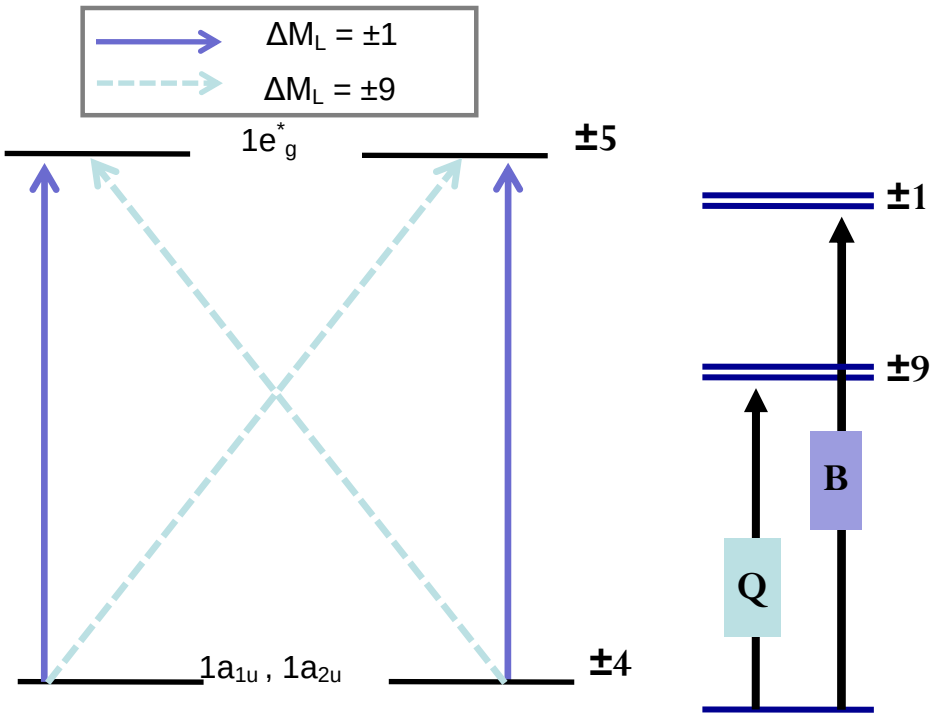

Figure 2-8 Summary of Gouterman's 4 orbital Linear Combination of Atomic Orbital (LCAO) model. The HOMO to LUMO transitions occur between the states with ±4 to ±5 units of angular momentum (M_L). Transitions between the HOMO and LUMO gives rise to the B and Q bands. The B band corresponds to a change in angular momentum (ΔM_L) of ±1 and is an allowed transition and, therefore, very intense. The lower energy Q band corresponds to a change in angular momentum of ΔM_L ±9 and is, therefore, forbidden. As the selection rules for absorption include $\Delta M_L = \pm 1$, it can be predicted that the Q bands should be forbidden [6].

The model shown in Figure 2-8 summarizes the features important to MCD spectral measurements from Gouterman's 4-orbital model, namely that the angular momentum in the Q and B states (S_1 and S_2 respectively) have very different, but generally positive, nonzero magnitudes. We can then predict that the MCD spectrum will exhibit two or more positive $\mathcal{A}_1$ terms with $\mathcal{A}_1/\mathcal{D}_0$ magnitudes that could differ by a factor of up to 9. Gouterman and his group were very successful using the theoretical capabilities of the 1960's (primarily Intermediate Neglect of Differential Overlap (INDO)) to predict many of the optical spectroscopic properties of porphyrinoids [26]. This was a remarkable discovery in view of the complexity of these-many

electron molecules. As has been commented on by many authors, the reason that these old techniques worked so well was that the optical spectrum is actually dominated by the Hückel Rule. In effect the top two electron pairs are wonderfully stable and for MCD measurements, it is the value of the ratio $\mathcal{A}_1/\mathcal{D}_0$ that becomes most important. The magnitude of $\mathcal{A}_1$ is related to the magnetic moment of the excited state; however, as is clear in the formal equation, it is the difference between the orbital angular momentum of the ground and excited states that is measured in the MCD spectrum.

A sample absorption and MCD spectrum, Figure 2-9, for the pseudo-D_{4h} symmetric Zn(II)-protoporphyrin IX or Zn(II)-PPIX in MeOH shows the similar properties and optical origin of the bands in the porphyrin ring. The use of zinc as a comparative model is well established [6] as suitable for determining the ring-based components of porphyrin spectroscopy. The filled 3d shell of Zn(II)-PPIX prevents the large number of charge transfer bands which are evident when looking at ferric heme and ferric heme binding proteins. Therefore, the B and Q bands can be readily identified. Figure 2-8, predicts that the Q band will be formally forbidden because of the selection rule that restricts absorption transitions to $\Delta M_J = \pm 1$. At this level, transitions to the B or Soret band are predicted to be fully allowed with a positive MCD $\mathcal{A}_1$ term. The electronic structure for Zn(II)-PPIX is shown in Figure 2-10. Of interest in the calculation of this electronic structure is that the HOMO (162 and 163) and LUMO (164 and 165) are essentially degenerate, and all orbital contributions come from the $18e^-$ conjugated π system on the PPIX ring. As many have shown previously, it is the accidental degeneracy of the HOMO pair of orbitals that results in the quenching of the oscillator strength of the Q band [6, 26].

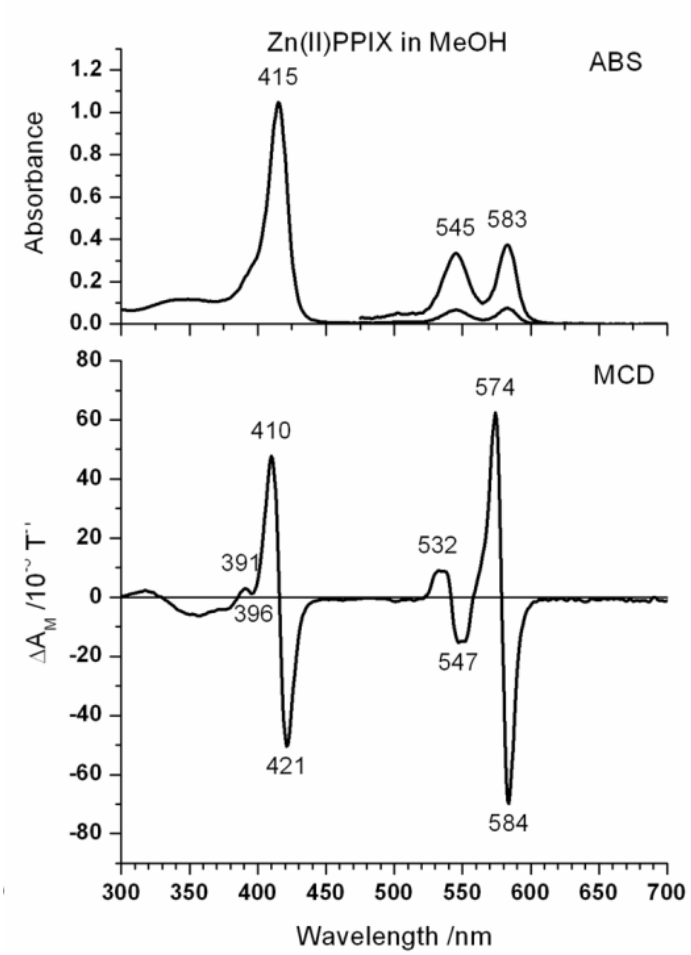

Figure 2-9 UV-visible absorption and MCD spectra Zn(II)-protoporphyrin IX (Zn(II)-PPIX). Zn(II)-PPIX in MeOH, B-band at 415 nm, Q_{vib} at 545 nm and Q_{00} at 583 nm. The MCD spectrum of Zn(II)-PPIX show pseudo A-terms centered on the B, Q_{vib} and Q_{00} bands. Reprinted with permission [27]. Copyright 2012 ACS Publications.

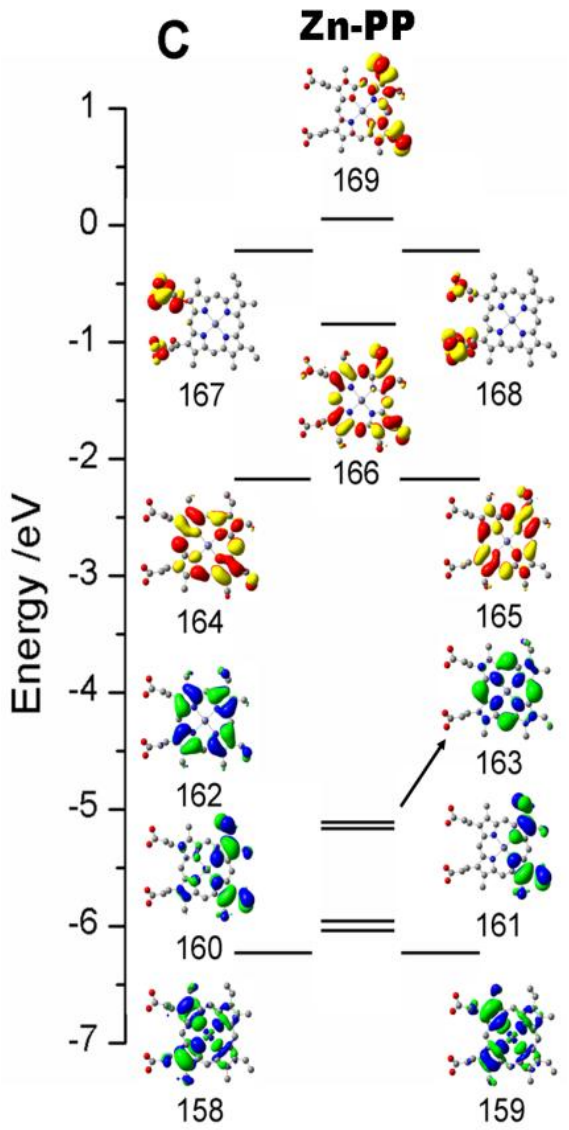

Figure 2-10 Energy level diagram for Zn(II)-PPIX. Shown are the energies and molecular orbital surfaces for the top five occupied MOs (green and blue phases) and the lowest five unoccupied MOs (red and yellow phases). Hydrogen atoms have been omitted from structures for clarity. The lowest shown molecular orbital for Zn(II)-PPIX is HOMO-5 at 158. Reprinted with permission [27]. Copyright 2012 ACS Publications.

2.6.4 Heme protein MCD spectra

In the last part of this MCD section, the focus will be on the application of MCD spectroscopy to the identification of amino acid heme binding ligands in heme proteins. This technique uses the exquisite fingerprinting information provided for a large number of heme binding proteins. The MCD spectrum is more useful than the absorption spectrum for this purpose because the

angular momentum of the π-π* and charge transfer transitions that together make up the absorption spectrum in the 300 – 800 nm region is highly dependent on the complexity of the electronic state structure. Coupling and mixing between these states results in a unique set of optical transitions, which are overlaid by the vibronic bands of the π-π* system. From the MCD spectral data for a protein it is possible to extract very accurate and detailed information about the heme environment and even elucidate the identity of the heme binding ligands. These studies are perhaps the most important of any using the MCD technique because of the exquisite fingerprinting information provided for a very wide range of proteins to characterize the heme binding ligands in many novel heme enzymes.

Heme proteins typically bind one molecule of Fe(III)-protoporphyrin IX (Fe(III)-PPIX). Fe(III)-PPIXs like other porphyrinoids have unique MCD spectral bands. There are two important π-π* transitions in hemes: the intense B band, often referred to as the Soret band, and the Q_{00} or α and the corresponding vibronic Q_{vib} band. The B band lies between 380 and 430 nm, with Q_{00} and the vibronic Q_{vib} bands, between 450 and 650 nm [5]. The complexity in the visible region spectra of porphyrins arises from the intensity-allowing mechanisms of the Q_{00} band, which is formally forbidden (especially when the two highest occupied molecular orbitals are accidentally degenerate) [6] and the overlap of the B, Q_{00} and Q_{vib} bands with metal-to-ligand (MLCT) and/or ligand-to-metal (LMCT) charge transfer bands between the iron center and the porphyrin ring. These greatly complicate the observed spectra however, as we will show below, the MCD spectrum provides significantly enhanced resolution of the individual transitions responsible for the overall, absorption band envelope and in doing so provides fingerprints sensitive to the heme environment [7]. Typically for heme binding proteins a scan between 250-800 nm will include all the necessary spectral features.

2.6.5 Elucidation of Heme-Binding Ligands

In a heme-protein, one or two amino acids bind the heme iron. Heme binding amino acid ligand identification can be achieved by probing the heme site with ligands (eg. CN^-, CO) and changing the heme-iron oxidation states. Anionic ligands bind to ferric hemes closely following the Spectrochemical Series with stronger field ligands displacing weaker-field ligands if the 5^{th} or 6^{th} positions are vacant and if there is spacial access in the protein. Axial coordination of the ferric heme in proteins with the 6^{th} position accessible (for example, in myoglobin (5 coordinate

with a histidine binding ligand), rather than in cytochrome c, (6 coordinate with a histidine and methionine binding ligand), Figure 2-11) is possible across the entire range of the Spectrochemical Series, starting with the very low Δ_{OCT} values of the halides and extending to the strong field ligand cyanide.

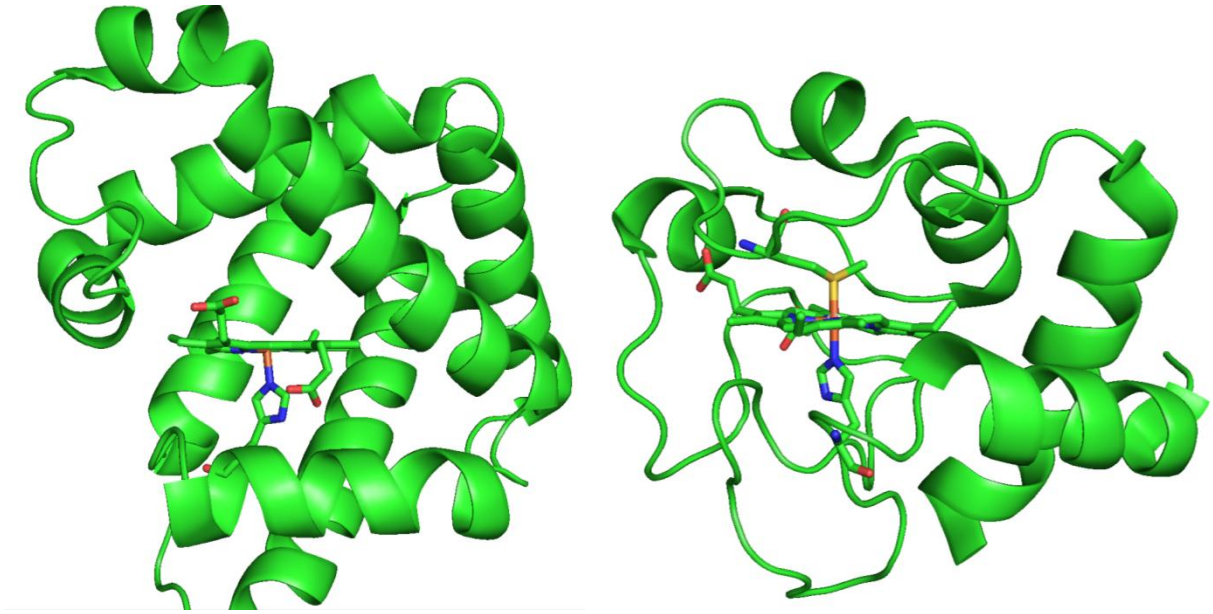

Figure 2-11 Cartoon protein structure of human myoglobin (left) and horse heart cytochrome C (right). Myoglobin (2W6W) has 5 coordinate heme with a histidine amino acid binding ligand. Cytochrome C (1HRC) has a 6 coordiante heme with a histidine and methionine amino acid binding ligands.

Ligation by anionic ligands such as cyanide is thermodynamically preferred and takes place with strong binding constants. Strong field ligands such as cyanide systematically force a change from high or intermediate to low spin if the existing ligand is a weaker field ligand. Spectral data for several heme proteins have been studied at both room temperature and helium temperatures, for example, myoglobin [28]. It is also well established that reduction to the ferrous heme is possible in many cases resulting in a characteristic MCD spectrum of the 5-coordinate iron. Addition of CO results in a major change in the MCD spectrum as the low spin, 6-coordinate iron usually forms. Together, these straightforward, chemically-induced changes provide definitive information about the electronic properties of the iron in the native, heme-containing protein. More subtle information about the identity/identities of the axial ligands comes from the relative intensities and band maxima of all bands in the MCD spectrum using fingerprinting from previously well-studied and characterized heme proteins [29-33]. Typically

the native protein is measured first then followed by addition of excess CN^-. Addition of a reducing agent such as sodium dithionite and a strong axial ligand, such as CO, can be used to probe the reduced state. The advantage of this type of ligand identification is that a single solution can be used and is much easier than protein mutation analysis. The main advantage of this technique stems from the fact that most heme-binding amino acids are common among many protein systems so many fingerprint spectra exist. Also, through this method, the native oxidation and spin state of the heme-iron are identified as well as the protein heme binding ligands. Where this technique starts to falter is when uncommon ligands are part of the heme binding site and comparative fingerprint spectra have not been previously reported. It is well established that all the band parameters change as a function of the protein environment of the heme. The spectral changes arise largely as a result of changes that take place at or near the iron, because charge transfer bands between the metal and the ring overlay the π to π^* bands of the porphyrin ring. These bands change in number, wavelength and intensity depending on the oxidation state (ferrous, ferric, ferryl) and spin state (low, intermediate, high) of the iron, and the axial ligands of the iron control the spin.

2.6.6 MCD spectral applications

The key to the interpretation of the MCD spectral data of complicated electronic systems is that the observed MCD bands lie at the same energy and exhibit approximately the same bandwidth as the absorption bands [5]. The absorption and MCD spectral data are very sensitive to the nature of the two axial ligands of the heme-iron, and to the heme-iron oxidation and spin state. These properties have such profound spectral effects that the key features in the observed MCD envelope morphology (sign, relative magnitude, and band wavelength maxima) systematically change for a range of heme proteins allowing 'fingerprinting' of the properties of a novel protein with those well-studied. In this manner, the identity of the two axial ligands (the proximal 5^{th} position, and the distal 6^{th} position), the oxidation state of the iron and its spin state, may be determined with considerable confidence for heme binding proteins directly from dilute solutions at room temperature.

However, an important point should be noted. This technique should be used in combination with electrospray mass spectrometry data in order to determine the number of bound heme molecules. If more than one heme is bound to the protein then the MCD spectra will be much

more complicated to analyze. Also, the stability and purity of solutions of the protein must be established. Mixtures of bound heme and free heme will also complicate the analysis. Finally, mixtures of oxidation states, spin states and ligation number will also render analysis unreliable. Despite the apparent complexity of the heme system, the MCD spectral bands are diagnostic of the axial ligand identity, spin state and oxidation state allowing in many cases unambiguous determination of each of these parameters. This diagnostic sensitivity has been used widely and successfully to interrogate the spin, oxidation and ligation state of the heme in a wide range of heme proteins, for example [24, 28, 33-40]. The MCD spectral data offer species identification far superior to that from the absorption spectroscopic data alone.

2.6.7 MCD spectral measurements

Protein solutions were prepared in a 10 mM PBS buffer at pH 7.4. Individual sample concentrations were calculated by UV-visible absorption spectroscopy before mixing and performing experiments. MCD measurements at room temperature were made in 1 cm cuvettes at 5.5 T in an Oxford Instruments SM2 superconducting magnet, aligned in a J-820 CD spectrometer (Jasco Inc, Japan). The stepped data pitch was 1 nm and the response time was 1 sec. Absorption measurements were made using a Cary 500 (Varian, Canada). All solutions were measured in the Cary 500 before and after being measured in the MCD spectrometer to ensure no changes were observed during experimentation.

2.7 Electrospray ionization mass spectrometry (ESI-MS)

2.7.1 Introduction to ESI-MS spectrometry

Mass spectrometry has become a widely used tool in both academic fields and industry due to its ability to identify, through mass analysis, different components in suitable mixed solutions [41, 42]. The application of ESI-MS to large biological molecules was initially developed by John B. Fenn, who was awarded the 2002 Nobel Prize in Chemistry for his contributions to this field [43, 44]. All mass spectrometers include the same basic components: a sample inlet, an ion source, a mass analyzer, a detector, a data system that outputs mass spectra, and a vacuum system [45, 46]. Mass spectrometry analysis involves the conversion of analyte molecules into gas-phase ionic species, the separation of these molecular ions based on their mass-to-charge ratio (m/z), the detection of the ions, and finally, the display of the mass spectrum [45, 46].

There are various methods to ionize molecules, which may be grouped into two categories [45, 46]. So called "hard" ionization methods like electron ionization (EI) often induce fragmentation of the parent molecule upon ionization while "soft" ionization methods like matrix-assisted laser desorption ionization (MALDI) and ESI induce little, or no, fragmentation of the parent molecule. Soft ionization is ideal for larger molecules, particularly proteins. While fragmentation may be useful for the identification of macromolecules like proteins, ionization of intact macromolecules allows for the study of inter- and intra-molecular interactions such as metalation to complexes. This important feature is exploited throughout this thesis and hence the focus of this section will be on the ESI technique as all the experiments that will be described involve the use of an ESI mass spectrometer.

2.7.2 Sample ionization and detection

In ESI-MS, the sample flowing through a capillary is dispersed into very small droplets through the use of high positive or negative voltages applied to the capillary tip, Figure 2-12. Figure 2-12A shows the "Z-spray" configuration for the ESI source in the Micromass LCT mass spectrometer system (Waters Micromass Inc., Canada) used for all the experiments described in this thesis unless otherwise stated. The sample solution is infused through a metal capillary that has an applied electric potential of +3-5kV. This produces an electrostatic field that disperses the solution into a fine mist of highly charged droplets [45]. Based on the "Charge Residue Model", these charged droplets undergo desolvation and fission until eventually the droplet contains only a single solute molecule [45]. Evaporation of the droplets is assisted by the flow of a hot nitrogen desolvation gas. The solvated ions undergo low energy collisions with the cone gas to remove the remaining solvent before being focused through a hexapole ion bridge and then immediately transferred into the high vacuum chamber of the mass analyzer [45].

Depending on the polarity of the voltage, droplets with excess positive or negative charge are formed. Desolvated, charged protein molecules, Figure 2-12B, then enter the mass analyzer and are ultimately measured at the detector [41]. One of the most common mass analyzers, and the type used to measure the data presented here, is a time of flight (TOF) analyzer, Figure 2-12C. TOF analyzers use an electric field (pusher) to move charged sample molecules within the analyzer. The principle is that light, highly charged molecules will travel faster than heavy molecules possessing few charges. Sample ions are timed between a shutter and the detector.

Measured by the instrument is the mass to charge ratio (*m/z*). The *m/z* ratio is then plotted against the relative intensities of all ions detected to produce a mass spectrum.

The mass spectrum displays a nearly Gaussian distribution of charge states with *m/z* values that are dependent on the number of charging species attached. Typically, protons are the charging species, thus the resulting charge state can be represented by $[M + nH]^{n+}$ where M stands for the molecular ion [45]. Possibly the greatest disadvantage of ESI is the technique's poor tolerance of salts like NaCl, which form adducts with the molecular ions and suppress signal-to-noise ratios of the molecular ions.

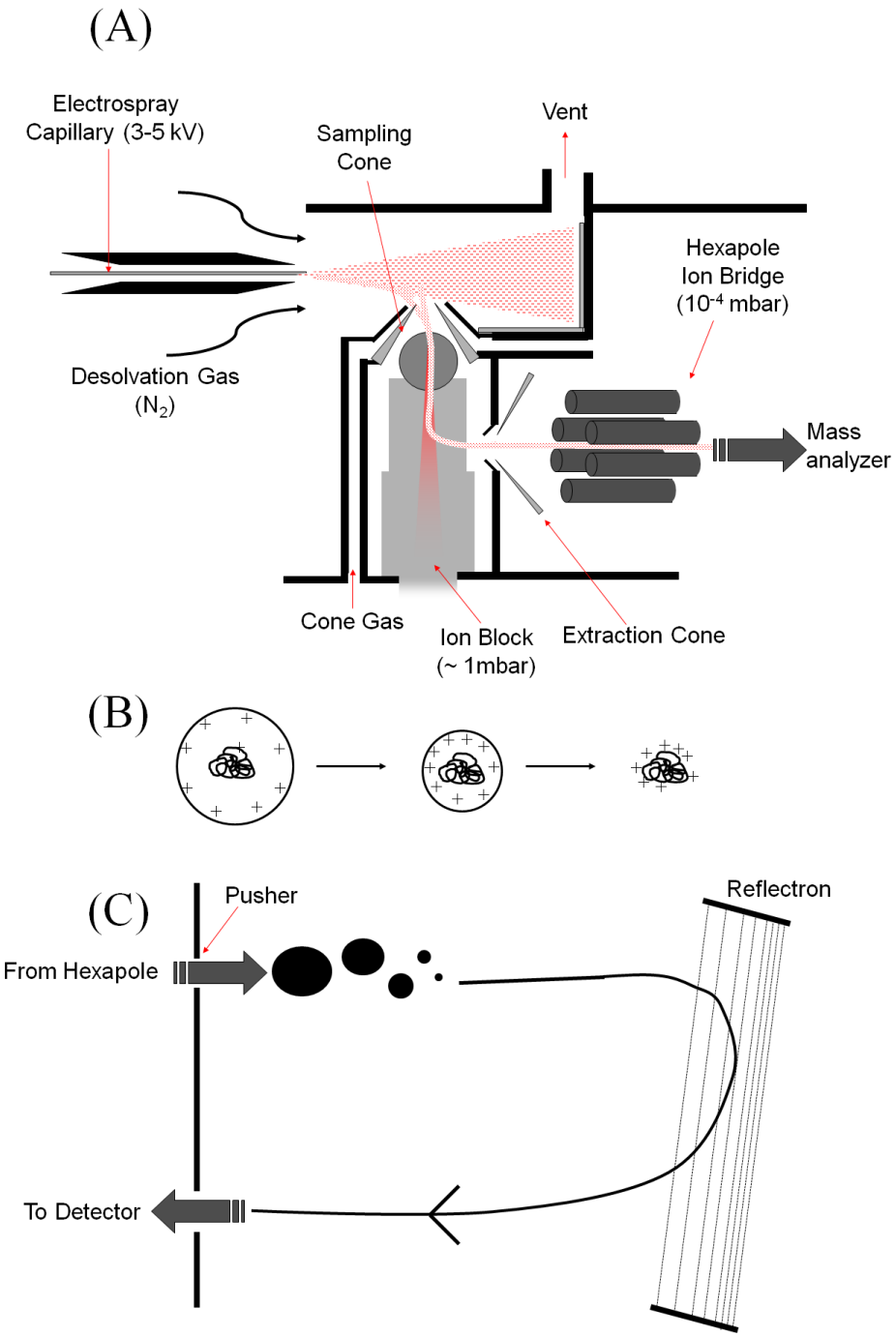

Figure 2-12 Schematic overview of electrospray ionization mass spectrometry machinery and formation of charged protein molecules. A) Schematic diagram of an electrospray ionization source B) charge residue model illustrating the formation of charged, gas phase protein molecules C) schematic diagram of a time of flight (TOF) mass analyzer.

2.7.3 Application of ESI-MS to heme proteins

Either negatively or positively charged analyte molecules can be produced at the ionization source and then detected by the instrument. All of the spectra presented in this thesis were recorded in positive ion mode, which is the common method for studying proteins. Nucleic acids on the other hand are commonly studied in negative ion mode due to the presence of numerous phosphate groups in a polynucleotide backbone [41]. In protein mass spectrometry, sample ions arise from the protonation of basic amino acid residues (lysine and arginine) or deprotonation of acidic residues (aspartic acid and glutamic acid). Depending on the number of exposed acidic/basic residues, the amount of charge on a protein molecule can vary, producing a number of charge states, Figure 2-13, unlike MALDI which typically produces analyte molecules with a single charge [47, 48]. This allows ESI-MS to be used to monitor the extent of folding of a protein. The exposed residues will be protonated/deprotonated before those residues that are buried in the structure; so that if the structure changes for example, as a function of heme binding or denaturation, then the number of residues exposed will change. Denatured proteins will show higher charge states than the properly folded protein due to the increase in exposure of accessible sites, Figure 2-13D. An observation that the center of the charge state distribution shifts to higher numbers is strong evidence that the structure has become less folded or more open [41, 48, 49].

ESI-MS is also a powerful tool to determine the number of heme molecules a protein can bind. Although typically proteins only bind one heme, the ESI-MS data produce unambiguous stoichiometric measurement of heme binding. Typically, this is done through deconvolution of the charge state spectra. Deconvolution software uses a maximum entropy algorithm to combine charge state (m/z) values and calculate the most probable parent mass spectrum (mass). Since the apo-protein mass is known, an increase of 616 Da indicates heme binding. Therefore, it is possible to track heme binding stoichiometrically, as well as heme transfer in a mixture of proteins in solution.

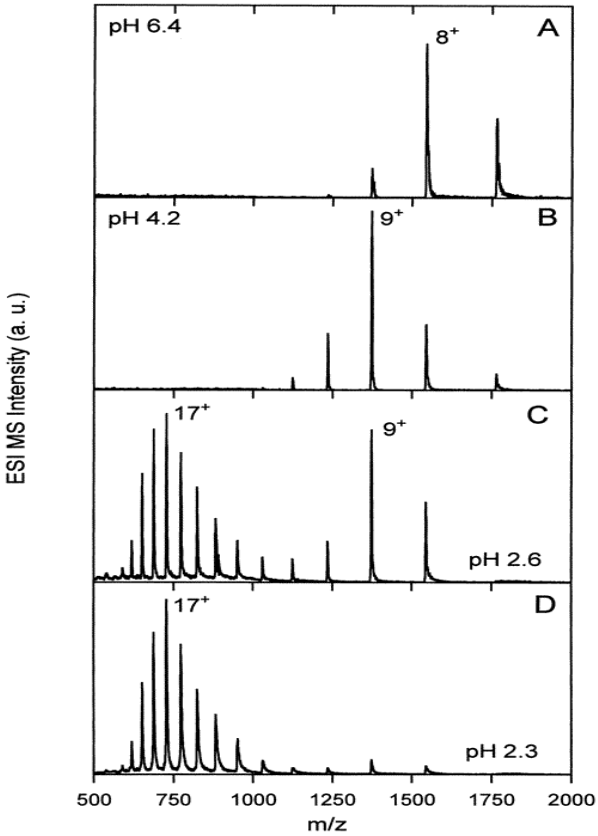

Figure 2-13 ESI mass spectra of cytochrome c at pH 6.4, pH 4.2, pH 2.6 and pH 2.3. As the pH of the solution is lowered, the protein becomes increasingly unfolded until complete unfolding at pH 2.3. Since more of this globular protein is solvent exposed upon unfolding, the charge states also increase from a maxima +8 at pH 6.4 to +17 at pH 2.3. Reprinted with permission [47]. Copyright 1997 American Chemical Society Publications.

2.7.4 Quantification of ESI-MS charge state spectra

ESI-MS charge state spectra are not directly quantifiable from the measured intensity directly. This is due to machine sensitivity to settings such as sample flow rate and ion suppression due to other samples or salts [41, 46]. However, since globular heme binding proteins, specifically the Isd proteins, have similar heme-bound (holo) and heme-free (apo) charge states [50], it can be assumed that the flying efficiency, similar to ε in absorption spectroscopy, of the proteins is the same for apo/holo pairs. Therefore, the concentrations of proteins can be calculated from the relative apo/holo pairs of Isd proteins if the starting concentration of proteins is known.

2.7.5 ESI-MS Sample Preparation (Desalting) and Measurements

Protein solutions were concentrated, desalted and buffer exchanged from 10 mM PBS buffer pH 7.4 to 20 mM ammonium formate pH 7.4 using Millipore Amicon ultra-4 centrifuge filter units (10 kDa MWCO) with a Beckman CS-6 swinging-bucket Centrifuge (3000 rpm for 10 minutes per run). Once thoroughly desalted, the protein concentrations were calculated using UV-visible absorption spectroscopy. The parameters used on the Micromass LCT mass spectrometer system (Waters Micromass Inc., Canada) are shown in Table 2-3.

Table 2-3: Micromass LCT ESI-MS settings used to measure Isd protein reactions

Setting	Value
Capillary	2800-3000 V
Sample Cone	23-25 V
Extraction Cone	18-20 V
RF Lens	800-1000 V
Desolvation Temperature	20 ^{o}C
Source Temperature	80 ^{o}C
Sample Flow	5-15 $\mu L \cdot min^{-1}$
Spectra Scan Time	4 sec

2.8 Conclusion

The aim of this chapter was to explain the methods used in preparing recombinant Isd protein, making UV-visible absorption measurements, the MCD spectroscopy technique in porphyrinoid applications and finally, the methods used with ESI-MS to study proteins.

Recombinant protein production enables the user to produce high purity, apo-protein in high yield. This technique is invaluable due to the advantages over extraction from the natural system, bacterial *Staphylococcus aureus.* Expression plasmids in *E. coli* RP523 avoids safety concerns that would have to be taken into consideration when working with *S. aureus* and due to *E. coli* RP523 being a *hemB* mutant, apo-protein can be expressed and purified without using harsh chemical techniques to extract heme. Furthermore, His-tagged proteins allow for less isolation steps and high purity samples for analysis.

Although UV-visible absorption spectroscopy has been used extensively in the past for heme protein amino acid ligand binding elucidation studies, MCD spectroscopy is a far superior

technique as explained above. However, UV-visible absorption spectroscopy still provides a quick and accurate method to calculate protein concentration via the common 280 nm band shared by all proteins consisting of the aromatic amino acids phenylalanine, tyrosine, tryptophan and histidine, which all Isd proteins have. Furthermore, UV-visible analysis provides a second check of MCD spectral results since all MCD bands lie under absorption bands.

MCD spectroscopy is a very powerful technique and has unfortunately often been overlooked because a good understanding of theoretical description has been deemed necessary. The value of MCD spectroscopy comes from the information provided, which combines the absorption energy, the absorption oscillator strength, and the magnetic moments of the ground and excited states. Room temperature MCD spectroscopy proves to be a very useful tool when studying heme binding proteins. Not only can MCD spectra be used to identify the oxidation and spin-state of the heme iron through extensive fingerprinting libraries, but also the spectral envelopes can be used to identify the axial ligands involved in binding the heme-iron. This property was used to elucidate heme transfer and heme binding ligands in the Isd series of proteins. Typically when this technique is coupled with ESI-mass spectrometry a great deal of chemical information can be extracted from an *in vitro* biochemical system.

ESI-MS data provide unambiguous results for heme binding stoichiometry, relative protein folding and tracking heme transfer reactions. The power of the ESI-MS technique stems from the ability to distinguish between apo- and holo-proteins. UV-visible absorption and MCD spectroscopy are not able to do this unless a significant change in the absorption bands between proteins exist. The power of the ESI-MS technique shines when looking at complex mixtures of proteins where the technique is able to track heme transfer and concentrations of proteins in solution.

2.9 References

1. Guzman, L. M.; Belin, D.; Carson, M. J.; Beckwith, J., *J. Bacteriol.* **1995,** 177, 4121-1430.
2. Li, J. M.; Uamanoff, H.; Proenca, R.; Russel, C. S.; Cosloy, S. D., *J. Bacteriol.* **1988,** 170, 1021-1025.
3. Nienhaus, K.; Nienhaus, G. U., Probing Heme Protein-Ligand Interactions by UV/Visible Absorption Spectroscopy, Humana Press Inc.: Totowa, NJ, 1992; Vol. 305, 215-241.
4. Mathews, C. K.; vanHolde, K. E.; Ahern, K. G., Biochemistry, Benjamin Cummings: San Francisco, CA, 2000; Vol. 3, 202-203.

5. Mack, J.; Stillman, M. J.; Kobayashi, N., *Coord. Chem. Rev.* **2007,** 251, 429-453.
6. Mack, J.; Yoshiaki, A.; Kobayashi, N.; Stillman, M. J., *J. Am. Chem. Soc.* **2005,** 127, 17697-17711.
7. Mack, J.; Stillman, M. J., Handbook of Porphyrins and Related Macrocycles, Academic Press: New York, 2003; Vol. 16, 43-1113.
8. Yoshida, M.; Kinoshita, T.; Horie, S.; Shimazono, N., *Biochem.* **1965,** 58, 334-347.
9. Piepho, S. B.; Schatz, P. N., Group Theory in Spectroscopy, Wiley-Interscience: 1983.
10. Buckingham, A. D.; Stephens, P. J., *Annu. Rev. Phys. Chem.* **1966,** 17, 399-432.
11. McCaffery, A. J., *Science.* **1971,** 232, 137-140.
12. Mason, W. R., A Practical Guide to Magnetic Circular Dichroism Spectroscopy, Wiley-Interscience: 2007; 223.
13. Briat, B., D. In Electronic States of Inorganic Compounds: New Experimental Techniques, Reidel Publishing: Boston, 1974; Vol. 20.
14. Mack, J.; Kirby, S.; Ough, E. A.; Stillman, M. J., *Inorg. Chem.* **1992,** 31, 1717-1719.
15. Ough, E.; Gasyna, Z.; Stillman, M. J., *Inorg. Chem.* **1991,** 30, 2301-2310.
16. Mack, J.; Stillman, M. J., *J. Am. Chem. Soc* **1994,** 116, 1292-1304.
17. Mack, J.; Stillman, M. J., *J. Phys. Chem.* **1995,** 99, 7935-7945.
18. Williamson, B. E.; VanCott, T. C.; Boyle, M. E.; Misener, G. C.; Stillman, M. J.; Schatz, P. N., *J. Am. Chem. Soc.* **1992,** 114, 2412-2419.
19. Ough, E. A.; Stillman, M. J., *Inorg. Chem.* **1995,** 34, 4317-4325.
20. Mack, J.; Bunya, M.; Lansky, D.; Goldberg, D. P.; Kobayashi, N., *Heterocycles* **2008,** 76, 1369-1380.
21. Chidawanyika, W.; Mack, J.; Shimizu, S.; Kobayashi, N.; Nyokong, T., *J. Porphryins Phthalocyanines* **2009,** 13, 1053-1062.
22. Tiedemann, M. T.; Stillman, M. J., *J. Porphyrins Phthalocyanines.* **2011,** 15, 1134-1149.
23. Kobayashi, N.; Katsunori, N., *Chem. Commun.* **2007**, 40, 4077-4092.
24. Vickery, L.; Nozawa, T.; Sauer, K., *J. Am. Chem. Soc.* **1975,** 98, 343-350.
25. Stillman, M. J.; Thompson, A. J., *J. Chem. Soc. Faraday Trans. 2* **1974,** 98, 343-350.
26. Gouterman, M., Electronic Spectra, 1 ed.; Academic Press: New York, 1978-1979; Vol. 3.
27. Pinter, T. B. J.; Dodd, E. L.; Bohle, S.; Stillman, M. J., *Inorg. Chem.* **2012,** 51, 3743-3753.
28. Springall, J.; Stillman, M. J.; Thomson, A. J., *Biochim. Biophys. Acta* **1976,** 453, 494-501.
29. Pluym, M.; Vermeiren, C. L.; Mack, J.; Heinrichs, D. E.; Stillman, M. J., *Biochem.* **2007,** 46, 12777-12787.
30. Pluym, M.; Muryoi, N.; Heinrichs, D. E.; Stillman, M. J., *J. Inorg. Biochem.* **2008,** 102, 480-488.
31. Vermeiren, C. L.; Pluym, M.; Mack, J.; Heinrichs, D. E.; Stillman, M. J., *Biochem.* **2006,** 45, 12867-12875.
32. Mack, J.; Vermeiren, C.; Heinrichs, D. E.; Stillman, M. J., *Biochem. Biophys. Res. Commun.* **2004,** 320, 781-788.
33. Tiedemann, M. T.; Muryoi, N.; Heinrichs, D. E.; Stillman, M. J., *J. Porphyrins Phthalocyanines* **2009,** 13, 1006-1016.
34. Eakanunkul, S.; Lukat-Rodgers, G. S.; Sumithran, S.; Ghosh, A.; Rodgers, K. R.; Dawson, J. H.; Wilks, A., *Biochem.* **2005,** 44, 13179-13191.

35. Cheek, J.; Dawson, J. H., Magnetic Circular Dichroism Spectrscopy of Heme Iron Systems, Academic Press: New York, 2000.
36. Browett, W. R.; Stillman, M. J., *Biochim. Biophys. Acta.* **1979,** 577, 291-306.
37. Sutherland, J. C., *Ann. Rev. Biosphys. Bioeng.* **1980,** 9, 293-326.
38. Browett, W. R.; Stillman, M. J., *Biophys. Chem.* **1984,** 19, 311-320.
39. Sook, B. R.; Block, D. R.; Sumithran, S.; Montanez, G. E.; Rodgers, K. R.; Dawson, J. H.; Eichenbaum, Z.; Dixon, D. W., *Biochem.* **2008,** 47, 2678-2688.
40. Pond, A. E.; Roach, M. P.; Thomas, M. R.; Boxer, S. G.; Dawson, J. H., *Inorg. Chem.* **2000,** 39, 6061-6066.
41. Laskin, J.; Lifshitz, C., Principles of Mass Spectrometry Applied to Biomolecules, John Wiley & Sons: Hoboken, 2006.
42. Kaltashov, I. A., Eyles, S. J., Mass Spectrometry in Biophysics, John Wiley & Sons: New Jersey, 2005.
43. Yamashita, M.; Fenn, J. B., *J. Phys. Chem.* **1984,** 88, 4451-4459.
44. Fenn, J. B.; Mann, M.; Meng, C. K.; Wong, S. F.; Whitehouse, C. M., *Science.* **1989,** 246, 64.
45. Dass, C., Principles and Pracitce of Biological Mass Spectrometry, Wiley Interscience: New York, 2001.
46. Skoog, D. A.; Holler, F. J.; Nieman, T. A., Principles of Instrumental Analysis, 5th Ed. ed.; Thomson Learning: Toronto, 1998.
47. Konermann, L.; Douglas, D. J., *Biochem.* **1997,** 36, 12296-12302.
48. Yan, X.; Watson, J.; Ho, P. S.; Deinzer, M. L., *Mol. Cell. Proteomics.* **2004,** 3, 10-23.
49. Simmons, D. A.; Wilson, D. J.; Lajoie, G. A.; Doherty-Kirby, A.; Konermann, L., *Biochem.* **2004,** 43, 14792-14801.
50. Muryoi, N.; Tiedemann, M. T.; Pluym, M.; Cheung, J.; Heinrichs, D. E.; Stillman, M. J., *J. Biol. Chem.* **2008,** 283, 28125-28136.

Chapter 3. Demonstration of the Iron-regulated Surface Determinant (Isd) Heme Transfer Pathway in *Staphylococcus aureus*[2]

3.1 Introduction

Iron is an essential nutrient for the majority of living organisms. Although the human body contains abundant iron, its low solubility in the ferric state of aerobic systems and the fact that the majority is intracellular, means that very little soluble iron (estimated as approx. 10^{-18} M [1]) is directly available to bacteria. As such, bacteria have developed multiple iron acquisition systems to facilitate their survival in such low iron environments. The most abundant potential iron source for bacteria is heme, or iron-protoporphyrin IX, which is typically bound in proteins such as hemoglobin and myoglobin. Pathogenic bacteria have evolved specialized mechanisms for acquiring heme-iron from the host [2-5].

The *isd* gene cluster of *Staphylococcus aureus* (*S.* aureus) was first identified in 2002 [6-8] and then in 2003 Mazmanian *et al*. [9] were the first to propose that the Isd series of proteins formulate a heme transfer pathway across the cell wall and through the membrane. Up to 2008, there has been a significant amount of research into defining the Isd-mediated heme acquisition system, especially in *S. aureus*. Briefly, the Isd system in *S. aureus* consists of nine iron-regulated proteins: IsdA, IsdB, IsdC, and IsdH, which are cell-wall anchored surface proteins, and IsdDEF, which constitute a membrane-localized transporter and, finally, IsdG and IsdI, which encode heme-degrading enzymes in the cytoplasm [10]. IsdA is highly expressed on the cell wall of iron-limited *S. aureus* and, in addition to several other reported functions [11-13], is effective at scavenging heme [14, 15]. Additional reported functions of Isd proteins include the binding by IsdB of hemoglobin [16], IsdH/HarA-dependent binding of haptoglobin and haptoglobin-haemoglobin [17], and heme binding by IsdC and IsdE [18-21]. IsdE, a lipoprotein and a member of the bi-lobed, alpha-helical backbone family of substrate binding proteins, binds heme into a shallow groove between the two lobes of the protein, using His and Met to coordinate to the heme-iron [18]. Conversely, proteins IsdA, IsdB, IsdC and IsdH each contain

[2] A version of this work has been published:
Muryoi N., Tiedemann M. T., Plyum M., Cheung J., Heinrichs D. E., Stillman M. J., J. Biol. Chem., **2008**, 283, 28125-28136.

at least one so-called Near Transporter (NEAT) domain that adopt a beta sandwich structure to bind one heme into a groove with heme-iron coordination via Tyr [14, 21, 22].

Together, the series of Isd proteins in *S. aureus* are believed to interact with heme proteins, extract the heme molecule and transport it across the cell wall through to the membrane where it is then translocated into the cytoplasm [23-26]. As described above, substrate binding by individual components has been demonstrated, as has the heme degrading ability of IsdG and IsdI [10]. Most recently, Liu and coworkers used UV-visible absorption spectroscopy to demonstrate that heme transfers from IsdA to IsdC [27].

In this chapter, the use of detailed magnetic circular dichroism (MCD) spectral data together with electrospray ionization mass spectrometry (ESI-MS) to determine the products, or lack of products, when a heme-donor (i.e. heme-bound protein) and heme-accepter (i.e. apo-protein) are mixed was described. MCD spectroscopy has been shown in many reports describing the heme binding environment of both the complete proteins IsdA, IsdB, IsdC, IsdE and as well the isolated NEAT domains of IsdA (IsdA-N), IsdB (domain 2) (IsdB-N2), IsdH (domain 3) (IsdH-N3), and IsdC (IsdC-N), to exhibit parameters sensitive to the heme binding axial ligands, oxidation state and spin state [15, 19, 20, 28-32]. Previous reports of the mass spectral data have shown that the heme-free native apo-protein can be readily distinguished from the heme-free denatured apo-protein and the native, heme-bound holo-proteins [15, 20, 30]. Extending the power of these two tools, direct evidence for an ordered, multi-protein, heme transfer system between the Gram-positive bacterial surface Isd proteins was demonstrated. Key to these experiments is that the MCD signal intensity is a fingerprint of the oxidation state, spin state and ligation state of the heme iron and that the ESI-MS technique indicates possible changes in folding as a function of heme binding, and for mixtures the ESI-MS data show all components in their relative fractions – so in total in heme exchange reactions, heme binding between the very similar Isd-NEAT containing Isd proteins and the IsdE protein can all be clearly identified, thus providing unambiguous information on the heme transfer.

3.2 Experimental Methods

3.2.1 Materials and Methods

General techniques and experimental procedures pertaining to protein growth, protein purification, protein sample preparation, instrumental techniques and analysis can be found in Chapter 2.

3.2.2 Gene cloning

Over the course of the study, two different cloning methods were used to generate each of His-tagged IsdB-N2 and IsdH-N3, resulting in a slight difference in amino acid composition in the His-tag region of recombinant protein (i.e. non-Isd protein sequence), even after thrombin cleavage. Sensitivity of MS illustrates these differences in mass. Construct 1 of each of the two proteins was used in Figures 3-1 and 3-5, and construct 2 was used in Figures 3-8 and 3-9. There was no change in heme binding properties between the two constructs.

3.2.3 Heme transfer reactions

To monitor heme transfer between the NEAT domains (IsdA-N, IsdC-N, IsdB-N2, IsdH-N3) and IsdE, the protein samples were mixed with an approximate 1.5x excess of the appropriate heme acceptor protein. The mixing times were varied from 10 min to 2 h. In all cases the spectra remained the same.

3.3 Results

3.3.1 ESI-MS as a method to discriminate apo from holo Isd proteins

The heme binding NEAT domains from IsdA, IsdB, IsdC and IsdH, as well as IsdE, were overexpressed in apo-form and purified. Holo-proteins were prepared by reconstitution of apo-proteins with hemin. The proteins were analyzed by mass spectrometry to confirm that each was heme-free (apo) or homogeneously heme bound (holo), and to establish the number of heme molecules bound to each protein in the case of the unexplored IsdH-N3 and IsdB-N2 proteins. The mass spectral data are shown as the charge states in Figure 3-1 with the deconvoluted spectra in Figure 3-2.

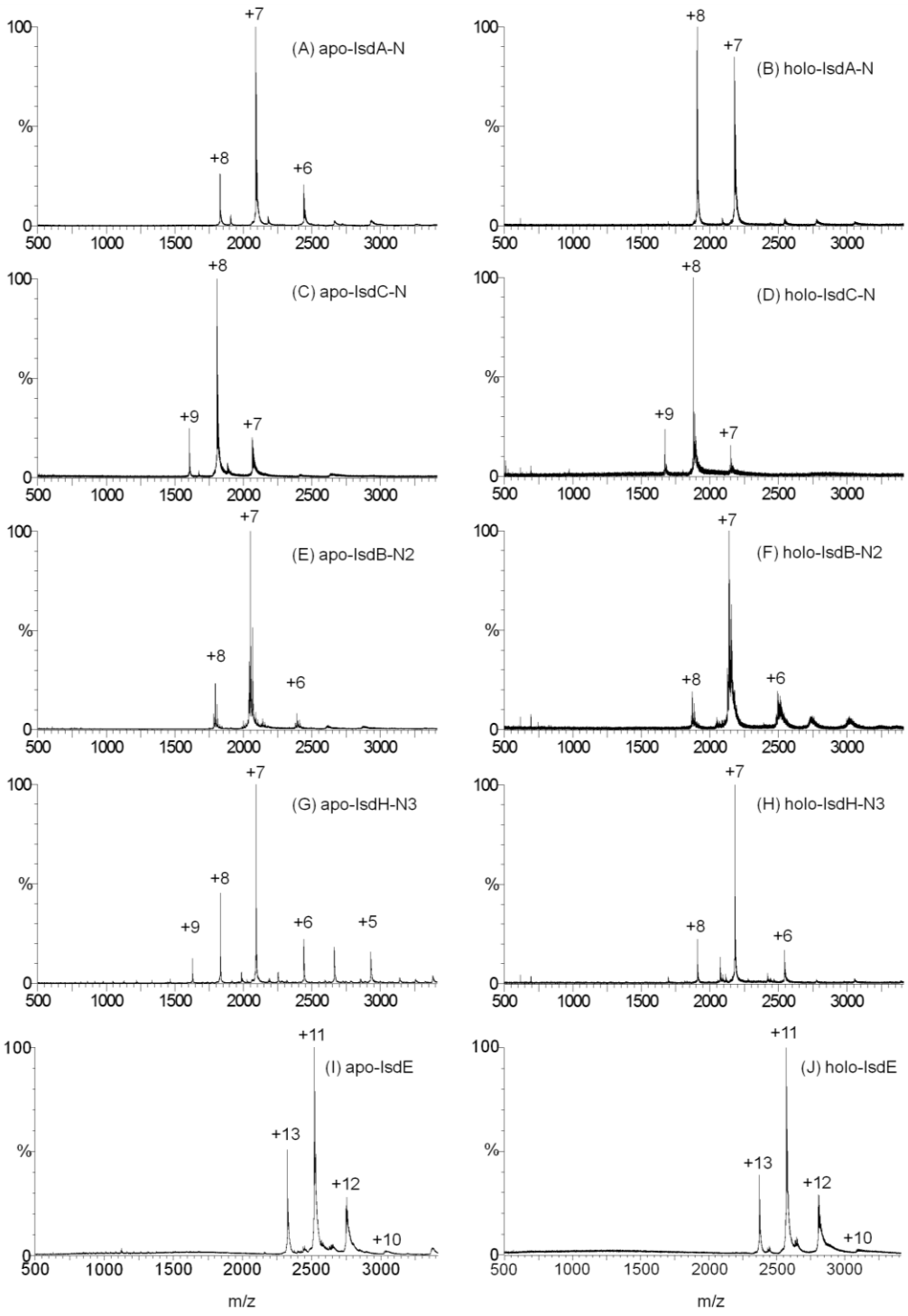

Figure 3-1 ESI-MS charge state spectra for four Isd NEAT domains and IsdE studied as the heme-free, apo-IsdA-N, -IsdC-N, -IsdB-N2, -IsdH-N3 and -IsdE species (A, C, E, G, I) and the heme-bound, holo-IsdA-N, -IsdC-N, -IsdB-N2, -IsdH-N3 and -IsdE species (B, D, F, H, J). The charge states provide information about the change in conformation associated with heme binding. The close similarities in charge state distribution between the apo-and holo- pairs of data show that the proteins do not significantly change in folding following heme binding. Each charge state arises from the same protein mass, as shown in Figure 3-2.

Charge states in ESI-MS provide an indication of the volume of the protein or solvent access to the protein's basic amino acid residues [20]. In Figure 3-1, the lack of changes in charge state distribution between the apo- and holo-species for IsdB-N2, and IsdC-N, in addition to the data previously published for IsdE [20], indicates that no significant structural changes take place with heme binding in any of these proteins. The ESI-MS data in Figure 3-1B and Figure 3-1A, indicate that there is a very slight change in conformation of IsdA-N upon heme binding because the charge state maximum increases to +8 from +7, suggesting solvent exposure of one additional basic residue when the heme binds. Similarly, there exists a change in the relative magnitude of the +9 and +8 charge states in Figure 3-1G and Figure 3-1H for apo and holo-IsdH-N3, respectively; again, the implication is that there are conformational changes upon binding the heme in holo-IsdH-N3, that, in this case, cause a reduction of solvent exposure. Compared with changes that take place following acid-induced denaturation of, for example, IsdE [20], the changes in conformation of IsdA-N and IsdH-N3 with heme binding are small and for IsdA-N in agreement with the published crystal structures of the holo versus apo forms of the protein [14].

Following heme loading, mass spectrometry was used again to confirm that the holo-proteins were formed (Figure 3-2A–J). The mass spectral data provide important evidence that the holo-proteins were the only source of heme in the transfer reactions due to the lack of a mass near 616 Daltons. This is an important test, as absorption spectroscopy is not a reliable technique to ensure the complete uptake and hence removal of free heme from a solution. The Soret band of free heme can appear as a blue-shifted shoulder on the Soret band of bound-heme and may be confused with its vibronic band, yielding complications in assessing heme transfer reactions spectroscopically. Moreover, because each of the heme-binding Isd NEAT domains possess heme-binding characteristics that result in similar optical properties, quantifying heme transfer proves very difficult. Table 3-1 summarizes the UV-visible absorption band maxima for each of the heme binding NEAT domains and IsdE. Given that the absorption spectroscopic properties of the hemes bound in IsdA, IsdB-N2, IsdC, and IsdH-N3 are all very similar, monitoring NEAT domain heme transfer reactions solely via absorption spectroscopy is, therefore, ambiguous and likely to be imprecise as the spectral envelopes of the reactants and products significantly overlap.

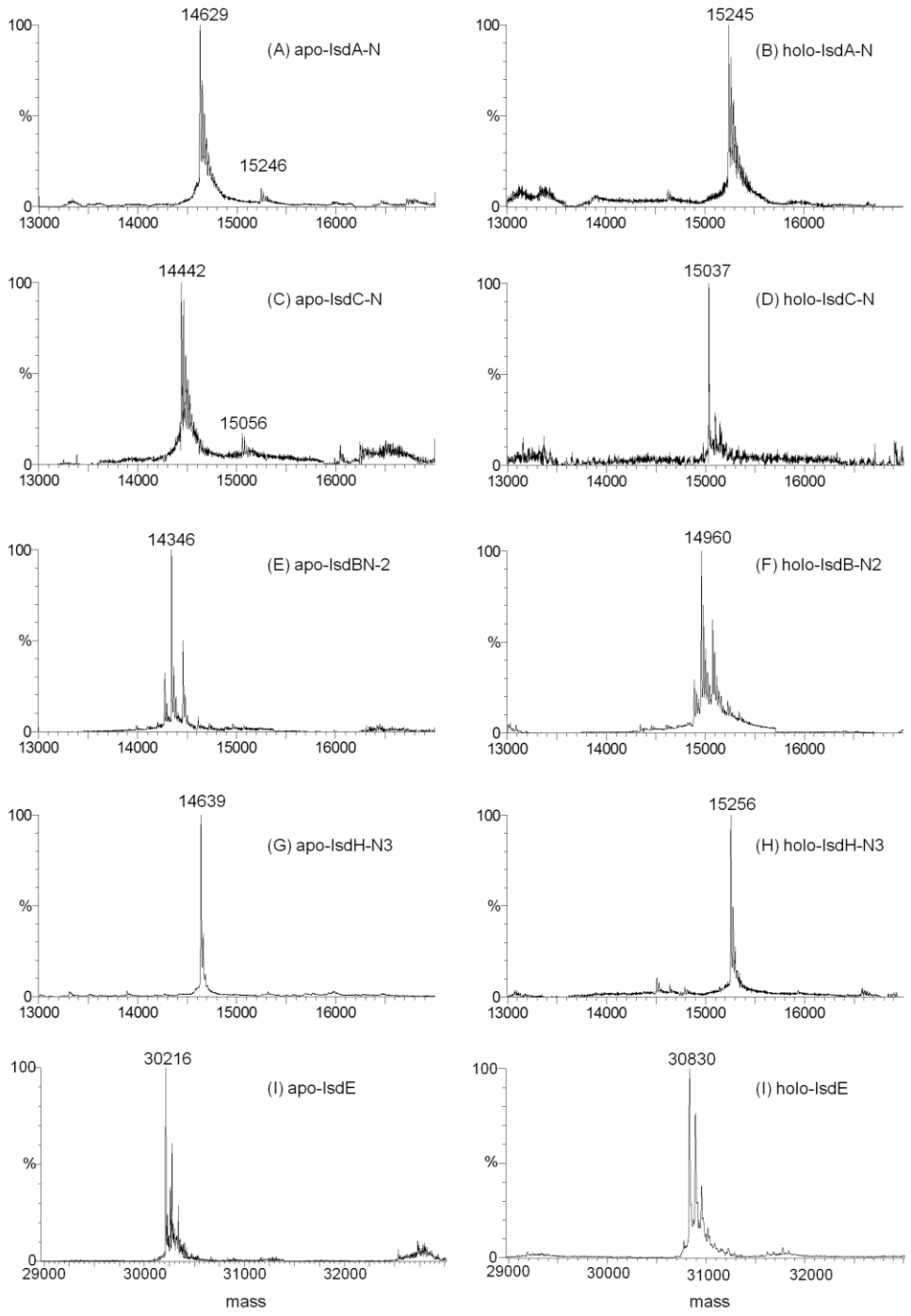

Figure 3-2 Deconvoluted ESI-mass spectra of the heme-free and heme-bound Isd proteins. Apo-IsdA-N, -IsdC-N, -IsdB-N2, -IsdH-N3 and -IsdE species (A, C, E, G, I) and Isd heme-bound-IsdA-N, -IsdC-N, -IsdB-N2, -IsdH-N3 and -IsdE species (B, D, F, H, J). The data show that only one heme binds to each of these species. The mass difference between the pairs of data for the apo- and holo-species is approximately 616 Da, the mass of a single heme.

Magnetic circular dichroism spectra do, however, exhibit additional assignment criteria that provide far more information from heme-containing proteins and we have demonstrated this sensitivity with both the full-length proteins and the isolated NEAT-domains [15, 20, 30]. When the data from MCD measurements are combined with mass spectrometric data, heme transfer reactions can be studied in detail and all protein species present can be identified together with their relative concentrations.

Table 3-1: Absorption spectra properties for the heme-bound NEAT domains of IsdA-N, IsdB-N2, IsdC-N and IsdH-N3, and IsdE

Protein	Soret λ_{max} (nm)	Visible region λ_{max} (nm)	Reference
IsdA-N	406	502, 535, 628	[15, 30]
IsdB-N2	404	505, 533, 627	This work
IsdC-N	403	502, 533, 627	[19, 30]
IsdH-N3	403	502, 533, 629	This work
IsdE	415	532, 563, 650	[19, 20]

The key focus of this study was determining the ability of heme to transfer among Isd proteins in order to directly address the hypothesis that the proteins function in concert as a heme shuttle system in the Gram-positive bacterial cell wall. A key test is whether the transfer reactions are quite general and independent of the donor or, on the other hand, highly specific to the heme-donor as would be the case if specific protein-protein interactions were involved. Since each NEAT domain contains a distinct amino acid composition and, therefore, a distinct mass (making mass spectral peak assignment straightforward; demonstrated in Figure 3-2), heme transfer reactions could therefore readily be followed using the ESI-MS technique.

3.3.2 Magnetic circular dichroism results

Magnetic circular dichroism spectral data indicate that heme transfer takes place from IsdA-N, through IsdC-N to IsdE - While the optical spectral properties of the heme-bound-NEAT domains are very similar due to the similarity in axial ligation of the heme-iron, IsdE contains a novel heme binding domain, which is quite distinct from the NEAT domains and, as a result, exhibits a very different absorption and MCD spectrum (see Table 3-1). Indeed, IsdE coordinates a single heme using both a histidine and a methionine residue, whereas the NEAT domains bind a single heme using a proximal tyrosine for heme-iron coordination [14, 15, 18,

20]. The Soret absorption band is red-shifted to 415 nm for IsdE, significantly separated from the ~404 nm Soret band of the NEAT domains. Heme transfer reactions could, therefore, be monitored using UV-visible absorption spectroscopy for Isd-NEAT to IsdE transfer reactions.

Despite the close similarity in absorption spectral properties between IsdA-N and IsdC-N, the MCD spectral properties are slightly different because the heme-iron in IsdC-N is slightly lower spin than in IsdA-N so the Soret region MCD bands distinctly change. Figure 3-3A shows the sequence of spectra recorded for holo-IsdA-N in the presence of increasing concentrations of apo-IsdC-N. Clearly, there is a change in the spectra but based on these data alone, it was ambiguous as to whether heme transfer took place. However, unambiguous data showing heme transfer in this reaction was obtained from the ESI-MS data shown below, confirming that the heme in IsdA-N transferred stoichiometrically to apo-IsdC-N. In other words, while the absorption data recorded for this transfer are very poor discriminators, and even the MCD data provide imprecise data, the ESI-MS data provide definitive data to support the conclusion that heme transfer took place.

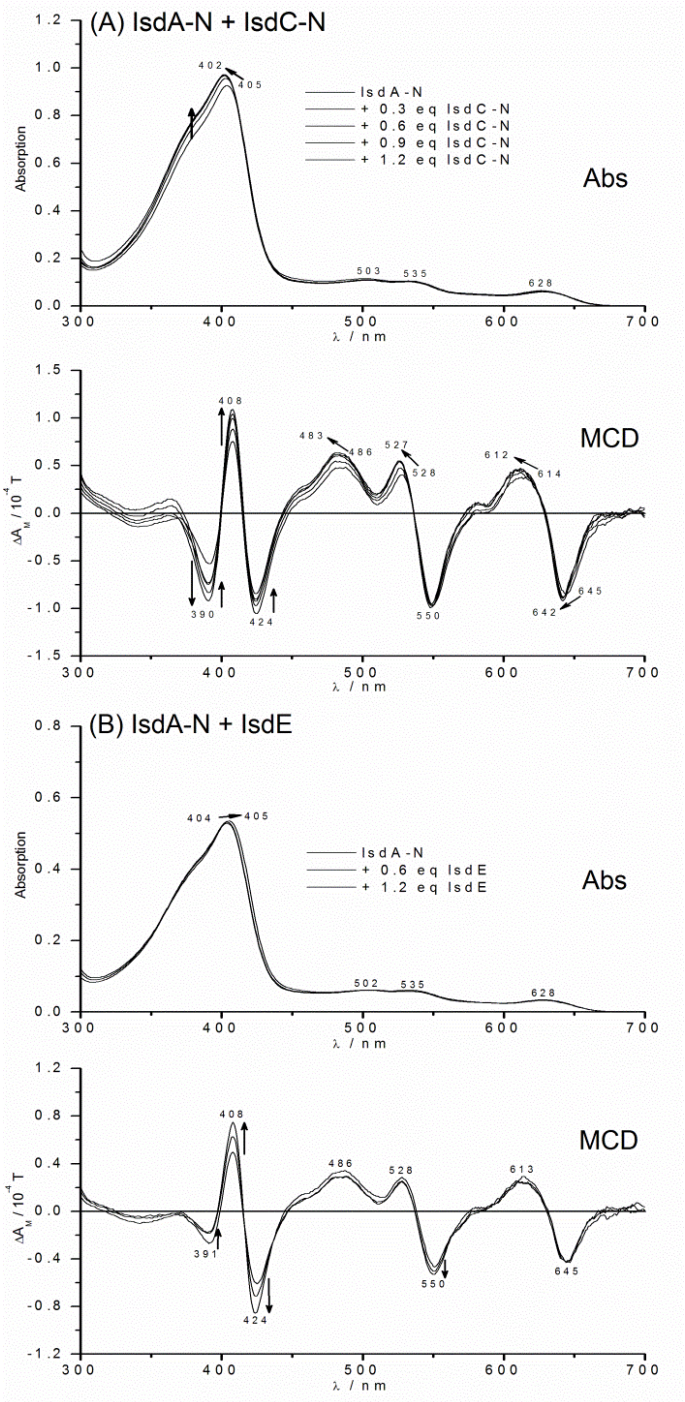

Figure 3-3 Absorption and magnetic circular dichroism (MCD) spectra recorded for heme transfer from Isd holo-IsdA-N to Isd apo-IsdC-N and for a mixed solution of Isd holo-IsdA-N and apo-IsdE. (A) Changes in the spectra when apo-IsdC-N is added to holo-IsdA-N in steps of 0.3 mol eq. Lines shown for additions to: 0, 0.3, 0.6, 0.9 and 1.2 mol eq. apo-IsdE. The spectra have been corrected for dilution effects. In the absorption spectrum the only significant change is the increase in absorbance at 390 nm and the slight blue shift from 405 to 402 nm; as marked by arrows. There is more change in the MCD spectrum because the MCD spectrum of the holo-IsdC-N product is slightly blue-shifted when compared with the holo-IsdA-

N reactant, and also exhibits a more prominent negative signal at 390 nm, a more positive signal at 408, and a less negative signal at 424 nm than holo-IsdC-N resulting in a significant change in the intensities of the bands at these wavelengths as the reaction proceeds. (B) Absorption and magnetic circular dichroism (MCD) spectra recorded when heme-free, apo-IsdE was added to a solution of heme-containing, Isd holo-IsdA-N. Three sets of spectra are shown: with a total of 0, 0.6 and 1.2 mol. eq. IsdE added. While there is little change in the absorption spectrum, addition of apo-IsdE results in intensification of the Soret MCD band envelope centered on 416 nm, a sign of increased low spin contribution in the ferric heme. There is no indication of the distinctly different absorption and MCD spectra of heme-containing, holo-IsdE. The changes are a result of interactions between the two proteins. Mass spectral data in Figure 3-7 also clearly show that no heme transfer took place and that the solution after mixing contains only holo-IsdA-N and apo-IsdE.

Figure 3-3B shows that the effect of adding apo-IsdE to holo-IsdA-N is essentially negligible in the absorption spectrum but is actually quite significant in the MCD spectrum. The MCD data clearly show that the heme does not transfer from IsdA-N to IsdE. However, an interesting finding was that the MCD data show that spectral changes do take place at the heme site in holo-IsdA-N (despite the fact that heme is not removed), which can be associated with a decrease in the high spin *g* factor of the ferric ground state, a situation encountered when a weak field ligand is replaced by a slightly stronger field ligand. The ESI-MS data described below confirm that no heme transfer took place between IsdA-N and IsdE but, unlike the data obtained from MCD, do not discriminate the fact that an interaction between the two proteins does occur.

Figure 3-4 shows results from heme transfer as increasing concentrations of apo-IsdE are added to a solution of holo-IsdA-N and apo-IsdC-N (the same solution as that used to generate the spectral data shown in Figure 3-3A – in fact, as shown conclusively above, that solution rapidly shifts to apo-IsdA-N and holo-IsdC-N). Since the spectral properties of the heme in holo-IsdE are completely different than when the heme is bound in either holo-IsdA-N or holo-IsdC-N, there are dramatic and systematic changes that are observed in both the absorption and MCD spectra. These data emphasize that transfers between NEAT-domains are difficult to quantify by optical measurements alone, but that heme transfer to IsdE is readily measurable, and the MCD spectra provide clear assignment criteria with respect to the exact heme-containing protein at the end of the reaction.

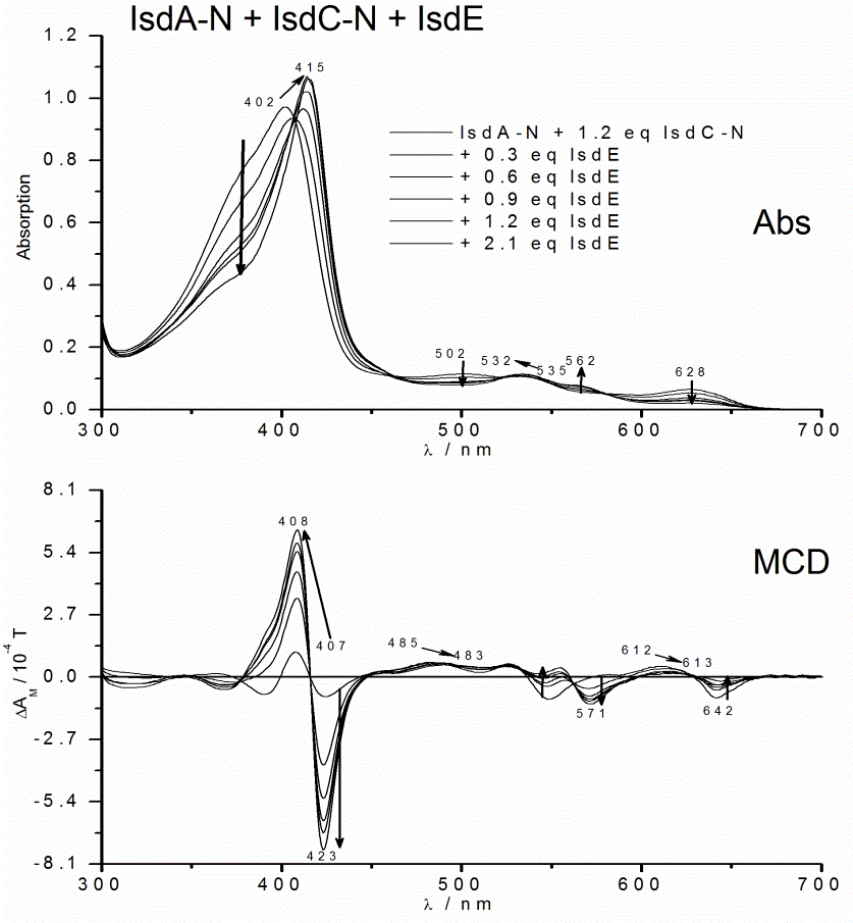

Figure 3-4 Changes in the absorption and magnetic circular dichroism spectra when heme-free, apo-IsdE is added to a solution of heme-containing, Isd holo-IsdA-N and apo-IsdC-N (the solution used in Figure 3-3A). Isosbestic change in spectral properties indicates the formation of heme-containing, holo-IsdE that was transferred from the holo-IsdA-N, to the apo-IsdC-N, then to the apo-IsdE. Spectra are shown for solutions with a total of: 0, 0.3, 0.6, 0.9, 1.2 and 2.1 mol eq apo-IsdE added. The lines show the direction of the spectral changes. The final absorption and MCD spectra closely resemble those of heme-loaded-IsdE (holo-IsdE).

3.3.3 Electrospray ionization mass spectrometry results

In the following sections, ESI-MS was used to demonstrate that specific heme transfer reactions occur between the NEAT domains of IsdH-N3, IsdB-N2, IsdA-N, and IsdC-N and the IsdE protein.

Apo-IsdC-N efficiently removes heme from holo-IsdA-N, holo-IsdB-N2, and holo-IsdH-N3 – In Figure 3-5, mass spectral data show that heme is transferred directly, rapidly and completely from holo-IsdA-N Figure 3-5A, holo-IsdB-N2 Figure 3-5B, and holo-IsdH-N3 Figure 3-5C to apo-IsdC-N. The heme donor proteins were mixed with an approximately 1.5x excess of the

heme acceptor protein. Three major peaks are seen in each of the deconvoluted spectra (adjacent panels in A, B and C in Figure 3-5), which are associated with (i) the heme-free form of the donor, (ii) the heme-free form of the acceptor and (iii) the heme-bound form of the acceptor. No remaining heme-bound form of the donor is observed (see Figure 3-2 for the masses of the holo species). It is interesting to note that the relative magnitudes of the %-abundances cannot be used to determine relative concentrations between different proteins because the uptake by the mass spectrometer is different for each protein. However, the relative concentrations of the heme-bound and heme-free species of the same protein can be related. In these data even though the apo- and holo- masses might be close, there is no direct overlap and within the precision of the experiment only three-separate species can be identified.

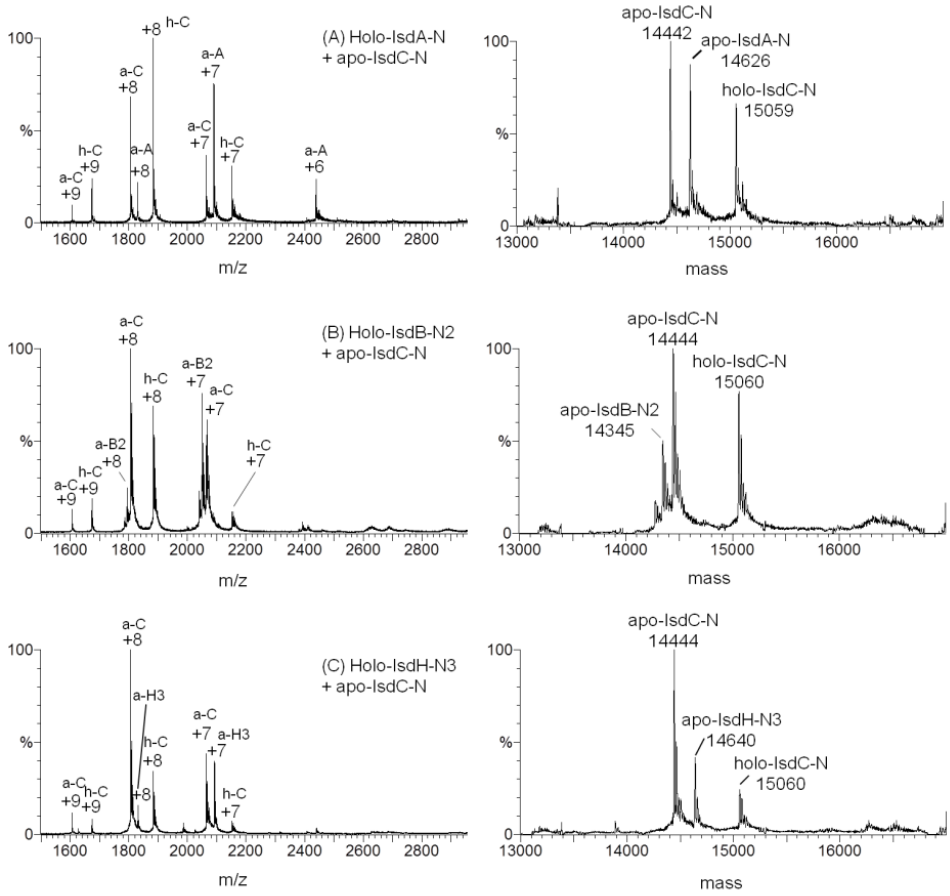

Figure 3-5 Mass spectral data for solution of mixed proteins showing heme transfer from the Isd holo-NEAT domains (IsdA-N, IsdB-N2, and IsdH-N3) to apo-IsdC-N. (A) Charge state and deconvoluted mass spectra measured for a mixture of heme-containing, Isd holo-IsdA-N and apo-IsdC-N. Excess heme-free, apo-IsdC-N was added. Three species coexist in solution and are identified in the charge state spectra with the abbreviations for apo-IsdC-N (a-C; with a mass of 14,442 Da), apo-IsdA-N (a-A; with a mass of 14,626 Da) and holo-IsdC-N (h-

C; with a mass of 15,059 Da). (B) Charge state and deconvoluted mass spectra measured for a mixture of heme-containing, holo-IsdB-N2 and apo-IsdC-N. Excess heme-free, apo-IsdC-N was added. Three species coexist in solution and are identified in the charge state spectra with the abbreviations for apo-IsdB-N2 (a-B2; with a mass of 14,345), apo-IsdC-N (a-C; with a mass of 14,444 Da), and holo-IsdC-N (h-C; with a mass of 15,060 Da). (C) Charge state and deconvoluted mass spectra measured for a mixture of heme-containing, Isd holo-IsdH-N3 and apo-IsdC-N. Excess heme-free, apo-IsdC-N was added. Three species coexist in solution and are identified in the charge state spectra with the abbreviations for apo-IsdH-N3 (a-H3; with a mass of 14,640 Da), apo-IsdC-N (a-C; with a mass of 14,444 Da), and holo-IsdC-N (h-C; with a mass of 15,060 Da). In each case heme transfer to IsdC-N was observed, resulting in a mixture of the heme-free-Isd-NEAT domain of IsdA-N, IsdB-N2, IsdH-N3) and heme-free apo-IsdC-N and heme-bound-holo-IsdC-N. No heme-bound-holo-IsdA-N (at 15,245 Da), IsdB-N2 (at 14,960 Da) or IsdH-N3 (at 15,256 Da) was observed in their respective mass spectra following mixing with apo-IsdC-N. In each case, excess (approximately 1.5x) of the heme-acceptor protein was used, so that there was also apo-heme-free protein remaining.

If the reverse reaction occurred in the presence of holo-acceptor protein, then four species would be observed since none of the possible protein species would be completely removed from solution. This was observed for only one experiment: namely for the heme transfer between IsdB-N2 and IsdH-N3, described below.

Conclusions from these data are that, unlike the data obtained from absorption and MCD spectra, the ESI-MS data unambiguously show that heme was transferred to apo-IsdC-N in every case. Next, the heme-transfer hypothesis and the MCD data described above was tested by adding IsdE to these solutions,

ESI-MS data show that apo-IsdE efficiently removes heme from holo-IsdC-N, -B2 and H3 – Figure 3-6 consolidates two experiments; in part A, the mass spectral data recorded following mixing of holo-IsdC-N and apo-IsdE are shown and, in part B, the separate absorption spectra for the two heme-bound proteins, holo-IsdC-N and holo-IsdE after heme-transfer from the holo-IsdC-N are shown. First, the mass spectral data (Figure 3-6A) shows that IsdC-N-bound-heme was transferred entirely to apo-IsdE. Only apo-IsdC-N at 14,443 Da, apo-IsdE at 30,258 Da and holo-IsdE, 615 Da heavier at 30,873 Da, are identified. The 616 Da mass is quite small with respect to the apo-heme-free mass of IsdE, so the charge states overlap and we observe a duplication from +11 to +13. There is only one set of charge states for the IsdC-N as there is no holo-IsdC-N remaining. The +6 charge state overlaps with the +13 of IsdE. Inspection of the charge states illustrate how heme binding does not change the overall conformation of either IsdE or IsdC-N significantly (Figure 3-6A and Figure 3-1), since the +12 state for IsdE and +8

for IsdC-N remain predominant following heme-binding. The absorption spectra in Figure 6B show how the Soret band for holo-IsdC-N red-shifts when apo-IsdE is added. For this combination, the absorption spectra are different because the maximum of IsdE lies 12 nm to the red near 415 nm, Table 3-1.

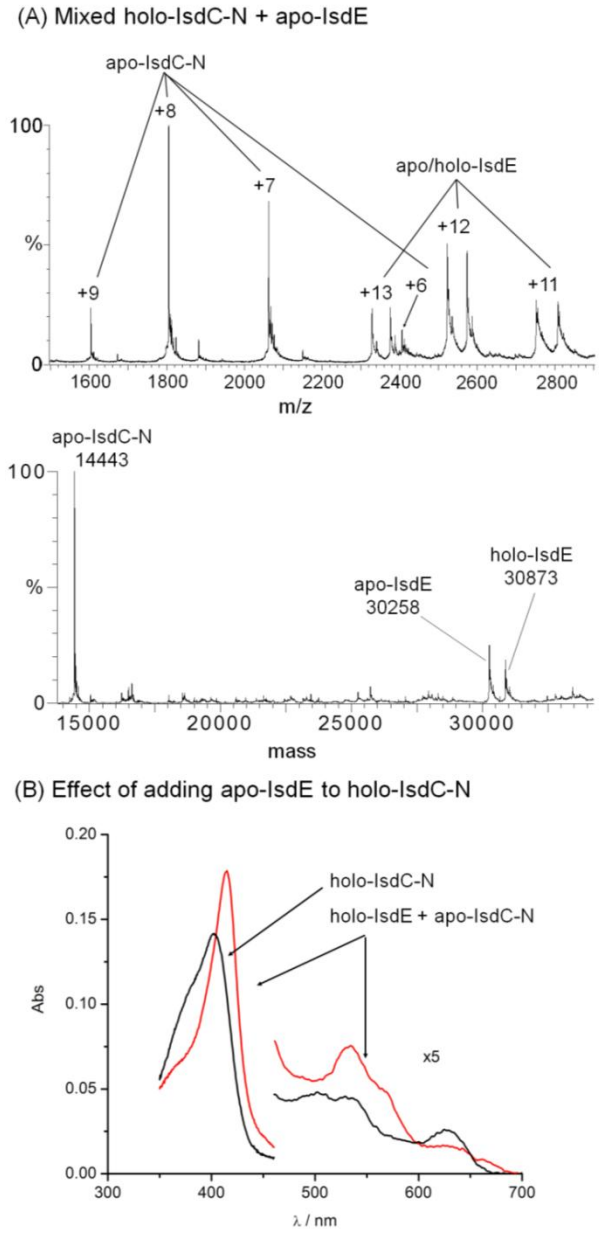

Figure 3-6 Heme transfer from holo-IsdC-N to apo-IsdE. (A) Charge state and deconvoluted mass spectra of the solution made by mixing holo-IsdC-N and apo-IsdE. Excess apo-IsdE was added. (B) Absorption spectra of holo-IsdC-N before (indicated by arrows) and following the addition of apo-IsdE. The significant change in the Soret band maxima following heme transfer to the apo-IsdE means that for this heme transfer experiment, absorption spectra can be used to monitor the progress of the

reaction. The absorption spectrum of holo-IsdE is quite different from that of either apo-IsdC-N or holo-IsdC-N.

Apo-IsdE does not accept heme from holo-IsdA-N – The ESI-MS data in Figure 3-7A show that there is no heme transfer when apo-IsdE is mixed with holo-IsdA-N. This is the only scenario, where no transfer to the heme-free Isd acceptor protein at all was observed. This lack of transfer is emphasized in the absorption spectra (Figure 3-7B) where the spectrum of holo-IsdA-N mixed with apo-IsdE is exactly the same as holo-IsdA-N – quite unlike the case in all the other spectra shown previously. However, recall that the MCD spectra in Figure 3-4 suggest that there is interaction between these two proteins, but without transfer of the heme.

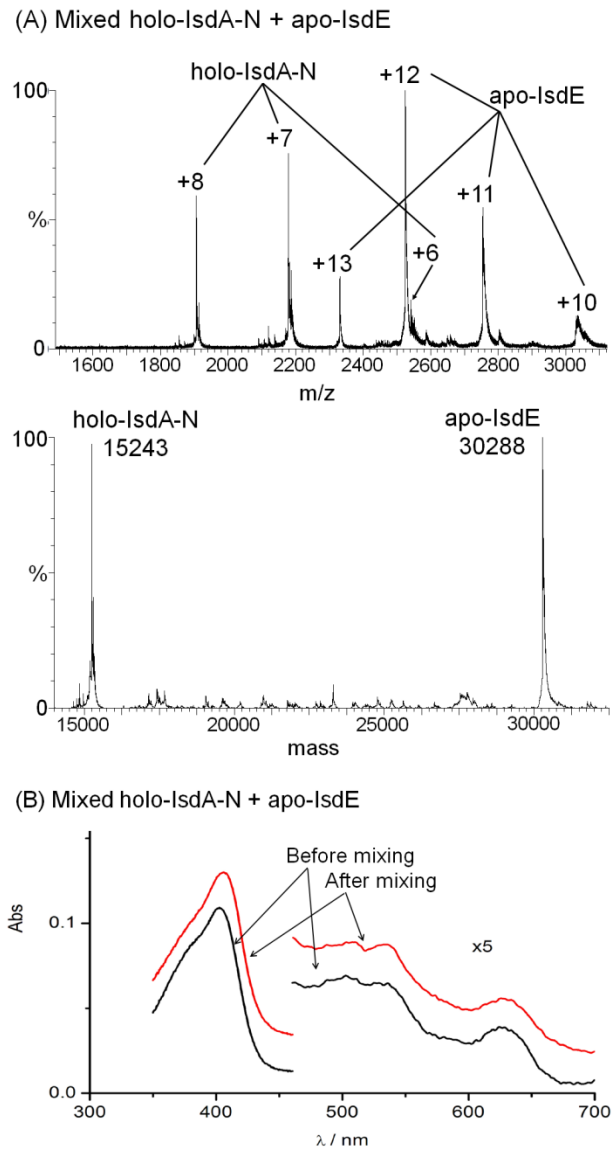

Figure 3-7 Demonstration that no heme transfer takes place from holo-IsdA-N to apo-IsdE. (A) ESI-MS spectra (charge states and deconvolution) for a mixture of holo-IsdA-N and apo-IsdE showing the presence of only holo-IsdA-N and apo-IsdE; there is no indication of the presence of either apo-IsdA-N or holo-IsdE showing that no heme transfer took place. (B) The absorption spectra recorded before and after addition of the apo-IsdE are characteristic of holo-IsdA-N for both solutions. There is no indication of formation of holo-IsdE, which has a significantly different absorption spectrum

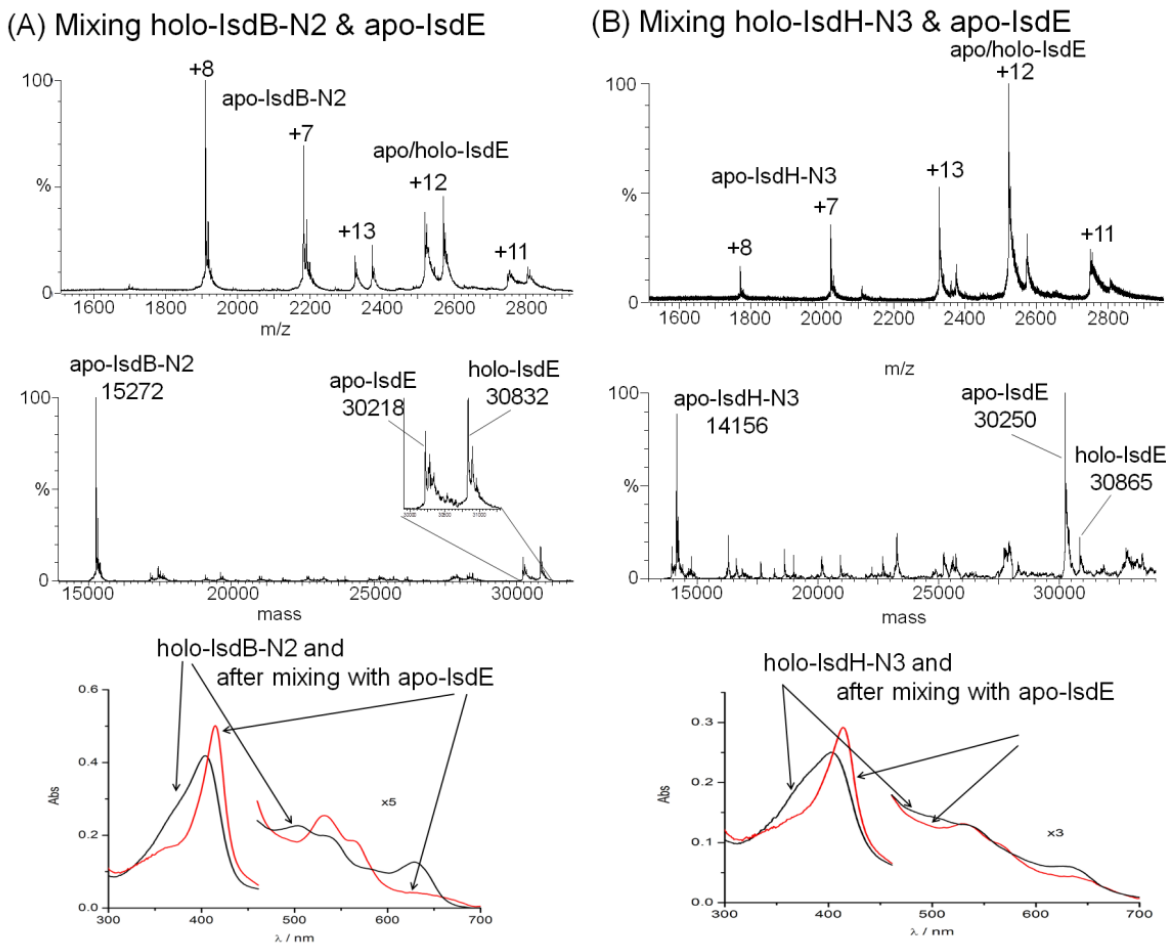

Figure 3-8 Heme transfer from holo-IsdB-N2 and holo-IsdH-N3 to apo-IsdE. Charge state and deconvoluted mass spectra and absorption spectra measured for mixtures of (A) holo-IsdB-N2 with apo-IsdE as a heme acceptor and (B) holo-IsdH-N3 with apo-IsdE as a heme acceptor. In (A) the data show that holo-IsdB-N2 transfers heme to apo-IsdE. In each mass spectrum are peaks that correspond to both the holo-and apo-proteins: peaks that correspond to apo-IsdE (+11 to +13) at 30,218 Da, peaks that correspond to holo-IsdE (+11 to +13) at 30,832 Da and peaks that correspond to apo-IsdB-N2 (+7 to +8) at 15,272 Da. The absorption spectra represent the holo-IsdB-N2 before the addition of IsdE (indicated by the arrow from the legend 'holo-IsdB-N2') and following mixing with IsdE for 25 min (indicated by the arrows from the legend 'after mixing with apo-IsdE'). The holo-IsdB-N2 was formed by binding heme to heme-free, apo-IsdB-N2 (construct 2), which was made using a different cloning strategy than that used to make IsdB-N2 which was used for the data in Figures 3-1, 3-2 and 3-5. Residues in the His-tag region (non-Isd) differ between the two constructs (see Experimental Procedures). The experimental results were unchanged by the use of the second construct. In (B) the data show that holo-IsdH-N3 transfers heme to apo-IsdE. In each mass spectrum are peaks that correspond to both the holo-and apo-proteins: peaks that correspond to apo-IsdE (+11 to +13) at 30,250 Da, peaks that correspond to holo-IsdE (+11 to +13) at 30,865 Da and peaks that correspond to apo-IsdH-N3 (+7 to +8) at 14,156 Da. The absorption spectra of the holo-IsdH-N3 before the addition of IsdE (indicated by arrows from the legend 'holo-IsdH-N3') and following mixing with apo-IsdE for 25 min (indicated by arrows from the legend 'after mixing with apo-IsdE').

The final spectrum corresponds to that of heme-containing, holo-IsdE. The apo-IsdH-N3 (construct 2) was made using a different cloning procedure than that used for the IsdH-N3 which was used to generate the data shown in Figures 3-1, 3-2 and 3-5. Residues in the His-tag region (non-Isd) were altered between the two constructs (see Experimental Procedures). The experimental results were unchanged by the use of the second construct.

Apo-IsdE accepts heme from holo-IsdB-N2 and holo-IsdH-N3 – The ESI-MS data in Figure 3-8 show unambiguously that heme, whether it was initially in IsdB-N2 (panel A) or IsdH-N3 (panel B), was transferred rapidly and completely to apo-IsdE. The absorption spectra in Figures 3-8A and 3-8B again illustrate that when IsdE is the heme acceptor there are significant differences in the absorption spectra. The spectra measured following mixing of holo-IsdB-N2 and apo-IsdE and of holo-IsdH-N3 and apo-IsdE are virtually identical, representing solely holo-IsdE.

Apo-IsdA-N accepts heme from holo-IsdB-N2 and holo-IsdH-N3 – The ESI-MS data in Figures 3-9A and 3-9B show that the heme in holo-IsdB-N2 and holo-IsdH-N3 transfers to apo-IsdA-N. The transfer from holo-IsdH-N3 to apo-IsdB-N2 is inefficient since the data in Figure 9C show the presence of all four species.

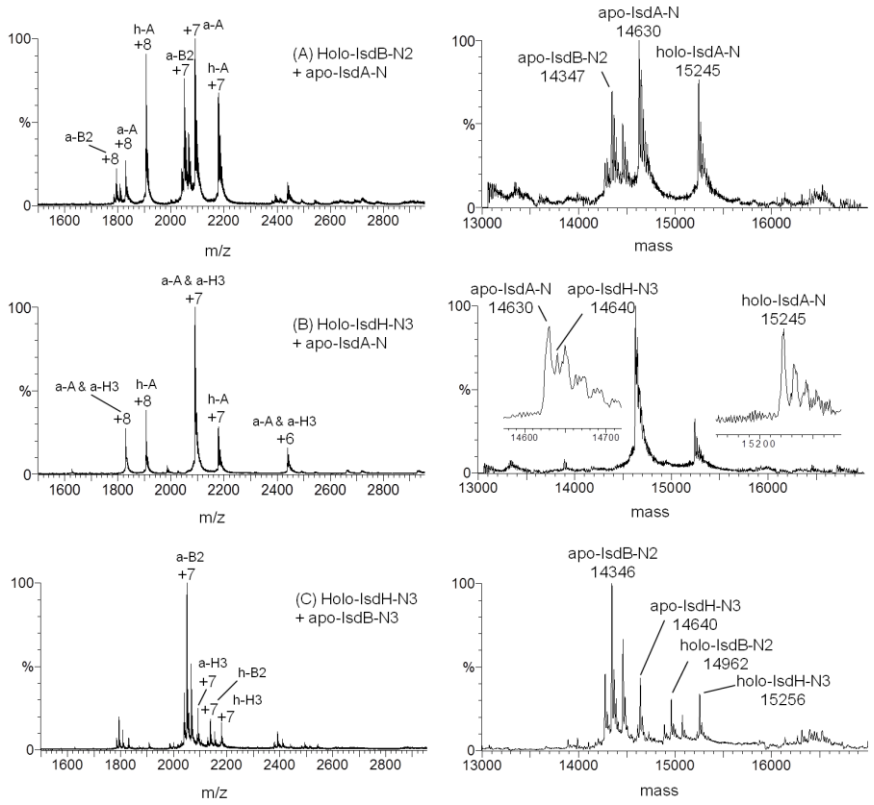

Figure 3-9 Heme transfer from holo-IsdB-N2 and holo-IsdH-N3 to apo-IsdA by ESI-MS. Charge state and deconvoluted mass spectra Heme transfer from holo-IsdB-N2 to apo-IsdA-N, and holo-IsdH-N3 to apo-IsdN-A and IsdB-N2. Charge state and deconvoluted mass spectra, and absorption spectra measured for mixtures of (A) holo-IsdB-N2 with apo-NEAT-A as a heme acceptor, (B) holo-IsdH-N3 with apo-IsdA-N as a heme acceptor, and (C) holo-IsdH-N3 with apo-IsdB-N2 as heme acceptor. In (A) the data show that holo-IsdB-N2 transfers heme to apo-IsdA-N. In each mass spectrum are peaks that correspond to both the holo-and apo-proteins: peaks in the mass spectra that correspond to apo-IsdA-N (a-A: +7 and +8) at 14,630 Da, peaks that correspond to holo-IsdA-N (h-A: +7 and +8) at 15,245 Da and peaks that correspond to apo-IsdB-N2 (a-B2: +7 to +8) at 14,347 Da. In (B) the data show that holo-IsdB-N2 transfers heme to apo-IsdA-N. In each mass spectrum are peaks that correspond to both the holo-and apo-proteins: peaks that correspond to apo-IsdA-N (a-A: +7 and +8) at 14,630 Da, peaks that correspond to holo-IsdA-N (h-A: +7 and +8) at 15,245 Da and peaks that correspond to apo-IsdH-N3 (a-H3: +7 to +8) at 14,640 Da. In (C) the data show that holo-IsdH-N3 transfers heme to apo-IsdB-N2. In each mass spectrum are peaks that correspond to both the holo-and apo-proteins: peaks that correspond to apo-IsdB-N2 (a-B2: +7 and +8) at 14,346 Da, peaks that correspond to holo-IsdB-N2 (h-B2: +7 and +8) at 14,962 Da, and peaks that correspond to holo-IsdH-N3 (h-H3: +7) at 15,256 Da, and to apo-IsdH-N3 (a-H3: +7 to +8) at 14,640 Da.

3.4 Discussion

The Isd series of proteins are proposed to represent a complete heme acquisition and transport system, together functioning to remove heme from proteins such as hemoglobin, then to shuttle heme across the Gram-positive bacterial cell wall right through to membrane ABC transporters, which translocate the heme molecule into the cytoplasm where it is eventually degraded by proteins IsdG and IsdI. While significant evidence now exists demonstrating substrate binding for the various proteins [9, 10, 14-21, 27, 30], the first direct evidence for heme transfer between Isd proteins was only very recently obtained for the IsdA to IsdC transfer reaction [27]. In the present study, a complete picture of heme transfer between all of the heme binding Isd proteins that reside on the outside of the bacterial cell has been obtained for the first time.

All heme-binding Isd NEAT domains possess overlapping heme-binding properties. Each has been shown to coordinate a single, 5-coordinate, high-spin ferric heme through a conserved tyrosine residue [14, 15, 21, 30] and, as such, the absorption spectroscopic properties of the hemes bound in IsdA, IsdB, IsdC, and IsdH are all very similar. The spectroscopic and structural data reported to date do not provide information on the process or mechanism that would be required if the Isd proteins are to capture and transfer heme molecules. Although the heme binding properties of the NEAT domains appear very similar, the data presented here show that the NEAT domains do, in fact, possess distinct qualities. The majority of heme transfer reactions occurred rapidly and in a unidirectional fashion (except for the transfer between IsdB-N2 and IsdH-N3) and, in the case of IsdA, very selectively, via apo-IsdC-N towards apo-IsdE

Together, the results suggest that specific protein-protein interactions must occur to promote the removal of heme from Isd proteins since concentrations of free heme were extremely low and if protein-protein reactions were not to occur, would result in very slow transfer rates. Experimentally, this is not what was observed. Also, in the absence of protein-protein interactions the presence of equilibria would be exected to be observed in both optical data (especially the MCD spectra) and ESI-mass spectra. No evidence for significant concentrations of both donor and acceptor was observed. It is likely, then, that one or more of the remaining, non-heme binding NEAT domains, that is, IsdB-N1 and/or IsdH-N1 or IsdH-N2 play crucial roles in extracting heme from myoglobin or hemoglobin. In support of this, it is noteworthy that IsdB-N1 binds hemoglobin [16] whereas IsdH-N1 binds hemoglobin-haptoglobin [17]. In the proposed Isd-mediated heme transport system, the surface exposed Isd proteins interact with

heme containing proteins such as hemoglobin (IsdB) or hemoglobin-haptoglobin (IsdH), which are found in serum following erythrocyte lysis. Extraction of the heme then occurs, followed by heme transfer to other Isd proteins present in spatially arranged locations within the cell wall architecture.

Analysis of the optical data illustrates the difficulties in obtaining precise information for transfer between the NEAT domains. Even though the MCD spectra provide far more information, there is only a small change following transfer from holo-IsdA-N to apo-IsdC-N. The situation is far better when the transfer takes place to IsdE. The transfer to IsdE was further confirmed by absorption spectroscopy since a gradual shift of the Soret band from 404 to 415 nm was observed. On the other hand, the mass spectrometric data show that holo-IsdH-N3 transferred heme to all other NEAT domains as well as to IsdE. Holo-IsdB-N2 showed similar behavior, even supplying heme to apo-IsdH-N3 with heme. This was the only example of bidirectional heme transfer that was observed in this study and suggests that IsdB and IsdH are functionally closely related, in agreement with predictions based on bioinformatic analyses.

A key result of this study is that the IsdA NEAT domain (IsdA-N) behaved quite differently than either IsdB-N2 or IsdH-N3. IsdA-N accepted heme from IsdB-N2 and IsdH-N3 in a unidirectional fashion, and only transferred heme to IsdC-N not to apo-IsdE. All three techniques, mass spectrometry, MCD and absorption spectroscopy, confirmed that IsdE was unable to accept heme from IsdA-N. Figures 3-3B and 3-7 show the MCD and absorption spectra of holo-IsdA-N before and following the addition of excess apo-IsdE. No shift in the Soret band or any change in the visible region was observed. IsdC has been proposed to function as the central conduit in the cell wall for heme passage to the bacterial cell membrane. The ability of IsdC-N to accept heme from IsdA-N, IsdB-N2, and IsdH-N3 (Figure 3-5) and to only transfer it to apo-IsdE (Figures 3-4 and 3-6) offers strong support for this proposal; no increase in holo-IsdE was observed after incubation with holo-IsdA-N whereas a significant increase in holo-IsdE was obtained following incubation of apo-IsdE with holo-IsdC-N (Figure 3-7 and Figure 3-6).

3.5 Conclusion

In conclusion, the data presented here support a model for heme transport as illustrated in Figure 3-10, in strong agreement with the proposal first offered by Mazmanian *et al*. [9]. Of

importance in these challenge experiments, is that the flow of heme is from the distally-located IsdH and IsdB through to the membrane-proximal IsdE protein. Key to the mechanistic analyses is that heme does not transfer from holo-Isd IsdA-N directly to apo-IsdE; apo-IsdC-N is the required facilitator. This fact, taken together with the demonstrated unidirectionality of the transfer reactions, suggests that specific protein-protein interactions must be a necessary part of the mechanism required to drive the heme transfer towards the membrane.

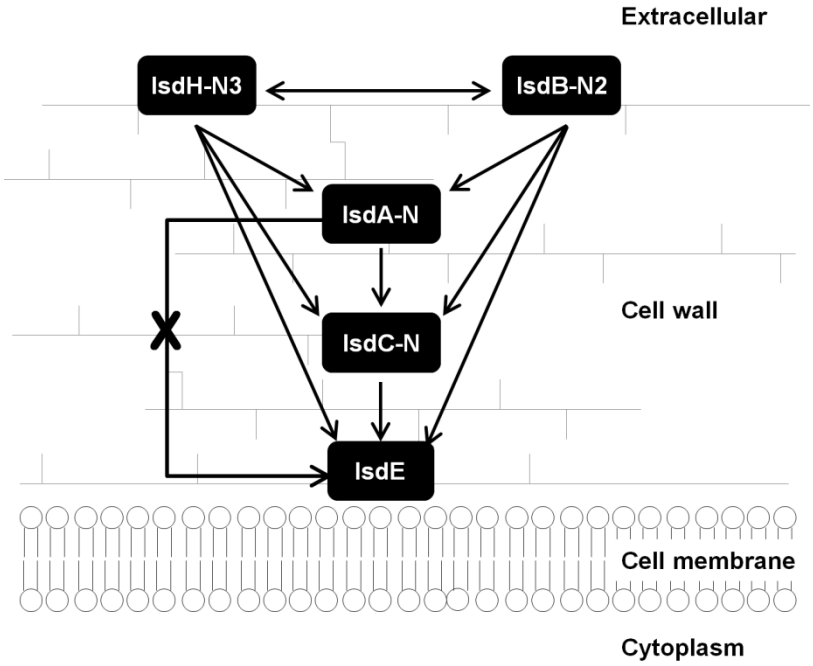

Figure 3-10 A heme transport model based on analysis of the magnetic circular dichroism and mass spectral data obtained from this study. Overall, heme transfer is from membrane distal IsdH (studied using NEAT domain H3) and IsdB (studied using the NEAT domain B2) proteins through to the membrane-proximal IsdE. There is unidirectional heme transfer from IsdA-N to IsdC-N to IsdE. There is no transfer from NEAT-A to IsdE. The mass spectral data to support the model are in agreement with the model first proposed by Schneewind and colleagues [9]. The absorption and MCD data of the equilibrated solutions fully support the conclusions reached from analysis of the mass spectral data.

3.6 References

1. Bullen, J.; Griffiths, E., Iron and Infecton: Molecular, Physiological, and Clinical Aspects, John Wiley and Sons: New York, 1999; Vol. 2, 409-415.
2. Genco, C. A.; Dixon, D. W., *Mol. Microbiol.* **2001,** 39, 215-220.
3. Skaar, E. P.; Schneewind, O., *Microbe. Infect.* **2004,** 6, 390-397.
4. Wandersman, C.; Delepelaire, P., *Annu. Rev. Microbiol.* **2004,** 58, 611-647.
5. Wandersman, C.; Stojiljkovic, I., *Curr. Opin. Microbiol.* **2000,** 3, 390-397.
6. Mazmanian, S. K.; Ton-That, H.; Su, K.; Scheenwind, O., *PNAS.* **2002,** 99, 2293- 2298.

7. Morrissey, J. A.; Cockayne, A.; Hammacott, J.; Bishop, K.; Denman-Johnson, A.; Hill, P. J.; Williams, P., *Infect. Immun.* **2002,** 70, 2399-2298.
8. Taylor, J. M.; Heinrichs, D. E., *Mol. Microbiol.* **2002,** 43, 1603-1614.
9. Mazmanian, S. K.; Skaar, E. P.; Gaspar, A. H.; Humayun, M.; Gornicki, P.; Jelenska, J.; Joachmiak, A.; Missiakas, D. M.; Scheenwind, O., *Science.* **2003,** 299, 906-909.
10. Skaar, E. P.; Gaspar, A. H.; Scheenwind, O., *J. Biol. Chem* **2004,** 279, 436-443.
11. Clarke, S. R.; Foster, S. J., *Infect. Immun.* **2008,** 76, 1518-1526.
12. Clarke, S. R.; Mohamed, R.; Bian, L.; Routh, A. F.; Kokai-Kun, J. F.; Mond, J. J.; Tarkowski, A.; Foster, S. J., *Cell Host Microbe.* **2007**.
13. Clarke, S. R.; Wiltshire, M. D.; Foster, S. J., *Mol. Microbiol.* **2004,** 51, 1509-1519.
14. Grigg, J. C.; Vermeiren, C. L.; Heinrichs, D. E.; Murphy, M. E., *Mol. Microbiol.* **2007,** 63, 139-149.
15. Vermeiren, C. L.; Pluym, M.; Mack, J.; Heinrichs, D. E.; Stillman, M. J., *Biochem.* **2006,** 45, 12867-12875.
16. Torres, V. J.; Pishchany, G.; Humayun, M.; Scheenwind, O.; Skaar, E. P., *J. Bacteriol.* **2006,** 188, 8421-8429.
17. Dryla, A.; Gelbmann, D.; Gabain, A. v.; Nagy, E., *Mol. Microbiol.* **2003,** 49, 7-53.
18. Grigg, J. C.; Vermeiren, C. L.; Heinrichs, D. E.; Murphy, M. E., *J. Biol. Chem.* **2007,** 282, 28815-28822.
19. Mack, J.; Vermeiren, C.; Heinrichs, D. E.; Stillman, M. J., *Biochem. Biophys. Res. Commun.* **2004,** 320, 781-788.
20. Pluym, M.; Vermeiren, C. L.; Mack, J.; Heinrichs, D. E.; Stillman, M. J., *Biochem.* **2007,** 46, 12777-12787.
21. Sharp, K. H.; Schneider, S.; Cockayne, A.; Paoli, M., *J. Biol. Chem* **2007,** 282, 10625-10631.
22. Tiedemann, M. T.; Muryoi, N.; Heinrichs, D. E.; Stillman, M. J., *Biochem. Soc. Trans* **2008,** 36, 1138-1143.
23. Reniere, M. L.; Torres, V. J.; Skaar, E. P., *Biometals* **2007,** 20, 333-345.
24. Grigg, J. C.; Mao, C. X.; Murphy, M. E. P., *J. Mol. Biol.* **2011,** 413, 684-698.
25. Tong, Y.; Guo, M., *Arch. Biochem. Biophys.* **2009,** 481, 1-15.
26. Reniere, M. L.; Torres, V. J.; Skaar, E. P., *Biometals* **2007,** 20, 333-345.
27. Liu, M.; Tanaka, W. N.; Zhu, H.; Xie, G.; Dooley, D. M.; Lei, B., *J. Biol. Chem* **2008,** 283, 6668-6678.
28. Cheek, J.; Dawson, J. H., Magnetic Circular Dichroism Spectrscopy of Heme Iron Systems. Academic Press: New York, 2000.
29. Eakanunkul, S.; Lukat-Rodgers, G. S.; Sumithran, S.; Ghosh, A.; Rodgers, K. R.; Dawson, J. H.; Wilks, A., *Biochem.* **2005,** 44, 13179-13191.
30. Pluym, M.; Muryoi, N.; Heinrichs, D. E.; Stillman, M. J., *J. Inorg. Biochem.* **2008,** 102, 480-488.
31. Pluym, M.; Vermeiren, C. L.; Mack, J.; Heinrichs, D. E.; Stillman, M. J., *J. Porphyrins Phthalocyanines* **2007,** 11, 165-171.
32. Springall, J.; Stillman, M. J.; Thomson, A. J., *Biochim. Biophys. Acta* **1976,** 453, 494-501.

Chapter 4. Characterization of IsdH (NEAT domain 3) and IsdB (NEAT domain 2) in *Staphylococcus aureus* [3]

4.1 Introduction

Critical to bacterial survival is the acquisition of iron which is an essential nutrient for bacterial metabolism. *Staphylococcus aureus* (*S. aureus*) uses an iron-siderophore system for iron acquisition and transport [1]. However, free iron is very limited in human hosts due to most of the iron being sequestered by proteins such as hemoglobin, myoglobin and ferritin. In order to flourish in these growth-limiting environments, pathogens like *S. aureus* have developed mechanisms to sequester or scavenge iron from heme containing proteins such as hemoglobin.

S. aureus is able to scavenge heme using a series of iron-regulated surface determinant proteins (Isd), which are heavily expressed in iron limited environments [2, 3]. This pathway consists of four proteins anchored to the bacterial cell wall, IsdH, IsdB, IsdA and IsdC. Each of these proteins contain at least one copy of a Near Transporter (NEAT) domain which comprises of a 150 amino acid motif. However, the exceptions are IsdH, which has three NEAT domains, and IsdB, which has two NEAT domains. Of these, only the third NEAT domain of IsdH (IsdH-N3) and the second NEAT domain of IsdB (IsdB-N2) are known to bind heme. NEAT domains are present in proteins whose genes are located in the vicinity of genes encoding putative Fe^{3+} scavenging transporters [4]. The final protein is an ABC membrane transport protein IsdDEF. The proposed scheme entails heme being transferred from IsdH and IsdB on the outside of the bacterial wall, to IsdA, IsdC and finally IsdE, and then transferred into the cytoplasm [2, 5]. The current transfer model [6, 7] is based on the proposal of Scheenwind [2]. In this proposal each of these proteins is involved in binding the heme in sequence. At present, the specificities for the oxidation state of the iron in the heme, ferric or ferrous, and for a specific spin state are not known. Spectroscopic analysis using MCD spectroscopy can provide evidence for stable protein conformations that may form with either ferric or ferrous hemes and with high and low spin states. The heme-iron binding site axial ligands of the wall-located heme binding Isd proteins (IsdA, IsdC and IsdE) have been previously characterized using ESI-MS, and UV-visible absorption and MCD spectroscopy [8-11]. Each of these NEAT domains binds one heme

[3] A version of this work has been published:
Tiedemann M. T., Muryoi N., Heinrichs D. E., Stillman M. J., J. Porphyrins Phthalocyanines, **2009**, 13, 1006-1016.

molecule axially in a heme binding pocket. IsdA contains a tyrosine ligand for the ferric (Fe^{3+}) state of the heme, switching to a histidine ligand for the ferrous (Fe^{2+}) state. IsdC contains only a tyrosine ligand and therefore, is found to not bind ferrous heme and finally, IsdE contains both histidine and methionine ligands [8, 10, 12]. Furthermore, it has been experimentally determined that the NEAT domain in the Isd proteins are the 'workhorses' of the heme binding system where the rest of the protein is potentially used only for scaffolding [9, 11, 12].

In this chapter, characterization of the heme binding environment in the first two heme binding NEAT domains in the Isd pathway, namely IsdB-N2 and IsdH-N3 is described. Identification of the heme binding properties was achieved using a combination of absorption and magnetic circular dichroism (MCD) spectroscopy and electrospray ionization mass spectrometry (ESI-MS). This study leads to a comprehensive understanding of the heme scavenging and potential heme transfer properties of the first five proteins in the Isd heme transfer pathway [6].

4.2 Experimental Methods

4.2.1 Materials and Methods

Experimental procedures have been previously reported; please refer to Chapter 2 for further protein growth, protein purification, ESI-MS and MCD spectroscopy preparatory and running procedures.

4.2.2 ESI-MS Protein Experiments

Denaturation experiments were performed by lowering the pH using dilute formic acid to pH 2.0. Renaturation was done using buffer exchange centrifugation with 20 mM ammonium formate pH 7.4 using Millipore Amicon ultra-4 centrifuge filter units (10 kDa MWCO) with a Beckman CS-6 swinging-bucket Centrifuge (3000 rpm for 10 minutes per run).

4.2.3 Protein Ligand Addition

Heme loaded proteins were diluted to give an absorbance of less than 1.0 absorbance units in the Soret region before performing experiments. In all cases, addition of ligands to the proteins was monitored by absorption spectroscopy until no further change was detected before measuring the MCD spectra. After the MCD spectra were measured, the absorption spectra were

taken again to ensure no change had taken place in the heme environment. Small amounts of crystalline sodium cyanide were added to the proteins in approximately 5-fold, 10-fold or in large excess (until no change in the absorption spectrum occurred) and then the MCD spectrum was measured. Reduction of the iron was achieved by adding small amounts of crystalline sodium hydrosulfite ($Na_2S_2O_4$). Following the reduction and measurement of the absorption and MCD spectra, CO was bubbled into the solution. Solutions were monitored closely to ensure that re-oxidation to the ferric heme did not occur. The absorption and MCD spectra were recorded for the same solution at the time the MCD spectrum was measured. The MCD spectra are corrected for the zero-field CD spectral envelope.

4.3 Results and Discussion

It has been previously shown are that the NEAT domains of IsdA and IsdC, and the protein IsdE, each bind one heme. Mass spectrometry (specifically ESI-MS) can provide specific information on the changes in conformation upon heme binding (very slight) and upon denaturation (heme is lost and the protein unfolds reversibly) [10-12]. On the other hand, while the ESI-MS data cannot specifically indicate any properties of the iron of the bound heme, magnetic circular dichroism (MCD) spectra have proven over many different systems to be extremely sensitive to the electronic and ligation status of the bound iron [13-20].

4.3.1 ESI-MS data for IsdB-N2 and IsdH-N3

The ESI-MS data for IsdB-N2 and IsdH-N3 show that both only bind one heme group and that the heme is bound with minimum conformational change, Figures 4-1 and 4-2. The ESI-MS deconvoluted masses for both apo-proteins closely match the theoretical masses: for IsdB-N2, experimental from Figure 4-1 is 15,303, theoretical mass is 15,300 Da, and for IsdH-N3, experimental from Figure 4-2 is 14,172 Da, theoretical mass is 14,170 Da. For IsdB-N2 the ESI-MS data clearly show that the +8 charge state dominates for both the heme-free and heme-bound native proteins. Denaturation with acid results in loss of heme and unfolding of the protein resulting in the +17 charge state dominating. Even under these conditions, there remains a small fraction of native protein. Addition of base to raise the pH back to neutral refolds the protein and the native form is found. Even though the deconvoluted masses for each of the heme-free species (in A, C and D) are the same within the experimental error of the instrument, the

dominant charge state for the refolded protein shifts from +8 to +7, indicating a slightly different folding. The mass spectral data are excellent indicators of conformational change for very specific conditions, namely heme-free native, heme-bound native and the denatured protein. The data in Figure 4-1 and Figure 4-2 very clearly shows that both IsdB-N2 and IsdH-N3 fold in the absence of the heme, resulting in conformations similar to those when the heme is bound. One might consider that this is an excellent attribute in that heme transfer does not disrupt the folded native structure. Indeed, heme transfer experiments suggest that each protein can transfer more than one heme in sequence, implying that the heme-free protein formed following transfer can subsequently bind heme again readily [7].

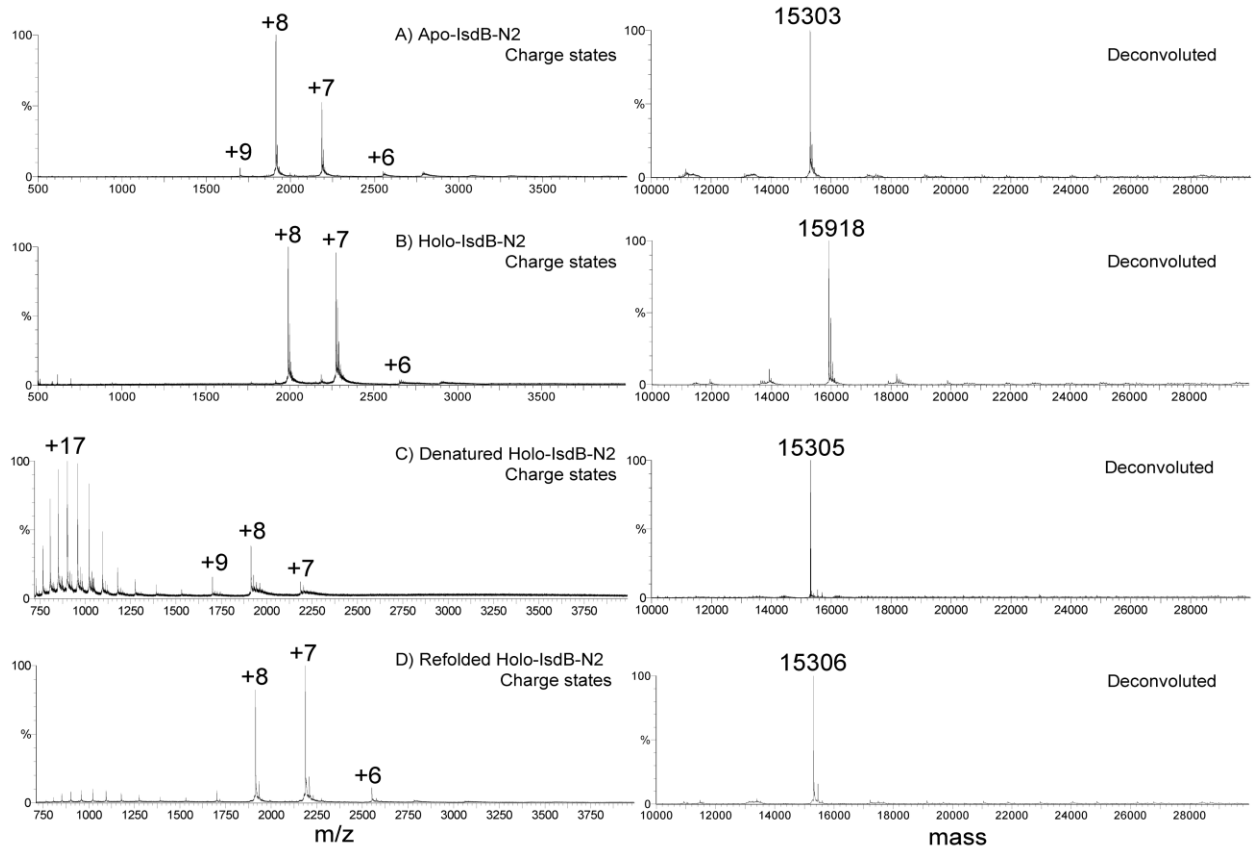

Figure 4-1 ESI-mass spectral data for IsdB-NEAT-domain 2 (IsdB-N2). (A) The charge states and deconvoluted spectrum of heme-free, native apo-IsB-N2. (B) The charge states and deconvoluted mass spectrum of heme-containing, native IsdB-N2. Note the increase in mass of 616 Da due to the iron protoporphyrin IX now bound. The charge state maximum at +8, which is the same as that for the heme-free, apo-protein in (A). (C) The charge states and deconvoluted mass spectrum of the denatured IsdB-N2 (using acid pH 2.0). Note the presence of a small fraction of heme-free, native apo-IsdB-N2 with charge states at +8. The deconvoluted spectrum shows that there is no heme bound. (D) The charge states and deconvoluted mass spectrum of the refolded (using base to raise the pH to 7.4) heme-free, native IsdB-N2.

Figure 4-2 shows the ESI-mass spectral data for IsdH-N3. The mass spectral data show that when the heme binds to the heme-free, apo-native IsdH-N3 that only very slight conformational changes occur. The dominant +7 charge state is measured for both species, with a slight shift to lower charge state values for the heme-bound, holo-protein, which suggests that there may be a minor conformational tightening with the heme bound. The deconvoluted mass difference between the apo and holo proteins is the 617 Da of the heme. Denaturation again results in the dominant charge state shifting to +15 representing an unwound protein; there is some folded protein as well. The refolding with base results in the native protein reforming together with a small fraction of heme-bound native that arises because a fraction of the released heme was still available for binding. Other groups have proposed that IsdH-N3 can bind up to four hemes [21]. This was not shown by the ESI-MS measurements in this study which utilizes a soft ionization technique; also free heme was not present in the spectra indicating that loosely associated heme was not present. This data is more consistent with the previously characterized NEAT domains and fit a biologically relevant model of heme transfer which we have previously proposed as involving a single heme in this domain.

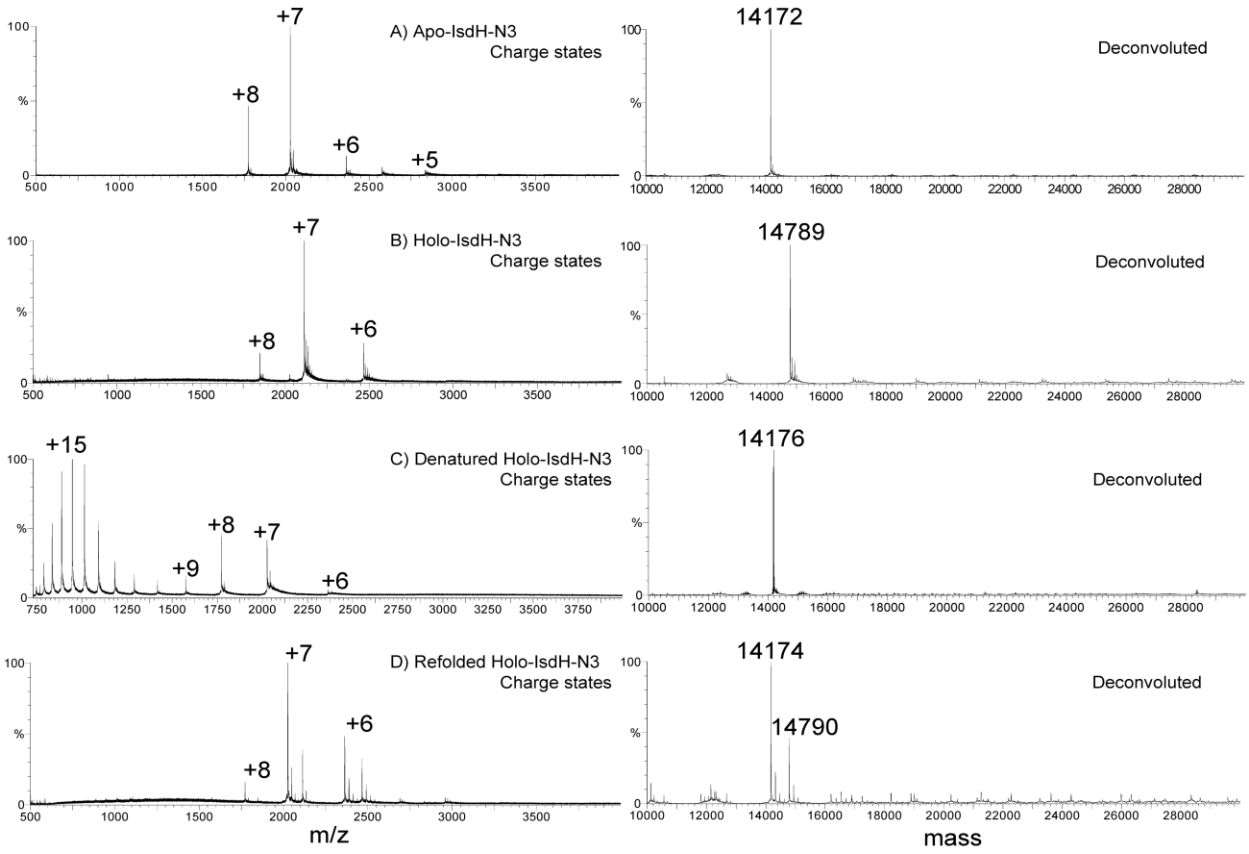

Figure 4-2 ESI-mass spectral data for IsdH-NEAT-domain 3 (IsdH-N3). (A) The charge states and deconvoluted spectrum of heme-free, native apo-IsdH-N3. (B) The charge states and deconvoluted mass spectrum of heme-containing, native IsdH-N3. Note the increase in mass of 617 Da due to the iron protoporphyrin IX now bound. The charge state maximum at +7, which is the same as that for the heme-free, apo-protein in (A). (C) The charge states and deconvoluted mass spectrum of the denatured (using acid pH 2.0) IsdH-N3. Note the presence of a small fraction of heme-free, native apo-IsdH-N3 with charge states at +8. The deconvoluted spectrum shows that there is no heme bound. (D) The charge states and deconvoluted mass spectrum of the refolded native protein, using base to raise the pH to 7.4 (mass 14,174 Da) and a small fraction of residual heme bound (mass 14,790 Da) native IsdH-N3.

4.3.2 Native heme binding of IsdB-N2 and IsdH-N3

The experiments above show that both NEAT domains exist as native heme-bound and native-heme-free forms and that denaturation is reversible. While the ESI-MS data clearly show only one heme binding, there is no information about the electronic or ligation state of the bound heme, which are critical properties for a heme transfer protein. Figures 4-3 and 4-4 compare the

absorption and MCD spectral data for IsdB-N2 and IsdH-N3 with the previously well-characterized spectra of IsdA, IsdC and IsdE. Figure 4-3 shows the absorption and MCD spectral data for the native NEAT domains of IsdH-N3 and IsdB-N2. Comparison with IsdE and the NEAT domains of IsdA and IsdC is valuable in assessing the coordination properties of the heme in each protein. The spectral envelope in three general regions centered on about 415, 540 and 630 nm can be used diagnostically. High- to intermediate-spin Fe(III) hemes are characterized by MCD spectral intensities in these three regions that are approximately equal. Specifically for high-spin Fe(III) it is common to observe a three feature envelope in the Soret region (393(-)/410(+)/430(-)) and derivative-like features at 530(+)/550(-) and 610(+)/640(-). This detail is clearly absent from the absorption spectra. This is because the MCD spectrum is dependent on both the electric and magnetic dipoles. We can conclude that IsdB-N2 and IsdH-N3 are very similar in the ligand field strength and ligand character. That is, the axial ligation of the Fe(III) in both these proteins is probably the same. Therefore, IsdB and IsdH most closely resembles IsdC, rather than the coordination in IsdE, where the heme is coordinated by tyrosine rather than histidine and 5-coordinate rather than 6. The coordination in IsdA is not like that in IsdE, and close inspection of the MCD data reveal that the differences arise from an increase in the ligand field strength but not a complete switch to low-spin Fe(III). Therefore, it can be concluded that the native ferric hemes of IsdH-N3 and IsdB-N2 are coordinated by tyrosine with the 6^{th} position empty. This conclusion about ferric bound heme to IsdH-N3 also matches the recently reported crystal structure of the protein showing a single tyrosine ligand binding the heme [21].

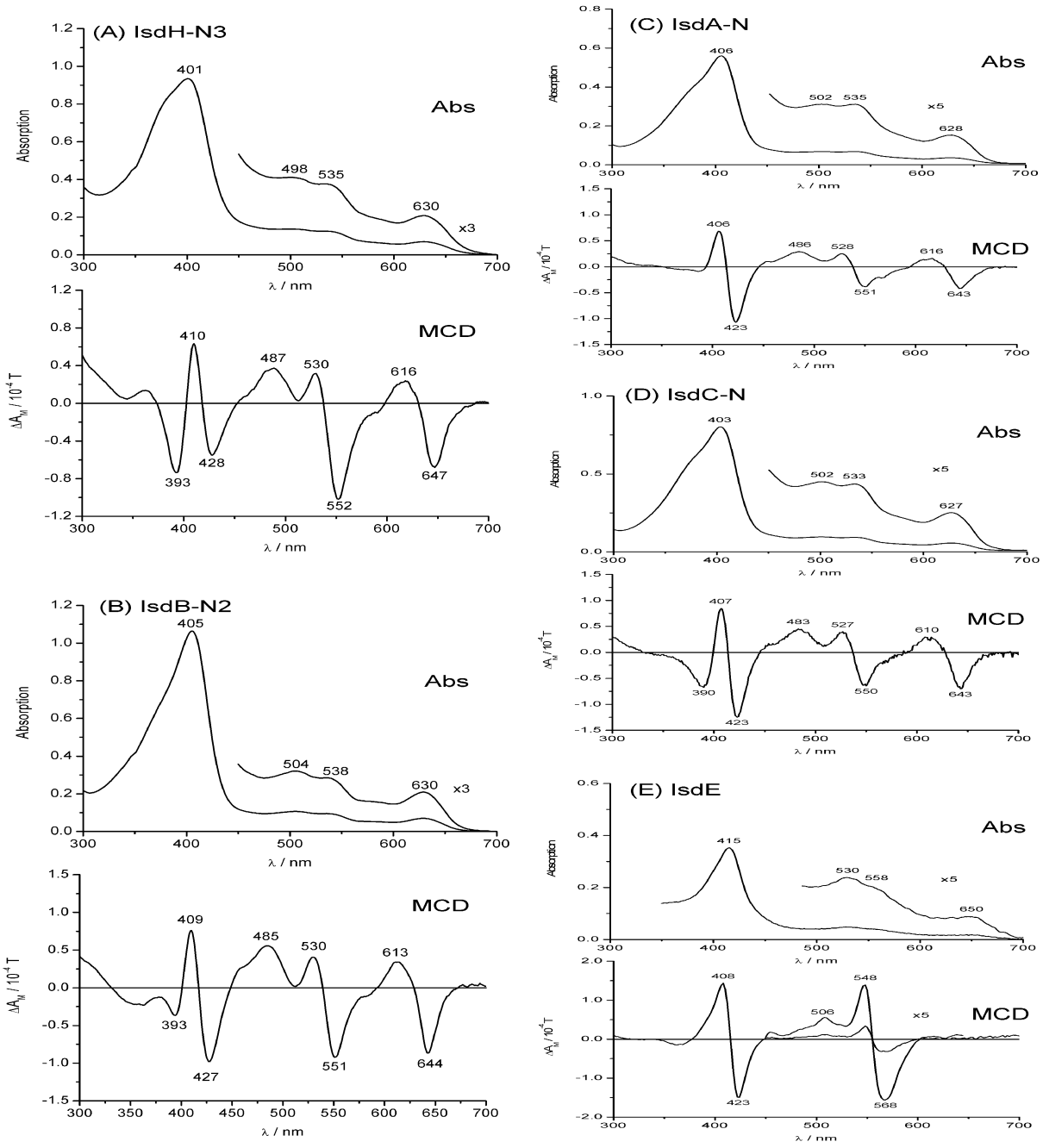

Figure 4-3 Absorption and MCD spectra of IsdH-NEAT domain 3 and IsdB-NEAT domain 2. (A) Native, heme-bound IsdH-N3. (B) Native IsdB-N2. (C) Native IsdA (NEAT domain). (D) Native IsdC (NEAT domain). (E) Native IsdE. The data for IsdA, IsdC and IsdE have been previously published [9, 10] and are presented here to allow direct comparison of the differences in spectral properties.

4.3.3 Addition of CN^- to IsdB-N3 and IsdH-N3

Figure 4-4 compares the absorption and MCD spectral data for the NEAT domains of IsdH-N3 and IsdB-N2 following the addition of CN^-. Cyanide is a well-known strong sigma donor and π-acid, resulting in low spin ferric hemes. The MCD spectral envelopes for both IsdH-N3 and IsdB-N2 exhibit the characteristic fingerprint for low spin Fe(III) with a strong derivative feature centered on the Soret band and a strong signal centered on 540 nm. The spectrum of IsdE with cyanide Figure 4-4E arises from a low spin Fe(III) heme. Neither IsdH-N3 nor IsdB-N2 exhibits this typical low spin spectral character with added cyanide. Both resemble IsdA, which was characterized as binding a low spin ferric heme. However, despite the addition of excess CN^- to IsdH-N3, it was found that there is equilibrium between bound and unbound iron. The CN^- bound heme gives the strong A term in the 420 nm region, whereas the remaining high spin heme results in the Soret band maximum at 406 nm. This would suggest that there is considerable congestion in the region of the 6^{th} position of the ferric heme resulting in much weaker binding for the CN^- than one would predict. The low spin ferric heme forms readily and nearly completely for IsdB-N2, with the Soret band maximum at 419 nm being essentially at the cross-over point of the A term.

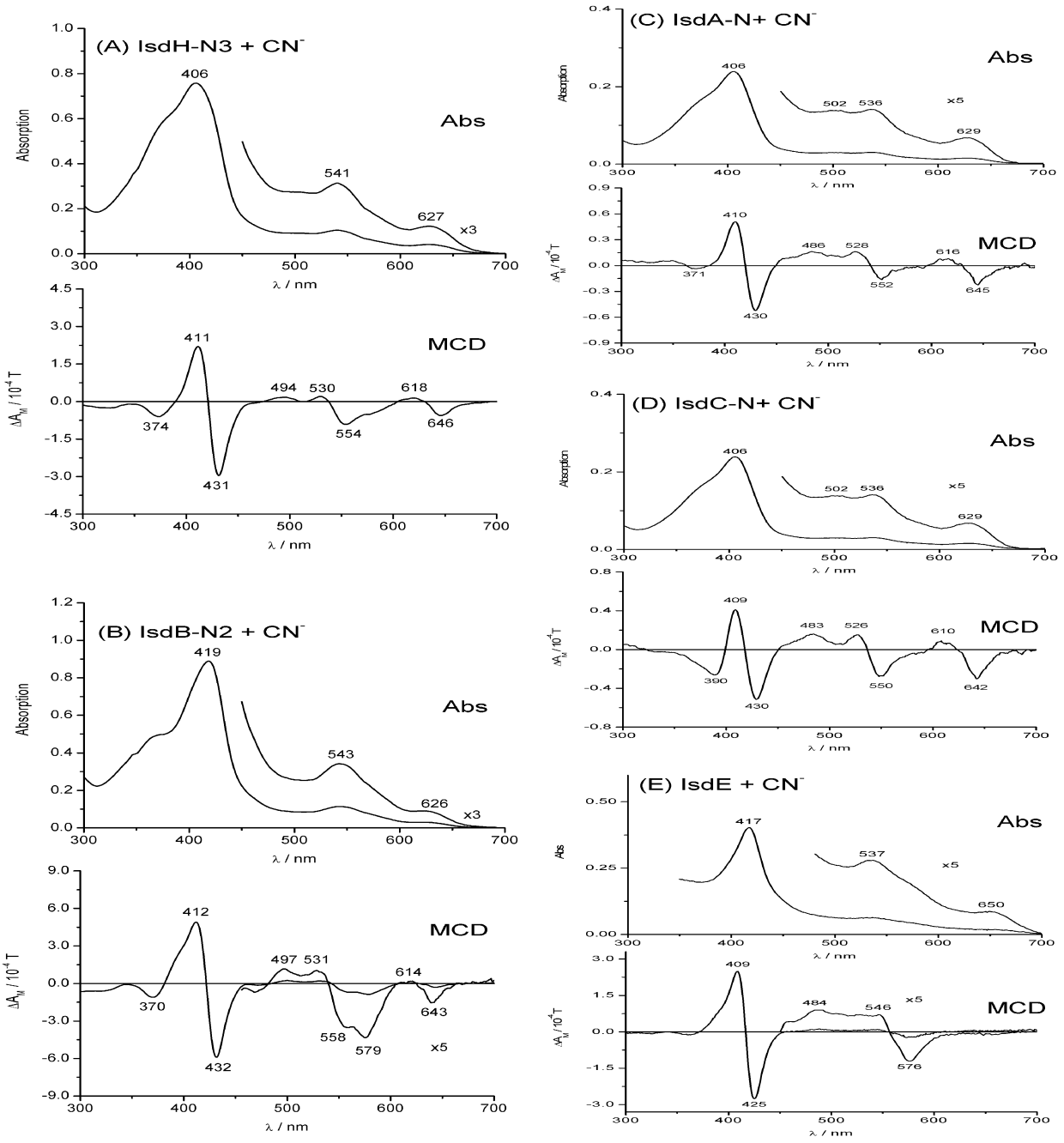

Figure 4-4 Absorption and MCD spectra of the cyanide complexed heme in IsdH-NEAT domain 3 and IsdB-NEAT domain 2. (A) Spectra when NaCN is added to native IsdH-N3. (B) Spectra when NaCN is added to native IsdB-N2. (C) Spectra when NaCN is added to native IsdA (NEAT domain). (D) Spectra when NaCN is added to native IsdC (NEAT domain). (E) Spectra when NaCN is added to native IsdE. The data for IsdA, IsdC and IsdE have been previously published [9, 10] and are presented here to allow direct comparison of the differences in spectral properties.

4.3.4 Reduced (Fe(II)) heme and CO ligand binding of IsdB-N3 and IsdH-N3

Figure 4-5 compares the absorption and MCD spectral data for the NEAT domains of IsdH-N3 and IsdB-N2 following the addition of $Na_2S_2O_4$, a well-known heme reducing agent. Upon heme reduction, both Soret bands red shift to 434 nm. Inspection of the ferrous heme spectra from IsdA and IsdE in Figure 4-5 immediately identifies differences: the ferrous hemes in IsdH-N3 and IsdB-N2 are six-coordinated like IsdE rather than the 5-coordination of IsdA. A key property of 5-coordinate ferrous heme is that the MCD spectrum appears inverted in the 430 nm region. A key property of 6-coordinate hemes is that the MCD spectrum in the Soret region exhibits a simple, positive A-term. The B:Q intensity ratio in the MCD spectra are approximately in a 1:1 ratio indicating that the heme binding environment is lower spin than in IsdE, but not the low spin found with CO added (Figure 4-6). The spectra now closely resemble that of IsdE with a characteristic derivative shaped A term centered at 559 nm. This is an indication of an unusual methionine ligand present in IsdE [10]. The increased intensity of the B band in IsdH-N3 and IsdB-N2 suggests that there has been a shift in axial ligands from tyrosine to histidine and methionine when heme was reduced from the ferric oxidation state to the ferrous oxidation state. This is not unexpected as the ferrous iron is more likely to bind to the neutral histidine nitrogen and soft methionine sulphur than to the anionic oxygen of the tyrosine. This oxidation state dependent ligand switch is modeled in Figure 4-7. Using the X-ray structure for IsdH-N3 (pdb code 2Z6F), it is possible to rotate histidine (His647) to allow the heme to be coordinated by both histidine (His647) and methionine (Met565). Finally, the data for addition of CO in Figure 4-6 result in the formation of the 6-coordinate ferrous heme for both proteins. The data more closely resemble those of a carbon monoxide bound ferrous myoglobin [13, 18] rather than IsdE, further confirming that one of the axial ligands binding the ferrous heme is now a histidine nitrogen.

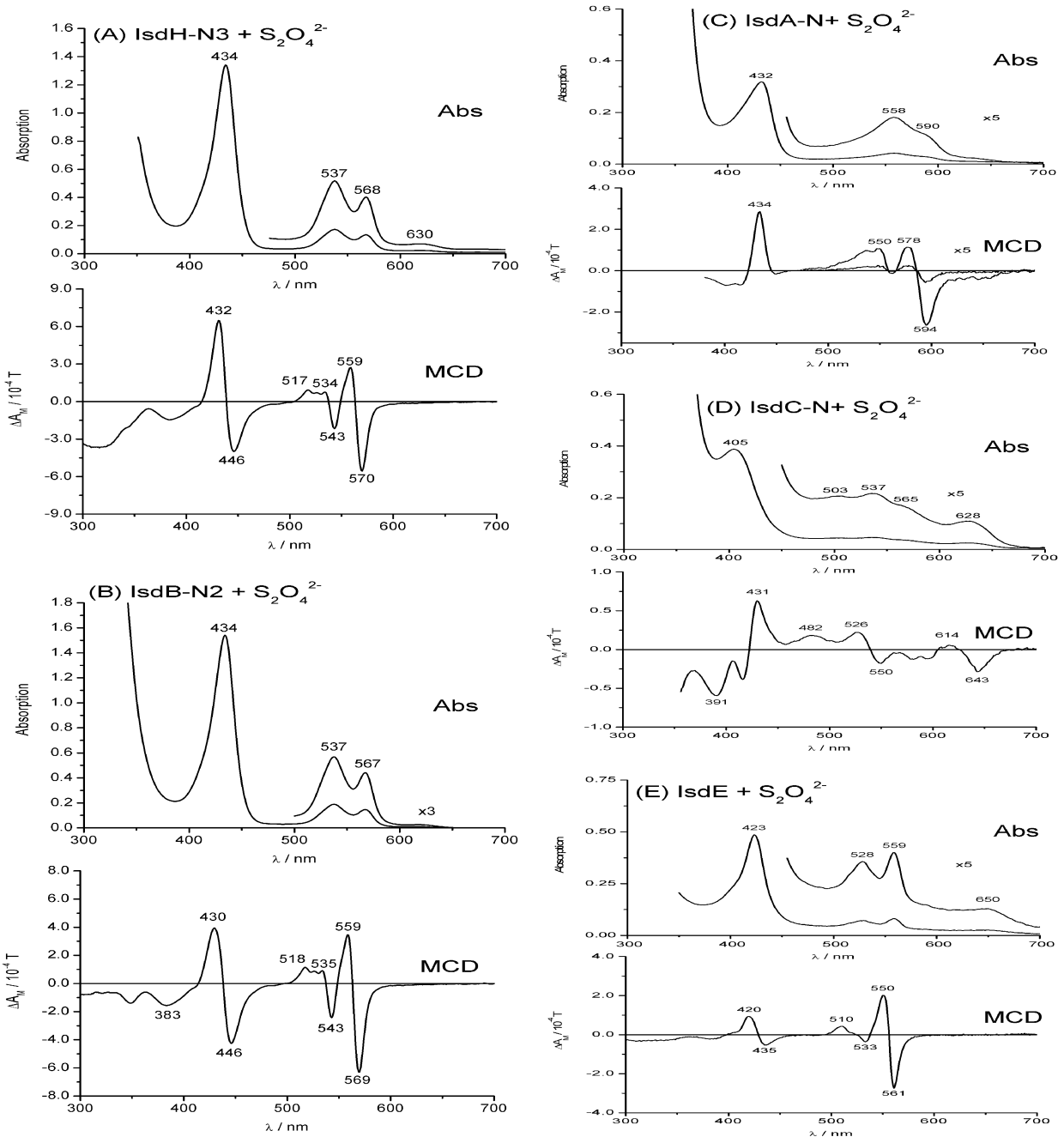

Figure 4-5 Absorption and MCD spectra of ferrous (FeII) heme in IsdH-NEAT domain 3 and IsdB-NEAT domain 2. (A) Spectra when $Na_2S_2O_4$ is added to native IsdH-N3. (B) Spectra when $Na_2S_2O_4$ is added to native IsdB-N2. (C) Spectra when $Na_2S_2O_4$ is added to native IsdA (NEAT domain). (D) Spectra when $Na_2S_2O_4$ is added to native IsdC (NEAT domain). (E) Spectra when $Na_2S_2O_4$ is added to native IsdE. The data for IsdA, IsdC and IsdE have been previously published [9, 10] and are presented here to allow direct comparison of the differences in spectral properties.

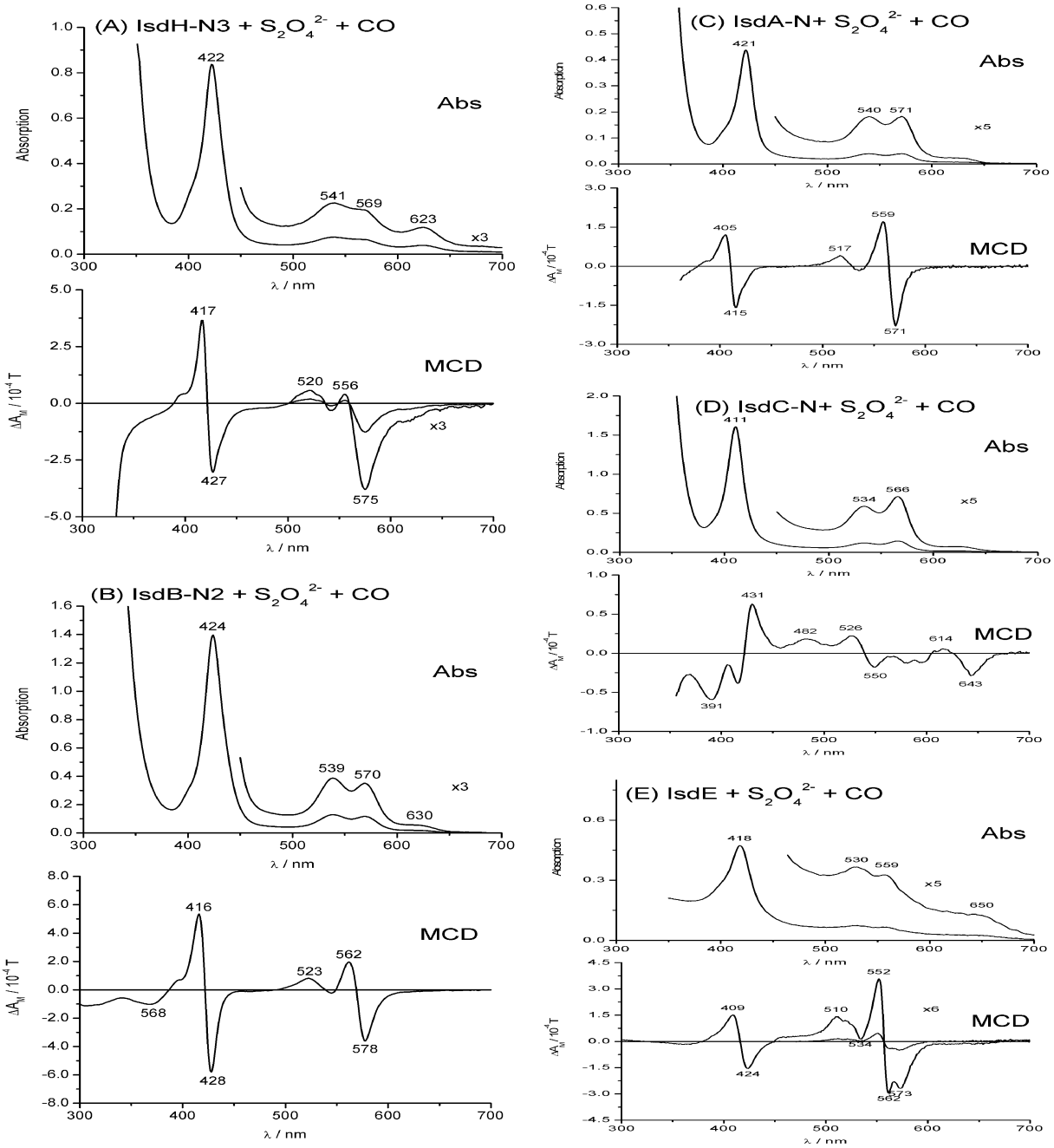

Figure 4-6 Absorption and MCD spectra of ferrous (Fe^{II}) heme with the addition of CO in IsdH-NEAT domain 3 and IsdB- NEAT domain 2. (A) Spectra when CO is added to native IsdH-N3. (B) Spectra when CO is added to native IsdB-N2. (C) Spectra when CO is added to native IsdA (NEAT domain). (D) Spectra when CO is added to native IsdC (NEAT domain). (E) Spectra when CO is added to native IsdE. The data for IsdA, IsdC and IsdE have been previously published [9, 10] and are presented here to allow direct comparison of the differences in spectral properties.

4.3.5 Conformation of IsdH-N3 crystal structure and protein conformation change upon reduced (Fe(II)) heme binding

Figure 4-7 compares the structure of the protein reported of IsdH-N3 (pdb number 2Z6F) [21], drawn using a ribbon for the protein backbone and showing the axial ligands of the heme iron. The heme iron is coordinated by tyrosine 642 in the fifth position with no ligand in the sixth position. In this native structure the heme is in a crevice with one surface exposed as shown in Figure 4-7 [21]. This coordination geometry fits the observed MCD spectral data well, resulting in a stable, high spin ferric heme. The image on the right hand side of Figure 4-7 shows the results of a calculation starting with the X-ray diffraction model using MM3 techniques in which the heme was rotated and bound axially to the nearest His (647) and Met (565). The calculation was carried out as follows: 1) The ground state geometry of the complete protein was calculated using MM3 methods with the ring bound to His647 and Met565; 2) following structural optimization, the heme and the axial ligands were subject to ground state structure optimization using ZINDO/1 methods. The structure shown is a composite of the MM3 optimization for the protein and ZINDO/1 optimization of the heme and its axial ligands. Examination of the folds of the tertiary structure of the two images reveals very little change suggesting that the ring could readily exchange axial ligands following reduction accounting for the spectral changes described above.

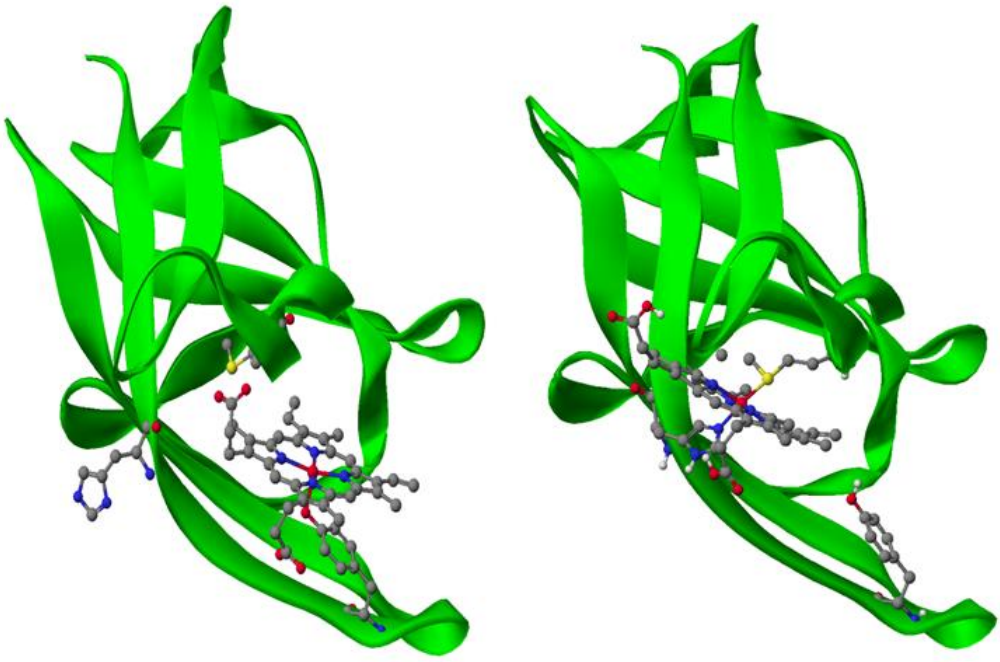

Figure 4-7 Structure of IsdH-N3 (pdb code 2Z6F). (Left) The structure as deposited in the protein data base [21], which shows the coordination of the heme iron by Tyr642. (Right) The structure calculated using MM3 and ZINDO/1 techniques showing the orientation of the heme when coordinated to His647 and Met565.

4.4 Conclusion

ESI-MS data for the heme-free forms (apo) and the heme-bound forms (holo) showed that both proteins, IsdH-N3 and IsdB-N2, remain in a folded state in the presence and absence of heme in the heme binding pocket and that each only binds one heme, in a similar manner to the other Isd proteins already characterized [8-10]. When denatured with acid, the heme dissociates and the unfolded, denatured state is observed by ESI-MS. Both proteins can then be refolded to a conformation that exhibits almost identical charge state properties as the folded apo-state. In the case of IsdH-N3, upon refolding, the protein was able to rebind some free heme, still in solution, showing that denaturation of the holo-protein is reversible. These results are in agreement with the current crystal structure of IsdH-N3, which indicate a tyrosine binding ligand in the ferric heme state and presence of a methionine in the binding pocket [21]. The absorption and MCD spectroscopy indicate that both IsdH-N3 and IsdB-N2 bind high-spin ferric hemes by tyrosine. The heme binding pocket of IsdB-N2 is accessible to small anionic ligands such as

cyanide while the heme binding pocket of IsdH-N3 is not nearly as accessible. The spectral data recorded in the reduced state indicate that the axial ligand of the iron changes from tyrosine to histidine and a methionine. This tri-ligand binding property of the two main heme scavenging proteins in the Isd pathway of *S. aureus* makes it versatile in heme transfer selectivity and able to bind heme regardless of the oxidation state. This becomes evident in our previous heme transfer study showing that IsdH-N3 and IsdB-N2 can transfer heme to all of the Isd proteins in the pathway while the other proteins are quite specific regarding which proteins can transfer heme [7]. Finally, upon reduction of the heme, the heme binding pockets open up and CO axial ligation is possible for both NEAT domains.

4.5 References

1. Andrade, M. A.; Ciccarelli, F. D.; Perez-Iratxeta, C.; Bork, P., *Genome Biol.* **2002,** 3, 1-5.
2. Skaar, E. P.; Schneewind, O., *Microbes Infect.* **2004,** 6, 390-397.
3. Mazmanian, S. K.; Skaar, E. P.; Gaspar, A. H.; Humayun, M.; Gornicki, P.; Jelenska, J.; Joachmiak, A.; Missiakas, D. M.; Scheenwind, O., *Science.* **2003,** 299, 906-909.
4. Pilpa, R. M.; Robson, S. A.; Villareal, V. A.; Wong, M. L.; Phillips, M.; Clubb, R. T., *J. Biol. Chem.* **2009,** 284, 1166-1176.
5. Skaar, E. P.; Gaspar, A. H.; Scheenwind, O., *J. Biol. Chem* **2004,** 279, (1), 436-443.
6. Tiedemann, M. T.; Muryoi, N.; Heinrichs, D. E.; Stillman, M. J., *Biochem. Soc. Trans* **2008,** 36, 1138-1143.
7. Muryoi, N.; Tiedemann, M. T.; Pluym, M.; Cheung, J.; Heinrichs, D. E.; Stillman, M. J., *J. Biol. Chem.* **2008,** 283, 28125-28136.
8. Mack, J.; Vermeiren, C.; Heinrichs, D. E.; Stillman, M. J., *Biochem. Biophys. Res. Commun.* **2004,** 320, 781-788.
9. Pluym, M.; Muryoi, N.; Heinrichs, D. E.; Stillman, M. J., *J. Inorg. Biochem.* **2008,** 102, 480-488.
10. Pluym, M.; Vermeiren, C. L.; Mack, J.; Heinrichs, D. E.; Stillman, M. J., *Biochem.* **2007,** 46, 12777-12787.
11. Pluym, M.; Vermeiren, C. L.; Mack, J.; Heinrichs, D. E.; Stillman, M. J., *J. Porphyrins Phthalocyanines* **2007,** 11, 165-171.
12. Vermeiren, C. L.; Pluym, M.; Mack, J.; Heinrichs, D. E.; Stillman, M. J., *Biochem.* **2006,** 45, 12867-12875.
13. Browett, W. R.; Stillman, M. J., *Biochim. Biophys. Acta.* **1979,** 577, 291-306.
14. Eakanunkul, S.; Lukat-Rodgers, G. S.; Sumithran, S.; Ghosh, A.; Rodgers, K. R.; Dawson, J. H.; Wilks, A., *Biochem.* **2005,** 44, 13179-13191.
15. Kobayashi, N.; Katsunori, N., *Chem. Commun.* **2007**, 4077-4092.
16. Mack, J.; Stillman, M. J.; Kobayashi, N., *Coord. Chem. Rev.* **2007,** 251, 429-453.
17. Risler, J.-L.; Groudinsky, O., *Eur. J. Biochem.* **1972,** 35, 201-205.
18. Springall, J.; Stillman, M. J.; Thomson, A. J., *Biochim. Biophys. Acta.* **1976,** 453, 494-501.

19. Sutherland, J. C., *Ann. Rev. Biosphys. Bioeng.* **1980,** 9, 293-326.
20. Vickery, L.; Nozawa, T.; Sauer, K., *J. Am. Chem. Soc.* **1975,** 98, 343-350.
21. Watanabe, M.; Tanaka, Y.; Suenaga, A.; Kurodo, M.; Yao, M.; Watanabe, N.; Arisaka, F.; Ohta, T.; Tanaka, I.; Tsumoto, K., *J. Biol. Chem.* **2008,** 283, 28649-28659.

Chapter 5. Heme binding to the IsdE(M78A; H229A) double mutant: Challenging unidirectional heme transfer in the Iron Regulated Surface Determinant (Isd) protein heme transfer pathway of *Staphylococcus aureus*[4]

5.1 Introduction

During infection, one pathway for *Staphylococcus aureus* (*S. aureus*) to scavenge iron is via the iron-regulated surface determinant (Isd) protein system. This system extracts iron from heme in hemoglobin following the lysing of red blood cells [1, 2]. The Isd system consists of nine iron-regulated proteins: IsdA, IsdB, IsdC, and IsdH are cell-wall anchored surface proteins; IsdDEF make up a membrane-localized ABC transporter; and finally, IsdG and IsdI encode heme-degrading enzymes in the cytoplasm [3, 4]. This system has been proposed [5-7] and shown [8] to pass heme through the gram-positive cell wall and cell membrane into the cytoplasm where heme is deconstructed and free iron is released. These nine proteins mediate the delivery of heme from the host's plasma into the *S. aureus* cytoplasm [9].

Traditionally, it has been considered that heme transfer pathways are facilitated through an association/dissociation mechanism. This means that heme transfer is intimately linked to the K_d of heme dissociation or K_a ($1/K_d$) of heme binding and the transfer of heme can be understood under highly predictable equilibrium conditions. However, the heme binding protein HasA (K_d~10^{-11} M) and its receptor HasR (K_d~10^{-6} M), interact which allows heme to transfer from the high-affinity protein to the lower-affinity protein [10]. In order for this to occur, there must be a protein-protein driven mechanism rather than an affinity-driven mechanism. The heme transfer is accomplished by shifts in the protein conformation and the spin state of the heme [10].

The Isd proteins of *S. auerus*, are a remarkable set of heme binding proteins because the overall heme transfer reactions span at least four proteins. Previous studies have shown that ferric heme transfer occurs in a unidirectional fashion and heme propagates down the pathway through the following sequence (with the heme proximal amino acid residue shown) IsdB-NEAT 2 (Tyr) $\rightarrow$ IsdA-NEAT (Tyr) $\rightarrow$ IsdC-NEAT (Tyr) $\rightarrow$ IsdE (His) or alternatively, initiating from

[4] A version of this work has been submitted:
Tiedemann M. T., Stillman M. J., J. Biol. Inorg. Chem., **2012**, JBIC-12-02-00019.

IsdH-N3, IsdH-N3 (Tyr) → IsdA-NEAT → IsdC-NEAT → IsdE. Significantly, IsdA does not transfer heme directly to IsdE under any conditions [11-13]. Typically the K_d of these proteins decrease along the chain of proteins, which means the heme binding becomes stronger. However, since the experimental data shows that IsdA does not transfer heme directly to IsdE, it is clear that the system does not function under an affinity mechanism. This unusual unidirectional property must require highly specific protein-protein interactions [11], which are currently unknown.

In terms of a mechanism for heme acquisition by the Isd system, previous work has shown that IsdB and IsdH capture heme from Hb released from erythrocytes by hemolysins [2, 13]. IsdH binds haptoglobin (a serum glycoprotein that protects the host from free hemoglobin) and the haptoglobin-hemoglobin complex [14, 15]. IsdA is proposed to function as a heme scavenging protein and a "heme reservoir" for IsdH and IsdB [16, 17]. IsdC, which is located in the cell wall, acts as the central conduit of heme transfer in the Isd system [9, 11, 18]. The membrane bound complex IsdDEF pumps heme across the membrane [19-22]. Heme is finally deconstructed by IsdG monooxygenase or its paralog, IsdI [3, 23]. The proteins IsdA, IsdB, IsdC and IsdH each contain at least one Near Transporter (NEAT) domain that adopts a beta sandwich structure to bind one ferric heme into a groove with heme-iron coordination via Tyr [1, 9, 11, 12, 16, 20, 22, 24, 25]. IsdE, a lipoprotein, binds heme into a shallow groove between two lobes of the protein using His to coordinate to the ferric heme-iron [19, 21]. Current studies on the Isd system in *S. aureus* are focusing on the structural aspects of the heme and heme analog binding [26], mechanistic details in terms of heme transfer/binding [27], and the heme degradation reaction [23]. However, none of these studies has yet addressed the question of how the heme transfer is constrained to a unidirectional mechanism in the sequence from IsdA to IsdC to IsdE.

In this study, the origin of the unidirectional heme transfer was investigated by utilizing the double mutant IsdE(M78A H229A) (IsdE(MH)). The double mutant effectively removes the two possible heme binding ligands within the heme binding cleft. It is shown that the protein structure of the double mutant is identical to that of native IsdE. As expected, knocking out the heme iron-amino acid ligands does significantly reduce heme binding but heme-protein associations through hydrophobicity and hydrogen bonding is not prevented, allowing heme associates in the crevice of the protein. Electrospray ionization mass spectrometry (ESI-MS), UV-visible absorption and magnetic circular dichroism (MCD) spectroscopy were used to probe

the heme binding and heme transfer properties of the double mutant of IsdE. The data shows that the amino acid ligands of the native IsdE protein also play a key role in the unidirectional heme transfer. The mutation disables the unidirectional mechanism of heme transfer to IsdE and imparts an affinity-like mechanism by heme transfer backwards up the chain from IsdE(MH) to IsdC-N and also to IsdA-N.

5.2 Materials and Methods

General techniques and experimental procedures pertaining to protein growth, protein purification, protein sample preparation, instrumental techniques and analysis can be found in Chapter 2.

5.2.1 Mutation techniques

Mutations were performed by the Heinrichs' lab. Site-specific mutations were introduced into the *isdE* gene using the QuikChange™ kit and procedure from Statagene, and confirmed by sequencing. The mass of IsdE (MH) matched the theoretical mass of 30,173 Da.

5.2.2 Equilibrium studies

For the mutant protein heme affinity measurements, stoichiometric amounts of heme in 20 mM ammonium formate buffer at pH 10, was added to apo-IsdE (MH) at pH 7.4. Samples were pH was adjusted to 7.4. ESI-mass spectral data were used to measure the relative proportions of the apo- and the reconstituted holo-IsdE(MH). The heme affinity of the IsdE was measured using a competitive reaction with apo-myoglobin. Myoglobin was made to >95% apo-form by a modified Teale's method [28]; the ratio of apo/holo was determined by mass spectrometry. 5 μM holo-IsdE was added to a solution 25 μM in apo-myoglobin. Heme transfer was monitored by ESI-mass spectrometry over a period of one hour.

5.2.3 Computational methods

Calculations were performed with CAChe 6.1.12.33 (Fujitsu, America). All calculations were carried out using the crystal structure of IsdE (Q6Q8). Using CAChe, M78 and H229 was changed to A78 and A229, respectively. Geometry optimization using the MM3 basis was performed to determine changes in protein conformation. All structural figures were created using Pymol.

5.3 Results

5.3.1 Structural Studies - native IsdE vs the mutant IsdE (MH)

ESI-mass spectral data were used to investigate the integrity of the mutant protein to see if it maintained a native structure. IsdE is a bilobed protein where the two lobes form a heme binding crevice [9]. This crevice is sensitive to the overall structure of the protein. Charge states in the ESI-mass spectral data provide an indication of the volume of the protein or solvent access to the basic amino acid residues [21, 29, 30]. A comparison of the ESI-MS charge state spectra of the mutant IsdE(MH) and intact IsdE, Figure 5-1, reveal that the mutant IsdE(MH) and the native IsdE essentially have an identical charge state distribution with a range from +13 to +10, +12 being the dominant peak for both proteins. Upon deconvolution the mass of the native and mutant proteins match their theoretical masses of 30,300 and 30,173 Da, respectively. Based on the similarity between the charged states of wild type and mutant proteins, it can be concluded that the overall structure of the protein is preserved in the mutant.

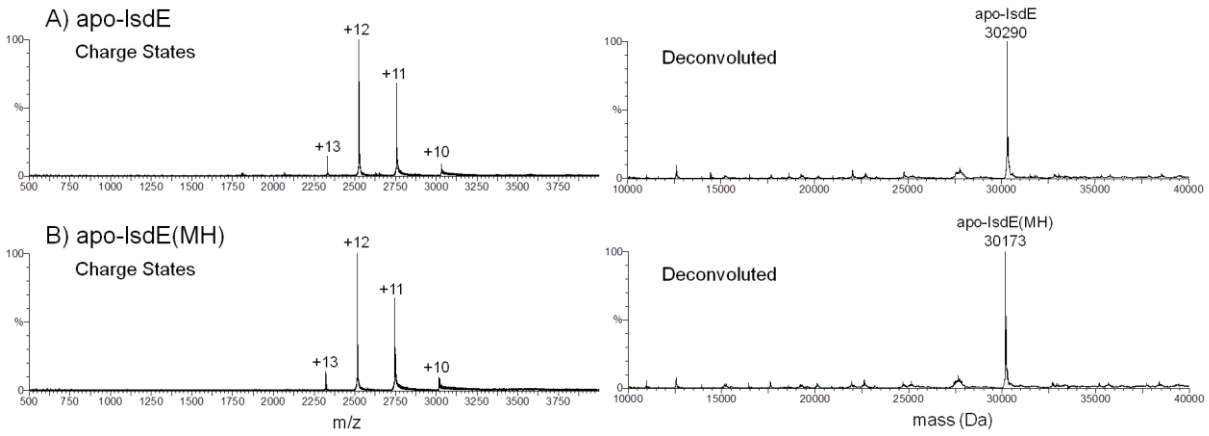

Figure 5-1 Mass/charge and deconvoluted ESI-mass spectra of the heme-free IsdE proteins (pH 7.4). A) Apo-IsdE and B) apo-IsdE(M78A; H229A) (IsdE(MH)), the mutant species. The almost identical charge state distributions, with maxima at +12, shows that the general structure and relative volumes of the two proteins are the same.

5.3.2 Equilibrium Studies with native IsdE and the mutant IsdE (MH)

No heme transfer from holo-IsdE to apo-Mb - In order to obtain a quantitative comparison of heme binding between the native IsdE and the mutant IsdE(MH) proteins, the heme binding affinity was measured under equilibrium conditions. The ESI-MS technique can be used as a quantitative technique with respect to the apo- and holo-protein pairs since both species have similar ionization efficiencies in the mass spectrometer due to the lack of conformational changes that take place upon heme binding [11]. First, in order to obtain a comparison, the heme binding properties of the native IsdE were measured. The Isd family of proteins are characterized by exceptionally strong heme binding [13, 31]. In order to accommodate this property, apo-myoglobin was used in conjunction with holo-IsdE to act as a competitor for heme binding. An important feature of the ESI-MS method is that the relative concentrations of all four species, namely, apo- and holo-myoglobin and apo- and holo-IsdE were determined simultaneously. In Figure 5-2A, the ESI-mass charge state spectra reveals that no heme transfer has taken place when 5 μM holo-IsdE is mixed with 5 equivalents of apo-myoglobin for 60 minutes, under equilibrium conditions. The dominant apo-myoglobin +7 to +10 charge states are present with no corresponding holo pairs, which would be present at the mass/charge ratio for holo-myoglobin. To support this claim, only the +13 to +10 charge states of holo-IsdE are observed in the spectrum. Upon deconvolution, the only two species that are present after one hour of the reaction are holo-IsdE at 30,916 Da and apo-myoglobin at 17,202 Da. Myoglobin has a well-known K_d of 10^{-14} M [32]. Therefore, it would be reasonable to conclude that the K_d of IsdE is less than 10^{-14} M. In that case, heme should transfer from IsdE to apo-myoglobin.

No heme transfer from holo-Mb to apo-IsdE - 5 μM holo-myoglobin was mixed with 5 equivalents of apo-IsdE for 60 minutes; this is the reverse of the experiment sequence shown in Figure 5-2A. In Figure 5-2B, the ESI-mass charge state spectra reveal that no heme transfer has taken place. Even after 60 minutes, only the holo-myoglobin (labeled HM) +7 and +8 charge states are present with no corresponding apo pairs (labeled AM in Figure 5-2A). Only the +13 to +11 charge states of apo-IsdE (labeled AE) are observed in the spectrum. No holo-IsdE (labeled HE) charge state peaks are found. Upon deconvolution, only two species are present after one hour of the reaction: apo-IsdE at 30,288 Da and holo-myoglobin at 17817 Da.

These apparently confusing results mean that there must be specific protein-protein release factors that contribute to the heme transfer reactions involving IsdE.

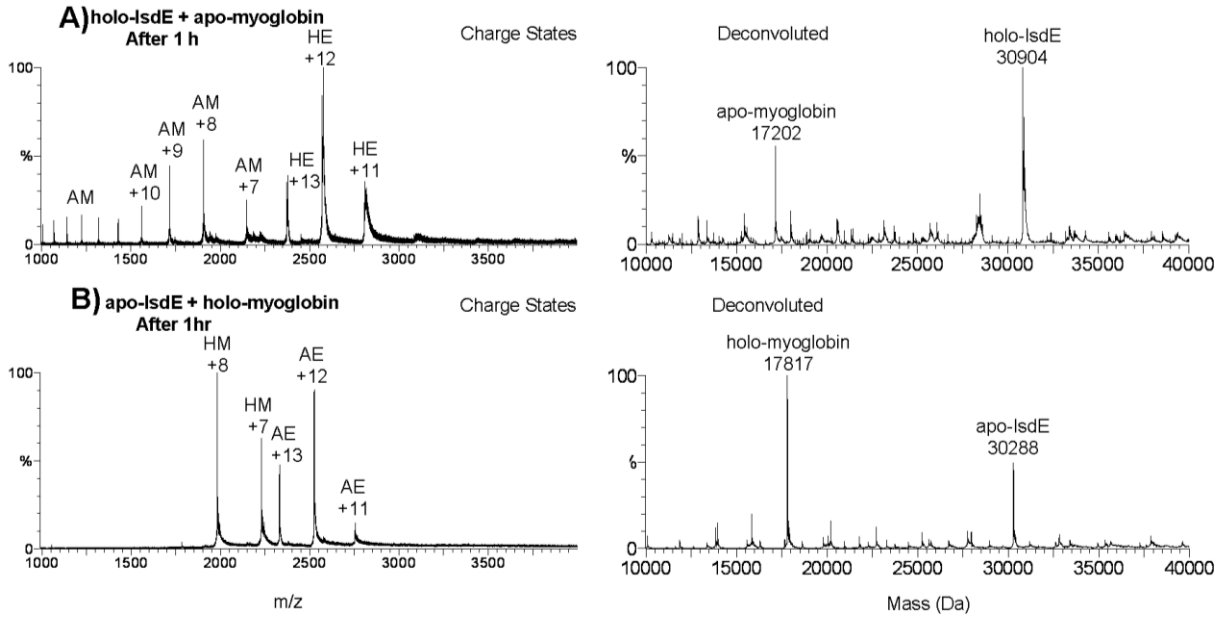

Figure 5-2 Charge state and deconvoluted ESI-mass spectra recorded during equilibrium experiments with IsdE and myoglobin (pH 7.4). A) Results after incubation of 5 μM holo-myoglobin (HM) with 5 equivalents of apo-IsdE (AE) for one hour. ESI mass spectra (charge states and deconvolution) for the mixture show the presence of only apo-IsdE and holo-myoglobin. There is no indication of the presence of either holo-IsdE (HE) or apo-myoglobin (AM) showing that no heme transfer or loss took place. B) Results after incubation of 5 μM holo-IsdE with 5 equivalents of apo-myoglobin for one hour. ESI mass spectra (charge states and deconvolution) for the mixture show the presence of only holo-IsdE and apo-myoglobin. There is no indication of the presence of either apo-IsdE or holo-myoglobin showing that no heme transfer or loss took place.

Determination of relative K_d for heme binding to IsdE(MH) - The K_d value for heme binding was obtained for the mutant IsdE(MH). Since the heme binding efficiency in the mutant was predicted to be low, it was possible to measure a direct equilibrium constant, Figure 5-3. 1.5 equivalents of heme were added to 3.0 μM apo-IsdE(MH) and under equilibrium conditions, ESI-MS was used to measure the relative heme binding. The charge states range from +13 to +11, the same as the parent apo-IsdE(MH) peaks, indicating that no major protein conformation changes have taken place. A free heme peak is present at 616 Da. Upon deconvolution, only two protein peaks are found, apo-IsdE(MH) at 30,174 Da (100% intensity) and holo-IsdE(MH) at 30,789 Da (40% intensity). The 615 Da increase in mass compared to the apo-protein, indicates heme binding. As there were no major protein conformation changes upon heme binding, it can be assumed that the protein ionization efficiency for both the apo- and holo-

IsdE(MH) are the same. Therefore, using the relative intensities of the deconvoluted mass spectra multiplied by their relative concentrations, the K_d values can be calculated directly from the deconvoluted mass spectrum with equation 1.

$$K_d = \frac{[\text{Heme}][\text{apo - IsdE(MH)}]}{[\text{holo - IsdE(MH)}]} = \frac{([\text{Heme}_0] - [\text{holo - IsdE(MH)}])[\text{apo - IsdE(MH)}]}{[\text{holo - IsdE(MH)}]} \quad (1)$$

The resultant K_d for IsdE(MH) is 9.1×10^{-6} M.

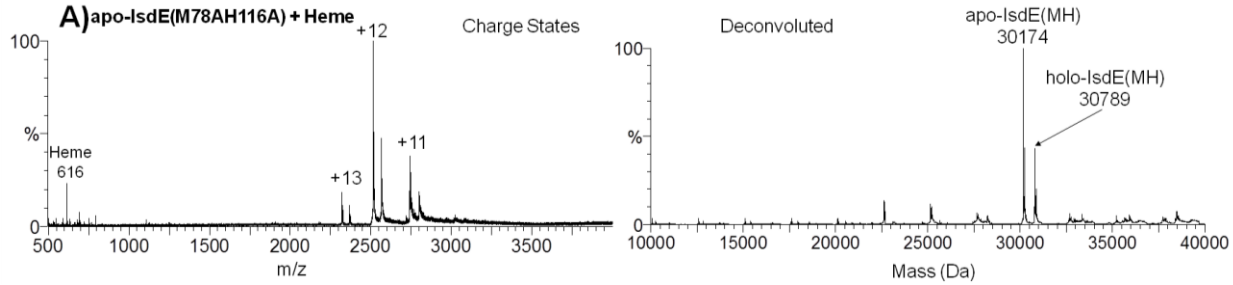

Figure 5-3 Charge state and deconvoluted ESI-mass spectra recorded during an equilibrium heme experiment with IsdE(MH) (pH 7.4) A) Results after incubation of 3 μM apo-IsdE(MH) with 1.5 equivalents of heme. Free heme is present in the charge state spectra at 616 m/z with apo- and holo-IsdE(MH) peaks with charge states +13 to +11. From analysis of the relative abundances in the deconvoluted spectra, it can be determined that the IsdE mutant protein is about 25% holo. The K_d of heme binding was calculated to be 9.1×10^{-6} M.

5.3.3 Nature of Heme Binding within IsdE (MH)

The location of the single heme found with ESI-MS cannot be on the outside of the protein. If this were the case, previous ESI-MS studies on IsdE would also show this result, indicating that IsdE would "bind" two hemes. Seeing as the mutations do not affect the overall protein conformation, the heme bound in holo-IsdE(MH) must be located in the heme crevice of the protein.

The optical spectra of heme proteins have been used to determine axial ligation of the heme in many proteins. In order to investigate the nature of heme binding in the protein crevice of IsdE(MH), UV-visible absorption and MCD spectroscopy were measured for solutions of holo-IsdE(MH) and free heme. The MCD and absorption spectra for free ferric heme in buffer (Figure 5-4, dotted line) match those that have been previously reported [33]. The MCD bands are a fingerprint for a high-spin ferric heme [34]. The addition of one equivalent of free heme to

apo-IsdE(MH) results in a shift in both the absorption and MCD spectra as seen in Figure 5-4. In the absorption spectrum (Figure 5-4A, full line), the B band broadens and red shifts from 393 to 397 nm. The shoulder to the blue of the B band peak is maintained. The broad Q band at 605 nm red-shifts to 610 nm. The MCD spectrum (Figure 5-4B, full line), is very sensitive to the heme environment and the spectral pattern changes significantly when the heme binds to the mutant. The magnitude of the B band region diminishes and the Q band magnitude increases so that the B and Q band envelopes are of about the same intensity. This is an indication of a high-spin complex, which contrasts the lower spin reported previously for the heme-bound to the native IsdE [11, 20, 21]. Overall, the MCD spectra of the free heme and the heme bound to IsdE(MH) indicate that the spin-state of the iron-heme changes only slightly when bound to the mutant protein. This differs to the dramatic spectral changes when bound by the His amino acid ligand in native IsdE [21].

The MCD spectrum in particular has been used successfully in the determination of the axial ligands binding the heme in many proteins. The major difference in the MCD spectrum of free heme compared with holo-IsdE(MH) is that the trough at 542 nm and the peak at 473 nm reverse in sign and there exists shifts in the bands from 360 to 366 nm, 395 to 400 nm and 416 to 422 nm. The sign of the MCD visible region envelope in the spectra of ferric hemes arises from the superposition of several transitions of similar magnitude but of the opposite sign. Minor changes in energies due to increases or decreases in spin can result in significantly different spectra. Therefore, the overall changes in the heme spectra indicate that the heme environment has changed when it is bound to apo-IsdE(MH). However, the MCD spectrum, is not characteristic of other heme binding proteins [12, 16, 21]. Consequently, we conclude that the heme is not directly bound by a normal amino acid residue in the protein but rather, it must be bound by π-π interactions with the heme ring, or hydrogen bonding with the heme carboxylic acid residues.

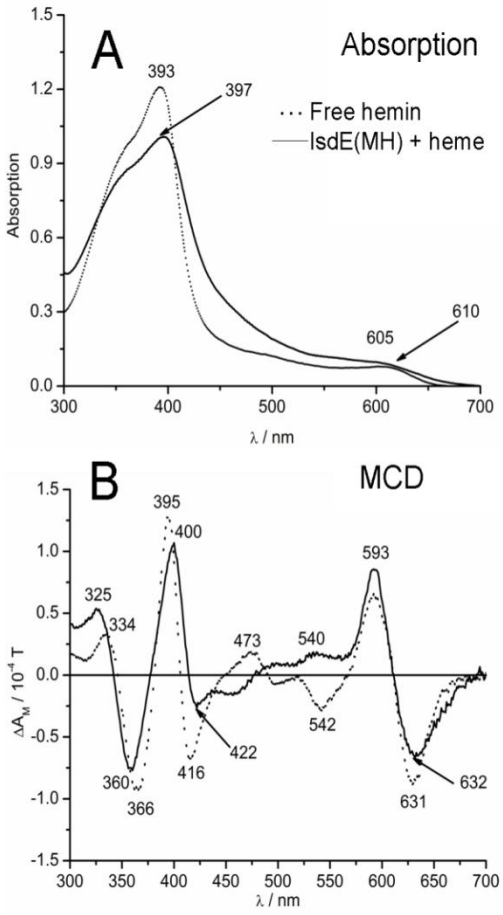

Figure 5-4 A) Absorption and B) MCD spectra recorded for free heme and heme bound to the mutant IsdE(MH) (pH 7.4)

Computational model - These results are supported by computational models. The crystal structure of IsdE (pdb: Q6Q8) [19] was used as a starting point for structure optimization and subsequently used as a model for the mutant IsdE(MH). A MM3 geometry optimization was carried out and the resultant structure was compared with the crystal structure to ensure there were no changes, Figure 5-5A. It can be seen for the calculation of the native IsdE that the MM3 optimized structure (green) is the same as the crystal structure (pink). The heme binding ligands in IsdE, M78 and H229, were then changed to A78 and A229, respectively. Another geometry optimization using MM3 forcefields was performed to view how the overall protein conformation and heme locations would change without heme binding ligands locking the heme into the heme crevice. As shown in Figure 5-5B, the heme in IsdE(MH) (red) is still located in the crevice. In order to approximate the interactions that keep the heme in the pocket, all

hydrophobic residues are colored orange, Figure 5-6. There are some potential hydrophobic interactions and π-π bonding orbital interactions with the heme ring. Furthermore, the buried carboxylic acid chain of heme is hydrogen bonded to the NH backbone of the protein from Val41 and the exposed carboxylic acid tail is hydrogen bonded with Lys62 [19].

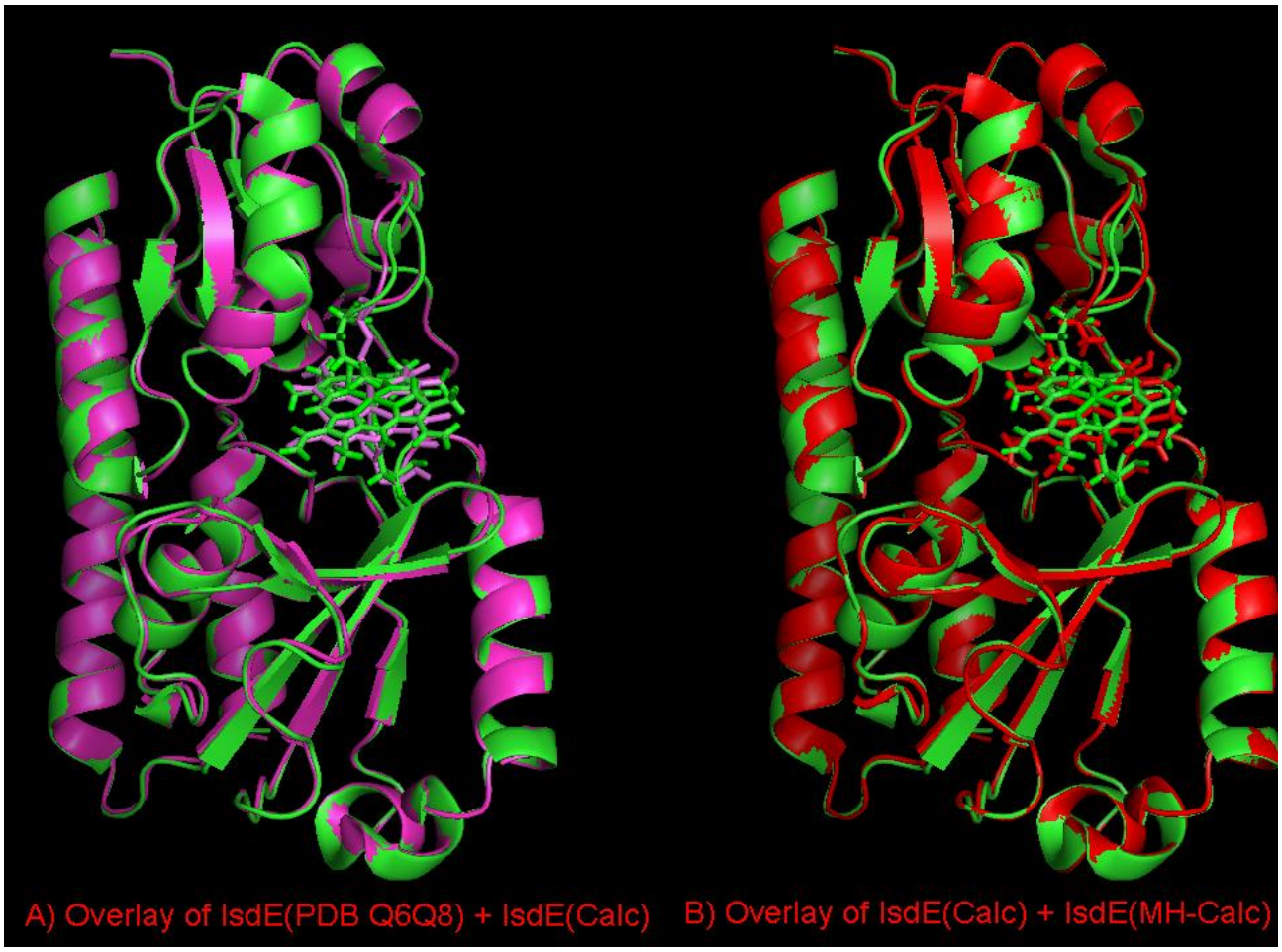

Figure 5-5 Computational model of IsdE and IsdE(MH) A) MM3 optimization (green) in comparison with the crystal structure of IsdE (pdb Q6Q8) (pink). Overall, no change in conformation is observed. B) MM3 optimization of IsdE(MH) (red) overlayed with the MM3 optimization of IsdE (green). There is no significant change in the heme location and protein conformation. Therefore, IsdE(MH) is still able to bind heme in the heme binding crevice without amino acid-heme-iron direct contact interactions.

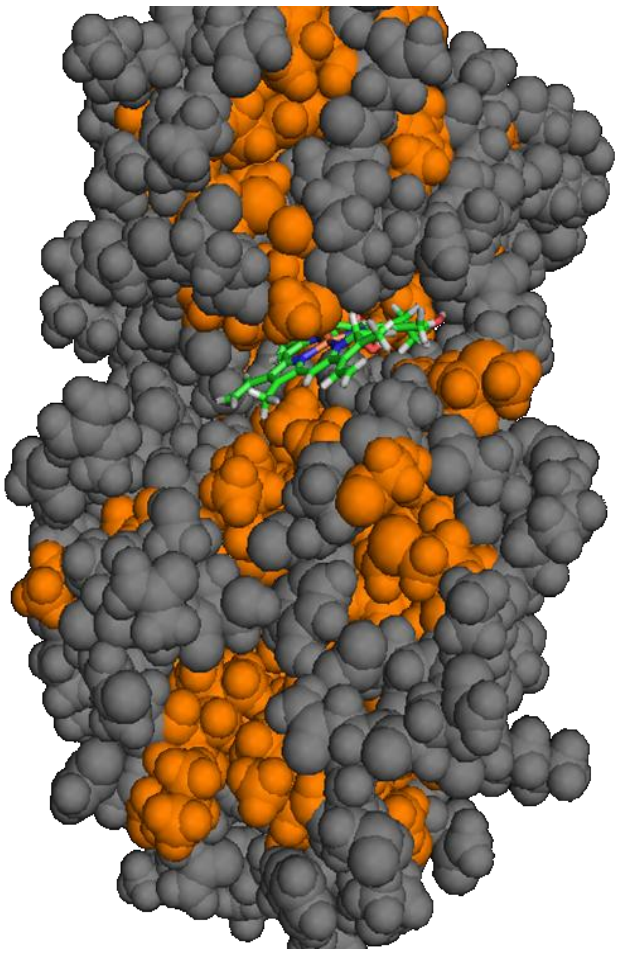

Figure 5-6 Calculation of IsdE(MH) with space filling atoms. The hydrophobic residues are colored orange to show potential interaction with the heme ring either through hydrophobicity or π-π interactions.

5.3.4 Heme Transfer from IsdC-N to IsdE(MH)

Figure 5-7 shows the UV-visible absorption, MCD spectra, and the ESI-MS charge state and deconvoluted spectrum recorded when 1.5 equivalents of apo-IsdE(MH) was added to holo-IsdC-N. It is clear that there are no shifts in the UV-visible absorption B band spectrum at 403 nm or in the Q band region at 490, 530, and 625 nm. The MCD spectrum shows the characteristic holo-IsdC-N peaks at (+) 610 nm, (+) 527 nm, (+) 483 nm, (+) 408 nm, and troughs at (-) 643 nm, (-) 550 nm, (-) 424 nm, (-) 390 nm. The lack of any changes in the optical spectra means that there are no ligand field effects or major heme environment changes when heme is bound to IsdC-N and heme transfer is initiated by addition of IsdE(MH). The lack of spectral changes suggests that no heme transfer or loss from holo-IsdC-N has taken place.

These observations are confirmed by the ESI-MS data, Figure 5-7C and Figure 5-7D. The charge state spectrum shows the previously reported +7 to +9 charge states for apo-IsdC-N and +13 to +10 for apo-IsdE(MH). However, under equilibrium conditions there is a new charge state (+14) for apo-IsdE(MH) while reacting with holo-IsdC-N. This suggests that the mutant apo-IsdE(MH) adopts a slightly more open conformation than the native apo-IsdE protein. The deconvoluted spectrum only shows two species, the holo-IsdC-N at 15,056 Da and the apo-IsdE(MH) at 30,173 Da.

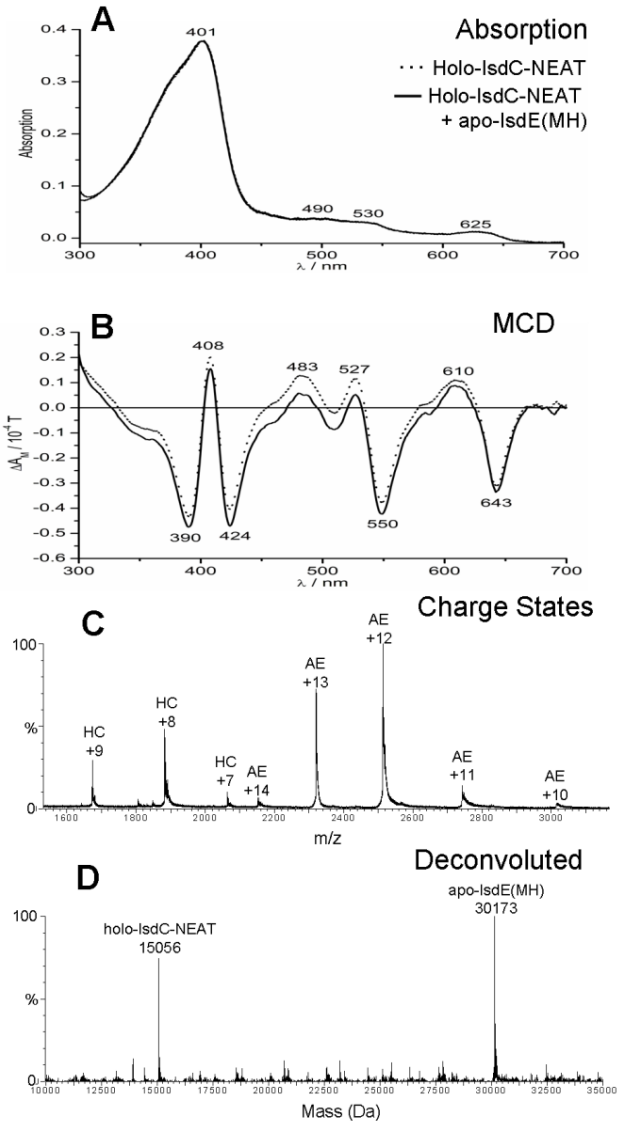

Figure 5-7 Absorption (A) and MCD (B) spectra recorded when heme-bound, native holo-IsdC-N was added to a solution of heme-free, apo-IsdE(MH) (pH 7.4). The two absorption spectra are almost superimposed. There is little change in the absorption and MCD

spectrum indicating no heme transfer between the two proteins. Mass spectral data, charge states (C) and deconvoluted (D) clearly show that no heme transfer took place and that the solution after mixing contains only holo-IsdC-N and apo-IsdE(MH).

5.3.5 The Loss of Forward Unidirectional Heme Transfer

A significant feature of the Isd pathway in *S. aureus* is the highly selective nature of heme transfer. Not only is heme transfer completely unidirectional from IsdA→IsdC and IsdC→IsdE, but there is no heme transfer from IsdA→IsdE [11]. Clearly, these highly specific reactions require protein-protein interactions. Holo-IsdE(MH) was used to challenge the irreversibility of heme transfer in the Isd system. The reverse heme transfer reactions (IsdE(MH)→IsdA, IsdE(MH)→IsdC and IsdE(MH)→IsdE) were tested in order to investigate the importance of the IsdA, IsdC, and IsdE heme binding ligands in establishing this phenomena. Reaction of holo-IsdE(MH) with either apo-IsdA-N or apo-IsdC-N or apo-IsdE yielded the same results under equilibrium conditions: the heme from IsdE(MH) transferred to each of IsdA-N, IsdC-N and IsdE.

Heme transfer from holo-IsdE(MH) to apo-IsdA-NEAT - The data in Figure 5-8A show the results of mixing 3 μM holo-IsdE(MH) with 5 μM apo-IsdA-NEAT, followed by incubation for 30 minutes. In the absorption spectrum, the B band shifts from 398 nm to 404 nm, which is typical when heme is bound to a tyrosine, as in IsdA-N. In the Q band region, a band at 627 nm appears. Further support for complete transfer of the heme to IsdA-N from the mutant IsdE is observed in the ESI mass spectral data, Figure 5-8. Under equilibrium conditions, the charge state spectra contain a mix of holo-IsdA-N (+8, +7), apo-IsdA-N (+8 to +6) and apo-IsdE(MH) (+13 to +11). Upon deconvolution it becomes apparent that the IsdE(MH), with mass 30,173 Da, contains no heme. There are now two IsdA-N peaks, one for apo-IsdA-N, at 14,632 Da and the second for holo-IsdA-N at 15,248 Da.

Heme transfer from holo-IsdE(MH) to apo-IsdC-NEAT - The data show the same result when a 3 μM holo-IsdE(MH) is incubated with 5 μM apo-IsdC-NEAT. The B band shifts from 398 nm to 402 nm. The appearance of the 627 nm band is a good indication of heme transfer to the heme binding tyrosine in IsdC-N Once again the charge state spectra only contain three species, the apo-IsdC-N (+9 to +7), the holo-IsdC-N (+9 to +7) and the apo-IsdE(MH) (+13 to +11). Upon deconvolution, only three protein species are present, the apo-IsdC-N, at 14,447 Da, the holo-

IsdC-N, at 15,063 Da and the apo-IsdE(MH) at 30,173 Da. The data show that all the heme had transferred from the mutant IsdE to the IsdC-N.

Heme transfer from holo-IsdE(MH) to apo-IsdE - The same result is found when 3 μM holo-IsdE(MH) is incubated with 5 μM apo-IsdE. Heme transfer to the native IsdE is signaled by the appearance of the strong 415 nm B band, which is characteristic of heme binding to the native IsdE due to histidine binding to the iron. The ESI mass spectral data again provide excellent conformation that all the heme transfers to the native IsdE. Figure 5-8C shows that only apo-IsdE (+13 to +11) and holo-IsdE (+13 to +11) and apo-IsdE(MH) (+13 to +11) are present in the charge state spectrum. This is confirmed by deconvolution, with only three species present in the deconvoluted spectra, the apo-IsdE at 30,300 Da, the holo-IsdE at 30,916 Da and the apo-IsdE(MH) at 30,173 Da. In each of these three cases, there is no heme bound to the mutant IsdE(MH). It is important to note that no major changes in the charge state distribution between the apo- and holo-species for either IsdA-N, IsdC-N, IsdE or IsdE(MH) were observed.

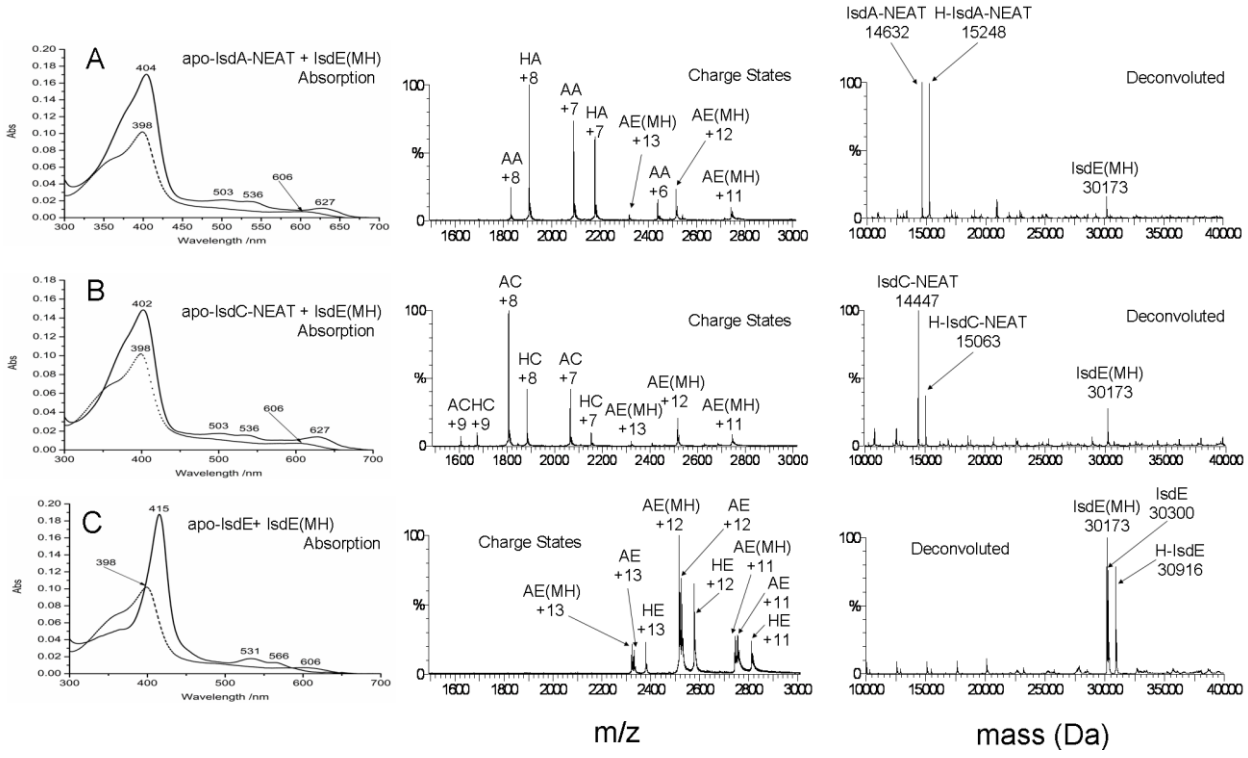

Figure 5-8 Absorption and mass spectral data for a mixture of holo-IsdE(MH) with 1.5x excess apo-IsdA-NEAT (A), apo-IsdC-NEAT (B) and apo-IsdE (C) (pH 7.4). (A) The absorption bands shift from a free-heme like spectra (Soret band centered at 398 nm) to a spectrum characteristic of holo-IsdA-NEAT (Soret band at 404 nm) indicating heme transfer. From the charge state and deconvoluted mass spectral data, three species are seen to be present in solution, apo-IsdA-NEAT (14,632 Da), holo-IsdA-NEAT (15248 Da) and apo-IsdE(MH)

(30173 Da). (B) The absorption bands shift from a free-heme like spectra (Soret band centered at 398 nm) to a spectrum characteristic of holo-IsdC-NEAT (Soret band at to 402 nm) indicating heme transfer. The charge state and deconvoluted mass spectral data show that there are three species present in solution: apo-IsdC-NEAT (14,447 Da), holo-IsdC-NEAT (15,063 Da) and apo-IsdE(MH) (30,173 Da). (C) The absorption spectrum changes from a free-heme like spectra (Soret band centered at 398 nm) to a spectrum characteristic of holo-IsdE (Soret band 415 nm) indicating heme transfer. The charge state and deconvoluted mass spectral data show that there are three species present in solution: apo-IsdE (30,300 Da), holo-IsdA-NEAT (30,916 Da) and apo-IsdE(MH) (30,173 Da).

5.4 Discussion

Typically, many heme transfer systems are thought to be affinity driven, where a dissociative/associative mechanism drives heme transfer. However, in some species, protein-protein interactions are used to circumvent heme affinity differences and to ensure heme transfer from high-affinity proteins to lower-affinity proteins [10, 35] especially with transfer from one protein with high ligand affinity, the "donor," to another with lower ligand affinity. The Isd system in *S. aureus* is also driven by protein-protein interactions and may be unique in that all of the heme transfer reactions studied in detail to date occur unidirectionally over a three-protein chain. Heme transfer in the Isd system cannot be dominated by a binding affinity mechanism. As shown in previous work on Isd proteins, protein-protein interactions drive heme transfer forward and down the protein chain (IsdA to IsdC to IsdE) [11]. Two significant properties are that heme cannot be transferred from IsdA to IsdE, skipping the IsdC intermediary, and heme cannot be transferred back from IsdE to IsdA. Clearly, if this system was under association/dissociation control, this reaction would take place resulting in equilibrium with measureable components. In the data reported in this study, a preliminary exploration of the molecular properties that control the protein-protein interactions in the Isd heme transfer system by changing the heme binding residues were investigated. It is important to note that this is a starting point for more selective mutations that can be carried out on this system to further explore the unidirectional protein-protein interaction driven system.

Figure 5-9 shows a summary of the data found in this work and a comparison of past results.

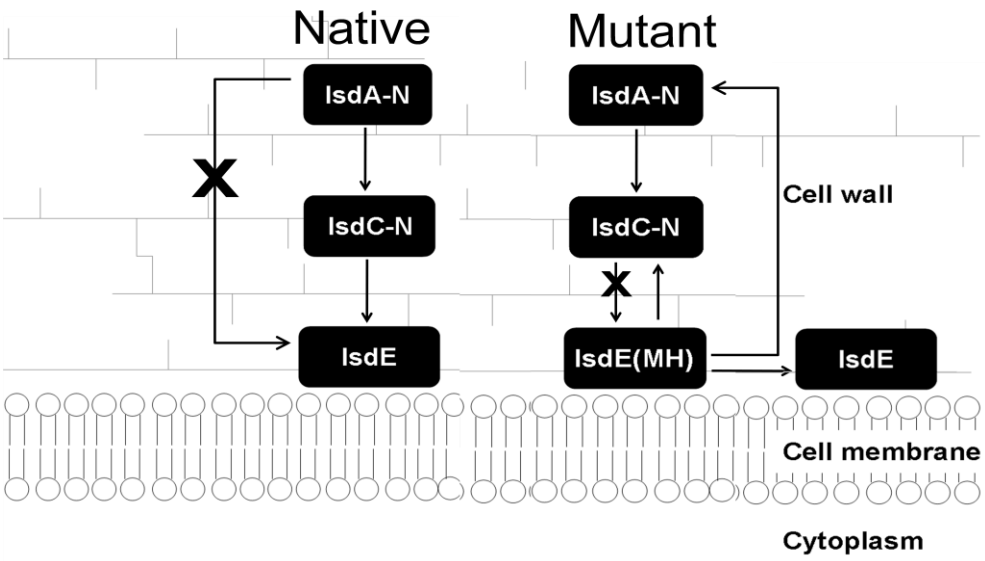

Figure 5-9 Summary of heme transfer mechanism for the native Isd proteins: IsdA, IsdC and IsdE (left) and the new results for the mutant IsdE(MH) (right) showing changes in heme transfer properties.

5.4.1 Conformation of the integrity of the IsdE double-mutant: the mutant is not denatured

IsdE is a bilobed protein, therefore, maintenance of structural protein integrity is important for comparisons of the mutant IsdE to be compared to native IsdE. The charge state distribution of proteins can be associated with the size (volume) of the protein, which can be related to the number of protonation sites. Furthermore, charge states from the ESI mass spectra very clearly distinguish between folded and unfolded or denatured proteins. Denaturation would dramatically change the heme binding properties and heme transfer properties of the IsdE protein. Denatured proteins show a high charge state value and also a large number of charge states, which typically results in a shift of charge state maxima to a lower mass to charge ratio, while a folded protein generally has fewer charge states and a prominent charge state value much lower than that of the unfolded protein [16, 21, 22]. The apo-IsdE and apo-IsdE(MH) proteins, Figure 5-1, exhibit the same charge states (+13 to +10) and charge state distribution of relative abundances are almost exactly the same. It can be concluded that altering the heme binding ligands inside the heme crevice did not affect the overall shape or folding of the protein of the mutant IsdE compared with the native IsdE. Hence, it may be proposed that the heme binding and heme transfer

properties of IsdE(MH) are entirely dependent on the available amino acids in the binding site with no contribution from changes in the structure of the protein.

5.4.2 Heme binding and affinity of IsdE(MH) compared with native IsdE

The equilibrium reaction studies show expected results where IsdE(MH) binds heme weaker than native IsdE, Figure 5-2 and Figure 5-3. Significantly, native IsdE does not bind heme from the dissociation of heme from myoglobin and myoglobin does not bind heme from the dissociation of heme from native IsdE. This result was not expected. This is specific evidence of the unique nature of IsdE in that protein-protein interactions are required to release heme. The mutant protein has a $K_d = 9.1x10^{-6}$ which is much higher than the other Isd proteins, indicating weak heme binding. Key to the heme binding and heme binding efficiency as expected, are the amino acid ligands of the ferric iron-heme. The K_d values for each Isd protein currently known are summarized in Table 5-1. The heme binding efficiency for the Isd proteins increases while moving down the heme transfer pathway. However, IsdE(MH) has a lower heme affinity than that of IsdA.

Table 5-3: Summary of heme dissociation constants (K_d) for the Isd system

Protein	Heme Dissociation Constant (K_d /M)	Reference
Myoglobin	$1x10^{-14}$	[32]
IsdA	$2.6x10^{-12}$	[31]
IsdC	$2.6x10^{-13}$	[31]
IsdE	Undetectable	This work, [13]
IsdE(M78 AH229A)	$9.1x10^{-6} \pm 0.9x10^{-6}$	This work

MCD spectroscopy was used to further investigate the location of the heme bound to the mutant IsdE. The MCD spectrum is sensitive to changes in the heme environment, not just through the specific donor atom of the amino acid binding to the heme but also through the heme binding site structure. Following addition of heme to IsdE(MH), there was a change in the MCD spectrum, however this change was not as significant as for heme binding to the native

IsdE where there are specific heme-amino acid binding ligand interactions [21]. Slight shifts in the B band region in the MCD spectrum result in a spectrum that does not resemble known spectra with ligation by donor atoms typically found binding ferric heme, such as tyrosine (with donor atom O), glutamic acid (O), histidine (N) or cysteine (S). However, while there are little changes in the B region, the MCD spectrum of the Q band region following heme binding to the mutant IsdE changes significantly as the troughs and peaks at 450 nm to 550 nm are inverted in sign. As this region is normally dominated by charge transfer between the ring and the Fe^{3+}, clearly the donor atoms of the proximal and distal residues play an important role. The lack of these residues in the double mutant results in a spectrum reflecting more the porphyrins Q band π-π^* nature and the effect of the electrostatic properties of the binding site. The changes in the heme spectra must arise because the heme is bound in the normal protein crevice. Further support that the heme can be bound even if loosely within the heme crevice comes from computational experiments. The MM3 geometry optimization calculations of IsdE(MH), Figure 5-5, show that the overall protein conformation does not change when the heme is bound. Overall, the ESI-MS and MCD data indicate that the heme is still in the crevice of protein and the computational modeling shows that other interactions besides the specific amino acid ligand-heme interactions, although weak, result in heme binding.

5.4.3 Challenging unidirectional heme transfer

The absence of heme binding ligands in IsdE(MH) is not only influential to the reduced heme binding affinity, but also critical in allowing forward unidirectional heme transfer to take place. The heme binding ligands must in some manner be involved in the (IsdC-N)(IsdE) protein-protein interactions that allow for heme transfer to take place in the native proteins.

The key mechanistic information reported in this paper can be summarized as follows in comparison to the mechanistic details known for the native proteins. Holo-IsdA-N does not transfer heme directly to IsdE and IsdE does not transfer heme to apo-IsdA-N. From both a protein-protein interaction point of view and an affinity based point of view, this means that there is a significant and highly unusual gate that restricts the heme transfer process. This study was aimed to begin to identify the controls of that gate. It was shown that holo-IsdE(MH) will transfer to apo-IsdA-N. In this case, heme was transferred backwards to the IsdA-N protein completely and irreversibly. This transfer is now under equilibrium control since the K_d of heme

binding for IsdE(MH) (~10^{-6}) is significantly higher than that of IsdA-N (~10^{-12}). Since heme transfer now takes place to all members of the Isd chain, it becomes apparent that the proximal and distal heme binding amino acid ligands in IsdE must control the gate and restrict the heme transfer direction. The mutations in IsdE(MH) eliminate the protein-protein interactions, unlocking the gate and allows the system to drive forward under affinity control. The system now works with an association/dissociation mechanism and heme transfer can now be accounted for using the relative K_d's of heme binding.

5.5 Conclusions

Heme transfer from protein to protein down the chain of proteins in the Isd system must be governed by a gate triggered by key protein-protein interactions. From this study, it is proposed that the gate residues are in the heme crevice that binds the heme in place and prevents loss due to dissociation. The heme affinities alone cannot explain the unidirectional heme transfer results from previous studies. The data show that only apo-IsdE can unlock holo-IsdC-N and only apo-IsdC-N can unlock holo-IsdA-N. Apo-IsdE cannot unlock the heme in holo-IsdA-N. Therefore, the Isd heme transfer system makes use of specific protein-protein interactions that are the key to the observed complete absence of reversal of the heme transfer reactions.

The important transfer reaction from the central conduit of the Isd system, IsdC-N to IsdE(MH) does not occur from holo-IsdC-NEAT to apo-IsdE(MH) meaning that important heme releasing triggers do not exist with IsdE(MH), effectively neutralizing important protein-protein interactions. Without the heme binding ligands the mutant IsdE now acts under affinity control transferring heme to apo-IsdA-N, apo-IsdC-N, and apo-IsdE.

In summary, the heme binding ligands in IsdE, the histidine, and methionine are essential elements in the reaction mechanism that drives the protein-protein interactions of heme transfer with regards to the unidirectional nature of the Isd system. Not only do the heme binding ligands play crucial roles in decreasing K_d values, from IsdA to IsdC and IsdE, but these ligands also dictate the selectivity and unidirectionality of the system. Finally, key protein-protein interactions and protein ligand-heme interactions must exist in order to facilitate selective transfer.

5.6 References

1. Pilpa, R. M.; Robson, S. A.; Villareal, V. A.; Wong, M. L.; Phillips, M.; Clubb, R. T., *J. Biol. Chem.* **2009,** 284, 1166-1176.
2. Torres, V. J.; Pishchany, G.; Humayun, M.; Scheenwind, O.; Skaar, E. P., *J. Bacteriol.* **2006,** 188, 8421-8429.
3. Reniere, M. L.; Skaar, E. P., *Mol. Microbiol.* **2008,** 69, 1304-1315.
4. Skaar, E. P.; Gaspar, A. H.; Scheenwind, O., *J. Biol. Chem.* **2004,** 279, 436-443.
5. Mazmanian, S. K.; Ton-That, H.; Su, K.; Scheenwind, O., *PNAS.* **2002,** 99, 2293- 2298.
6. Morrissey, J. A.; Cockayne, A.; Hammacott, J.; Bishop, K.; Denman-Johnson, A.; Hill, P. J.; Williams, P., *Infect. Immun.* **2002,** 70, 2399-2298.
7. Taylor, J. M.; Heinrichs, D. E., *Mol. Microbiol.* **2002,** 43, 1603-1614.
8. Mazmanian, S. K.; Skaar, E. P.; Gaspar, A. H.; Humayun, M.; Gornicki, P.; Jelenska, J.; Joachmiak, A.; Missiakas, D. M.; Scheenwind, O., *Science.* **2003,** 299, 906-909.
9. Grigg, J. C.; Vermeiren, C. L.; Heinrichs, D. E.; Murphy, M. E., *Mol. Microbiol.* **2007,** 63, 139-149.
10. Tong, Y.; Guo, M., *Arch. Biochem. Biophys.* **2009,** 481, 1-15.
11. Muryoi, N.; Tiedemann, M. T.; Pluym, M.; Cheung, J.; Heinrichs, D. E.; Stillman, M. J., *J. Biol. Chem.* **2008,** 283, 28125-28136.
12. Tiedemann, M. T.; Muryoi, N.; Heinrichs, D. E.; Stillman, M. J., *Biochem. Soc. Trans.* **2008,** 36, 1138-1143.
13. Zhu, H.; Xie, G.; Liu, M.; Olson, J.; Fabian, M.; Dooley, D.; Lei, B., *J. Biol. Chem.* **2008,** 283, 18450-18460.
14. Dryla, A.; Gelbmann, D.; Gabain, A. v.; Nagy, E., *Mol. Microbiol.* **2003,** 49, 37-53.
15. Watanabe, M.; Tanaka, Y.; Suenaga, A.; Kurodo, M.; Yao, M.; Watanabe, N.; Arisaka, F.; Ohta, T.; Tanaka, I.; Tsumoto, K., *J. Biol. Chem* **2008,** 283, 28649-28659.
16. Pluym, M.; Muryoi, N.; Heinrichs, D. E.; Stillman, M. J., *J. Inorg. Biochem.* **2008,** 102, 480-488.
17. Vermeiren, C. L.; Pluym, M.; Mack, J.; Heinrichs, D. E.; Stillman, M. J., *Biochem.* **2006,** 45, 12867-12875.
18. Villareal, V. A.; Pilpa, R. M.; Robson, S. A.; Fadeev, E. A.; Clubb, R. T., *J. Biol. Chem* **2008,** 283, 31591-31600.
19. Grigg, J. C.; Vermeiren, C. L.; Heinrichs, D. E.; Murphy, M. E., *J. Biol. Chem.* **2007,** 282, 28815-28822.
20. Mack, J.; Vermeiren, C.; Heinrichs, D. E.; Stillman, M. J., *Biochem. Biophys. Res. Commun.* **2004,** 320, 781-788.
21. Pluym, M.; Vermeiren, C. L.; Mack, J.; Heinrichs, D. E.; Stillman, M. J., *Biochem.* **2007,** 46, 12777-12787.
22. Tiedemann, M. T.; Muryoi, N.; Heinrichs, D. E.; Stillman, M. J., *J. Porphyrins Phthalocyanines.* **2009,** 13, 1006-1016.
23. Reniere, M. L.; Ukpabi, G. N.; Harry, S. R.; Stec, D. F.; Krull, R.; Wright, D. W.; Bachmann, B. O.; Murphy, M. E.; Skaar, E. P., *Mol. Microbiol.* **2010,** 75, 1529-1538.
24. Grigg, J. C.; Mao, C. X.; Murphy, M. E. P., *J. Mol. Biol.* **2011,** 413, 684-698.
25. Pilpa, R. M.; Fadeev, E. A.; Villareal, V. A.; Wong, M. L.; Phillips, M.; Clubb, R. T., *J. Mol. Biol.* **2006,** 360, 435-447.

26. Grigg, J. C.; Ukpabi, G.; Gaudin, C. F. M.; Murphy, M. E. P., *J. Inorg. Biochem.* **2010,** 104, 341-348.
27. Robson, S. A.; Peterson, R.; Bouchard, L.-S.; Villareal, V. A.; Clubb, R. T., *J. Am. Chem. Soc.* **2010,** 132, 9522-9523.
28. Yonetani, T., *J. Biol. Chem.* **1967,** 242, 5008.
29. Felitsyn, N.; Peschke, M.; Kebarle, P., *Int. J. Mass Spectrom.* **2002,** 219, 39-62.
30. Ruotolo, B. T.; Giles, K.; Campuzano, I.; Sandercock, A. M.; Bateman, R. H.; Robinson, C. V., *Science.* **2005,** 310, 1658-1661.
31. Liu, M.; Tanaka, W. N.; Zhu, H.; Xie, G.; Dooley, D. M.; Lei, B., *J. Biol. Chem.* **2008,** 283, 6668-6678.
32. Eakanunkul, S.; Lukat-Rodgers, G. S.; Sumithran, S.; Ghosh, A.; Rodgers, K. R.; Dawson, J. H.; Wilks, A., *Biochem.* **2005,** 44, 13179-13191.
33. Shimizu, T.; Nozawa, T.; Hatano, M., J. *Bioinorg. Chem.* **1976,** 6, 119-131.
34. Tiedemann, M. T.; Stillman, M. J., *J. Porphyrins Phthalocyanines.* **2011,** 15, 1134-1149.
35. Krieg, S.; Huche, F.; Diederichs, K.; Izadi-Pruneyre, N.; Lecroisey, A.; Wandersman, C.; Delepelaire, P.; Welte, W., *PNAS.* **2009,** 106, 1045-1050.

Chapter 6. The multi-protein heme shuttle pathway in *Staphylococcus* aureus: Isd cog-wheel kinetics[5]

6.1 *Introduction*

Iron is an essential nutrient to all forms of life being critical for a range of functions including oxygen transport and energy metabolism. However, free ferric (Fe^{3+}) iron is almost insoluble in aerobic systems with an estimated concentration of approximately 10^{-18} M [1, 2]. Under normal biological conditions iron is sequestered in ferritin, transferrin, and heme proteins in mammals. As a result, bacteria have developed multiple iron acquisition systems to facilitate their survival [3-6]. A readily accessible, and the most abundant iron source for bacteria in mammals, is iron-protoporphyrin IX (heme), which is typically bound in proteins such as hemoglobin and myoglobin. Bacteria can extract heme from hemoglobin and myoglobin using protein-based extraction pathways that generally isolate and subsequently bind the heme to the amino acid ligands His and Tyr [7-9]. The heme is then transferred through the bacterial cell wall via a series of heme binding proteins and finally to an ABC heme transporter to cross the membrane into the cytoplasm where the iron is then extracted from the protoporphyrin IX with heme degrading proteins. Examples of bacterial heme acquisition systems include the *phu* system in *Pseudomonas aeruginosa*, the *has* system in *Serratia marcescens*, and the *shu* system in *Shigella dysenteriae [9]*. The *isd* system in *Staphylococcus aureus* also carries out this function and is the heme scavenging protein system that is the focus of this present study [9].

Antibiotic-resistant bacterial infections by *S. aureus* cause a range of infections and diseases, most significantly life-threatening pneumonia, meningitis, endocarditis, and septicemia [10, 11]. The iron-regulated surface determinant (Isd) protein system extracts iron from heme in hemoglobin and myoglobin [12, 13]. The *isd* gene cluster was first identified in 2002 [14-16] and in 2003 Mazmanian *et al*. [17] proposed that the Isd series of proteins act as a heme transfer pathway across the cell wall and through the membrane of the Gram positive *S. aureus*. In *S. aureus* the Isd system consists of nine iron-regulated proteins: IsdA, IsdB, IsdC, and IsdH, which are cell-wall anchored surface proteins, and IsdEF, which constitute a substrate binding protein

[5] A version of this work is to be submitted.

and cognate membrane-localized ABC transporter and, finally, IsdG and IsdI, which are heme-degrading enzymes in the cytoplasm [18-20].

Considerable research has provided the structures and some mechanistic details of the Isd-mediated heme acquisition systems in *S. aureus*. A number of individual reactions of the Isd protein system have been reported including the binding of hemoglobin by IsdB [13, 21], the IsdH-dependent binding of haptoglobin and haptoglobin-hemoglobin [22, 23], and heme binding by IsdA, IsdB, IsdC, IsdE, and IsdH [8, 24-27]. The proteins IsdA, IsdB, IsdC and IsdH each contain at least one Near Transporter (NEAT) domain that adopts a beta sandwich structure to bind one ferric heme into a groove with heme-iron coordination via Tyr [28, 29]. IsdE, a lipoprotein and member of the class III substrate binding proteins, binds heme into a shallow groove between two α/β lobes of the protein, using His and Met to coordinate to the ferric-heme-iron [30].

Key to the proposal for the role of the Isd series of proteins in iron acquisition in *S. aureus*, is that heme passes from protein to protein in such a manner as to move spatially through first the ~90 nm thick bacterial wall and then through the bacterial membrane into the cytoplasm. Experimental evidence for the trans-wall and trans-membrane sections of the mechanism for this channeling process have not been reported to date. Techniques previously used to study the Isd system include UV-visible absorption spectroscopy (heme transfer from IsdA to IsdC), crystallography for protein structure and heme binding ligands, magnetic circular dichroism (MCD) spectral data to elucidate ligand binding to heme, and ESI-MS to elucidate the heme transfer pathway. Individual heme transfer reactions have been predominantly studied by UV-visible spectroscopy where the heme transfer kinetics between pairs of proteins has been analyzed by stopped flow spectroscopy [13, 21, 27, 31, 32]. However, a major difficulty arises when using UV-visible spectroscopy to monitor heme binding when the amino acid residues binding the iron of the heme in both the donor and receiver proteins are similar or the same, which is the case for several proteins within the Isd system. This results in very similar optical spectra leading to very small ΔA changes in the spectra during heme transfer. However, mass spectral data overcome the UV-visible absorption limitations by readily distinguishing the heme-free apo-proteins from heme-free denatured apo-proteins and from the native heme-bound holo-proteins. In previous work, it was shown that ferric heme transfer occurs in a unidirectional fashion down the pathway of the series of Isd proteins, where we indicate the proximal amino

acid residue in parenthesis, IsdB (Tyr)→ IsdA (Tyr) → IsdC (Tyr) → IsdE (His) or, alternatively, initiating from IsdH, IsdH (Tyr) → IsdA → IsdC → IsdE. Finally it was shown that heme transfer through the cell wall must occur via IsdC indicating that IsdC acts as the central conduit of the Isd system [32].

Here, the first real-time measurement of heme transfer between the three key proteins in the Isd system involved in the trans-wall channeling are reported. By exploiting the unidirectional nature of the Isd system (that is heme transfer only takes place from IsdA → IsdC → IsdE) and by using limiting concentrations of IsdC, we have explored the real-time heme transfer kinetics across these three proteins by ESI-MS. Time-resolved mass spectral data provide firm evidence for a sequential, multi-protein, heme transfer system. Determining the reaction rates from kinetic measurements for heme transfer between these three Isd proteins provides new information that directly addresses the hypothesis that the proteins function in concert as a heme shuttle system in the Gram-positive bacteria cell wall.

6.2 Experimental Methods

6.2.1 Materials and Methods

Experimental procedures have previously been reported; please refer to Chapter 2 for further protein growth, protein purification, ESI-MS and MCD spectroscopy preparatory and running procedures.

6.2.2 ESI-MS measurements

ESI-MS sample preparation can be found in previous work [32]. A Bruker micrOTOF II ESI-TOF mass spectrometer (Bruker, Canada) operated in the positive ion mode was used for all ESI-MS measurements. Samples were infused into the spectrometer at a rate of 600 μL h^{-1} using a microliter infusion pump. The instrument was calibrated with an external CsI standard solution. Data were processed using the Bruker DataAnalysis 4.0. Parameters: sample range = 500-4000 m/z; rolling average = 2 × 0.5 Hz; end plate offset = -500 V; nebulizer = 2.0 Bar; dry gas temp = 293 K; flow rate = 8.0 L/min; capillary voltage = 4200 V; capillary exit = 180 V; skimmer 1 = 22 ; hexapole = 22.50 V; hexapole rf = 600 V. The complete kinetic run was measured from a single mixture.

6.2.3 Heme transfer reactions

To monitor heme transfer between the two NEAT domains (IsdA-N and IsdC-N) and IsdE, apo-IsdC-N (for MCD) or holo-IsdC-N (for ESI-MS) was added to a mixture of holo-IsdA-N and apo-IsdE. Previous reports have shown that there is no heme transfer between holo-IsdA-N and apo-IsdE and that no free heme can be detected so that this mixture is stable [32]. Following mixing of the holo-IsdA-N and the apo-IsdE, apo-IsdC-N was added. The solution was rapidly mixed and then immediately infused into the mass spectrometer. Data were measured continuously for up to 30 minutes; however, only the first 20 minutes of data are shown. The protein concentrations were deduced from the normalized relative abundances summed from the charge states of the apo/holo pairs of the respective proteins at each time interval. The samples were held at a thermostatted temperature of 15 ˚C during infusion for ESI-MS measurements. Each transfer reaction is an average of three separate runs.

6.2.4 Kinetic Analysis

The concentration data for each species (holo-IsdA-N, apo-IsdA-N, holo-IsdC-N, apo-IsdC-N, holo-IsdE, and apo-IsdE) at each time interval for the complete kinetic reaction were analyzed using the program Copassi [33]. The reaction scheme used is described below in results section. Errors were calculated using the standard deviation for each k calculated from the fit.

6.2.5 MCD spectral measurements

MCD spectra were measured using an SM2 5.5 T superconducting magnet (Oxford, UK) attached to a J-810 CD spectrometer (Jasco Inc., Japan) with a range of 500-350 nm at 2 nm steps with a 1 sec response time and no delay between scans. A T_o spectra was measured with a solution containing holo-IsdA-N and apo-IsdE with the absence of apo-IsdC-N (No heme transfer). Spectra were then measured continuously for 40 minutes. A T_∞ spectra was taken 90 minutes after the kinetic run.

6.2.6 UV-visible absorption spectral measurements

Continuous UV-visible absorption scans were measured on a Cary50 Bio spectrometer (Varian, USA) using the Scanning Kinetics Application with a range of 200-700 nm at a scan rate of 4800 $nm \cdot min^{-1}$ with two cycles (0.2 min delay between scans for 3 minutes and 1.0 min

delay between scans for 50 minutes). Apo-IsdC-NEAT was denatured by adding SDS (2% by m/v) and then boiling the protein for 30 minutes.

6.3 Results

6.3.1 Problems with species identification with MCD spectroscopy

MCD spectroscopy has been shown to be a powerful technique not only in ligand identification of the Isd heme binding proteins but also tracking heme transfer [26, 32, 34, 35]. A solution of 6 μM holo-IsdA-N, 0.6 μM apo-IsdC-N and 9 μM IsdE was studied with continuous scanning MCD spectroscopy, Figure 6-1. As shown previously, holo-IsdA-N possesses a much different MCD spectral trace than holo-IsdE due to a switch in amino acid binding ligands, Tyr (IsdA-N) to His (IsdE) and the heme spin shift from high to low spin [32, 34, 35]. This is shown by a large increase in the B band MCD signal at 408 nm (+) and 423 nm (-) in the MCD spectrum. Due to the substoichiometric amount of apo-IsdC-N present in solution and the significant overlap of the spectral envelops of holo-IsdA-N and holo-IsdE species in solution, it was not possible to track the concentration of holo-IsdC-N and very difficult to track the concentration holo-IsdA-N in solution by MCD spectroscopy. Therefore, in order to track all species in solution and create an accurate kinetic map of the reaction, ESI-MS was used to solve the problem.

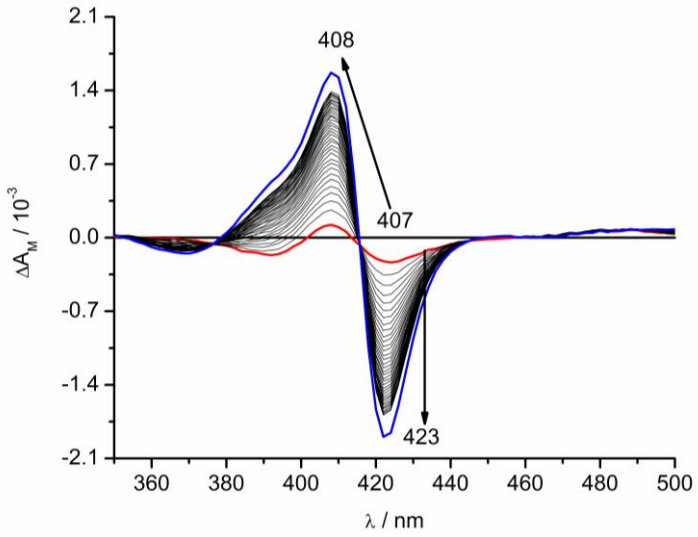

Figure 6-1 MCD spectra of the reaction between holo-IsdA-N, stoichiometrically-limiting apo-IsdC-N and apo-IsdE. Spectral changes are observed for the heme transfer from IsdA-N to IsdE through IsdC-N. The large difference between the MCD spectra of holo-IsdA-N and holo-IsdE is due to a heme binding ligand switch from Tyr (IsdA-N) to His (IsdE). A large increase in B band intensity at 423 nm (-) and 408 nm (+) can be observed throughout the reaction.

6.3.2 ESI-MS data show real-time transfer of heme from IsdA-N to isdC-N and then to IsdE

The ESI-MS technique is able to identify all of the six protein species involved in the heme transfer reaction which include heme-bound, holo-IsdA-N, holo-IsdC-N and holo-IsdE. ESI-MS can also measure spectroscopically silent apo-IsdA-N, apo-IsdC-N and apo-IsdE. The mass spectral data were obtained from a single mixed solution.

From previous work, it was shown that apo-IsdC-N efficiently removes heme from holo-IsdA-N, and then transfers heme to apo-IsdE [21, 32]. Apo-IsdE does not remove heme from holo-IsdA-N. Each NEAT domain contains a distinct amino acid composition, and therefore, a distinct mass. Hence, a similar reaction to the MCD experiment was performed using time-resolved ESI-MS, Figure 6-2, with Isd species concentration of 6 μM holo-IsdA-N, 0.45 μM holo-IsdC-N and 12 μM IsdE. Holo-IsdC-N was used because using ESI-MS the first measured point was approximately 0.5 minutes. Therefore, by starting with holo-IsdC-N, the first filling step of apo-IsdC-N is skipped and the kinetic map is more accurate. With these concentrations the stoichiometric ratio of IsdA-N:IsdC-N:IsdE was approximately 1:0.075:2 meaning that IsdC-

N must turnover approximately 13 times to complete the reaction and transfer all heme to apo-IsdE thereby imparting the role of heme shuttle onto IsdC-N.

Over the course of time the charge state data reveal all six possible species in solution. IsdA-NEAT (AA), apo-IsdC-NEAT (AC), and apo–IsdE (AE) species and the heme-bound, holo-IsdA-NEAT (HA), holo-IsdC-NEAT (HC), and holo–IsdE (HE) species. +8 and +7 charge states were observed for IsdA-N, +9 and +8 for IsdC-N and +13 to +11 for IsdE. Early in the reaction (0.5 min), the formation of holo-IsdE is detected. Only holo-IsdC-N and no apo-IsdC-N is detected indicating that the filling of IsdC-N from IsdC-N is faster than transfer to IsdE. Progressing through the reaction the disappearance of holo-IsdA-N is observed with the appearance of apo-IsdA-N charge states. By the 10 minute mark, only apo-IsdA-N peaks are observed with no holo-IsdA-N charge state peaks. After 20 minutes, some holo-IsdC-N peaks are left, only apo-IsdA-N is observed. IsdE is approximately 50% holo which corresponds stoichiometrically to the predicted stiochiometry of the reaction.

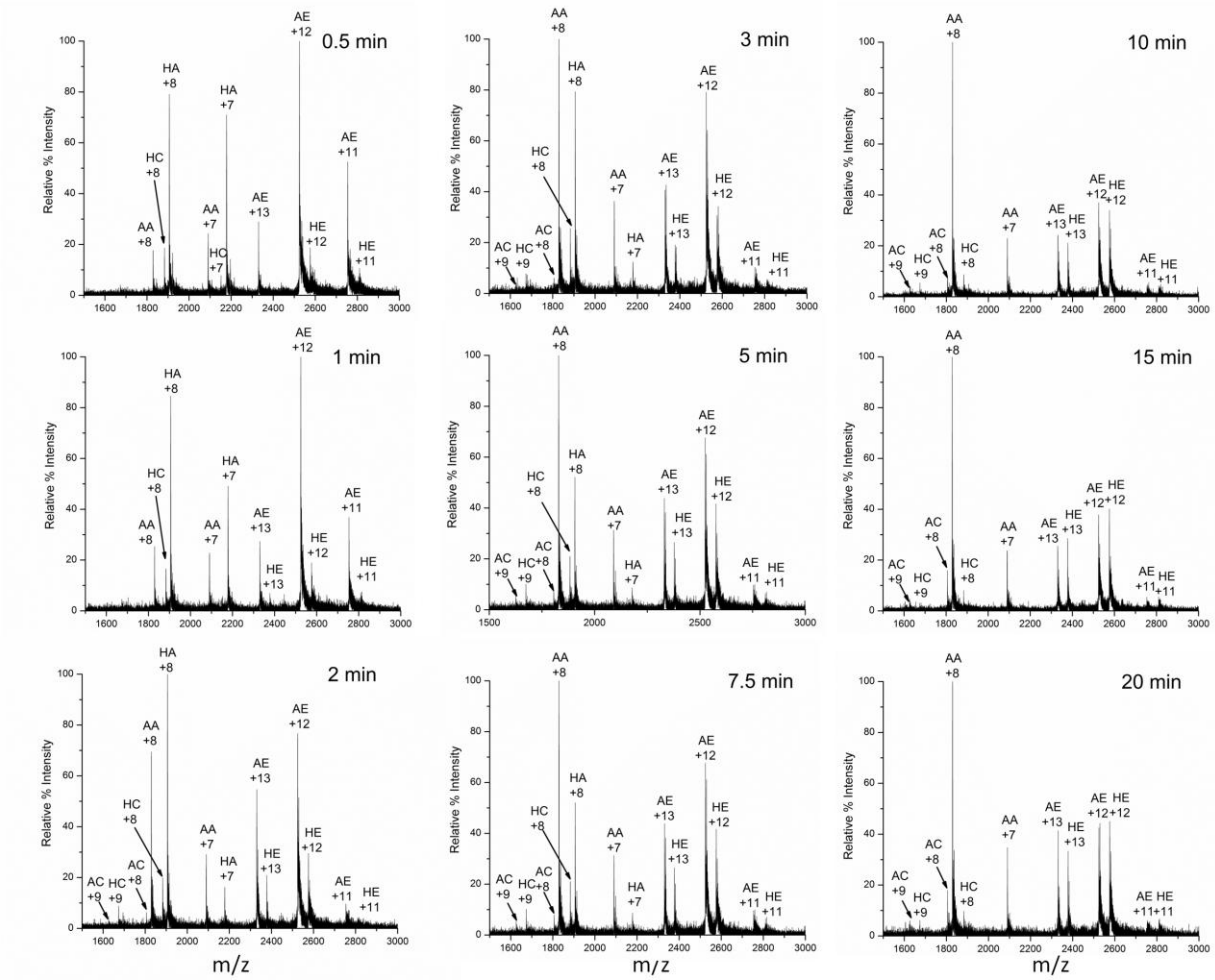

Figure 6-2 Mass spectral data recorded during heme transfer from IsdA-N to IsdE via IsdC-N. ESI-MS charge state at nine time intervals (0.5, 1.0, 2.0, 3.0, 5.0, 7.5, 10, 15 and 20 min) for the heme-free, apo-IsdA-NEAT (AA), apo-IsdC-NEAT (AC), and apo–IsdE (AE) species and the heme-bound, holo-IsdA-NEAT (HA), holo-IsdC-NEAT (HC), and holo–IsdE (HE) species. +8 and +7 charge states were observed for IsdA-N, +9 and +8 for IsdC-N and +13 to +11 for IsdE. At the start of the reaction the concentrations were: HA= 6.0 μM, AC = 0.45 μM, and AE = 12 μM. The temperature was 15 ^{o}C.

6.3.3 Determination of the reaction mechanism and the rates of reaction

To determine the mechanism of the reaction and the associated reaction rates, multifunctional analysis [33] was carried out. Quantification of charge state data requires that both apo- and holo-Isd proteins have a similar charge state distribution and, therefore, by measuring the intensity of the apo- and holo- peaks relative to each other, it is possible to calculate concentrations [32, 36]. For this analysis, all data points were fitted with a set of sequential bimolecular reaction equations. The changes in the concentrations of each of the six species as a

function of time are best seen in the three summary plots, Figure 6-3 with predicted fits and Figure 6-4 with an actual fit. Figure 6-3A shows concentration data extracted from the continuous series of ESI mass spectral scans with an irreversible scheme shown below.

$$\text{holo-IsdA-N} + \text{IsdC-N} \xrightarrow{k_1} \text{IsdA-N} + \text{holo-IsdC-N} \quad (1)$$

$$\text{holo-IsdC-N} + \text{IsdE} \xrightarrow{k_2} \text{IsdC-N} + \text{holo-IsdE} \quad (2)$$

Scheme 1: Irreversible heme transfer from holo-IsdA-N to apo-IsdC-N to apo-IsdE.

Scheme 1 was based primarily on known chemistry which shows that static transfer from holo-IsdA-N to apo-IsdC-N and transfer from holo-IsdC-N to apo-IsdE is complete and irreversible [32]. Figure 6-3A shows the time dependant ESI-MS data and multivariable fit. Clearly, this scheme does not fit this reaction. Importantly, although the IsdA-N and IsdE line fits are off, the IsdC-N fit is completely misaligned and do not overlap. Observed in the raw data, Figure 6-2, is that holo-IsdC-N never fully does transfer heme to apo-IsdE. Therefore, a reversible fit with scheme below was tried next.

$$\text{holo-IsdA-N} + \text{IsdC-N} \underset{k_2}{\overset{k_1}{\rightleftharpoons}} \text{IsdA-N} + \text{holo-IsdC-N} \quad (1)$$

$$\text{holo-IsdC-N} + \text{IsdE} \underset{k_4}{\overset{k_3}{\rightleftharpoons}} \text{IsdC-N} + \text{holo-IsdE} \quad (2)$$

Scheme 2: Reversible heme transfer from holo-IsdA-N to apo-IsdC-N to apo-IsdE.

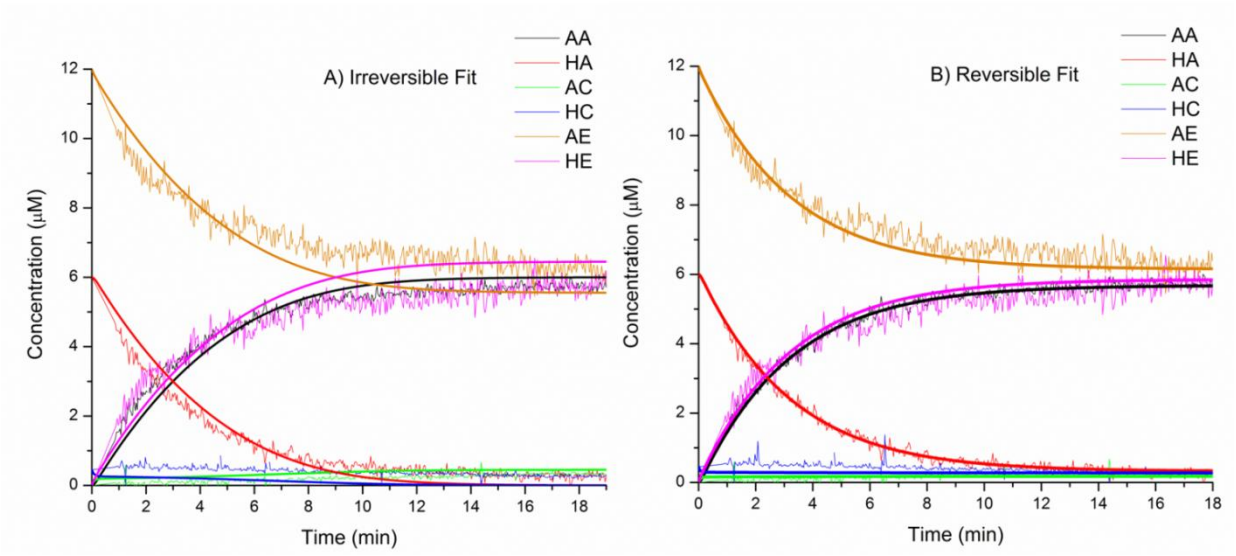

Figure 6-3 Time dependence fit using Scheme 1 and Scheme 2 with the data from Figure 6-2. A) Irreversible fit showing that this mechanism does not match what is experimentally observed. The thin lines are the experimentally determined concentrations; the thick lines represent the best fit to all the data based on Scheme 1. B) Reversible fit showing that this mechanism does potentially match the experimentally observed data except in the starting region with holo-IsdC-N. The thin lines are the experimentally determined concentrations; the thick lines represent the best fit to all the data based on scheme 2. At the start of the reaction the concentrations were: HA= 6.0 μM, AC = 0.45 μM, and AE = 12 μM. The temperature was 15 ^{o}C.

Although the reversible fit from Scheme 2 correctly fits the data, Figure 6-3B, there is significant error in first half of the fit with regards to holo-IsdC-N. A summary of the reaction rate constants can be found in Table 6-1.

Table 6-4: Bimolecular rate constants for Figure 6-3B: A reversible mechanism

Kinetic parameters using the Scheme 2 mechanism (Second order rate constants)	Specific rate constant /L μmol^{-1} s^{-1}
k_1	$2.3\text{x}10^{-2} \pm 0.2\text{x}10^{-2}$
k_2	$8.6\text{x}10^{-3} \pm 0.5\text{x}10^{-3}$
k_3	$1.1\text{x}10^{-3} \pm 0.1\text{x}10^{-3}$
k_4	$1.4\text{x}10^{-2} \pm 0.1\text{x}10^{-2}$

From these rate constants, the forward rate constant of the transfer from holo-IsdC-N to apo-IsdE (k_3) is approximately 20 times smaller than the forward rate constant of the transfer from holo-IsdA-N to apo-IsdC-N (k_1). The reversible rate constant for the transfer of holo-IsdA-N to apo-IsdC-N (k_1) is only approximately 3 times greater than the reverse transfer rate (k_2). This would have been a detectable result with ESI-MS during static experiments [32]. To further complicate analysis, the forward rate constant of holo-IsdC-N to apo-IsdE (k_3) is approximately 13 times smaller than the reverse rate constant of the reverse reaction (k_4). This result does not account for the fact that holo-IsdC-N fully and irreversibly transfers heme to apo-IsdE [32]. Therefore, this scheme must not be correct.

The cog-wheel like mechanism of heme transfer where IsdC-N acts as a heme shuttle is not a straightforward reaction. Key to the analysis is that most reactions studied in terms of heme transfer only involve the turn-over of heme once [21, 32]. Therefore, the origin of the strange chemistry that results in some of the heme being frozen in IsdC-N must lie in the turnover of IsdC-N itself. That is, the filling of apo-IsdC-N from holo-IsdA-N and transfer to apo-IsdE. This is taken into account with Scheme 3. Scheme 3 adds a third reaction: heme transfer from holo-IsdA-N to apo-IsdC-N which results in apo-IsdA-N and holo-IsdC-N*. Where holo-IsdC-N* is an inactive heme transfer protein. The time dependent ESI-MS results from Figure 6-2 are plotted using Scheme 3 and can be found in Figure 6-4. A summary of the reaction constants can be found in Table 2. The rate constant for transfer from holo-IsdA-N to apo-IsdC-N (k_1) is approximately 2.5 times as fast as transfer from holo-IsdC-N to apo-IsdE (k_2). The reaction rate constant that disables IsdC-N is approximately 9 times slower than heme transfer from holo-IsdC-N to apo-IsdE. Therefore, the progression to the disabled IsdC-N is slow and progressive.

$$\text{holo-IsdA-N + IsdC-N} \xrightarrow{k_1} \text{IsdA-N + holo-IsdC-N} \quad (1)$$

$$\text{holo-IsdC-N + IsdE} \xrightarrow{k_2} \text{IsdC-N + holo-IsdE} \quad (2)$$

$$\text{holo-IsdA-N + IsdC-N} \xrightarrow{k_3} \text{IsdA-N + holo-IsdC-N*} \quad (3)$$

Scheme 3. Reaction mechanism used to fit the experimental data

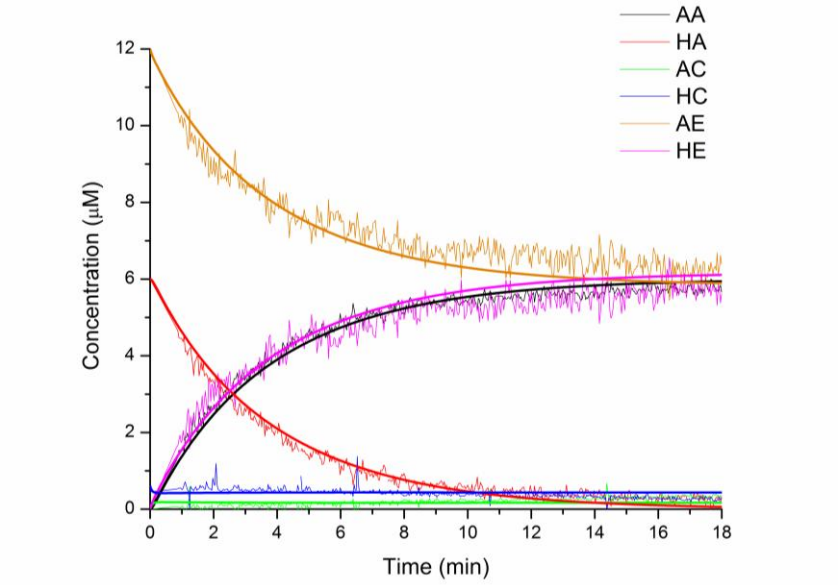

Figure 6-4 Time dependence fit using Scheme 3 with the data from Figure 6-2. The thin lines are the experimentally determined concentrations; the thick lines represent the best fit to all the data based on Scheme 3. At the start of the reaction the concentrations were: HA= 6.0 μM, AC = 0.45 μM, and AE = 12 μM. The temperature was 15 ^{o}C.

Table 6-5: Bimolecular rate constants for Figure 6-2B: A mechanism based on Scheme 3

Kinetic parameters using the Scheme 3 mechanism (Second order rate constants)	Specific rate constant /L μmol^{-1} s^{-1}
k_1	$2.3\text{x}10^{-2} \pm 0.2\text{x}10^{-2}$
k_2	$9.6\text{x}10^{-3} \pm 0.3\text{x}10^{-3}$
k_3	$1.1\text{x}10^{-3} \pm 0.1\text{x}10^{-3}$

Reaction Scheme 3 was tested by performing the same reaction as Figure 6-2 but with an increase in holo-IsdC-N, Figure 6-5. At the start of the reaction the concentrations were: HA= 6.0 μM, AC = 1.2 μM, and AE = 12 μM. By doubling the amount of holo-IsdC-N, both parts of the reaction would be affected by a concentration change. This reaction was fit with the kinetic parameters from Table 2. The fit from Figure 6-5 confirms the results from Table 2. This model is an accurate and simple explanation of the kinetics observed when IsdC-N acts as a heme shuttle and turnovers heme from IsdA-N to IsdE.

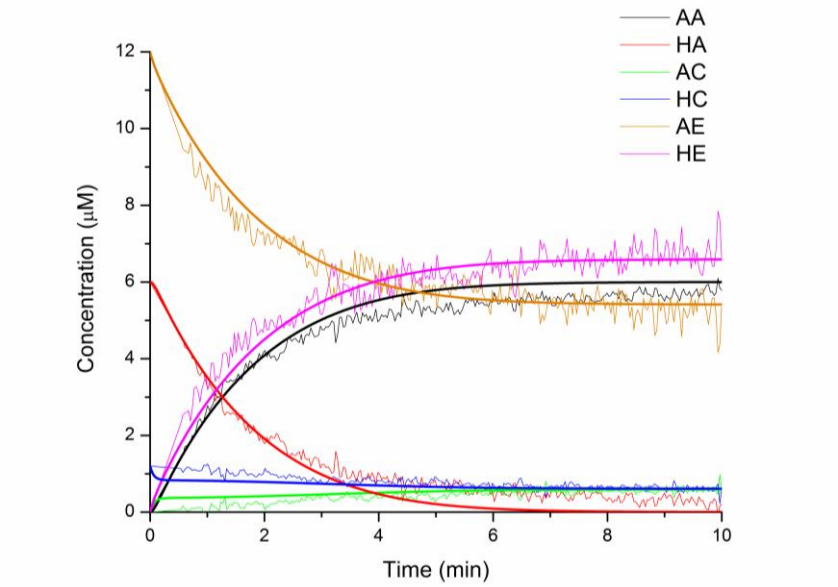

Figure 6-5 Time dependence fit using Scheme 3 with a second data set. At the start of the reaction the concentrations were: HA= 6.0 μM, AC = 1.2 μM, and AE = 12 μM. The temperature was 15 ˚C. This fit supports the mechanism from Scheme 3. The thin lines are the experimentally determined concentrations; the thick lines represent the best fit to all the data based on Scheme 3.

6.3.4 UV-visible absorption data indicate that protein conformation is important for heme transfer

The mass spectral data in Figure 6-2 provide one more important piece of information about the reaction. Charge states in the ESI mass spectrum are sensitive to changes in the volume of the protein and, therefore, provide a measure of changes in solvent access to the protein's basic amino acid residues. Protein integrity during the heme transfer reaction can be determined directly from the charge state distribution [25, 26, 32, 34, 35]. The data show that no major changes in the charge state distribution occur for the apo- and holo-species of IsdA-N, IsdC-N and IsdE. This indicates that no significant structural changes took place as a result of heme binding or release in any of these proteins. No protein degradation was observed; this observation was particularly important with respect to IsdC-NEAT following its turnovers.

A control experiment was performed in order to test if intact apo-IsdC-N must bind heme from holo-IsdA-N in order to transfer heme to apo-IsdE or if IsdC-N acts as an independent facilitator, whereby apo-IsdC-N acts as a trigger to facilitate heme transfer between holo-IsdA-NEAT and apo-IsdE, Figure 6-6. Figure 6-6A shows that heme does not dissociate or transfer from holo-

IsdA-NEAT to IsdE within the timeframe of the kinetic measurements. The Soret band for holo-IsdA-N and holo-IsdC-N is at 403 nm due to Tyr ligand binding while it would shift to 413 nm for holo-IsdE due to His binding. However, this Soret band shift is immediately observed when apo-IsdC-N is added to a solution of holo-IsdA-N and apo-IsdE, Figure 6-6B, showing that heme transfer from holo-IsdA-N to apo-IsdE has occurred. This result was mirrored in Figure 6-1 with the time dependant MCD results. In a further test, denatured apo-IsdC-N was added to a mixture of holo-IsdA-N and apo-IsdE to test if native IsdC-N is required for the heme transfer reaction to take place, Figure 6-6C. The data show that no heme transfer from holo-IsdA-N occured to apo-IsdE within the experimental timeframe, although a slight wavelength change is detectable in the Soret band of the holo-IsdA-N. This could indicate slight interactions with SDS that was added to the solution when apo-IsdC-N was added. Nonetheless no heme transfer was observed.

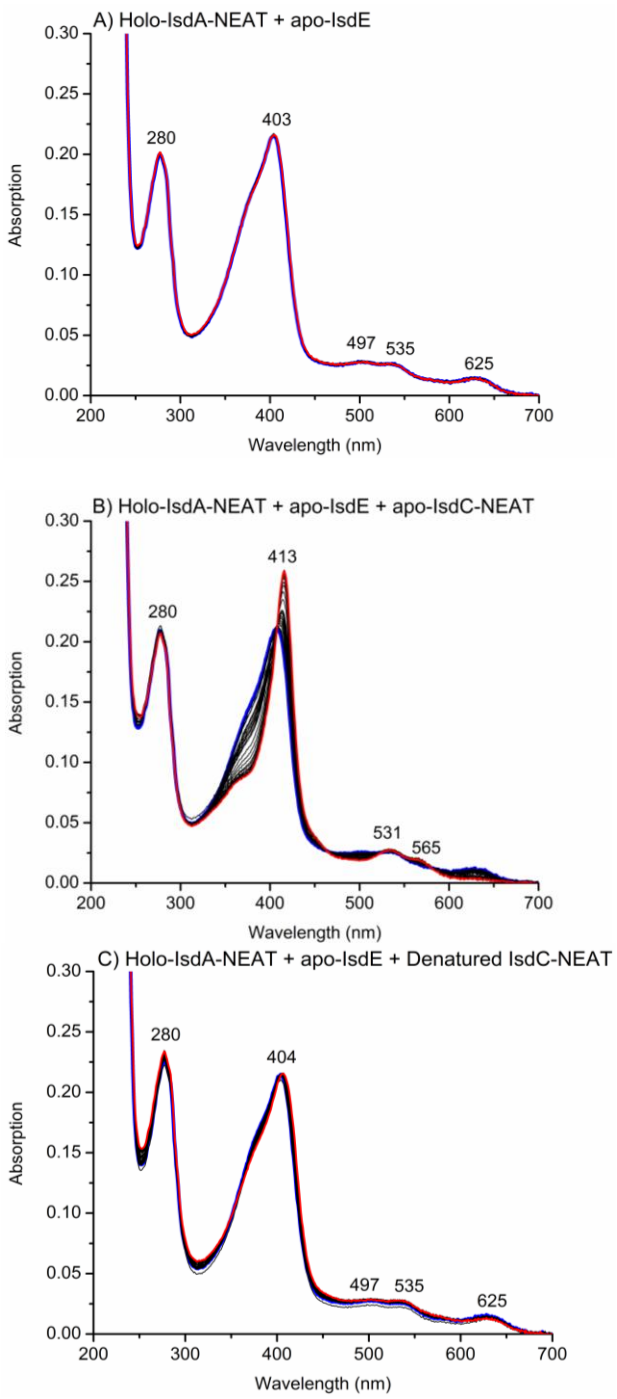

Figure 6-6 Heme transfer reactions investigating the importance of intact IsdC-N by UV-visible absorption spectroscopy. A) 6.0 uM holo-IsdA-N with 12 uM apo-IsdE showing lack of heme transfer due to no shift in the Soret band (403 nm IsdA-N (Tyr) to 413 nm IsdE (His)) B) 6.0 uM holo-IsdA-N, 0.6 uM apo-IsdC-N and 12 uM apo-IsdE showing heme transfer from IsdA-N→IsdC-N→IsdE (Shift in the Soret band from 403 nm to 413 nm indicating heme transfer to IsdE) and C) 6.0 uM holo-IsdA-N, 0.6 uM denatured apo-IsdC-N and 12 uM apo-IsdE indicating no heme transfer. Each experiment was run for 30 minutes (within the experimental timeframe of the other kinetic experiments presented)

6.4 Discussion

The proposed role of the Isd proteins is to shuttle heme through the cell wall and membrane of *S. aureus*. Two important questions are: (i) what is the actual mechanism for the heme transfer following heme acquisition? And, (ii) can the Isd system act as a catalyst with respect to heme transfer? With respect to question (i), previous equilibrium studies have shown that heme transfer that takes place from holo-IsdA-N to apo-IsdC-N and also from holo-IsdC-N to apo-IsdE is unidirectional [21, 32] implying protein to protein transfer is involved rather than a dissociative reaction mechanism, which would not impose the specificity of the reaction observed. These weak protein-protein interactions have been shown by other groups where heme transfer results from a hand-clasp model between the alpha and beta loops in the Isd protein structure just outside of the heme pocket. These interactions facilitate the NEAT domains of IsdA-N and IsdC-N coming together and forming an interactive complex [31]. Furthermore, it was determined that the heme transfer rate from IsdA to IsdC and IsdC to IsdE were >70,000 times faster than simple heme dissociation due to protein-protein interactions [27]. The data presented in this work also show a requirement for protein-protein interactions rather than a series of coupled dissociative/associative reactions.

Key to being able to answer question (ii) is the development of a technique that can differentiate between spectroscopically similar species and spectroscopically silent species regardless of the number of protein species in solution. Time dependant ESI-MS is able to perform this task. Quantitative analysis of charge state data can be performed since the apo- and holo- conformation of the Isd proteins contain similar charge states. Hence, apo- and holo- charge states can be used relatively to eac hother to quantitate the Isd species measured by ESI-MS [7, 26, 32, 37]. To answer question (ii), consideration to the complete system and the values of the rate constants reported here must be taken. IsdB or IsdH were proposed as the starting points of the heme transfer through the relatively thick (ca. 90 nm) peptidoglycan cell wall with transfer via IsdA to IsdC and then on to IsdE. It is reasonable to assume that IsdE, which is located at the membrane surface, serves as the acceptor for heme prior to its passage through the membrane and into the cytoplasm where heme is then met by the heme degrading enzymes IsdG and IsdI [18-20].

6.4.1 Relative rates of heme transfer between Isd species

The values of the specific rate constants for heme transfer from Table 6-1 for the model that fits the reactions mechanism in Scheme 3 are $2.3x10^{-2}$ $\mu M^{-1}s^{-1}$ for the first step from holo-IsdA-N to apo-IsdC-N (k_1) and $9.6x10^{-3}$ $\mu M^{-1}s^{-1}$ for the second step from holo-IsdC-N to IsdE (k_2). The reaction rates are different by a factor of ~2.5 (k_1/k_2). Since NEAT to NEAT heme transfer is relatively fast [21], this difference between the first step and the second step has a major ramification: heme will rapidly build up in IsdC in the cell wall before slowly transferring to IsdE, the protein located on the membrane as part of the ABC transporter.

Overall, these results may explain the importance of a multi-step heme passage mechanism. The introduction of the requirement for the intervention of a single protein in the heme transfer mechanism is restrictive. The data presented here, and specifically the disparity in transfer rates, suggest a possible explanation: if heme transfer was slow from IsdA to IsdC then free heme exposed during the extraction from hemoglobin, which involves IsdH and IsdB, might be lost to the bacterium. With a fast heme transfer rate into a wall-bound protein (IsdC), heme is moved deeper into the cell wall of the bacterium where it is more protected from the extracellular milieu. The subsequent slower heme transfer from IsdC to IsdE can act as a throttle for the system to control the eventual heme transport into and build up in the cytoplasm; indeed Skaar and coworkers have demonstrated heme toxicity in *S. aureus* [38].

The disabling step of IsdC-N is slow. Interestingly, this protein would still contain the same charge state mass as normal IsdC-N. This slow progressive step, ~9 times slower than normal transfer from IsdC-N to IsdE, affects the overall kinetic model and the heme transfer kinetic results. Key to the reaction is the treatment of IsdC-N. The limited concentration of IsdC-N imparts a catalytic role on this protein so that IsdC-N acts a central cog-wheel in the heme transfer system. IsdC plays the role of shuttling heme from IsdA-N to IsdE, where IsdC-N would need to turnover approximately 10 times before the reaction is finished under the experimental conditions used in this work. This disabling step might also impart protection of the Isd system. Since the Isd system is efficient at heme extraction, the central conduit of the Isd system may impart further protection from heme toxicity due to the disabling of IsdC-N.

6.4.2 *Intact Isd proteins are required to transfer heme*

The UV-visible absorption experiments show how important intact IsdC-N is to protein-protein interactions with regards to heme transfer. Importantly, disruption of the hand-clasp model by protein denaturation completely disables heme transfer [31].

6.5 Conclusion

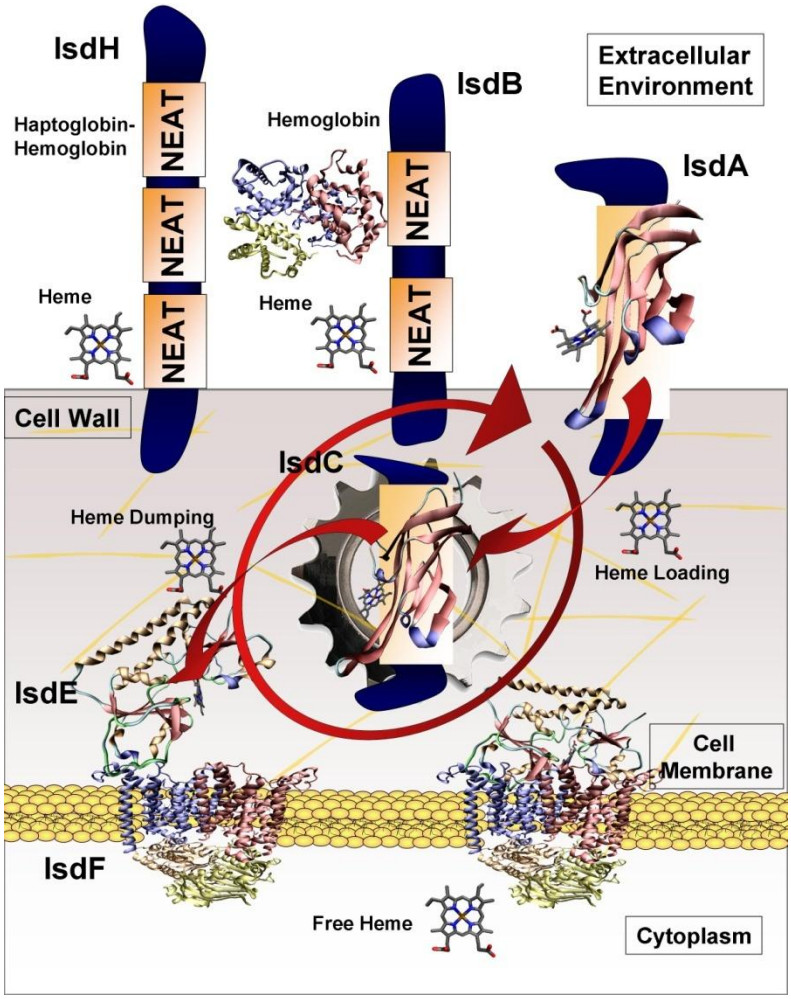

Figure 6-7 A heme transport model based on analysis of the mass spectral data obtained from this study. Unidirectional heme transfer takes place from IsdA-NEAT to IsdC-NEAT to IsdE, and the diagram indicates that IsdC-NEAT cycles round acting as a cog-wheel in the overall transfer reaction. There is no direct transfer from holo-IsdA-NEAT to apo-IsdE. The mass spectral data to support the model are in agreement with the model first proposed by Schneewind and colleagues [17].

Overall, the model proposed treats IsdC-N as a catalyst in the important through cell wall heme transfer pathway of the Isd system (IsdA-N, IsdC-N and IsdE). The model suggests that intact catalytic amounts of IsdC-N are crucial to heme transfer from IsdA-N to IsdE because heme does not transfer from IsdA-N directly to IsdE. Overall, the rate of transfer from IsdA-N to IsdC-N is faster than transfer from IsdC-N to IsdE, which may impart heme cytotoxicity relief on the bacterium by throttling the heme transfer reaction into the cell interior. Key to the transfer reaction mechanism used to account for the experimental data is the disabling of IsdC-N, which also may important heme toxicity protection. Figure 6-7 summarizes the results found in this research. The conclusions are that IsdC (here studied as IsdC-N) is the central cog-wheel in heme transfer through the *S. aureus* wall, and acts as a courier between IsdA and IsdE, by cycling between IsdC and IsdE multiple times and that the differential in rates support an hypothesis that heme stockpiling in the wall may take place as a result of efficient scavenging but more restricted influx via the membrane transporters reduces possible subsequent heme toxicity.

6.6 References

1. Papanikolaou, G.; Pantopoulos, K., *Tox. Appl. Pharm.* **2005,** 202, 199-211.
2. Bullen, J. J.; Rogers, H. J.; Griffiths, E., *Curr. Top. in Micro. Imm.* **1978,** 80, 1-35.
3. Genco, C. A.; Dixon, D. W., *Mol. Microbiol.* **2001,** 39, 215-220.
4. Skaar, E. P.; Schneewind, O., *Microbes Infect.* **2004,** 6, 390-397.
5. Wandersman, C.; Delepelaire, P., *Annu. Rev. Microbiol.* **2004,** 58, 611-647.
6. Wandersman, C.; Stojiljkovic, I., *Curr. Opin. Microbiol.* **2000,** 3, 390-397.
7. Grigg, J. C.; Mao, C. X.; Murphy, M. E. P., *J. Mol. Biol.* **2011,** 413, 684-698.
8. Tiedemann, M. T.; Muryoi, N.; Heinrichs, D. E.; Stillman, M. J., *Biochem. Soc. Trans* **2008,** 36, 1138-1143.
9. Tong, Y.; Guo, M., *Arch. Biochem. Biophys.* **2009,** 481, 1-15.
10. Gordon, R. J.; Lowy, F., *Clin. Infect. Dis.* **2008,** 46, (Suppl 5), S350-359.
11. McGowan, J. E.; Tenover, F. C., *Nature Rev.* **2004,** 2, 251-259.
12. Pilpa, R. M.; Robson, S. A.; Villareal, V. A.; Wong, M. L.; Phillips, M.; Clubb, R. T., *J. Biol. Chem* **2009,** 284, 1166-1176.
13. Torres, V. J.; Pishchany, G.; Humayun, M.; Scheenwind, O.; Skaar, E. P., *J. Bacteriol.* **2006,** 188, 8421-8429.
14. Mazmanian, S. K.; Ton-That, H.; Su, K.; Scheenwind, O., *PNAS.* **2002,** 99, 2293- 2298.
15. Morrissey, J. A.; Cockayne, A.; Hammacott, J.; Bishop, K.; Denman-Johnson, A.; Hill, P. J.; Williams, P., *Infect. Immun.* **2002,** 70, 2399-2298.
16. Taylor, J. M.; Heinrichs, D. E., *Mol. Microbiol.* **2002,** 43, 1603-1614.
17. Mazmanian, S. K.; Skaar, E. P.; Gaspar, A. H.; Humayun, M.; Gornicki, P.; Jelenska, J.; Joachmiak, A.; Missiakas, D. M.; Scheenwind, O., *Science.* **2003,** 299, 906-909.
18. Skaar, E. P.; Gaspar, A. H.; Scheenwind, O., *J. Biol. Chem.* **2004,** 279, 436-443.

19. Lee, W. C.; Reniere, M. L.; Skaar, E. P.; Murphy, M. E., *J. Biol. Chem.* **2008,** 283, 30957-30963.
20. Reniere, M. L.; Ukpabi, G. N.; Harry, S. R.; Stec, D. F.; Krull, R.; Wright, D. W.; Bachmann, B. O.; Murphy, M. E.; Skaar, E. P., *Mol. Microbioll.* **2010,** 75, 1529-1538.
21. Zhu, H.; Xie, G.; Liu, M.; Olson, J.; Fabian, M.; Dooley, D.; Lei, B., *J. Biol. Chem.* **2008,** 283, 18450-18460.
22. Dryla, A.; Gelbmann, D.; Gabain, A. v.; Nagy, E., *Mol. Microbiol.* **2003,** 49, 37-53.
23. Watanabe, M.; Tanaka, Y.; Suenaga, A.; Kurodo, M.; Yao, M.; Watanabe, N.; Arisaka, F.; Ohta, T.; Tanaka, I.; Tsumoto, K., *J. Biol. Chem.* **2008,** 283, 28649-28659.
24. Mack, J.; Vermeiren, C.; Heinrichs, D. E.; Stillman, M. J., *Biochem. Biophys. Res. Commun.* **2004,** 320, 781-788.
25. Pluym, M.; Vermeiren, C. L.; Mack, J.; Heinrichs, D. E.; Stillman, M. J., *J. Porphyrins Phthalocyanines.* **2007,** 11, 165-171.
26. Tiedemann, M. T.; Muryoi, N.; Heinrichs, D. E.; Stillman, M. J., *J. Porphyrins Phthalocyanines.* **2009,** 13, 1006-1016.
27. Liu, M.; Tanaka, W. N.; Zhu, H.; Xie, G.; Dooley, D. M.; Lei, B., *J. Biol. Chem.* **2008,** 283, 6668-6678.
28. Grigg, J. C.; Vermeiren, C. L.; Heinrichs, D. E.; Murphy, M. E., *Mol. Microbiol.* **2007,** 63, 139-149.
29. Sharp, K. H.; Schneider, S.; Cockayne, A.; Paoli, M., *J. Biol. Chem* **2007,** 282, 10625-10631.
30. Grigg, J. C.; Vermeiren, C. L.; Heinrichs, D. E.; Murphy, M. E., *J. Biol. Chem.* **2007,** 282, 28815-28822.
31. Villareal, V. A.; Spirig, T.; Robson, S. A.; Liu, M.; Lei, B.; Clubb, R. T., *J. Am. Chem. Soc.* **2011,** 133, 1417-14179.
32. Muryoi, N.; Tiedemann, M. T.; Pluym, M.; Cheung, J.; Heinrichs, D. E.; Stillman, M. J., *J. Biol. Chem.* **2008,** 283, 28125-28136.
33. Hoops, S.; Sahle, S.; Gauges, R.; Lee, C.; Pahle, J.; Simus, N.; Singhal, M.; Xu, L.; Mendes, P.; Kummer, U., *Bioinf.* **2006,** 22, 3067-3074.
34. Pluym, M.; Muryoi, N.; Heinrichs, D. E.; Stillman, M. J., *J. Inorg. Biochem.* **2008,** 102, 480-488.
35. Pluym, M.; Vermeiren, C. L.; Mack, J.; Heinrichs, D. E.; Stillman, M. J., *Biochem.* **2007,** 46, 12777-12787.
36. Ngu, T.; Lee, J.; Rushton, M. K.; Stillman, M. J., *Biochem.* **2009,** 38, 8806-8816.
37. Grigg, J. C.; Ukpabi, G.; Gaudin, C. F. M.; Murphy, M. E. P., *J. Inorg. Biochem.* **2010,** 104, 341-348.
38. Torres, V. J.; Stauff, D. L.; Pishchany, G.; Bezbradica, J. S.; Gordy, L. E.; Iturregui, J.; Anderson, K. L.; Dunman, P. M.; Joyce, S.; Skaar, E. P., *Cell Host Microbe.* **2007,** 1, 85-87.

Chapter 7. Mechanism of heme scavenging from bovine hemoglobin by IsdB from *Staphyloccocus aureus*: Importance of the intact Isd protein[6]

7.1 *Introduction*

Staphylococcus aureus (*S. aureus*) is an invasive Gram-positive coccoid bacterium that innocuously colonizes the anterior nares of approximately 30% of the human population [1, 2]. In hospitals, *S. aureus* is one of the most commonly acquired bacterial infections as it is the leading cause of nosocomial infections [3]. Bacterial infection requires the acquisition of host iron. Iron is an essential component of living biological systems [4] due to the ability to undergo changes in oxidation and to take part in ligand binding. Since free iron is not typically available, it is sequestered by host proteins. As a result, invasive organisms need high affinity systems to acquire and store iron [5]. *S. aureus* responds to the iron-restricted environment of the host with an array of iron-uptake and acquisition systems. It has been shown that *S. aureus* is able to grow on heme, hemoglobin, hemoglobin-haptoglobin, transferrin and ferric or ferrous iron [6-8].

Interestingly, approximately 75% of the total host body-iron is locked up in heme. This source of iron is considered largely inaccessible to siderophores [9]. Furthermore, about 70% of the total body iron is contained within hemoglobin (Hb), making it a particularly attractive iron source for invading microbes. *S. aureus* has also evolved mechanisms to exploit and scavenge heme as an iron source. *S.* aureus secretes hemolysins [10] to lyse host red blood cells and release Hb into the serum where it is accessible to the bacteria. Utilization of Hb in *S. aureus* is mediated by the Isd heme transfer system [6, 11], whose motif is also found in other Gram-positive pathogens such as *Bacillus anthracis, Clorstridium tetani* and *Listeria monocytogenes* [12-14].

The *S. aureus* iron-regulated surface determinant (*isd*) gene cluster was first identified in 2002 [8, 11, 15], and then in 2003, Mazmanian *et al.* [6] reported that, when grown in iron-limiting medium, *S.* aureus expresses genes that are involved in iron acquisition and were the first to propose that the Isd series of protein formulate a heme transfer pathway across the cell wall and through the cell membrane. The Isd system consists of nine iron-regulated proteins, named

[6] A version of this work will be submitted.

IsdA, IsdB, IsdC, and IsdH, which are cell-wall anchored, surface proteins, and IsdDEF, which together constitute a membrane-localized ABC transporter and, finally, IsdG and IsdI, which encode heme-degrading enzymes in the cytoplasm [16, 17]. This system was proposed [8, 11, 15] and later demonstrated [6] to be able to pass heme through the gram-positive cell wall and cell membrane into the cytoplasm where heme is deconstructed and free iron is released. These nine proteins mediate the delivery of heme from the host's plasma into the *S aureus* cytoplasm [18]. IsdB and IsdH are exposed to the environment, while IsdA is partially exposed and IsdC is buried within the cell wall [6]. In terms of a mechanism for heme acquisition IsdB and IsdH capture heme from Hb released from erythrocytes by hemolysins [14, 19]. IsdH binds haptoglobin (a serum glycoprotein that protects the host from free hemoglobin) and the haptoglobin-hemoglobin complex [7, 20, 21]. IsdA is proposed to function as a heme scavenging protein and a "heme reservoir" for IsdH and IsdB [22, 23]. IsdC, which is located in the cell wall, acts as the central conduit of heme transfer in the Isd system [24-26]. The membrane bound complex IsdDEF complex pumps heme across the cell membrane [18, 27]. Heme is finally deconstructed by IsdG monooxygenase or its paralog, IsdI [17, 18]. The proteins IsdA, IsdB, IsdC and IsdH each contain at least one Near Transporter (NEAT) domain that adopts a beta sandwich structure to bind one ferric heme into a groove with heme-iron coordination via Tyr [22-25, 28-30].

Previous studies have shown that ferric heme transfer takes place in a unidirectional fashion as heme propagates down the pathway in the sequence (with the heme proximal amino acid residue shown) IsdB-N2 (Tyr)→ IsdA-N (Tyr) → IsdC-N (Tyr) → IsdE (His) or, alternatively, initiating from IsdH-N3, IsdH-N3 (Tyr) → IsdA-N → IsdC-N → IsdE. Significantly, IsdA does not transfer heme directly to IsdE under any conditions [25, 27, 28, 31]. In order to facilitate such transfer protein-protein interactions have been shown to be key factors in heme transfer from IsdA-N to IsdC-N [32]. Heme is transferred by a handclasp model of the transfer complex and reveal that kinetics of heme transfer between IsdA and IsdC can be attenuated by alternating key β7/β8 loops and 3_{10} helices in the proteins. Overall, weak transient stereospecific interactions facilitate the selective transport seen in the Isd system.

Recent studies on IsdH show that the NEAT domain interaction with Hb capture is important to heme extraction. IsdH-N1 interacts weakly through loop interactions with the α-chain of Hb (αHb) and mutants of Hb are defective in IsdH-N1 binding [21, 30]. Therefore it was speculated

that IsdB may also function in a similar manner with Hb binding through weak interactions of the IsdB-N1 domain and heme extraction with the heme binding IsdB-N2 domain due to IsdB-N1 having 40% sequence identity to IsdH-N1 and IsdB-N2 possessing 56% sequence similarity to IsdH-N3. Past studies on IsdB binding to Hb have revealed that oxidized metHb directly transfers heme to apo-IsdB, but apo-IsdA, apo-IsdC or apo-IsdE are not able to extract heme from metHb. However, holo-IsdB transfers heme from metHb in much that same way as heme is transferred from recombinant holo-IsdB-N2 [19, 25]. Overall, heme transfer facilitated by protein-protein interactions is much faster than a dissociated mechanism [19].

Interestingly, the mechanism of heme transfer and the importance of metHb compared to ferrous oxy (^{O2}Hb) or the importance of the intact IsdB protein when looking at heme transfer remains unknown. In this study the individual IsdB NEAT domains, IsdB-N1 and IsdB-N2 and their interaction with metHb and ferrous oxyHb by electrospray ionization mass spectrometry was investigated. Separated, the NEAT domains do not alter any Hb solutions. Furthermore, intact IsdB-N1N2 is not able to interact with ferrous oxy Hb. However, when the intact domains (IsdB) are added to metHb significant denaturation of Hb occurs and heme is "stolen" from Hb. Extraction of heme from metHb is enhanced with the addition of IsdC-N.

7.2 Experimental Methods

7.2.1 Materials and Methods

General techniques and experimental procedures pertaining to protein growth, protein purification, protein sample preparation, instrumental techniques and analysis can be found in Chapter 2.

7.2.2 Gene cloning and protein expression

DNA encoding residues 144-462 of IsdB (IsdB-N1N2) was, 144-269 of IsdB (IsdB-N1) and 337-462 of IsdB (IsdB-N2) were incorporated into *E. coli* so recombinant protein could be produced. The proteins were analyzed by ESI-mass spectrometry to confirm that each was heme-free (apo).

7.2.3 Hemoglobin Preparation

Bovine ferrous ^{oxy}Hb was was prepared from fresh hemolysate via slightly modified method from standard procedures [33, 34]. Fresh bovine blood was extracted into a chilled glass bottle containing sodium citrate as an anticoagulant to a final concentration of 0.3% (w/v). Centrifugation at 5,500*g* for 20 min gave a RBC pellet. Plasma and buffy coat (containing white blood cells and platelets) were removed with suction. Isolated RBCs were resuspended and washed in isotonic 0.9% (w/v) sodium chloride and then centrifuged again at 5,500*g* for 20 min. This washing step was repeated four times to rid the samples of plasma proteins and cellular debris. Hemolysate was obtained through osmotic shock, and stromal impurities were extracted into an organic phase. This was achieved by mixing the packed RBCs with an equal volume of distilled water containing 10% (v/v) toluene. Centrifugation at 15,000*g* for 30 min yielded an aqueous layer of purified hemolysate, which was then dialyzed at 4 °C against 10 mM ammonium acetate over a period of 36 h with multiple buffer exchanges.

In order to produce ferric metHb, a small amount of crystalline potassium ferricyanide was added to ferrous oxyHb prepared above in order to oxidize the Hb. Potassium ferricyanide was then separated from ferric metHb using G-25 sephadex column chromatography. Samples were further purified by buffer exchange using using Millipore Amicon ultra-4 centrifuge filter units (10 kDa MWCO) with a Beckman CS-6 swinging-bucket centrifuge (3000 rpm for 10 minutes per run).

Acid denaturation of Hb was performed by titrating dilute formic acid into hemoglobin samples until the desired pH was obtained.

7.3 Results

7.3.1 Apo-Isd proteins and bovine hemoglobin using ESI-MS

Figure 7-1 shows the ESI-MS spectra of the Isd proteins apo-IsdBN1, apo-IsdBN2 and apo-IsdBN1N2. ESI-mass spectrum of apo-IsdB-N1 results in a charge state distribution similar to other Isd NEAT domains such as IsdA and IsdC with charge states +8 to +6 [23, 25, 28]. The deconvoluted mass matches the theoretical mass of 15.1 kDa with a mass of 15127 Da. The ESI-MS data of IsdB-N2 is similar to previously reported results with a charge state distribution of +8 to +5 with a deconvoluted mass of 15303 Da. The * indicates a +11 charge state dimer of

apo-IsdB-N2 [28]. IsdB-N1N2 is a larger protein with a theoretical mass of 37.8 kDa. Apo-IsdB-N1N2 has a five charge state manifold, +14 to +10, with a deconvoluted mass of 37783 Da. The charge state manifold of IsdB-N1N2 is more similar to IsdE than to the smaller NEAT domain proteins due to the size of the protein [35]. Previous studies have shown that IsdB-N1 does not bind heme [7, 14, 20], IsdB-N2 binds one heme through a tyrosine amino acid ligand and IsdB-N1N2 binds one heme in a similar manner as IsdB-N2 [19, 28, 36].

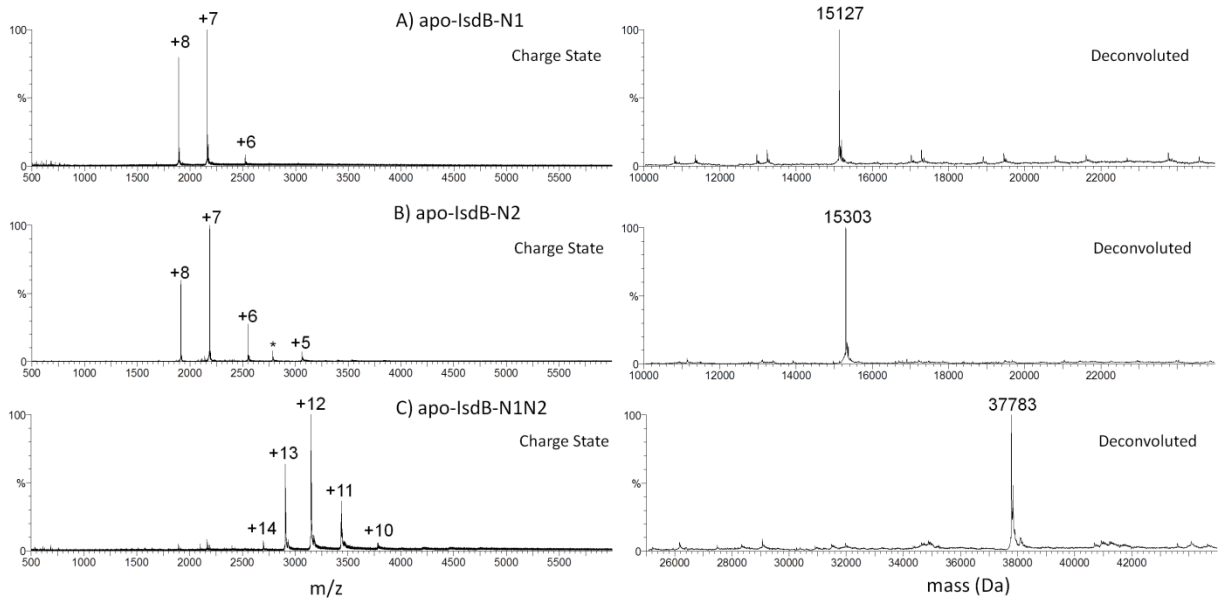

Figure 7-1 ESI-MS spectra for A) apo-IsdB-N1, B) apo-IsdB-N2 and C) apo-IsdBN1N2. A) Charge state and deconvoluted mass spectra of apo-IsdB-N1. The ESI-mass spectrum of apo-IsdB-N1 shows three charge states (+8, +7, +6) which deconvolute to 15127 Da. B) Charge state and deconvoluted mass spectra of apo-IsdB-N2. These results match those that have been previously reported [25, 28]. The ESI-mass spectrum of apo-IsdB-N2 shows four charge states (+8 to +5). The * indicates dimer-apo-IsdB-N2. The charge states deconvolute to 15303 Da. C) Charge state and deconvoluted mass spectra of apo-IsdB-N1N2. Apo-IsdB-N1N2 possesses five charge states (+14 to +10), which deconvolute to 37783 Da.

For comparison, the ESI-MS spectra of bovine hemoglobin pH 7.40 and pH 1.21 are shown in Figure 7-2. These results match the spectra that were previously reported [34, 37]. Briefly, four Hb components can be found in a solution of blood extracted Hb: tetramer holo-Hb $(\alpha^h\beta^h)_2$ with charge states of +15 to +18, dimer holo-$\alpha^h\beta^h$ with charge states of +10 to +12 , apo-α strands with charge states of +7 and +8 and holo-α strands with charge states of +7 and +8. Overall, the amount of tetramer present in solution is much greater than the amount of dimer and single strands [34, 37]. Typically, when heme proteins are acid denatured and hence unfolded,

protonation of the protein amino acids is increased and a distinct increase in charge states is observed [28, 34, 38]. Upon formic acid denaturation, the denaturation of tetramer into single strand components (α and β) and loss of heme is observed with ESI-MS, Figure 7-2B. The efficiency of ionization of the α strand is much greater than the β strand which results in a greater intensity and distribution of denatured α than denatured β. Apo-α has a centered denatured charge state of +16 while apo-β has a centered denatured charge state at +11. Overall, the deconvoluted masses of bovine hemoglobin are 64513 Da for $(\alpha^h\beta^h)_2$, 32254 Da for $(\alpha^h\beta^h)$, 15055 Da for apo-α and 15955 Da for apo-β.

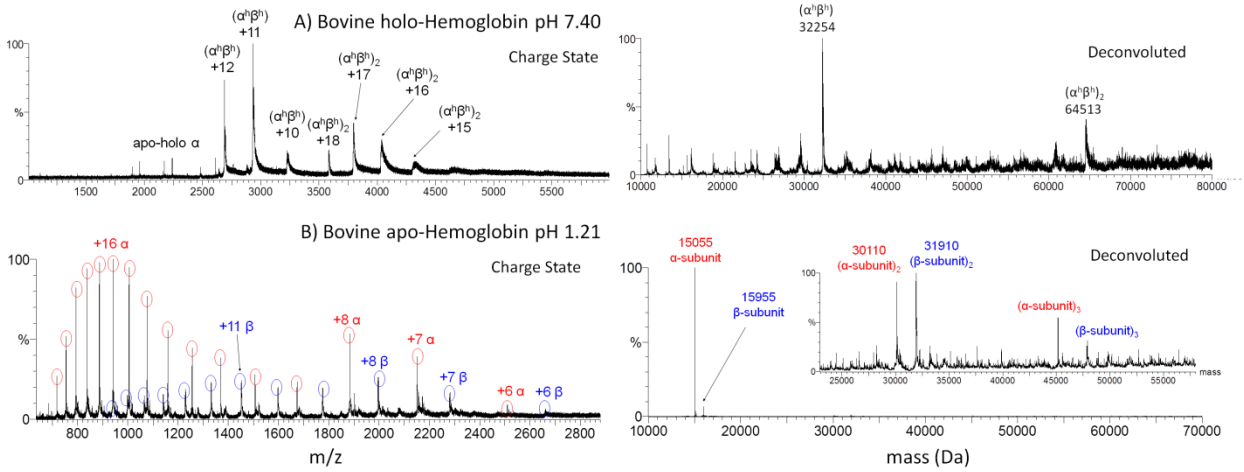

Figure 7-2 ESI-mass spectra of intact bovine hemoglobin at pH 7.40 and denatured bovine hemoglobin at pH 1.21. These ESI-mass spectra match results that have been previously reported for bovine hemoglobin [34, 38]. A) Measured results for bovine hemoglobin at pH 7.40. Tetramer holo-Hb $(\alpha^h\beta^h)_2$ are observed with charge states of +18 to +15 and deconvoluted mass of 64513 Da. Dimer holo-$(\alpha^h\beta^h)$ are observed with charge states +12 to +10 and deconvoluted mass 32254. Small peaks are observed for the apo/holo pair of single intact α bands at +8 and +7. B) Measured results for acid denatured bovine hemoglobin at pH 1.21. The denatured charge states for apo-α and apo-β have a peak maximum of +16 and +11, respectively. Non-denatured apo-α and apo-β have charge states of +8 to +7. The deconvoluted apo-α and apo-β subunit mass is 15055 Da and 15955 Da, respectively.

7.3.2 Heme scavenging from Hb by apo-IsdB-N1 using ESI-MS

The importance of the first NEAT domain of IsdB, IsdB-N1, with regards to heme extraction from Hb was investigated. Upon addition of 4 μM apo-IsdB-N1 with 4 μM metHb, Figure 7-3A, no change in the charge states of IsdB-N1 and metHb were observed. For both ferrous and ferric Hb, IsdB-N1 still has a charge state manifold of +8 to +6. Only tetramer Hb with a charge

state distribution of +18 to +16 was present. No apo-tetramer Hb charge states are observed. Dimer $^{hh}(\alpha\beta)$ is present with a charge state manifold of +12 to +10. Overall, the Hb charge states remain similar to that observed with a solution consisting of holo-Hb. The same result is obtained with the addition of 4 μM apo-IsdB-N1 and 4 μM ferrous Hb, Figure 7-3B. No significant changes in the charge states are observed and Hb remains intact.

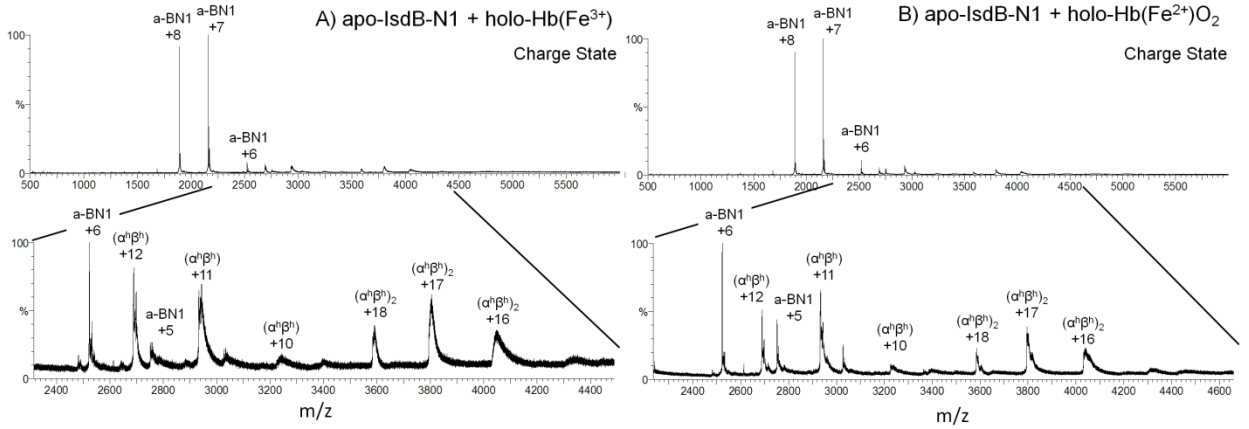

Figure 7-3 Interaction of 4 μM IsdB-N1 with A) 4 μM ferric Hb and B) 4 μM ferrous Hb. A) Charge state data for the addition of apo-IsdB-N1 with ferric Hb from 500-6000 m/z and the zoomed in region 2300-4500 m/z. +8 to +6 charge states are present for apo-IsdB-N1 (a-BN1). No peaks indicating heme binding are present. The overall charge manifold of ferric Hb remains intact for Hb. No interaction with Hb is evident. B) Charge state data for the addition of apo-IsdB-N1 with ferrous Hb from 500-600 m/z and the zoomed in region 2300-4500 m/z. Again, no interaction with Hb is evident as no change in the charge manifold of apo-IsdB-N1 and Hb was observed.

7.3.3 Heme scavenging from Hb by apo-IsdB-N2 using ESI-MS

The importance of the second NEAT domain of IsdB, IsdB-N2, with regards to heme extraction and heme binding from Hb was investigated next. Upon addition of 4 μM apo-IsdB-N2 with 4 μM ferric Hb, Figure 7-4A, no changes in the charge states of IsdB-N2 and ferric Hb were observed. Interestingly, although IsdB-N2 has been found to be a heme binding NEAT domain [28], IsdB-N2 is not able to extract heme from ferric Hb as either the tetramer, dimer or single heme bound strands. For both ferrous and ferric Hb reactions, IsdB-N2 still has a charge state manifold of +8 to +5. Only tetramer Hb with a charge state distribution of +18 to +16 were present. No apo-tetramer Hb charges states were observed. Dimer $^{hh}(\alpha\beta)$ is present with a charge state manifold of +12 to +10. Overall, the Hb charge states remain similar to that

observed with a solution consisting of holo-Hb. The same result is obtained with the addition of 4 μM apo-IsdB-N2 and 4 μM ferrous Hb, Figure 7-4B. No significant changes in the charge states are observed and the Hb remains intact.

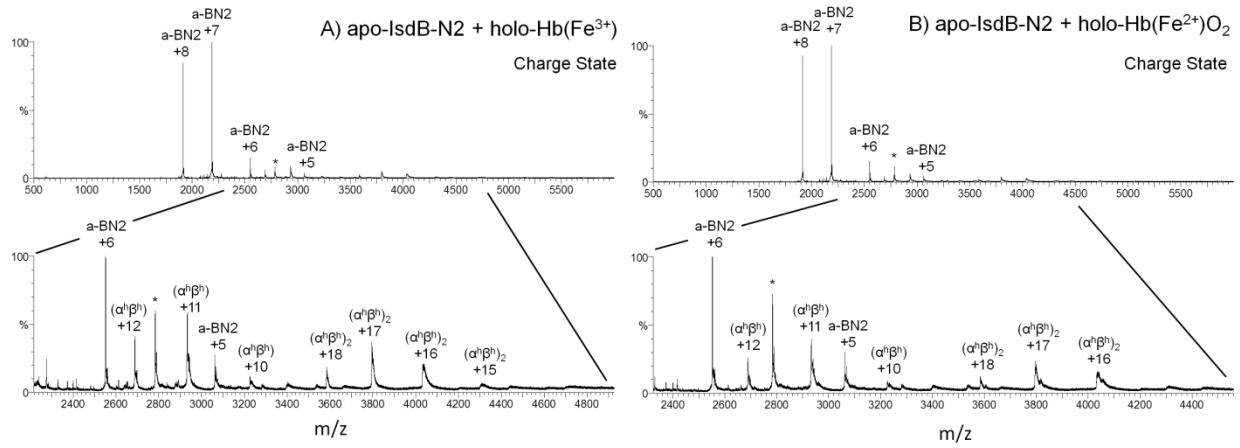

Figure 7-4 Interaction of 4 μM IsdB-N2 with A) 4 μM ferric Hb and B) 4 μM ferrous Hb. A) Charge state data for the addition of apo-IsdB-N2 with ferric Hb from 500-6000 m/z and the zoomed in region 2300-4500 m/z. +8 to +5 charge states are present for apo-IsdB-N2 (a-BN2). The dimer charge state peak is indicated with a *. No peaks indicating heme binding are present. The overall charge manifold of ferric Hb remains intact for Hb. No interaction with Hb is evident. B) Charge state data for the addition of apo-IsdB-N2 with ferrous Hb from 500-600 m/z and the zoomed in region 2300-4500 m/z. Again, no interaction with Hb is evident as no change in the charge manifold of apo-IsdB-N2 and Hb was observed. Apo-IsdB-N2 does not extract or bind heme from ferrous Hb.

7.3.4 Heme scavenging from Hb by apo-IsdB-N1 and apo-IsdB-N2 using ESI-MS

The importance of the first and second NEAT domain of IsdB, IsdB-N1 and IsdB-N2, was explored. Upon addition of 4 μM apo-IsdB-N1 and 4 μM apo-IsdB-N2 to a solution of 4 μM ferric Hb, Figure 7-5A, no changes in the charge states of IsdB-N2 and ferric Hb were observed. For ferrous Hb, IsdB-N1 still has a charge state manifold of +8 to +5 and IsdB-N2 still has a charge state manifold of +8 to +5. Tetramer holo-Hb with a charge state distribution of +18 to +16 was observed. No tetramer apo-Hb species were present. Also, only holo dimer $^{hh}(\alpha\beta)$ were observed with a charge state manifold of +12 to +10. Interestingly, the separate domains combined in solution do not interact with Hb. No heme extraction to IsdB-N2 or significant alteration in the charge states of Hb was observed. This result is surprising as IsdB-N1N2 has

been previously shown to interact with and extract heme from ferric Hb [19]. Overall, the Hb charge states remain similar to what is observed with a solution of just holo-Hb. The same result is obtained with the addition of 4 μM apo-IsdB-N1 and 4 μM apo-IsdB-N2 with 4 μM ferrous Hb, Figure 7-5B. No significant changes in the charge states are observed and the Hb remains intact.

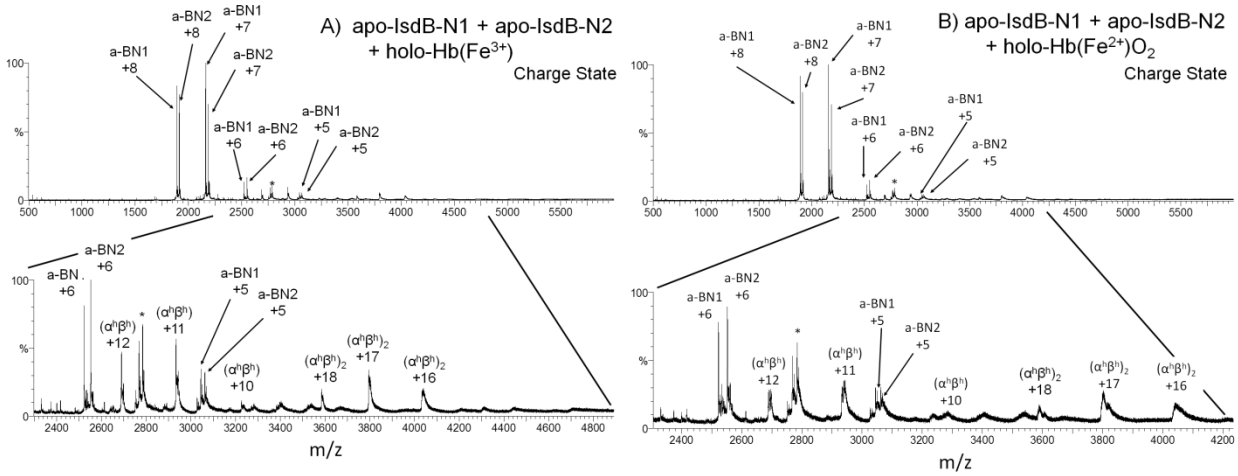

Figure 7-5 Interaction of 4 μM IsdB-N1 and 4 μM IsdB-N2 with A) 4 μM ferric Hb and B) 4 μM ferrous Hb. A) Charge state data for the addition of apo-IsdBN1 (a-BN1) apo-IsdB-N2 (a-BN2) with ferric Hb from 500-6000 m/z and the zoomed in region 2300-4500 m/z. +8 to +5 charge states are present for both apo-IsdB-N1 and apo-IsdB-N2. The dimer charge state peak is indicated with a *. No peaks indicating heme binding of apo-IsdB-N2 are present. The overall charge manifold of ferric Hb remains intact for Hb. No interaction with Hb is evident. B) Charge state data for the addition of apo-IsdB-N1 apo-IsdB-N2 with ferrous Hb from 500-600 m/z and the zoomed in region 2300-4500 m/z. Again, no interaction with Hb is evident as no changes in the charge manifold of apo-IsdB-N1 and apo-IsdB-N2 and Hb were observed.

7.3.5 Heme scavenging from ferrous Hb by apo-IsdB-N1N2 using ESI-MS

With null results regarding the interaction of IsdB-N1 and IsdB-N2 with Hb, the effect of the combined protein, IsdB-N1N2 with ferrous Hb, Figure 7-6, was investigated. Again, only apo charge states are present for IsdB-N1N2 (+14 to +11). No heme extraction from Hb had occurred. The overall charge state manifold for Hb remains the same as a solution of free Hb without the Isd protein. Only tetramer holo-Hb with a charge state distribution of +18 to +16 and holo dimer $^{hh}(\alpha\beta)$ with a charge state manifold of +12 to +10 were observed. Therefore, it may be concluded that IsdB is not able to extract heme from ferrous Hb despite evidence suggesting that IsdB-N2 can bind ferrous heme [28].

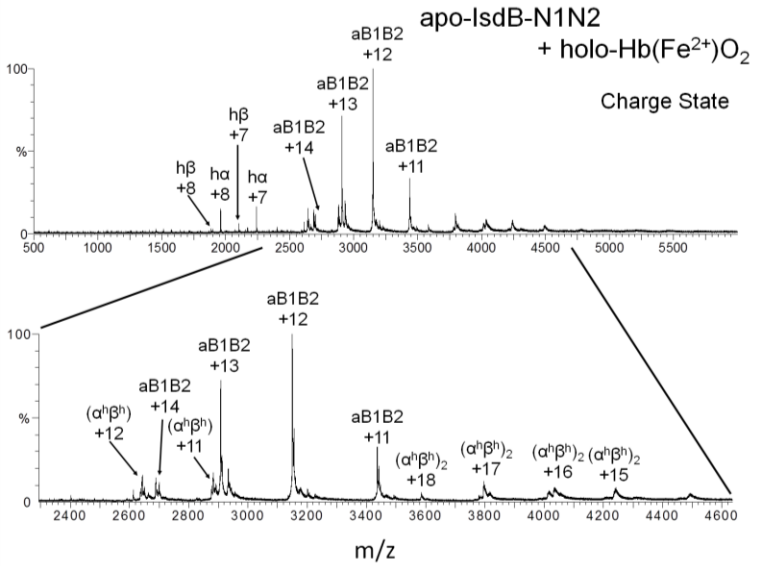

Figure 7-6 Interaction of 4 apo-IsdB-N1N2 with ferrous Hb. 4 μM apo-IsdB-N1N2 with 4 μM ferrous Hb. Charge state data for the addition of apo-IsdBN1 (a-BN1) apo-IsdB-N2 (a-BN2) with ferric Hb from 500-6000 m/z and the zoomed in region 2300-4500 m/z. +8 to +5 charge states are present for both apo-IsdB-N1 and apo-IsdB-N2. The dimer charge state peak is indicated with a *. No peaks indicating heme binding of apo-IsdB-N2 are present. The overall charge manifold of ferric Hb remains intact for Hb. No interaction with Hb is evident.

7.3.6 Heme scavenging from metHb by apo-IsdB-N1N2 using ESI-MS

With null results observed regarding heme extraction by IsdB-N1 and IsdB-N2 with Hb, heme extraction from 1 μM metHb with 4 μM apo-IsdB-N1N2 by time dependant ESI-MS, Figure 7-7, was investigated next. To aid in the explanation of the mass spectral data, time-dependent relative trace data for the apo/holo-IsdB-N1N2 +13 charge state, the +12 charge state of the dimer (αβ) and the +8 charge state for the single intact apo-α strand, Figure 7-8, is shown below. Mass spectral data analysis cannot be used quantitatively to analyze raw charge states. The charge states must be made relative to a protein with a similar conformation in order to be interpreted quantitatively. For heme binding proteins this can be carried out using the apo/holo charge state pairs [25, 39]. Therefore, since single intact holo-β, denatured holo-β, denatured holo-α and apo-tetramer Hb are not present in the mass spectral data then therefore, these traces cannot be analyzed quantitatively.

In the early stages of the reaction following addition of apo-IsdB-N1N2 with metHb at about 1 minute, there are significant changes in the mass spectral data compared to the previous null reactions above. The appearance of holo-IsdB-N1N2 charge states is evident by one minute but

significantly most of the IsdB-N1N2 protein is now apo indicating a slow heme transfer relative to other Isd-NEAT to Isd-NEAT transfers [19, 31]. Over time, by 5 minutes, the appearance of holo-IsdB-N1N2 charge states matching the apo-IsdB-N1N2 charge states of +13 to +11 become apparent. From Figure 7-8A, it can be seen that heme extraction by IsdB-N1N2 is slow and that the overall shape appears to be multiphasic, meaning IsdB-N1N2 may be able to extract heme from not only from intact tetramer Hb but also from dimer (αβ) Hb and single stranded α and β strands. Over time, approximately 50% of IsdB-N1N2 binds heme meaning this reaction is slow and not as complete as seen with the other Isd proteins [19, 25, 31].

Interestingly, holo-tetramer metHb is present throughout the reaction with apo-IsdB-N1N2. No apo-tetramer metHb charge states were present. Therefore, when apo-IsdB-N1N2 interacts with tetramer metHb the tetrameric structure of metHb is disrupted into smaller components. Present in Figure 7-7 are the +13 to +11 charge states of the (αβ) dimer proteins. At first the relative amount of $^{ah}(\alpha\beta)$ and $^{aa}(\alpha\beta)$ are the same while the amount of $^{hh}(\alpha\beta)$ is very low. Progressing through the heme extraction reaction, it is clear that the relative amounts of $^{aa}(\alpha\beta)$ increases while $^{hh}(\alpha\beta)$ and $^{ah}(\alpha\beta)$ decreases. Analysis of Figure 7-8B shows the disappearance of $^{hh}(\alpha\beta)$, which is present in the starting metHb solution, and slow tailing of $^{ah}(\alpha\beta)$ indicating the formation of these species from the interaction of IsdB-N1N2 with metHb.

Normal metHb production produces a small amount of single stranded non-denatured apo-α and holo-α strands. Relative to acid denaturation the amount of single α strands is very low. This is the same case for single non-denatured β strands which is not present in purified metHb solutions. Figure 7-7 shows that early in the reaction the presence of apo- and holo-α strands are present with charge states +8 to +6. The relative amount of non-denatured α strands are shown in Figure 7-8C. A steady increase of apo-α is produced and a tailing decrease in holo-α is observed. Single α strands are produced from dissociation of tetrameric and dimer metHb. Only apo-β strands are present which may indicate a preference of IsdB-N1N2 towards extracting heme from the β domain of Hb first and then subsequently from the α strand. This is supported by the appearance of denatured apo-α and apo-β with charge state maximum of +14 and +11 respectively. When compared with the ESI-MS data for acid denatured metHb from Figure 7-2, the charge state maxima for denatured apo-α was measured as +16 and for denatured apo-β was measured as +11. Therefore, the denatured apo-β strands from heme extraction by IsdB-N1N2 resemble acid denatured conformations compared with apo-α which while still denatured, would

be slightly more folded as charge state envelopes have been shown to indicate size of the protein [23, 28, 35]. When IsdBN-N1N2 extracts heme from metHb, a higher ratio of denatured apo-β to apo-α compared with acid denatured metHb was observed. This is shown by the large difference of relative abundance between denatured apo-α and apo-β in acid denatured metHb (approximately a 5:1 ratio from maximal charge states) from Figure 7-2B and the small difference between denatured apo-α and apo-β in heme extracted apo-IsdB-N1N2 (approximately a 2:1 ratio from maximal charge states) from Figure 7-7.

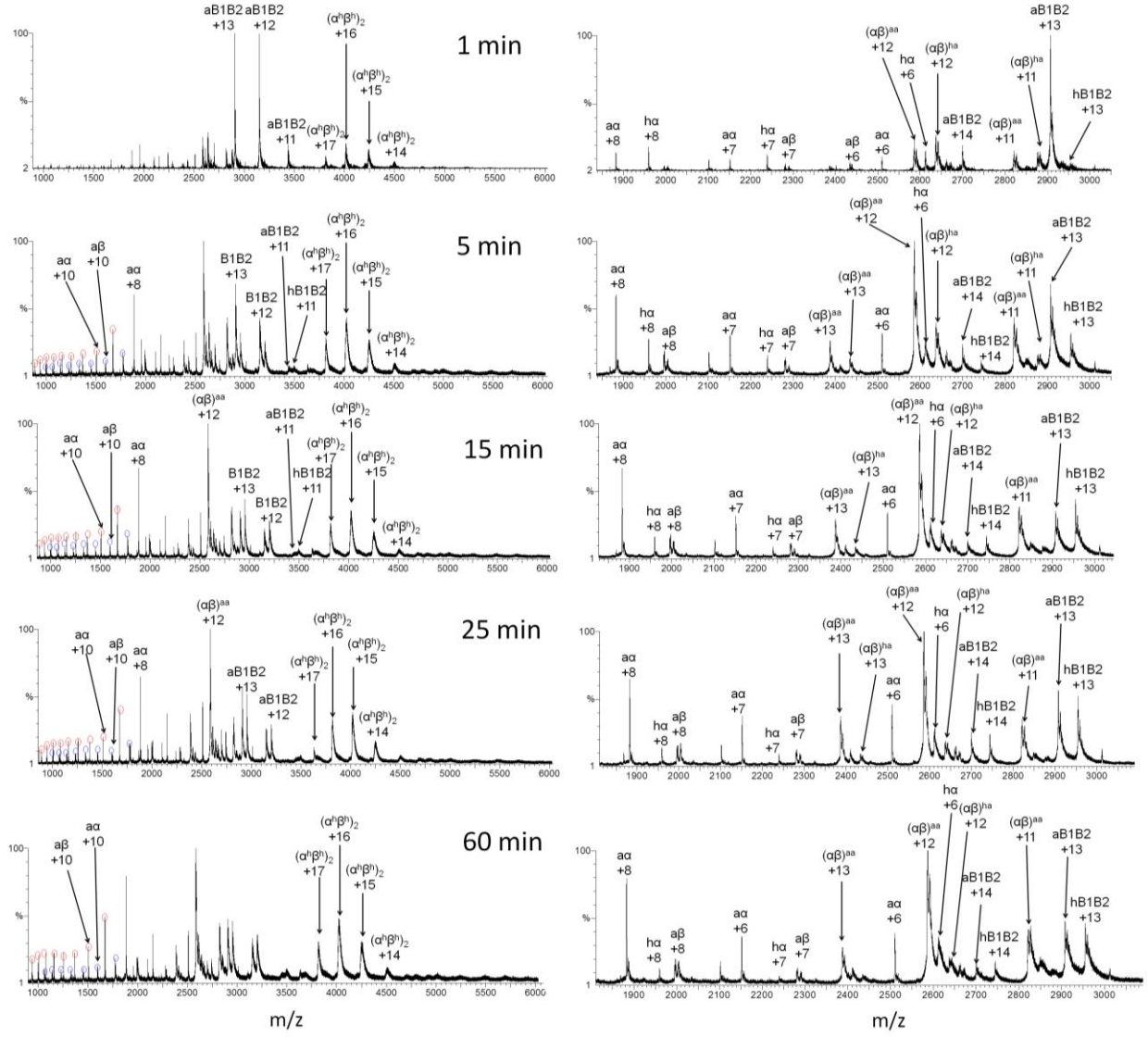

Figure 7-7 Heme extraction from 1 µM metHb and binding by 4 µM IsdB-N1N2 over a time period of one hour. 1 min: The appearance of mostly apo and a small fraction of holo IsdB-N1N2 peaks with charge states +13 to +11. Holo-tetramer charge state peaks at +17 to 14 were observed. No apo-tetramer charge states were measured. Over time, the appearance of holo-$^{hh}(\alpha\beta)$, single heme bound-$^{ah}(\alpha\beta)$ and fully apo-$^{aa}(\alpha\beta)$ Hb dimer are present with charge

states +12 and +11. Also intact apo/holo pairs of single stranded α and β strands are present with charge states of +8 and +7 are present. 5-60 min: Important changes in the mass spectra are observed in the 1000 to 2000 m/z region where the appearance of denatured apo α and β strands (red and blue highlights respectively) are measured. The ratio of apo-IsdB-N1N2:holo-IsdB-N1N2 charge state pairs decrease over time. No apo-tetramer Hb peaks are present in any of the resulting spectra. The holo-$^{hh}(\alpha\beta)$ charge states decrease while single heme bound-$^{ah}(\alpha\beta)$ and fully apo-$^{aa}(\alpha\beta)$ increases as heme is extracted and bound by IsdB-N1N2.

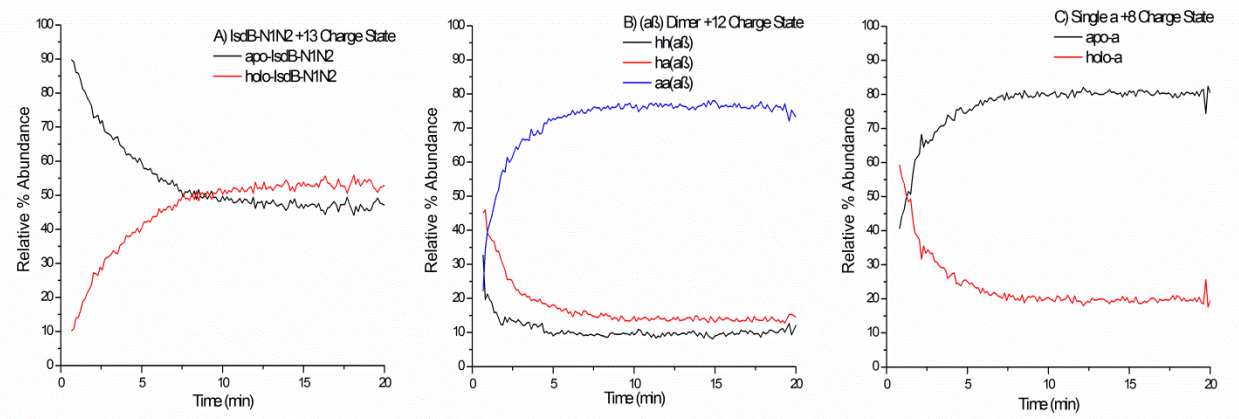

Figure 7-8 Time dependant mass spectral charge state data for A) IsdB-N1N2 B) αβ of Hb dimer and C) intact single stranded α of Hb extracted from the data from Figure 7-7. A) Relative % abundances of apo-IsdBN1N2 and holo-IsdB-N1N2 +13 charge state data. A steady increase in the relative amount of holo-IsdB-N1N2 is observed with a decrease in the relative amount of apo-IsdB-N1N2. B) Relative % abundance of the αβ dimer +12 charge state data. Four species are possible for the αβ dimer ($^{hh}(\alpha\beta)$, $^{ha}(\alpha\beta)$, $^{ah}(\alpha\beta)$ and $^{aa}(\alpha\beta)$). It should be noted that there is no mass distinction between $^{ha}(\alpha\beta)$ and $^{ah}(\alpha\beta)$ and hence these data are plotted together. $^{hh}(\alpha\beta)$ steadily decreased early in the reaction while $^{ah}(\alpha\beta)$ lagged behind. Ultimately $^{aa}(\alpha\beta)$ is formed as a result of heme extraction by IsdB-N1N2. C) Relative % abundance of α intact single strand from Hb +8 charge state data. Heme extraction from metHb by apo-IsdB-N1N2 produced single stranded holo-α. IsdB-N1N2 is also able to interact with the single domain and extract heme.

7.3.7 Extraction of heme with apo-IsdB-N1N2 from metHb and transfer to apo-His-IsdC-N using ESI-MS:

Addition of 2.5 μM metHb to a mixture of 3 μM apo-IsdB-N1N2 and 20 μM apo-His-IsdC-N tests heme extraction by apo-IsdB-N1N2 and transfer to apo-His-IsdC-N, Figure 7-9. Apo-His-IsdC-N was used because some Hb charge state peaks overlap with native IsdC-N charge state peaks. The His-tag results in an increase in mass and circumvents this problem. Importantly, neither apo-IsdC-N nor apo-His-IsdC-N extracts heme from metHb or causes any denaturation of metHb as seen with apo-IsdB-N1N2 above [19]. After 30 minutes, there exists a mixture of apo- and holo-His-IsdC-N with a charge state manifold of +13 to +6. These charge states are different

from those of normal apo-IsdC-N which has a charge state manifold of +8, +7 and +6 [25]. The large range of charge states is due to the 6xHis-tag on IsdC-N which significantly increases the overall charge volume and protonatable basic amino acid residues of the protein and hence the charge state manifold. Approximately 30% of His-IsdC-N is holo meaning that 4 μM heme is left in metHb of the original 10 μM of heme. Interestingly, only apo-IsdB-N1N2 is present with a charge state manifold of +15 to +12. Any heme present in apo-IsdB-N1N2 has been transferred to apo-His-IsdC-N. No tetramer metHb peaks are present in the range from 3700 to 4600 m/z. Apo-IsdB-N1N2 has deconstructed tetramer holo-metHb. The resultant metHb species exist as either the αβ dimer (^{hh}(αβ), ^{ha}(αβ), ^{ah}(αβ) and ^{aa}(αβ)) with a charge state manifold of +13 to +11 or as denatured single strand apo-α or apo-β with a charge state manifold from +15 to +8 or +17 to +10 respectively.

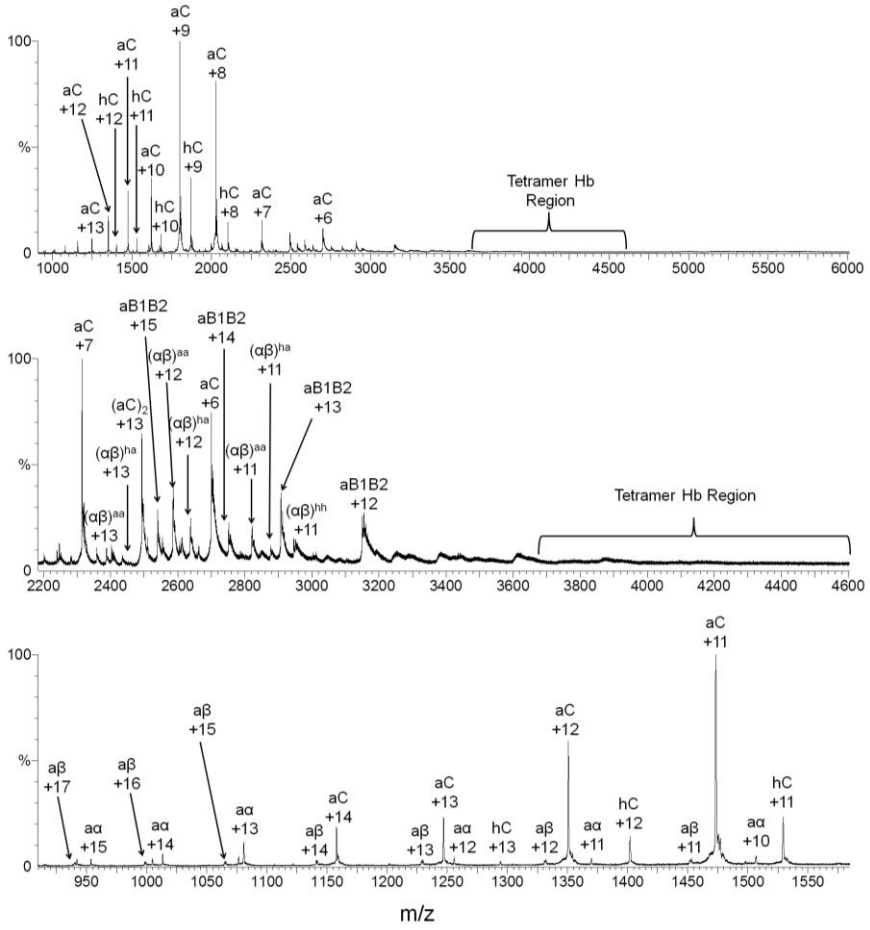

Figure 7-9 Heme extraction from 2.5 μM metHb and binding by 3 μM apo-IsdB-N1N2 and 20 μM apo-His-IsdC-N after 30 minutes. A mixture of apo- and holo-His-IsdC-N is observed with charge states +13 to +6. The large range of charge states is due to the His-tag on

IsdC-N, which significantly increases the overall number of charges on the protein and hence the charge state manifold. Apo-IsdB-N1N2 is present with a charge state manifold of +15 to +12. No tetramer metHb peaks are present in the range from 3700 to 4600 m/z. All metHb species exist as either the αβ dimer (^{hh}(αβ), ^{ha}(αβ), ^{ah}(αβ) and ^{aa}(αβ)) with a charge state manifold of +13 to +11 or as denatured single strand apo-α or apo-β with a charge state manifold from +15 to +8 or +17 to +10, respectively.

7.3.8 Extraction of heme from metHb by apo-IsdB-N1N2 and subsequent transfer to other Isd proteins using UV-visible absorption and MCD spectroscopy

The ESI-MS results above were confirmed by UV-visible absorption and MCD spectroscopy with transfer down the core of the Isd system through apo-IsdA-N, apo-IsdC-N and apo-IsdE, Figure 7-10. MetHb (blue line) exhibits a B band at 407 nm, which is mirrored in the MCD spectrum with an A term peak maximum at 403 nm and trough at 420 nm. A large B:Q ratio of ~10 is observed with a solution of MetHb. Stepwise addition of apo-IsdB-N1N2 to metHb results in a decrease in intensity of the B band and a significant red-shift from 579 nm to 553 nm in the Q band region in the MCD spectrum. Overall, the spectra start to resemble typical IsdB-N2 binding [28]. Addition of small amounts of IsdE did not result in a spectral shift. IsdE possesses a much different MCD fingerprint spectrum than Isd-NEAT domain proteins due to a shift in amino acid heme binding ligands from tyrosine to histidine [25, 28]. However, addition of IsdA-N and IsdC-N results in a B band shift to 415 nm. A Q band shift to 572 nm and a decrease of the 642 nm band is a fingerprint of heme transfer and binding to IsdE [25, 28]. Heme is transferred by IsdA-N to IsdC-N and then to IsdE.

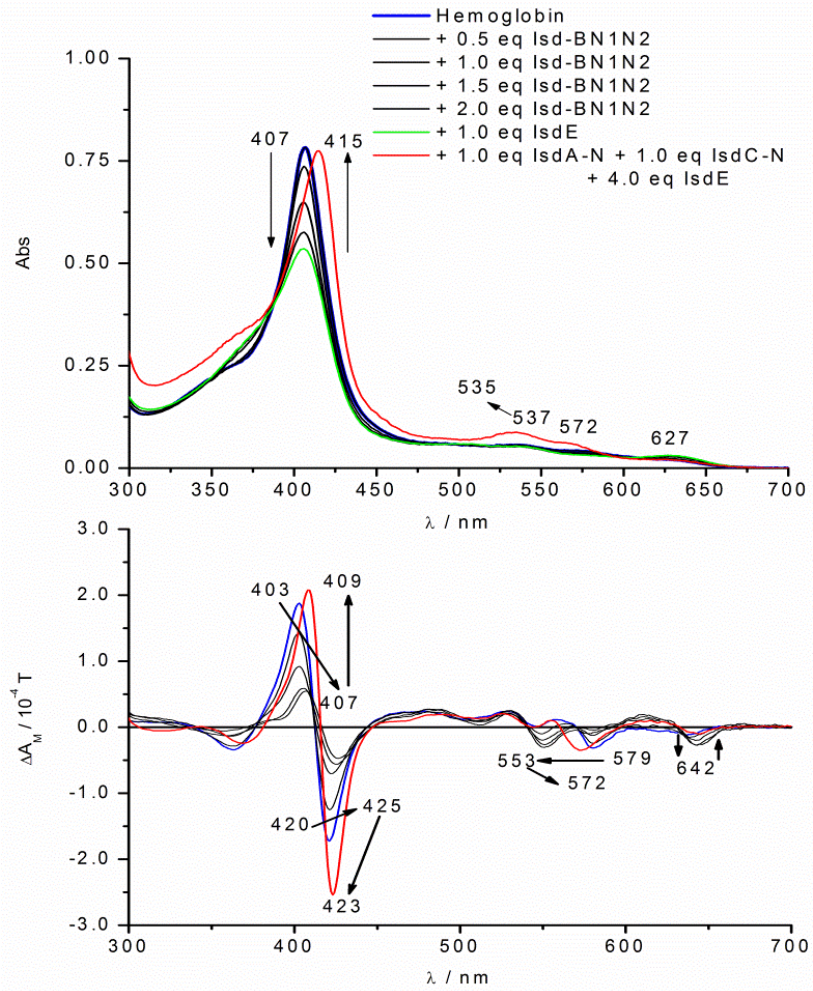

Figure 7-10 UV-visible absorption and MCD spectroscopic results for heme extraction by apo-IsdB-N1N2 and heme transfer to apo-IsdE via apo-IsdA-N and apo-IsdC-N for a stepwise titration. MetHb heme is possesses a large B:Q ratio of ~10. Upon addition of apo-IsdB-N1N2 and following heme extraction the absorption B band decreases while the MCD B band starts to shift from 403 nm to 407 nm. A significant decrease in the B:Q ratio from ~10 to ~3 is observed. This ratio is much more typical of Isd NEAT domain binding [25, 28]. Addition of IsdE does not change the MCD spectra to typical IsdE heme bound spectrum [25, 35]. However, addition of apo-IsdA-N and IsdC-N result in a spectra typical of holo-IsdE due to heme transfer from holo-IsdBN1N2 to IsdE via IsdA-N and IsdC-N. The B:Q ratio increases back to 10:1 and the resulting spectra are indicative of IsdE. Previous studies have shown that IsdA-N, IsdC-N and IsdE are not able to extract heme from metHb [19].

7.4 Discussion

7.4.1 Bovine Hb as a model for human Hb

The importance of freshly extracted Hb from bovine blood compared to lyophilized, commercially bought Hb has been stressed by other groups using ESI-MS [34, 37, 38].

Importantly, Hb extracted from fresh blood results in Hb that has much greater tetrameric fractions whereas lyophilized commercially-available Hb contains a very low fraction of tetrameric Hb. Due to this fact, we have used bovine Hb as a model for human Hb heme extraction by the Isd heme scavenging system in *S. aureus*. Interestingly, humans are not the only hosts susceptible to infection by *S. aureus*. Cows have also been found with *S. aureus* infections [40-42]. Potentially, the Isd system is able to extract heme from bovine Hb in the same way as human Hb since Hb is a very well conserved protein.

7.4.2 Importance of intact IsdB-N1N2 and oxidation of state of Hb for heme extraction

Apo-IsdBN1, apo-IsdBN2 and combinations of apo-IsdBN1 and apo-IsdB-N2 in solution do not extract heme from metHb or native oxyHb. The charge states of the IsdB proteins and both forms of Hb do not change in the mass spectral data. Charge states can indicate the overall size of proteins as unfolded or larger proteins have a higher surface area with solvent access to basic amino acids and hence more and higher charge states [25, 38, 43]. Therefore, with no changes in charge states the overall protein conformation of Hb and the IsdB components do not change. This interesting result is not what is observed with IsdH, the other Isd protein that interact with haptoglobin-hemoglobin complex and hemoglobin. Other work has shown that IsdH-N1 and IsdH-N2 interacts and binds to the αHb chain.

However, when intact IsdB-N1N2 is added to a solution of metHb significant changes in the structure of metHb are observed and the heme is trasnferred to IsdB-N1N2. In summary, tetramer metHb is shredded to dimer $^{hh}(\alpha\beta)$. Dimer $^{hh}(\alpha\beta)$, is further deconstructed into single stranded α and β chains which are subsequently denaturated upon heme extraction by apo-IsdB-N1N2. The denatured apo- α and apo-β strands resemble acid denatured apo-α and apo-β strands meaning that full denaturation of these strands has occurred. Overall, the only apo-Hb structures present during heme extraction are $^{ah}(\alpha\beta)$ $^{aa}(\alpha\beta)$ and apo-α and apo-β strands. Never present in solution is apo-tetrameric metHb, which indicates important protein-protein interactions exist with intact IsdB-N1N2 which interact with metHb to enable heme extraction and subsequent deconstruction and denaturation of metHb. Importantly, just as IsdH contains two non-heme binding NEAT domains that interact with metHb, IsdB might also require two contact points for

heme extraction from metHb. One, which would be located in the non-heme binding NEAT domain, IsdB-N1 and another, in the linker region between the two IsdB NEAT domains.

Furthermore, intact IsdB-N1N2 can only extract heme from metHb and not ferrous oxyHb. This result is important for two reasons: 1) heme in Hb found in the human body is ferrous. Therefore, *S. aureus* must secrete an oxidizing compound that is able to oxidize the heme in Hb in order to be able to extract heme. It is possible to speculate that this maybe another form of regulatory control since *S. aureus* is sensitive to heme as free heme is cytoxic [44]. 2) IsdC is the central conduit of Isd heme transfer system [18, 19, 25, 45]. Therefore, IsdC must bind and transfer heme through the system. However, IsdC is not able to bind ferrous heme [23, 46]. Therefore, the importance of starting with ferric heme extraction is crucial in the flow of heme through the system.

7.4.3 Extraction of heme by IsdB-N1N2 becomes efficient with IsdA-N and IsdC-N

From Figure 7-7 and Figure 7-8A it is clear the heme extraction by solely IsdB-N1N2 is not efficient or complete as is seen with heme transfer between other Isd NEAT domain proteins [25]. Approximately 50% of the IsdB-N1N2 is apo and there still exists tetrameric Hb. Addition of metHb to a solution of apo-IsdB-N1N2 and apo-His-IsdC-N results in holo-His-IsdC-N. As apo-His-IsdC-N does not extract heme from metHb, heme could only then be transferred from holo-IsdB-N1N2 which extracts heme from metHb. Interestingly, denaturation of α strands and β strands results and no tetrameric metHb mass spectral charge states are observed in solution. Apo-His-IsdC-N with a combination of apo-IsdB-N1N2 in solution results in a more efficient system where all tetrameric metHb is deconstructed to either the αβ dimer or the single stranded species.

A summary of the transfer and mechanism of heme extraction is presented in Figure 7-11. Heme extracted from metHb by IsdB-N1N2 does not transfer directly to IsdE. Addition of apo-IsdC-N and apo-IsdA-N results in heme transfer to IsdE. Since IsdA is partially exposed on the cell surface, [6, 13] the importance of IsdA-N as a mediator as heme reservoir in the Isd system becomes apparent as other groups have shown that heme transfer from IsdB-N1N2 to IsdA-N is relatively fast but transfer to IsdC-N is relatively slow [19]. Therefore, just as addition of apo-

His-IsdC-N to apo-IsdB-N1N2 and metHb results in a more efficient system, addition of apo-IsdA-N enhances the heme scavenging and extraction properties of the system.

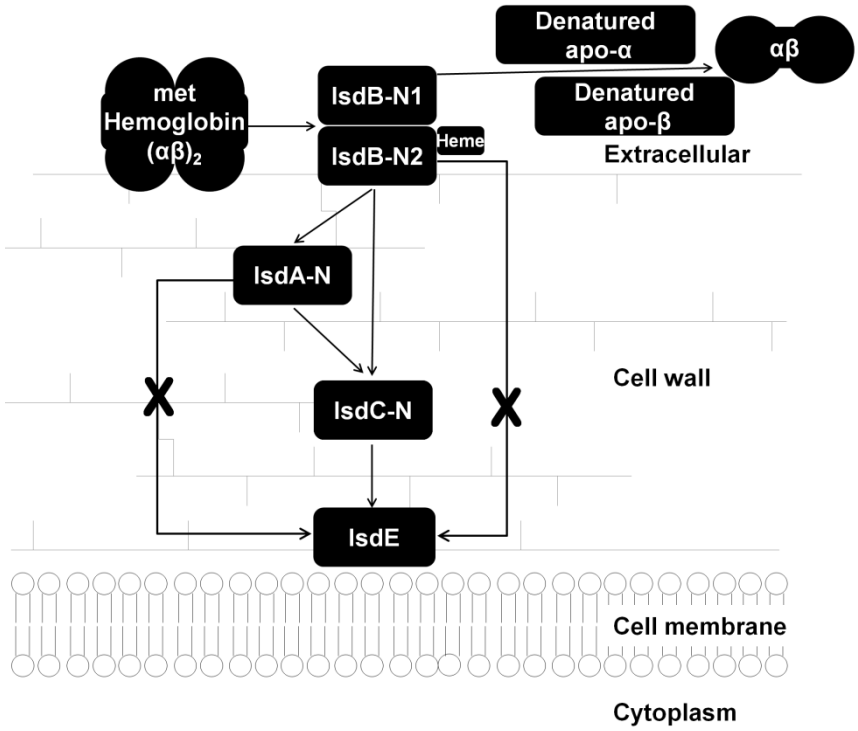

Figure 7-11 Schematic showing the pathways of heme extraction from metHb by IsdB-N1N2. Heme extraction by IsdB-N1N2 results in denatured α strands and β strands as well as dimeric $^{ha}(\alpha\beta)$, $^{ah}(\alpha\beta)$, $^{aa}(\alpha\beta)$ species. Holo-IsdB-N1N2 is not able to transfer to IsdE however, holo-IsdB-N1N2 is able to transfer heme to IsdA-N and IsdC-N.

7.5 Conclusion

In summary, unique protein-protein interactions exists with apo-IsdB-N1N2 and Hb with regards to heme extraction and the mechanism of heme removal. Interestingly, only fully intact apo-IsdB-N1N2 is able to extract heme from ferric metHb. Protein-protein ineractions must be located in the first NEAT domain of IsdB and the linker region between the two NEAT domains. Upon heme extraction, IsdB-N1N2 is able to denature and deconstruct metHb into subunit components that compose of $^{ah}(\alpha\beta)$ $^{aa}(\alpha\beta)$ dimer and the apo-α and apo-β strands. Heme scavenging is not efficient as tetramer metHb still exists in the presence of IsdB-N1N2. However, addition of apo-IsdC-N makes heme scavenging from metHb more efficient. With the presence of apo-IsdC-N in a solution with IsdB-N1N2 and metHb, the disapearance of all tetrameric metHb is observed. Interestingly, IsdB-N1N2 is not able to transfer heme from Hb to

IsdE but can transfer to IsdA-N and IsdC-N. Overall, when looking at heme extraction from metHb, the Isd system forms an efficient machine that is able to "shred" metHb and extract the precious iron containing heme resource inside.

7.6 References

1. Haley, K. P.; Skaar, E. P., *Mirobe. Infect.* **2011,** 14, 217-227.
2. Kuehnert, M. J.; Kruszon-Moran, D.; Hill, H. A.; McQuillan, G.; McAllister, S. K.; Fosheim, G.; McDougal, L. K.; Chaitram, J.; Jensen, B.; Fridkin, S. K.; Killgore, G.; Tenover, F. C., *J. Infect. Dis.* **2006,** 193, 172-179.
3. Wisplinghoff, H.; Bischoff, T.; Tallent, S. M.; Seifert, H.; Wenzel, R. P.; Edmond, M. B., *Clin. Infect. Dis.* **2004,** 39, 309-307.
4. Wandersman, C.; Delepelaire, P., *Annu. Rev. Microbiol.* **2004,** 58, 611-647.
5. Radtke, A. L.; O'Riordan, M. X., *Cell Microbiol.* **2006,** 8, 1720-1729.
6. Mazmanian, S. K.; Skaar, E. P.; Gaspar, A. H.; Humayun, M.; Gornicki, P.; Jelenska, J.; Joachmiak, A.; Missiakas, D. M.; Scheenwind, O., *Science.* **2003,** 299,m906-909.
7. Dryla, A.; Gelbmann, D.; Gabain, A. v.; Nagy, E., *Mol. Microbiol.* **2003,** 49, 37-53.
8. Taylor, J. M.; Heinrichs, D. E., *Mol. Microbiol.* **2002,** 43, 1603-1614.
9. Ratledge, C.; Dover, L. G., *Annu. Rev. Microbiol.* **2000,** 54, 881-941.
10. Nilsson, I. M.; Hartford, O.; Foster, T.; Tarkowski, A., *Infect. Immun.* **1999,** 67, 1045-1049.
11. Morrissey, J. A.; Cockayne, A.; Hammacott, J.; Bishop, K.; Denman-Johnson, A.; Hill, P. J.; Williams, P., *Infect. Immun.* **2002,** 70, 2399-2298.
12. Andrade, M. A.; Ciccarelli, F. D.; Perez-Iratxeta, C.; Bork, P., *Genome Biol.* **2002,** 3, 1-5.
13. Skaar, E. P.; Schneewind, O., *Microbes Infect.* **2004,** 6, 390-397.
14. Torres, V. J.; Pishchany, G.; Humayun, M.; Scheenwind, O.; Skaar, E. P., *J. Bacteriol.* **2006,** 188, 8421-8429.
15. Mazmanian, S. K.; Ton-That, H.; Su, K.; Scheenwind, O., *PNAS.* **2002,** 99, 2293- 2298.
16. Skaar, E. P.; Gaspar, A. H.; Scheenwind, O., *J. Biol. Chem.* **2004,** 279, 436-443.
17. Reniere, M. L.; Skaar, E. P., *Mol. Microbiol.* **2008,** 69, 1304-1315.
18. Grigg, J. C.; Ukpabi, G.; Gaudin, C. F. M.; Murphy, M. E. P., *J. Inorg. Biochem.* **2010,** 104, 341-348.
19. Zhu, H.; Xie, G.; Liu, M.; Olson, J.; Fabian, M.; Dooley, D.; Lei, B., *J. Biol. Chem* **2008,** 283, 18450-18460.
20. Watanabe, M.; Tanaka, Y.; Suenaga, A.; Kurodo, M.; Yao, M.; Watanabe, N.; Arisaka, F.; Ohta, T.; Tanaka, I.; Tsumoto, K., *J. Biol. Chem* **2008,** 283, 28649-28659.
21. Kumar, K. K.; Jacques, D. A.; Pishchany, G.; Cardoc-Davies, T.; Spirig, T.; Malmirchegini, G. R.; Langley, D. B.; Dickson, C. F.; Mackay, J. P.; Clubb, R. T.; Skaar, E. P.; Guss, J. M.; Gell, D. A., *J. Biol. Chem.* **2011,** 286, 38439-38447.
22. Vermeiren, C. L.; Pluym, M.; Mack, J.; Heinrichs, D. E.; Stillman, M. J., *Biochem.* **2006,** 45, 12867-12875.
23. Pluym, M.; Muryoi, N.; Heinrichs, D. E.; Stillman, M. J., *J. Inorg. Biochem.* **2008,** 102, 480-488.

24. Grigg, J. C.; Vermeiren, C. L.; Heinrichs, D. E.; Murphy, M. E., *Mol. Microbiol.* **2007,** 63, 139-149.
25. Muryoi, N.; Tiedemann, M. T.; Pluym, M.; Cheung, J.; Heinrichs, D. E.; Stillman, M. J., *J. Biol. Chem.* **2008,** 283, 28125-28136.
26. Villareal, V. A.; Pilpa, R. M.; Robson, S. A.; Fadeev, E. A.; Clubb, R. T., *J. Biol. Chem.* **2008,** 283, 31591-31600.
27. Tiedemann, M. T.; Muryoi, N.; Heinrichs, D. E.; Stillman, M. J., *Biochem. Soc. Trans.* **2008,** 36, 1138-1143.
28. Tiedemann, M. T.; Muryoi, N.; Heinrichs, D. E.; Stillman, M. J., *J. Porphyrins Phthalocyanines.* **2009,** 13, 1006-1016.
29. Mack, J.; Yoshiaki, A.; Kobayashi, N.; Stillman, M. J., *J. Am. Chem. Soc.* **2005,** 127, 17697-17711.
30. Pilpa, R. M.; Robson, S. A.; Villareal, V. A.; Wong, M. L.; Phillips, M.; Clubb, R. T., *J. Biol. Chem.* **2009,** 284, 1166-1176.
31. Liu, M.; Tanaka, W. N.; Zhu, H.; Xie, G.; Dooley, D. M.; Lei, B., *J. Biol. Chem.* **2008,** 283, 6668-6678.
32. Villareal, V. A.; Spirig, T.; Robson, S. A.; Liu, M.; Lei, B.; Clubb, R. T., *J. Am. Chem. Soc.* **2011,** 133, 1417-14179.
33. Antonini, E.; Brunori, M., North-Holland Publishing Company: Amsterdam, 1971; Vol. 21.
34. Boys, B. L.; Kuprowski, M. C.; Konermann, L., *Biochem.* **2007,** 46, 10675-10684.
35. Pluym, M.; Vermeiren, C. L.; Mack, J.; Heinrichs, D. E.; Stillman, M. J., *Biochem.* **2007,** 46, 12777-12787.
36. Gaudin, C. F. M.; Grigg, J. C.; Arrieta, A. L.; Murphy, M. E., *Biochem.* **2011,** 50, 5443-5452.
37. Simmons, D. A.; Wilson, D. J.; Lajoie, G. A.; Doherty-Kirby, A.; Konermann, L., *Biochem.* **2004,** 43, 14792-14801.
38. Konermann, L.; Douglas, D. J., *Biochem.* **1997,** 36, 12296-12302.
39. Ngu, T.; Lee, J.; Rushton, M. K.; Stillman, M. J., *Biochem.* **2009,** 38, 8806-8816.
40. Shoshani, E.; Leitner, G.; Hanochi, B.; Saran, A.; Shpigel, N. Y.; Berman, A., *J. Dairy. Res.* **2000,** 67, 155-169.
41. Sears, P. M.; Smith, B. S.; English, P. B.; Herer, P. S.; Gonzalez, R. N., *J. Dairy. Res.* **1990,** 73, 2785-2789.
42. García-Álvarez, L.; Holden, M. T.; Lindsay, H.; Webb, C. R.; Brown, D. F.; Curran, M. D.; Walpole, E.; Brooks, K.; Pickard, D. J.; Teale, C.; Parkhill, J.; Bentley, S. D.; Edwards, G. F.; Girvan, E. K.; Kearns, A. M.; Pichon, B.; Hill, R. L.; Larsen, A. R.; Skov, R. L.; Peacock, S. J.; Maskell, D. J.; Holmes, M. A., *Lancet Inf. Dis.* **2011,** 11, 70126-70128.
43. Konermann, L.; Douglas, D. J., *J. Am. Soc. Mass Spec.* **1998,** 9, 1248-1254.
44. Torres, V. J.; Stauff, D. L.; Pishchany, G.; Bezbradica, J. S.; Gordy, L. E.; Iturregui, J.; Anderson, K. L.; Dunman, P. M.; Joyce, S.; Skaar, E. P., *Cel. Host Microbe.* **2007,** 19, 109-119.
45. Grigg, J. C.; Mao, C. X.; Murphy, M. E. P., *J. Mol. Biol.* **2011,** 413, 684-698.
46. Pluym, M.; Vermeiren, C. L.; Mack, J.; Heinrichs, D. E.; Stillman, M. J., *J. Porphyrins Phthalocyanines.* **2007,** 11, 165-171.

Chapter 8. Insight into blocking heme transfer by exploiting molecular interactions in the core Isd heme transporters IsdA-NEAT, IsdC-NEAT and IsdE of *Staphylococcus aureus*[7]

8.1 Introduction

Iron is an essential component of living biological systems [1] due its ability to undergo changes in oxidation and to take part in ligand binding. Since free iron is not typically available, as it is sequestered by proteins, invasive organisms need high affinity systems to acquire and store iron [2]. *S. aureus* responds to the iron-restricted environment of the host with an array of iron-uptake and acquisition systems. It has been shown that *S. aureus* is able to grow using heme, hemoglobin, hemoglobin-haptoglobin, transferrin, ferric iron or ferrous iron as the sole iron source [3-5]. Siderophores are examples of iron uptake through the use of low molecular weight iron binding molecules (usually 400-1000 Da) that are secreted by bacteria into their extra-cellular environments. Siderophores have high affinity for iron and are found in numerous bacterial systems, those secreted by bacteria are able to remove iron from transferrin. *S. aureus* is no exception as two structurally characterized polycarboxylate-type siderophores, Staphyloferrin A and Staphyloferrin B [6].

Since the majority of iron is sequestered and bound as heme-iron, *S. aureus* has also evolved mechanisms to exploit and scavenge heme as an iron source. The iron-regulated surface determinant (*isd*) gene cluster was first identified in 2002 [5, 7, 8], and then in 2003, Mazmanian *et al.* [3] reported that, when grown in iron-limiting medium, *S.* aureus expresses genes that are involved in iron acquisition and were the first to propose that the Isd series of protein formulate a heme transfer pathway across the cell wall and through the cell membrane. The Isd system consists of nine iron-regulated proteins, named IsdA, IsdB, IsdC, and IsdH, which are cell-wall anchored, surface proteins, and IsdDEF, which together constitute a membrane-localized ABC transporter and, finally, IsdG and IsdI, which encode heme-degrading enzymes in the cytoplasm [9, 10]. This system was proposed [5, 7, 8] and later demonstrated [3] to be able to pass heme

[7] A version of this work has been submitted:
Tiedemann M. T., Tyler B.J., M. J. Stillman, Metallomics., **2012.**

through the gram-positive cell wall and cell membrane into the cytoplasm where heme is deconstructed and free iron is released. These nine proteins mediate the delivery of heme from the host's plasma into the *S aureus* cytoplasm [11]. IsdB and IsdH are exposed to the cell exterior, while IsdA is partially exposed and IsdC is buried within the cell wall [3]. In terms of a mechanism for heme acquisition IsdB and IsdH capture heme from Hb released from erythrocytes by hemolysins [12, 13]. IsdH binds haptoglobin (a serum glycoprotein that protects the host from free hemoglobin) and the haptoglobin-hemoglobin complex [4, 14]. IsdA is proposed to function as a heme scavenging protein and a "heme reservoir" for IsdH and IsdB [15, 16]. IsdC, which is located in the cell wall, acts as the central conduit of heme transfer in the Isd system [17-19]. The membrane bound complex IsdDEF complex pumps heme across the membrane [11, 20]. Heme is finally deconstructed by IsdG monooxygenase or its paralog, IsdI [10, 11]. The proteins IsdA, IsdB, IsdC and IsdH each contain at least one Near Transporter (NEAT) domain that adopts a beta sandwich structure to bind one ferric heme into a groove with heme-iron coordination via Tyr [15-18, 21-23].

Previous studies have shown that ferric heme transfer takes place in a unidirectional fashion. Heme propagates down the pathway in the sequence (with the heme proximal amino acid residue shown) IsdB-NEAT 2 (Tyr)→ IsdA-NEAT (Tyr) → IsdC-NEAT (Tyr) → IsdE (His) or, alternatively, initiating from IsdH-N3, IsdH-N3 (Tyr) → IsdA-NEAT → IsdC-NEAT → IsdE. Significantly, IsdA does not transfer heme directly to IsdE under any conditions [18, 20, 21, 24].

The heme uptake mechanisms of bacterial pathogens present an ideal path for targeted drug delivery because these pathogens accumulate heme via active transport and are maximally expressed in iron-limiting conditions of the host, which happens during infection [25]. It is thought that metal-substituted protoporphyrins (PPIXs) could be inserted into enzymes by the bacteria and render them useless for catalytic activity [25-27]. However, most studies do not focus on how the metal-substituted PPIX can affect the heme uptake pathway. With the detailed characterization of the Isd heme transfer system of *S.* aureus, we propose that a compound that could be transferred only partially through the heme uptake system and could have a greater efficacy in potentially serving as an actual route for potentially killing the bacteria by preventing the bacteria from uptaking important iron resources.

IsdA-N and IsdH-N3 will bind rings with metals other than Fe. GaPPIX and MnPPIX bind and form nearly indistinguishable three-dimensional structures when bound to IsdH-N3 and

exhibit similar ring transfer properties to apo-IsdA as for the native heme [28]. Similar results have been reported for CoPPIX binding to IsdA-N [11, 29] and for Zn(II)-PPIX binding to IsdC-N [19]. Despite claims for an antibacterial "Trojan horse" approach in which these compounds gain access to the interior of the cell via Isd transfers [25, 27, 28], there have been no reports of the effects of metal substituted-PPIXs on the heme transfer with IsdA, IsdC and IsdE, the core proteins located in the cell wall of *S. aureus*. A second controlling feature in the highly specific and unidirectional nature of the Isd heme transfer mechanism may well involve the peripheral substituents of the heme, not just the coordination properties of the ferric iron. The role of the carboxylic acid tails of the heme in binding and transfer properties may be challenged by changing the carboxylic acids to the relatively non-polar dimethyl ester side chain.

In this study, the effects of metal and the ring periphery substitution on the PPIX transfer in the Isd system of *S. aureus* are investigated using Co(III)PPIX (CoPPIX), Mn(III)PPIX (MnPPIX) and Fe(III)PPIX-dimethyl ester (FePPIX-DME). Electrospray ionization mass spectrometry (ESI-MS), UV-visible absorption and magnetic circular dichroism (MCD) spectroscopies were used to probe ring binding and ring transfer properties of the IsdA-N, IsdC-N and IsdE proteins. IsdA binds to each of the rings but the subsequent transfer properties to IsdC-N or IsdE are not the same as found with heme. FePPIX-DME transfers from IsdA-N to IsdC-N but neither protein transfers the ring to IsdE. IsdA-N does not transfer CoPPIX to IsdC-N or IsdE. IsdA-N does transfer MnPPIX to both IsdC-N and IsdE. Significantly, it is possible that since CoPPIX and FePPIX-DME bind to IsdA-N, the lack of transfer to IsdC-N and subsequently to IsdE for CoPPIX could prove to be used as a potential disruption agent to the *S. aureus* heme transfer system and may identify as a possible anti-microbial agent against this bacteria.

8.2 Experimental Methods

8.2.1 Materials and Methods

Experimental procedures have previously been reported; please refer to Chapter 2 for further protein growth, protein purification, ESI-MS and MCD spectroscopy preparatory and running procedures.

8.2.2 Porphyrin synthesis and addition to Isd proteins

CoPPIX and MnPPIX chloride were purchased from Frontier Scientific (Logan, UT). All samples used for binding were dissolved in DMF. FePPIX-DME was prepared from free-base PPIX-DME purchased from Frontier Scientific (Logan, UT) using standard metal insertion procedures [30] and dissolved in pyridine. FePPIX-DME synthesis was confirmed from the UV-visible absorption spectrum where a blue shift in the Soret band from ~405 nm (free base PPIX-DME) to ~385 nm (FePPIX-DME) was observed. The reaction purity was confirmed with ESI-MS analysis. The experimental data of a mass peak of 644.2 Da (FePPIX-DME - H) matched the theoretical mass of 645.55 Da. No free base PPIX-DME (mass 590.71 Da) was found in the mass spectrum (Appendix Figure 8-14). All porphyrins masses were checked by ESI-MS to ensure sample purity.

To insert the porphyrin into the heme-free proteins, concentrated (10x stoichiometric excess) solutions of M-PPIXs were added to each of the apo-Isd proteins and subsequent holo-Isd proteins formed were purified to separate excess free PPIX from PPIX-bound protein using G-25 size exclusion chromatography with 10 mM PBS buffer pH 7.4.

8.3 Results

8.3.1 FePPIX-DME binding to IsdA-N: absorption, MCD and ESI-mass spectra.

Figure 8-1A shows the UV-visible absorption and MCD spectra of FePPIX-DME in pyridine. The axial coordination of the Fe^{3+} by pyridine resembles axial ligation from the His in the Isd proteins. Even in neat pyridine a mixture of species is observed in the MCD spectrum emphasizing the much higher resolution of this technique when studying porphyrins. The assignment of the B or Soret absorption band to the 400 nm region (401 nm) with its accompanying positive MCD pseudo-A term (401/416 nm) is straightforward, the assignment of the absorption bands in the 500-700 nm region is complicated by the superposition of both the first π-π^* band, the Q_{00} and associated Q_{vib} bands and the charge transfer bands (LMCT or MLCT). In Figure 8-1A, the 550/559 MCD band envelope are assigned as the Q_{00} and the 594/629 nm envelope as LMCT. In Figure 8-1B the spectral data when excess FePPIX-DME was added to apo-IsdA-N and the resulting complex purified by column chromatography are

shown. In comparison to the uncomplexed PPIX-DME ring significant UV-visible absorption and MCD spectral bands shifts when it is bound to the IsdA-N are observed. The MCD Soret band blue shifts from a pseudo-A term centered at 412 nm to one centered on 417 nm. The absorption and MCD spectra in Figure 8-1B arise solely from the FePPIX-DME bound to the protein, because FePPIX-DME is not soluble in 10 mM PBS buffer pH 7.4 and the chromatographic isolation of the protein will have separated the protein from any remaining free FePPIX-DME, the spectra must be from the protein bound ring. It is clear that there is a mixture of high and low spin species due to underlying charge transfer bands found in the Soret absorption band at 405 nm, which distort the MCD spectral alignment. There are significant changes in the Q band region. The appearance of a band at 626 nm in the absorption spectrum associated with a 614/643 nm derivative-like envelope in the MCD spectrum is strongly correlated with ring binding [16, 31]. The Q:B MCD band ratio is also reduced from ~3:1 for FePPIX-DME to ~2:1 upon binding with IsdA-N. The MCD spectrum of FePPIX-DME bound to IsdA-N in Figure 8-1B is very similar to that reported for heme-bound IsdA-N, which exhibits a similar B:Q ratio as well as similar spectral features [16]. In view of this similarity, and the differences from the pyridine solution, Figure-1A, it can be concluded that IsdA-N binds FePPIX-DME through the same tyrosine ligand that binds heme [16, 29].

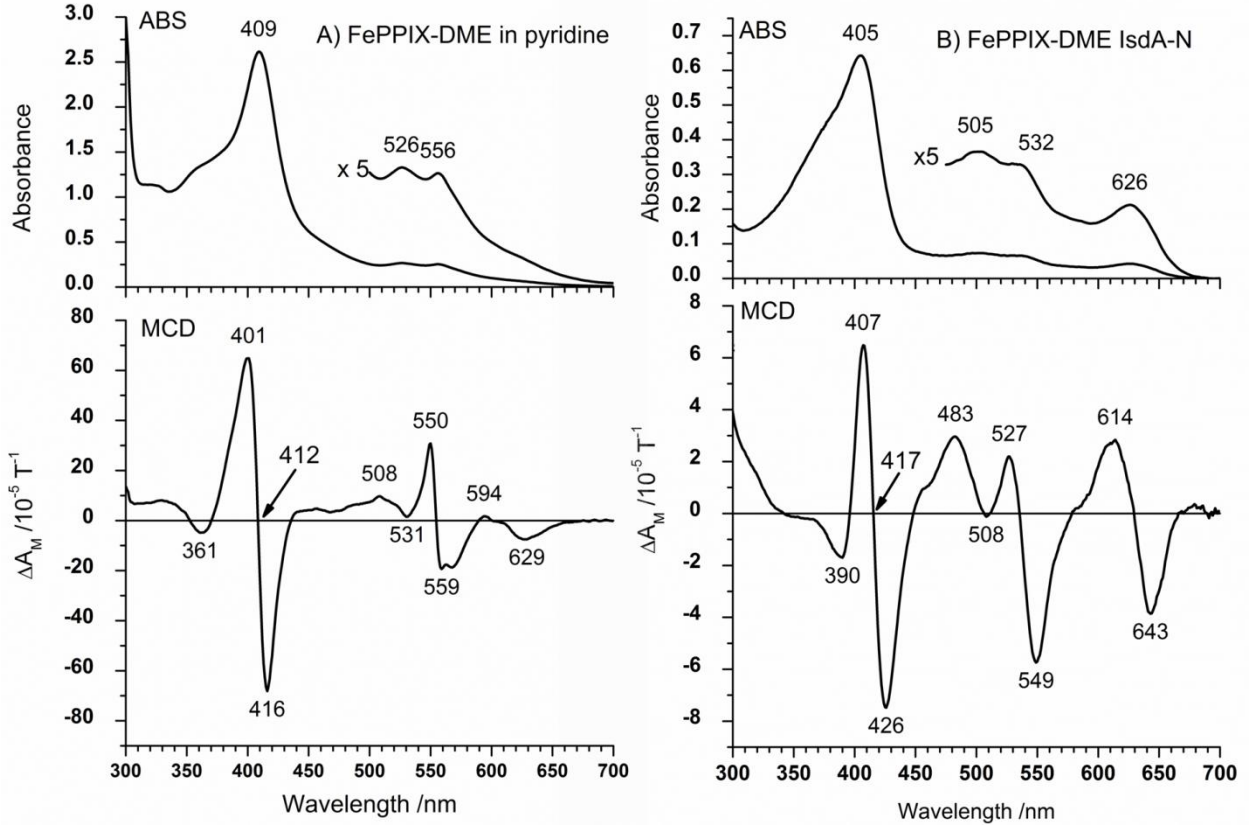

Figure 8-1 Absorption and MCD spectra of A) FePPIX-DME in pyridine and B) FePPIX-DME bound to IsdA-N purified by column chromatography. Significant UV-visible absorption and MCD spectral band shifts following binding of free PPIX-DME to IsdA-N are observed. The MCD spectrum now shows the presence of two species as the cross-over red shifts to 417 nm from 409 of the free heme. The appearance of the 614 nm and 643 nm MCD bands under the more intense 626 nm absorption band indicate that the FePPIX-DME is much more high spin than when not bound.

Figure 8-2A shows the charge states and deconvoluted mass spectra of the species in solution following reaction of 3 µM IsdA-N with excess (30 µM) FePPIX-DME. Apo-IsdA-N (aA) has a charge state distribution of +6 to +8, which match previously reported data [18]. Upon binding FePPIX-DME, holo-IsdA-N forms (hA), with charge states between +7 and +9, indicating that the protein overall volume remains similar to the apo-conformation. The deconvoluted data show a shift in the mass associated with apo-IsdA-N (14,627 Da) to that for holo-(FePPIX-DME)-IsdA-N (15,269 Da). The difference matches the theoretical mass of FePPIX-DME of ~644 Da. Approximately 40% of the apo-IsdA-N binds FePPIX-DME even though the FePPIX-DME is in excess. This means that the binding constant is significantly less than that for heme.

Typically, over 95% of apo-IsdA-N binds heme in the presence of excess heme to form holo-IsdA-N [18].

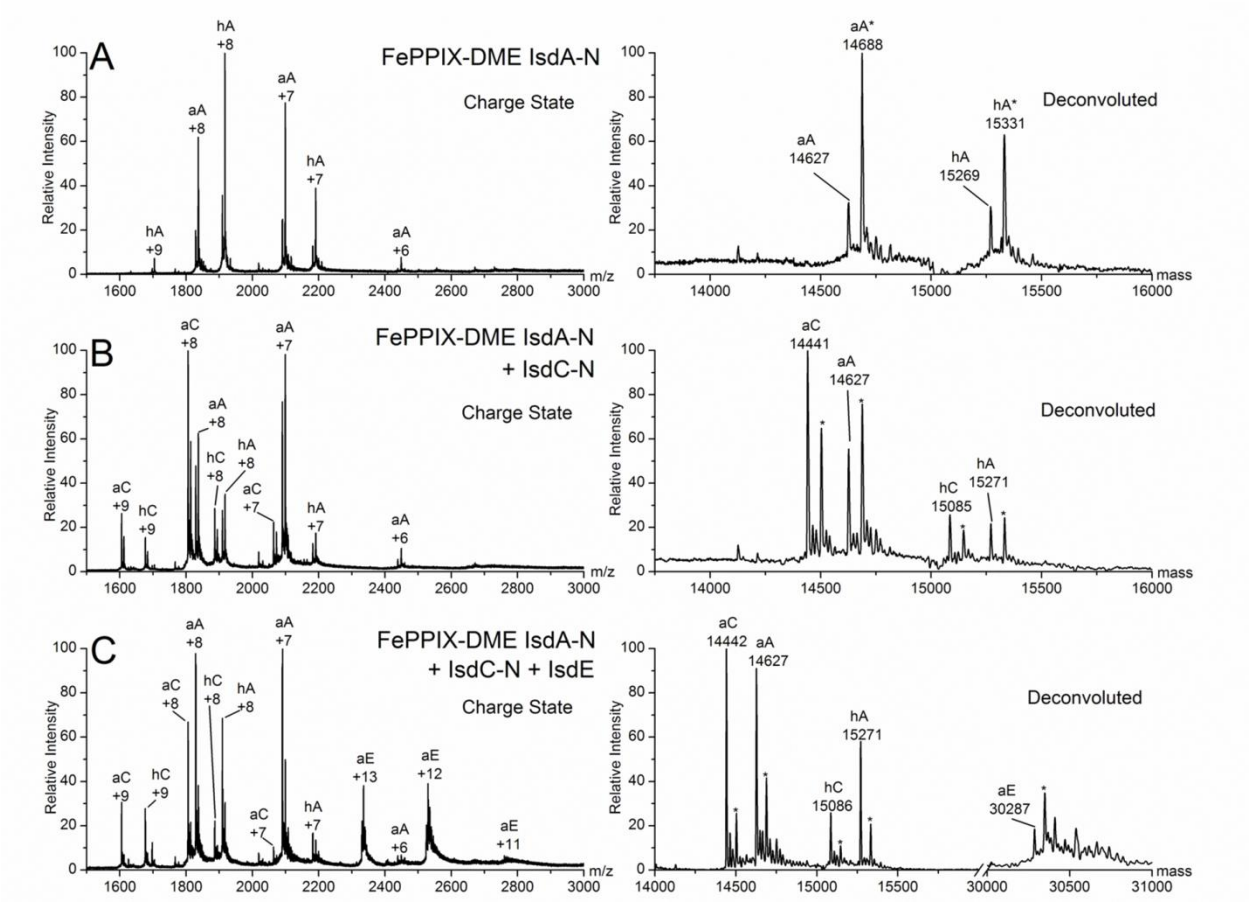

Figure 8-2 ESI-Mass spectral data recorded following reaction of FePPIX-DME with IsdA-N. A) Charge state and deconvoluted mass spectra after the reaction of 3 µM IsdA-N with excess (30 µM) FePPIX-DME. Apo-IsdA-N and holo-IsdA-N are both observed. Apo-IsdA-N(aA, 14627 Da) has a charge state distribution of +6 to +8 and following binding, holo-IsdA-N (hA, 15269 Da) there is a shift to a +7 to +9 distribution. B) Charge state and deconvoluted mass spectra after the reaction of 3 µM holo-IsdA-N with excess (6 µM) apo-IsdC-N. Four species are present in solution, apo and holo-IsdA-N, with charge states +6 to +8, and apo and holo-IsdC-N (14441/15058 Da), with charge states +7 to +9. The data show that IsdA-N does transfer FePPIX-DME to IsdC-N. C) Charge state and deconvoluted mass spectra after the reaction of 6 µM holo-IsdA-N with 3 µM apo-IsdC-N and 6 µM apo-IsdE. Five species are present in solution, apo and holo-IsdA-N (+7 and +8), apo and holo-IsdC-N (+7 to +9) and apo-IsdE (30287 Da, +11 to +13). The data clearly show that no holo-IsdE is present. No FePPIX-DME has transferred to IsdE. The peaks are adducted by a common 62 Da adduct found after centrifugation sample preparation (labeled * in the deconvoluted spectra)

8.3.2 FePPIX-DME binding and transfer determined by ESI-MS and MCD techniques

Since IsdA-N binds FePPIX-DME the heme transfer mechanism was tested to determine the effects of reducing the polar carboxylic acid side chains of heme to the relatively non-polar methyl-esters using ESI-MS and UV-visible and MCD absorption spectroscopy. The mass spectral data for the reaction of 3 µM holo-IsdA-N mixed with 6 µM (excess) apo- IsdC-N are shown in Figure 8-2B. Charge state data indicate that four species are present in solution: apo/holo-IsdA-N, with charge states +6 to +8 as previously reported [18], and apo/holo-IsdC-N, with charge states +7 to +9. Deconvolution shows that there is approximately 25% holo-IsdA-N and 25% holo-IsdC-N. indicating that indeed holo-IsdA-N does transfer the FePPIX-DME to apo-IsdC-N. There were no further changes after one hour.

Figure 8-3A shows absorption and MCD data for the same reaction as described in Figure 8-1A. 30 µM FePPIX-DME was mixed with 3 µM apo-IsdC-N and purified by column chromatography to remove excess free FePPIX-DME. When the spectral data are compared with those for FePPIX-DME bound in holo-IsdA-N, it clear that there is a blue shift in the Soret band from 405 nm to 400 nm. This is reflected in the MCD spectrum with slight blue shifts in the A-like term (by 2 nm from (-)390, (+)407 and (-)426 nm to (-)388, (+)405 and (-)424 nm). These spectroscopic changes of binding FePPIX-DME binding to IsdC-N are similar to those reported for heme binding apo-IsdC-N [20]. Therefore, IsdC-N coordinates the FePPIX-DME with a tyrosine amino acid ligand. This result is not unexpected as other porphryins are bound in much the same way as the heme [19].

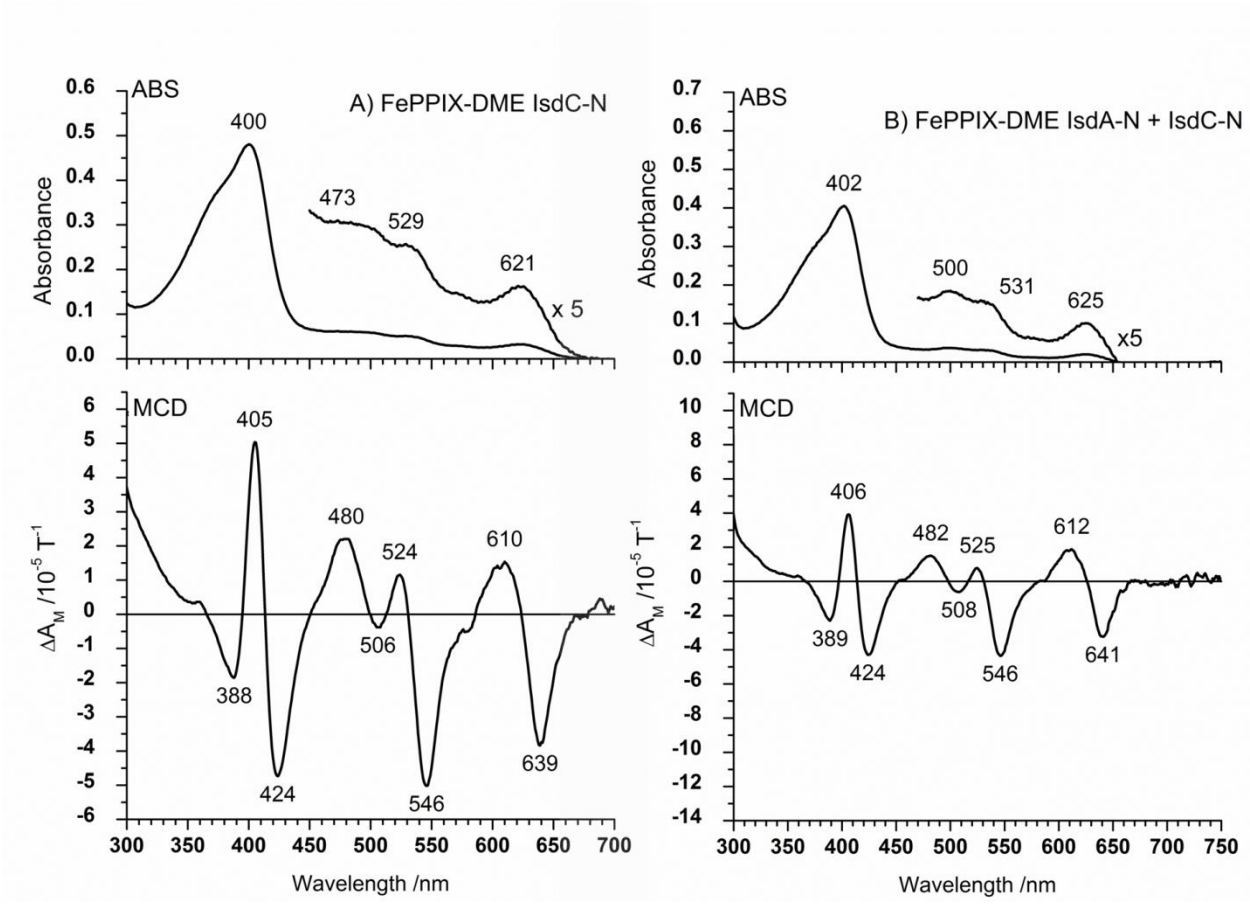

Figure 8-3 Absorption and MCD spectra of A) FePPIX-DME bound to IsdC-N and B) FePPIX-DME transferred from IsdA-N to IsdC-N. A) A solution of FePPIX-DME mixed with apo-IsdC-N. When compared to FePPIX-DME bound holo-IsdA-N, there is a blue shift in the Soret band from 405 to 400 nm. This is reflected in the MCD spectrum with slight blue shift in the A term-like band centered at 405 nm. The overlapping MCD bands in the Soret region indicates the presence of mixed species. B) A solution of 3 µM holo-IsdA-N mixed with 6 µM apo-IsdC-N. The complicated, overlapped appearance is due to a mixture of holo-IsdA-N and holo-IsdC-N in solution.

The ESI-MS data, Figure 8-2B, showed that FePPIX-DME was transferred from holo-IsdA-N to IsdC-N when holo-IsdA-N was mixed with apo-IsdC-N. The optical spectral data in Figure 8-3B confirm this. When 3 µM holo-IsdA-N was added to 6 µM apo-IsdC-N new spectra that resemble an average of holo-IsdA-N and holo-IsdC-N was observed. The Soret band at 402 nm is midway between those for the two individual FePPIX-DME bound species. There is a significant decrease in the B and Q band intensities in the MCD spectrum relative to the 294 nm band, due to the presence of the two holo species in solution, where the decrease in signal arises from cancelling of band intensities. Therefore these data confirm the ESI-MS results: IsdA-N is

able to transfer FePPIX-DME to IsdC-N but not completely, unlike with heme transfer, where heme is transferred completely from IsdA-N to IsdC-N [13, 18].

The most important reaction in the Isd system is the transfer of heme from IsdA-N via IsdC-N to IsdE, that is through the cell wall to the membrane. The data described in Figure 8-2C show the resultant FePPIX-DME-bound species when 6 μM holo-IsdA-N was mixed with 3 μM apo-IsdC-N and 6 μM apo-IsdE. The charge state data show that there are five species present in solution: apo/holo-IsdA-N (+7 and +8), apo/holo-IsdC-N (+7 to +9) and apo-IsdE (+11 to +13). There are no charge states attributable to holo-IsdE present. Deconvolution showed that FePPIX-DME transfer had occurred from IsdA-N to IsdC-N but not to the apo-IsdE. Therefore, clearly, neither IsdA-N nor IsdC-N can transfer FePPIX-DME to IsdE.

The same three-protein experiment was carried out monitoring the results by absorption and MCD spectroscopy, Figure 8-4. A spectroscopic advantage with FePPIX-DME is that the spectroscopy closely resembles the absorption spectra to heme since only the periphery carboxylic acid tails are changed. Therefore, the binding amino acids can be readily predicted by comparing the spectra to that of well characterized heme binding properties in the Isd system. The spectra measured were very similar to the set measured following mixing holo-IsdA-N with apo-IsdC-N, Figure 8-2, which resulted in a mixture of holo/apo-IsdA-N and holo/apo-IsdC-N. IsdE binds heme with a proximal histidine, which is different from the tyrosine that binds heme in IsdA-N and IsdC-N [16, 17, 31, 32]. This change from a nitrogen donor to an oxygen donor for the iron, red shifts the Soret band from 402 to 415 nm, in much the same way that these donor atoms change the spectrum of myoglobin [33]. If IsdE bound FePPIX-DME under the conditions of the experiment, a large change in the absorption spectrum would be expected as is seen when IsdE binds heme [18, 31]. Since no spectral changes are seen compared with a mixed solution of holo-IsdA-N and holo-IsdC-N, no FePPIX-DME transfer has taken place.

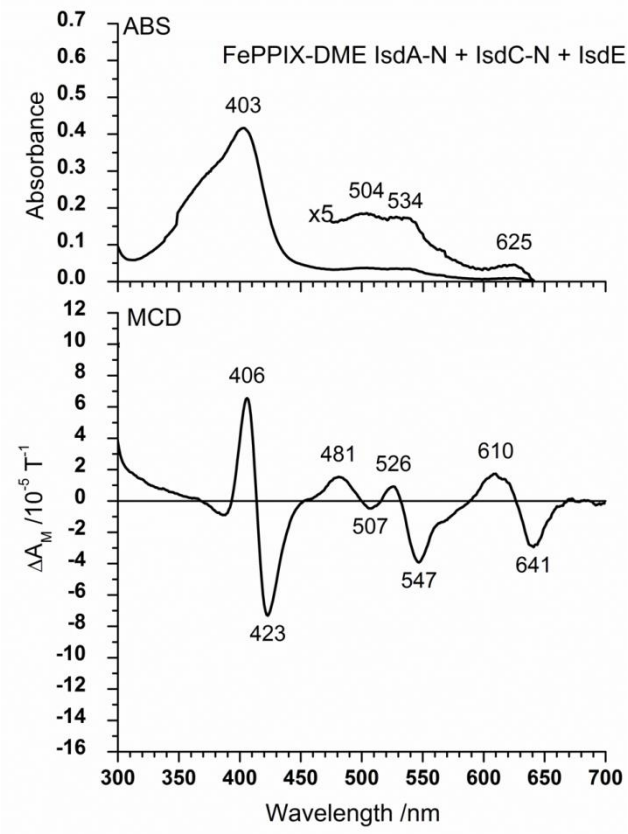

Figure 8-4 Absorption and MCD spectral data recorded when apo-IsdE and apo-IsdC-N were mixed with holo(FePPIX-DME)-IsdA-N. 3 µM holo-IsdA-N was mixed with 3 µM apo-IsdC-N and 6 µM apo-IsdE. The spectra are typical of holo-IsdA-N and holo-IsdC-N not holo-IsdE indicating that neither holo-IsdA-N nor holo-IsdC-N are able to transfer FePPIX-DME to apo-IsdE.

8.3.3 Effects of central metal of heme on heme transfer

The focus of this study now shifts to looking at the effect of the central metal on PPIX transfer between the core Isd proteins. CoPPIX and MnPPIX were chosen as ideal candidates since these metals straddle Fe in the Periodic Table. In these experiments, the axial ligand preferences are essentially testing the effects of hardness of the metal, where Co(III) is a harder metal than Fe(III), which is harder than Mn(III). The importance of a +3 charge on the metal has been demonstrated previously [25-27], where it appears that +3 metals mimic Fe(III) and have a higher efficacy of anti-bacterial properties when compared to +2 metal substituted PPIXs.

8.3.4 CoPPIX binding to IsdA-N monitored by MCD spectroscopy.

It has been shown previously that IsdA-N binds CoPPIX in the same manner as IsdA-N binds heme [11, 29]. The X-ray crystallography data show that overall protein confiormation is similar indicating that while ring shape is an important factor in binding, perhaps the metal is not as critical a factor for protein binding. However, if the ligand binding properties of each metal are different then it would be expected that changes in ring transfer properties with each metal would occur. Free CoPPIX has different spectral properties than CoPPIX bound to IsdA-N, Figure 8-5. The Soret band at 421 nm red shifts to 426 nm upon CoPPIX binding. This is mirrored in the MCD spectrum with a shift in the Soret peak (+)417 nm to (+)420 nm and the trough from (-)430 to (-)433 nm. In comparison to heme binding, the Q bands also shift by 2 nm upon binding [16]. Sensitive measures of the excited state modifications by the environment are found in the ratios of the MCD B (Soret) band magnitude compared with the Q band span. The B:Q band ratio changes from >1 to <1 upon CoPPIX binding. This change is similar to heme binding with IsdA-N because the heme bound to IsdA-N exhibits a significantly higher spin than the free heme [16]. These results coincide with the results from the crystal structure of IsdA-N with CoPPIX, where the CoPPIX ring is bound by the same tyrosine ligand that would bind heme [11, 29].

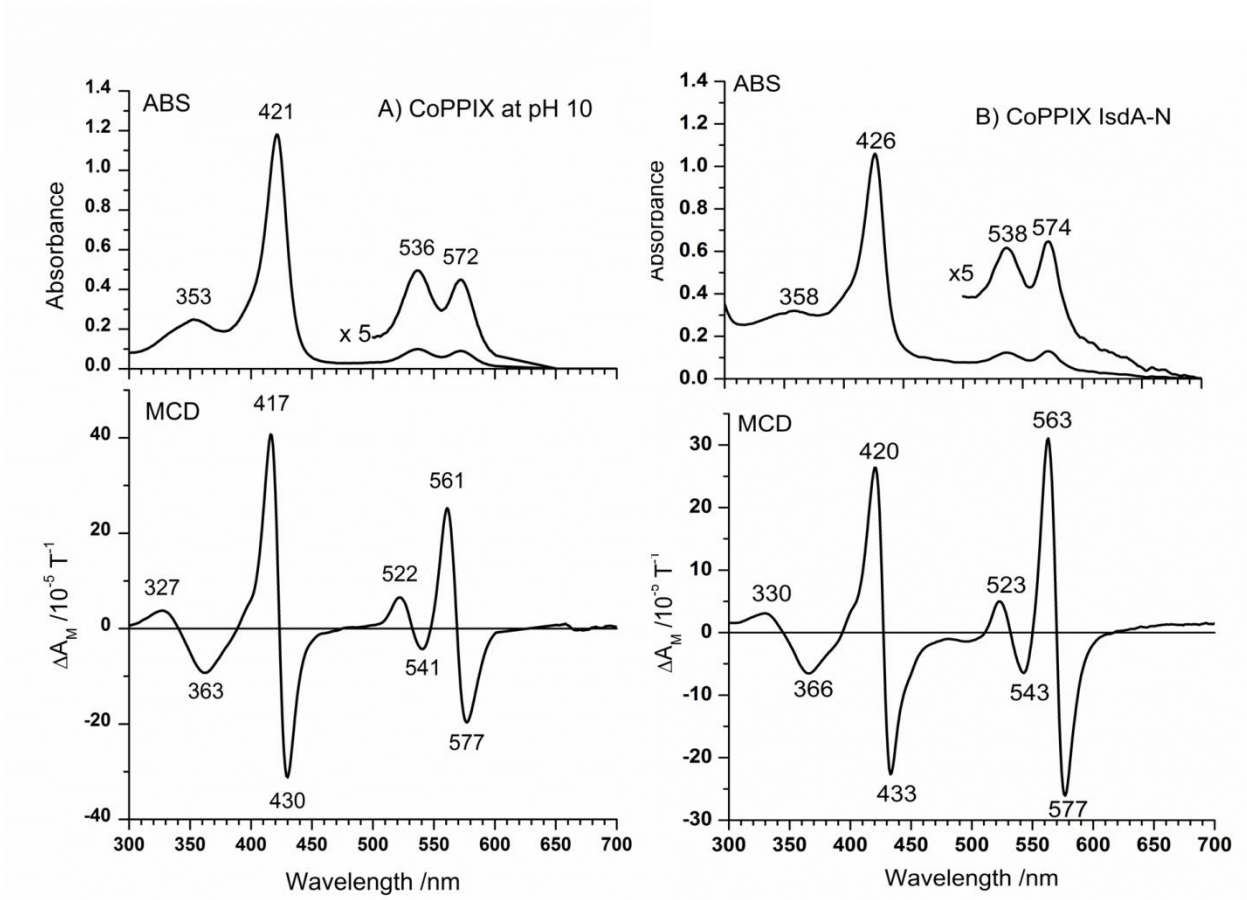

Figure 8-5 Absorption and MCD spectra of A) free Co-PPIX at pH 10 and B) CoPPIX added in excess to apo-IsdA-N. The Soret band at 421 nm red shifts to 426 nm following CoPPIX binding, which is mirrored in the MCD spectrum. The Q bands also shift by 2 nm with CoPPIX binding to apo-IsdA-N. The B:Q band ratio changes from >1 to <1 upon Co-PPIX binding.

CoPPIX binding to apo-IsdA-N was confirmed by ESI-MS, Figure 8-6A. Apo-IsdA-N (aA) has a charge state distribution of +6 to +8. Upon binding CoPPIX (hA), the charge states remain the same. This means that the overall volume remains similar to the apo-conformation, this result is also seen with heme binding to IsdA-N [16, 18]. Deconvolution, shows that both apo-IsdA-N (14624 Da) and holo-IsdA-N (15241 Da) exist in solution. An increase of ~617 Da corresponds to an increase in mass that matches CoPPIX. Approximately 75% of IsdA-N binds CoPPIX, meaning that the binding to IsdA-N is significantly less favourable than with heme. Typically, when adding excess heme to IsdA-N, followed by purification steps, >95% of the protein is holo-IsdA-N [16, 18]. However, these ESI-MS results confirm the UV-visible absorption and MCD spectroscopic results.

8.3.5 CoPPIX binding and transfer monitored by ESI-MS and MCD spectroscopy

CoPPIX transfer from holo-CoPPIX-IsdA-N to apo-IsdC-N was investigated using ESI-MS. Mass spectral data, Figure 8-6B, for a solution of 3 µM holo-IsdA-N mixed with 6 µM apo-IsdC-N show no charge states attributable to holo(CoPPIX)-IsdC-N: only the +7 and +8 charge states of apo-IsdA-N and holo-IsdA-N, and the +7 to +9 of apo-IsdC-N are observed in the spectrum. Deconvolution shows only apo-IsdC-N (14444 Da) with a mixture of apo-IsdA-N (14623 Da) and holo-IsdA-N (15239 Da), this means that no Co-PPIX transfer has taken place.

Transfer of CoPPIX from holo-IsdA-N directly to apo-IsdE was also investigated by ESI-MS, Figure 8-6C. No transfer took place when 3 µM IsdA-N was mixed with excess (6 µM) apo-IsdE; the ESI mass spectral data show the presence of only holo-IsdA-N and apo-IsdE. Deconvolution showed that apo-IsdA-N (14622 Da), holo-IsdA-N (15241 Da) and apo-IsdE (30278 Da) were present.

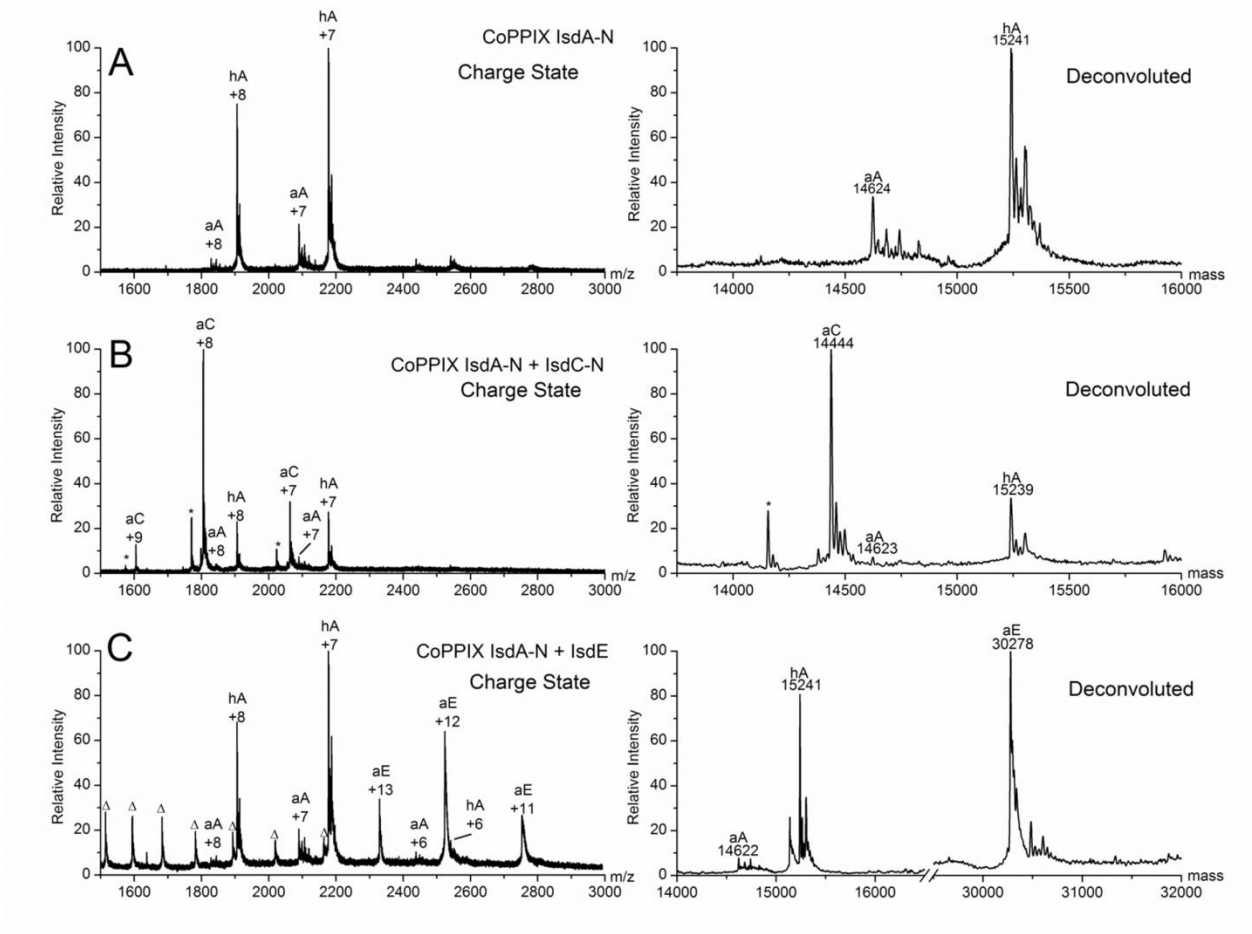

Figure 8-6 ESI-mass spectral data recorded following reaction of Co-PPIX with apo-IsdA-N, apo-IsdC-N and apo-IsdE. A) Mass spectral data recorded when excess CoPPIX was added to apo-IsdA-N. Apo-IsdA-N (aA, 14,624 Da) has a charge state distribution of +6 to +8. Upon binding to form the holo-IsdA-N (hA, 15,241 Da), the charge state distribution remains the same. Approximately 0.75 mol equivalents of the apo-IsdA-N binds to the CoPPIX even though there is excess of the CoPPIX. B) Mass spectral data recorded when 6 µM apo-IsdC-N is mixed with 3 µM holo-CoPPIX-IsdA-N. The mass spectrum only shows the +7 to +8 charge states for apo-IsdA-N (aA) and holo-IsdA-N (hA) and the +7 to +9 charge states for apo-IsdC-N (aC, 14444 Da). Clearly, no Co-PPIX transfer has taken place. C) Mass spectral data recorded when 6 µM apo-IsdE is mixed with 3 µM holo-CoPPIX- IsdA-N. In addition to the mixture of apo-IsdA-N and holo-IsdA-N, the +11 to +13 charge states of apo-IsdE (AE, 30278 Da) peaks are observed. No CoPPIX transfer from hA to apo-IsdE has taken place.

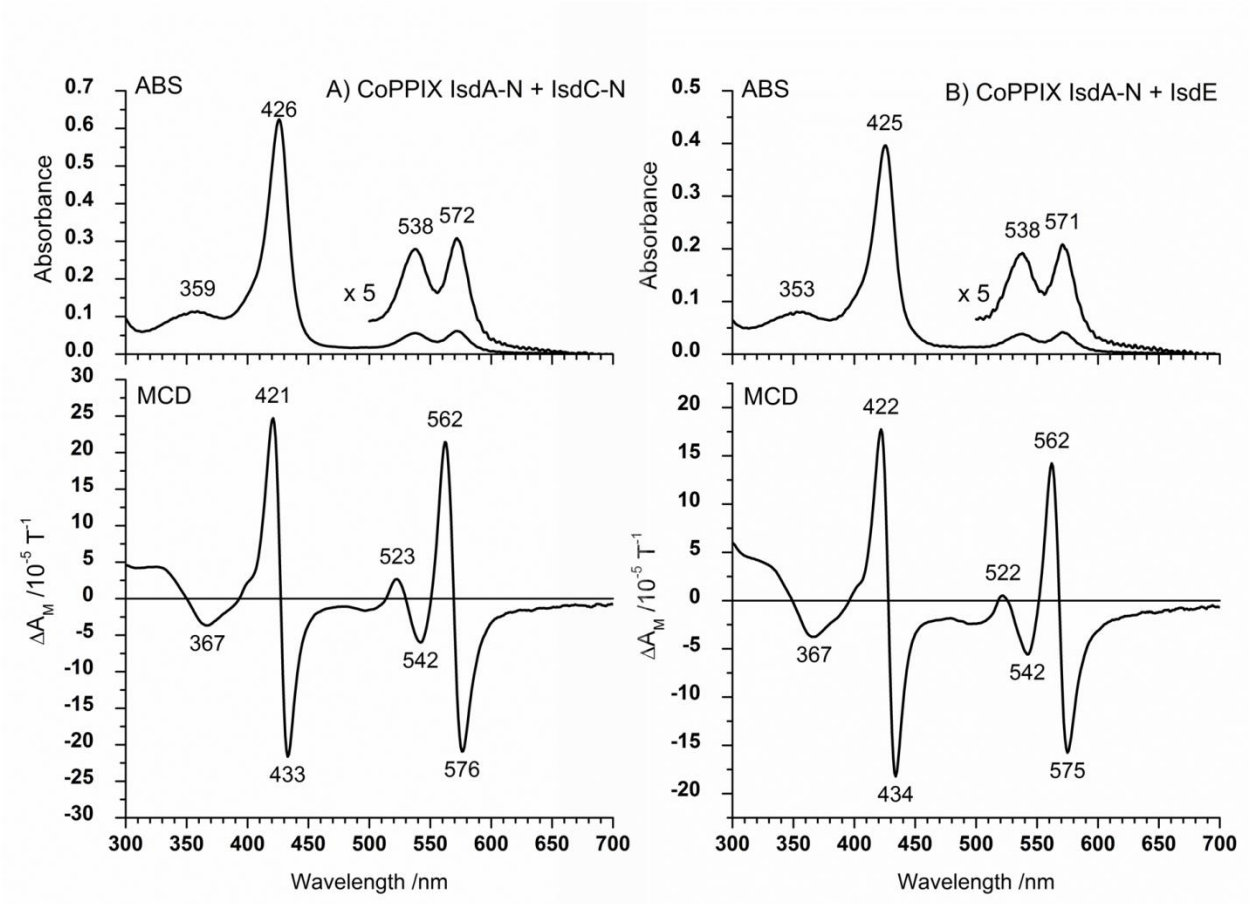

Figure 8-7 Absorption and MCD spectral data recorded for CoPPIX when apo-IsdC-N (A) and apo-IsdE (B) were mixed with holo-IsdA-N. A) Spectra recorded following mixing 6 µM apo-IsdC-N with 3 µM holo-IsdA-N. The UV-visible absorption and MCD spectra did not change when apo-IsdC-N is added indicating that no CoPPIX transfer took place. B) Spectra recorded following mixing of 6 µM apo-IsdE with 3 µM holo-IsdA-N. The UV-visible absorption and MCD spectra did not change when apo-IsdE was added indicating no CoPPIX transfer took place.

The null transfer results were confirmed by UV-visible absorption and MCD spectroscopy, Figure 8-7. The spectral data for a solution of 3 µM holo-IsdA-N mixed with 6 µM apo-IsdC-N are the same as for the original holo-IsdA-N. Although, the actual heme binding spectrum of IsdA-N and IsdC-N are very similar, there are slight differences in the MCD spectrum [16]. The same spectral result is found when 3 µM holo-IsdA-N was mixed with 6 µM apo-IsdE as no significant changes in the UV-visible absorption and MCD spectra were found. The overall spectral envelope and Q:B band ratio remain approximately the same. Since IsdE binds heme through a histidine ligand, a dramatic shift in the spectrum would be expected if CoPPIX was

transfered from holo-CoPPIX-IsdA-N to apo-IsdE [18]. Although IsdA-N binds Co-PPIX, ring transfer does not occur from IsdA-N to either IsdC-N or IsdE.

8.3.6 MnPPIX binding to IsdA-N by MCD spectroscopy and ESI-MS

Previous studies have shown that IsdH-N3 is able to bind MnPPIX and transfer the ring to apo-IsdA-N [28]. In the study described here, the transfer of IsdA-N-bound MnPPIX across the three core proteins: from holo-MnPPIX-IsdA-N, to apo-IsdC-N and on to apo-IsdE was investigated. The absorption spectral data in Figure 8-8 resembles the spectra reported when MnPPIX is transferred from IsdH-N3 to IsdA-N, with two prominent bands in the UV-visible absorption spectrum, at 368 and 468 nm and weaker bands at 563 and 614 nm [28]. While there are only minor shifts in the absorption spectrum when MnPPIX binds to IsdA-N, there are significant changes in the MCD spectrum. The MCD band at centered at 387 nm shifts to 381 nm and there is significant resolution in the Q bands between 450 and 650 nm. As such, the B-like terms at 447 nm and 492 nm become more resolved while the psuedo-A-term at 589 and 605 nm is defined. Complicating some of the spectra measured was the presence of free MnPPIX which after protein purification can only result due to the ring being labile within the protein.

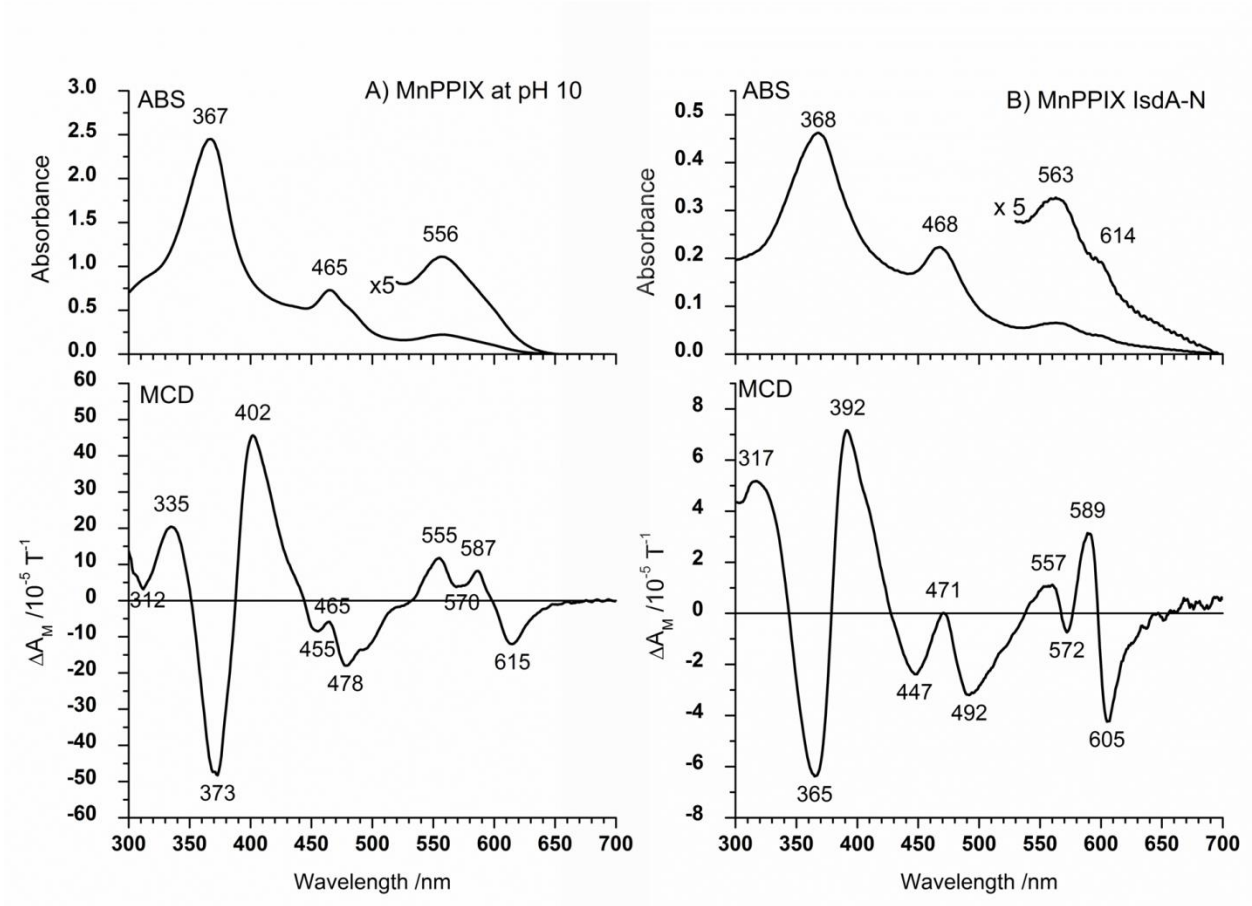

Figure 8-8 Absorption and MCD spectral data recorded for MnPPIX at pH 10 and when added to apo-IsdA-N. (A) Free MnPPIX at pH 10 and (B) spectra recorded following mixing of excess MnPPIX with apo-IsdA-N. The change in the UV-visible and MCD spectra when apo-IsdA-N is added indicate that MnPPIX binding took place. Significantly increased resolution is observed in the Q bands between 500 and 650 nm which supports a change in the environment of the MnPPIX.

The MnPPIX binding was confirmed with ESI-MS, Figure 8-9A. Reaction of apo-IsdA-N with excess MnPPIX results in ESI mass spectra that show masses from apo-IsdA-N and holo-IsdA-N, both with a charge state distribution of +6 to +8. Observation of the same charge state distribution is an indication that IsdA-N binds MnPPIX with little change in overall volume of the holo protein, which is the same as for heme binding. Deconvolution shows an approximately 50% mix of apo-IsdA-N (14626 Da) and holo-IsdA-N (15298 Da). Typically, when adding excess heme to IsdA-N, followed by purification steps, we find >95% of the protein is holo-IsdA-N [18]. This means that MnPPIX binding is not as favourable as heme binding to the IsdA-N.

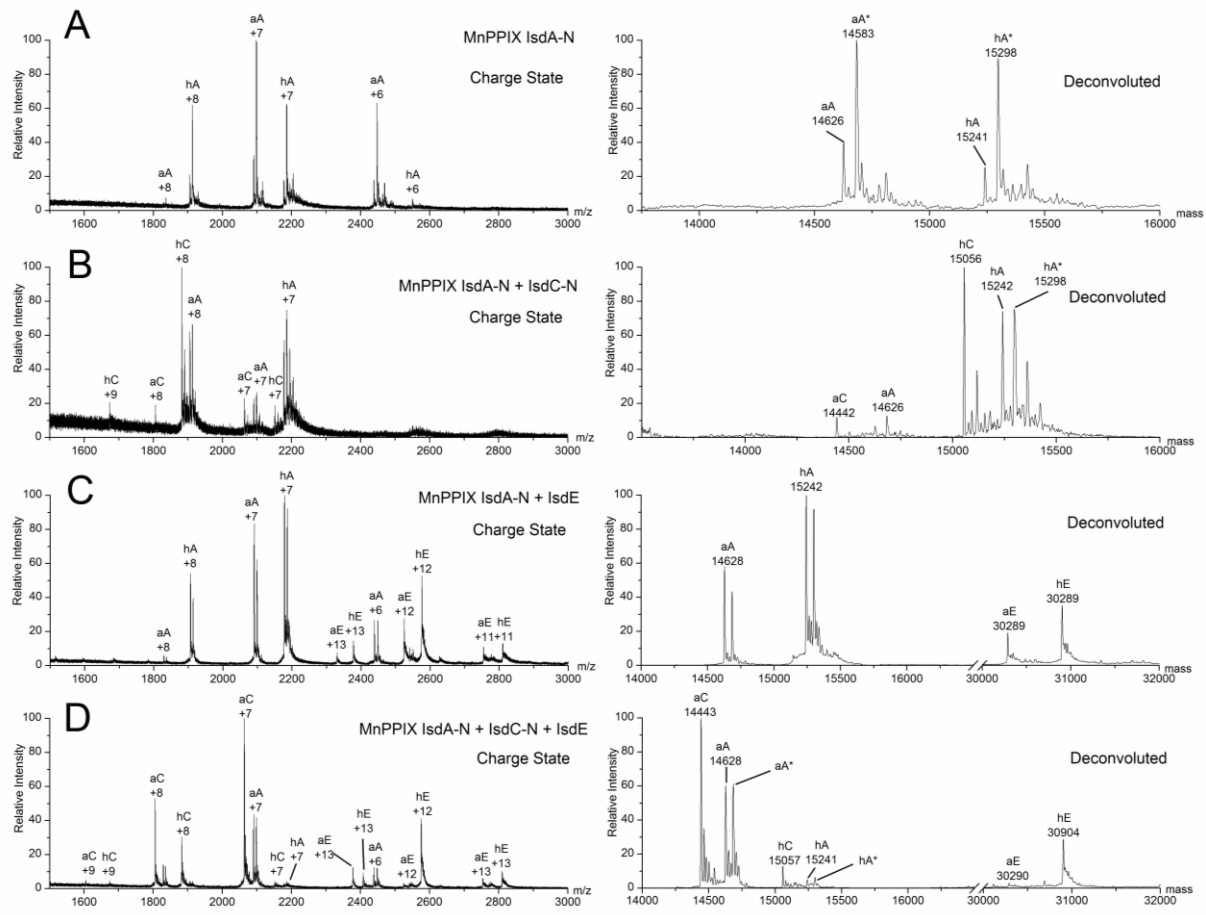

Figure 8-9 ESI-Mass spectral data recorded following reaction of MnPPIX with apo-IsdA-N, apo-IsdC-N and apo-IsdE. A) Reaction of IsdA-N with excess MnPPIX. Apo-IsdA-N(aA, 14,626 Da) has a charge state distribution of +6 to +8. Following mixing with MnPPIX, holo-(MnPPIX)-IsdA-N (hA, 15,298 Da) is formed, which exhibits the same charge state distribution. B) Four species are observed in solution (apo/holo-IsdA-N and apo/holo-IsdC-N (apo-14,442 Da holo-15,056 Da) when 2.5 µM apo-IsdC-N is mixed with 3 µM holo-IsdA-N. While holo-IsdAN transfers MnPPIX to IsdC-N, transfer is not complete. C) MnPPIX transfers from holo-IsdAN (3 µM) to apo-IsdE(3 µM). Both IsdE (apo-30289 Da and holo-30904 Da) species exist in solution. D) MnPPIX transfer from holo-IsdA-N (6 µM) to apo-IsdC-N (3 µM) and then to apo-IsdE (6.5 µM). All six apo/holo species (IsdA-N: apo-14628 Da and holo-15241 Da; IsdC-N: apo-14443 Da and holo-15057 Da; and IsdE: apo-30290 Da and holo-30904 Da) are observed.

8.3.7 MnPPIX binding and transfer monitored by absorption and MCD spectroscopy and ESI mass spectrometry

Figure 8-9B shows the ESI mass spectrum of a solution containing 2 µM holo-IsdA-N mixed with 3 µM apo-IsdC-N. The data show that holo-IsdAN does transfer MnPPIX to IsdC-N. Four

species are present in the charge state spectra: apo/holo-IsdA-N (+7 and +8), apo-IsdC-N (+7 and +8) and holo-IsdC-N (+7 to +9). A slight increase in the charge state envelope of IsdC-N upon binding MnPPIX could indicate a slightly more open conformation. This result is expected as it has been shown that IsdC-N contains a flexible heme pocket and was able to bind Zn(II)PPIX [19]. Deconvolution shows that transfer is not complete, however, when compared with heme binding [18], with all four species (apo-IsdC-N (14442 Da), holo-IsdC-N (15056 Da), apo-IsdA-N (14626 Da) and holo-IsdA-N (15242 Da)) present in solution.

This same reaction was examined using absorption and MCD spectra. Excess apo-IsdC-N was added to MnPPIX bound IsdA-N. The UV-visible absorption and MCD spectra, Figure 8-10A do change slightly when compared with holo-MnPPIX-IsdA-N. The Soret band centered at 369 nm becomes much more resolved in the MCD spectrum confirming a change in environment of the MnPPIX. We should note that the heme bound spectra of IsdA-N and IsdC-N are also very similar, due to the same ring binding ligand (tyrosine).

The ESI mass spectrum, Figure 8-9C, of a solution containing 5 µM holo-IsdAN mixed with 6.5 µM apo-IsdE showed charge states for four species: apo/holo-IsdA-N (+7 and +8) and apo/holo-IsdE (+11 to +13). Clearly, MnPPIX does transfer from holo-IsdA-N to apo-IsdE. Deconvolution shows that there exists approximately equal concentrations of apo-IsdA-N (14628 Da) and holo-IsdA-N (15242 Da), and also IsdE (apo-IsdE (30289 Da) and holo-IsdE (30904 Da). Therefore, although MnPPIX does transfer it does not transfer completely. Significantly, heme does not transfer from holo-IsdA-N to IsdE [18]. In the case of MnPPIX, it is possible that the transfer takes place via a dissociative/associative mechanism rather than the highly specific protein-protein interactions that are required for the transfer of heme from IsdC-N to IsdE [18].

Absorption and MCD spectra confirm that a change in the MnPPIX take splace when 3 µM holo-IsdA-N is mixed with 6 µM apo-IsdE, Figure 8-10B. MnPPIX transfer from the holo-IsdA-N to apo-IsdE. The Soret band red shifts from 369 to 372 nm while the Q band shoulder blue shifts from 606 to 600 nm. Overall, the spectrum is complicated and not as resolved as for the IsdA-N to IsdC-N transfer. Therefore, it is probable that these spectra represent a mixture of apo/holo-IsdA-N, apo/holo-IsdE and free MnPPIX in solution as shown in the ESI mass spectrum, Figure 8-9C.

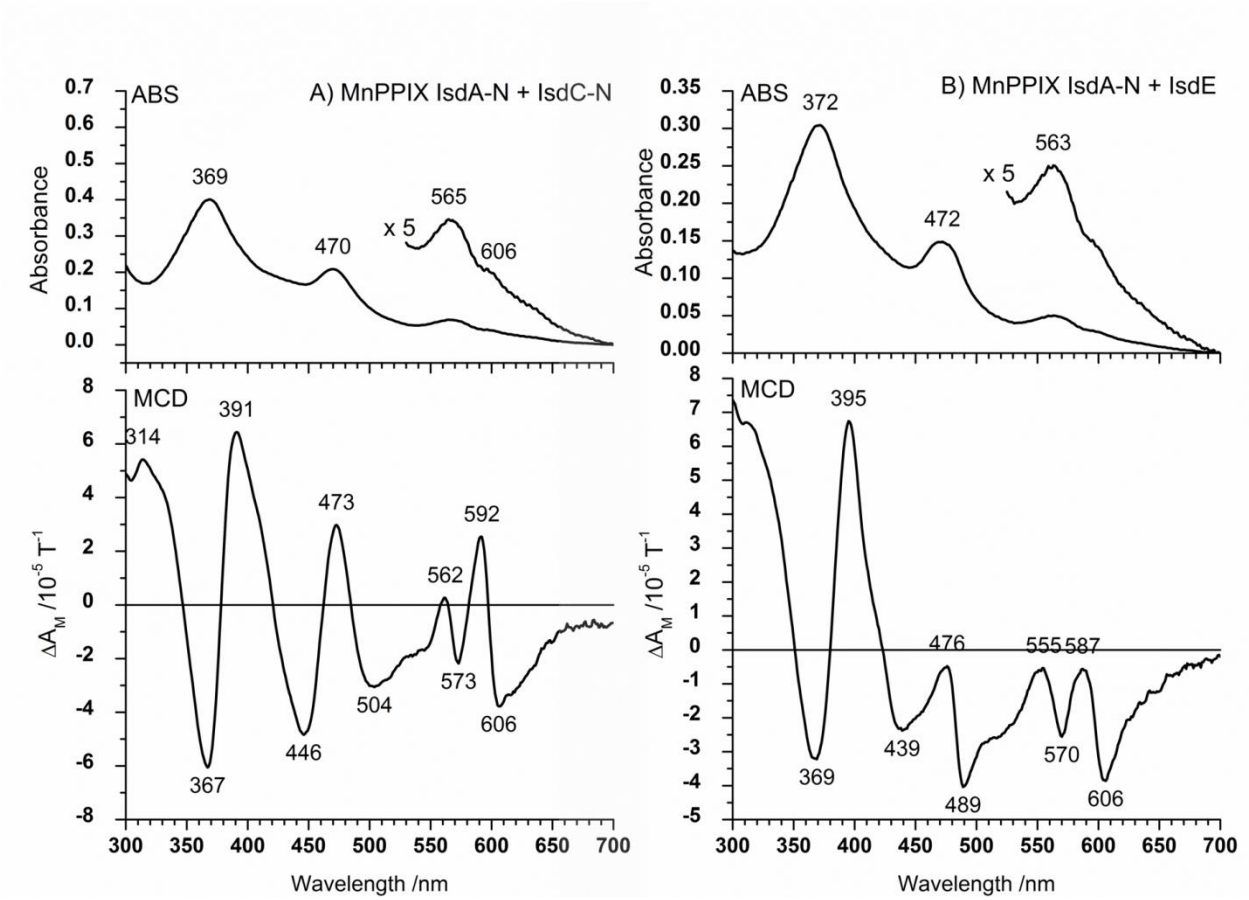

Figure 8-10 UV-visible absorption and MCD spectra recorded following reaction of MnPPIX with apo-IsdA-N, apo-IsdC-N and apo-IsdE. A) Reaction of holo-(MnPPIX)-IsdA-N (3 μM) with apo-IsdC-N (6 μM). The UV-visible absorption and MCD spectra change reflecting the formation of holo-IsdC-N. The Soret band centered at 369 nm becomes more resolved. B) MnPPIX transfer from holo-IsdA-N (3 μM) to apo-IsdE (6 μM). The Soret band red shifts from 369 to 372 nm while the Q band shoulder blue shifts from 592 to 587 nm.

The complete transfer of MnPPIX across all three core Isd proteins was monitored by ESI-MS, Figure 8-9D. Holo-(MnPPIX)-IsdA-N (6 μM) was mixed with apo-IsdC-N (3 μM) and apo-IsdE (5 μM). The ESI-mass spectrum shows that all six apo/holo pairs exist in solution meaning that transfer has taken place and is almost complete, as very little apo-IsdE remains in solution. It has been reported that IsdE has the highest heme affinity [13] and therefore, if MnPPIX is labile within the heme pocket of the IsdA-N and IsdC-N, it might preferentially bind to IsdE.

The absorption and MCD spectral data for this same reaction, Figure 8-11, show the results of mixing a solution of 3 μM holo-IsdA-N with 3 μM apo- IsdC-N and 6 μM apo-IsdE. There is further redshifting of the Soret band to 374 from 372 nm. The Q band region is less resolved

with shoulders at 490 nm and a broad MCD band at 619 nm. This suggests the presence of each of the holo-species in solution, IsdA-N, IsdC-N and IsdE and also the free MnPPIX. Evidence for free MnPPIX in solution is shown by the double band at ~619 nm. The 619 nm peak was not prominent in any other MCD spectrum except for free MnPPIX at pH 10 with a peak at 615 nm. With size-exclusion chromatography performed on all holo-protein solutions, free Mn-PPIX in the MCD spectrum leads us to conclude that binding is not very tight and the ring is labile.

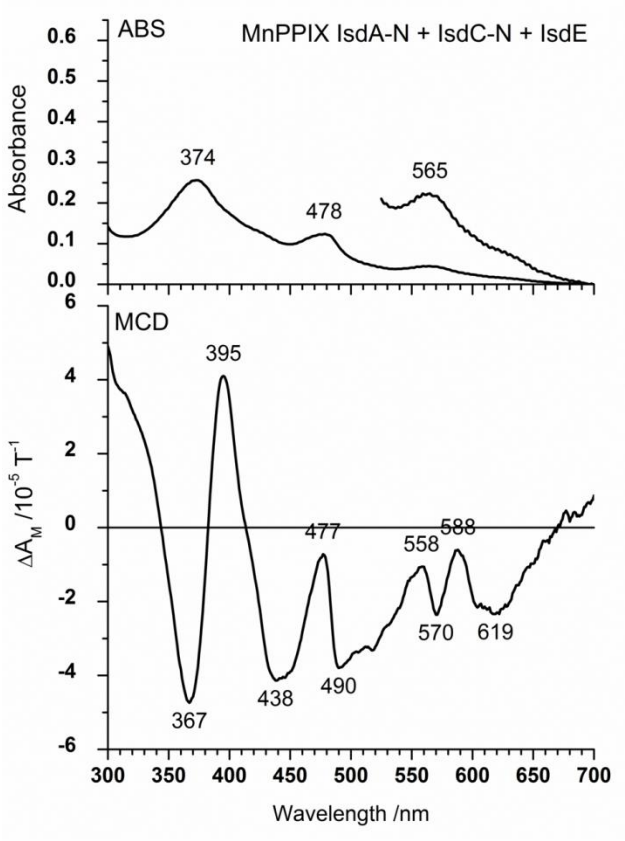

Figure 8-11 UV-visible absorption and MCD spectra recorded for the reaction of holo-IsdA-N (3 µM) with apo- IsdC-N (3 µM) and apo-IsdE (6 µM). The Soret band shifts to 374 from 372 nm. The Q band region is less resolved with shoulder peaks at 490 nm and a broad MCD band envelope is recorded at 619 nm. These data suggest a complicated mixture of MnPPIX species.

8.4 Discussion

8.4.1 Importance of the propionic side chains of heme in heme transfer.

The Isd heme transfer system of *S. aureus* is a novel target for new antibiotic compounds. This system can potentially be abused with a "Trojan Horse" approach [25-28]. With new

studies looking at different metal substituted porphryins in the Isd system as potential antibiotic agents and their effects on binding [11, 28] it becomes important to study other aspects of the system such as the importance of the heme binding ligands [29] and the critical components of the heme ring itself. In this study, the effects of changing the propionic sidechain to the dimethyl ester and of changing the Fe(III) to Co(III) and Mn(III) are reported.

The crystal structures of IsdA-N, IsdC-N and IsdE can be compared with that of myoglobin, Figure 8-12. It appears that the carboxylic acid orientation is important in these proteins. From the crystal structures of the heme bound in myoglobin, IsdA-N and IsdC-N, the propionic side chains of the heme are facing away from the binding site out towards the bulk solvent while the opposing vinyl side of the protoporphyrin ring is buried into the hydrophobic pocket in all of the structures except for IsdE and myoglobin. The heme bound the IsdE protein have both propionic side chains facing into the heme pocket [11, 17, 19, 32, 34]. Therefore, there has been considerable speculation about the mechanism of heme transfer [29] and that it is possible that hydrogen bonding interactions as well as ligands playing a key role in protein-protein interactions.

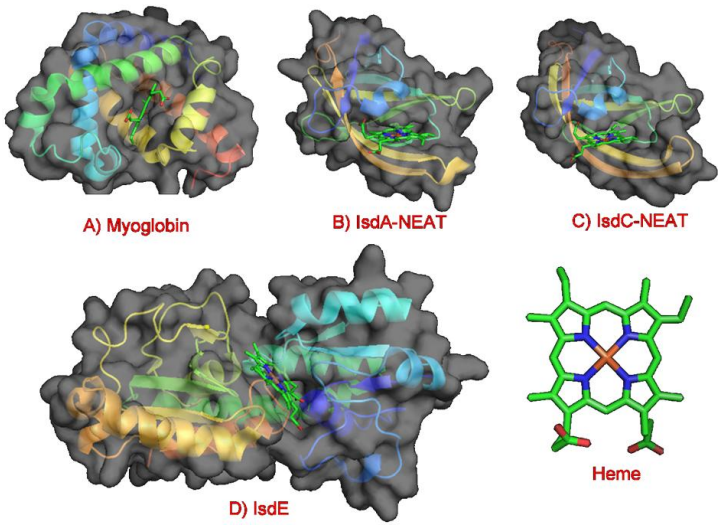

Figure 8-12 Crystal structures of holo heme binding proteins A) Myoglobin (1MBN) [34], B) IsdA-NEAT (2ITF) [17], C) IsdC-NEAT (2O6P) and D) IsdE (2Q8Q) [32]. The cartoon ribbons of their structures are colored blue to red for the direction N to C terminal. The calculated surfaces are shown in grey with the heme pockets oriented forward. The structure of heme is shown as a reference. The crystal structures of the heme bound proteins myoglobin, IsdA-N and IsdC-N show the propionic side chains facing away from the binding site out towards bulk solvent while the opposing vinyl side of the protoporphyrin ring is buried into the hydrophobic pocket in all of the structures except for IsdE.

The results of the PPIX (FePPIX-DME, CoPPIX. MnPPIX) transfer experiments investigated in this study are summarized in Figure 8-13. Upon close inspection of these X-ray crystallography structures, the hydrophobic pocket appears to be unable to accept porphyrin rings much larger than protoporphyrin IX and, therefore, FePPIX-DME is an ideal candidate to look at the effects of heme transfer with regards to heme structure. The ESI-MS, UV-visible absorption and MCD spectral data show that IsdA-N is able to bind FePPIX-DME and transfer it to IsdC-N. However, neither IsdA-N nor IsdC-N is able to transfer FePPIX-DME to IsdE. This may be due to IsdE binding the heme with the propionic side chains buried inside the protein. Therefore, important hydrogen bonding interactions that would stabilize the heme within the bi-lobed [32] heme pocket are not now present. Since this interaction would be stripped away from this PPIX compound, IsdE is not able to bind or accept through transfer FePPIX-DME.

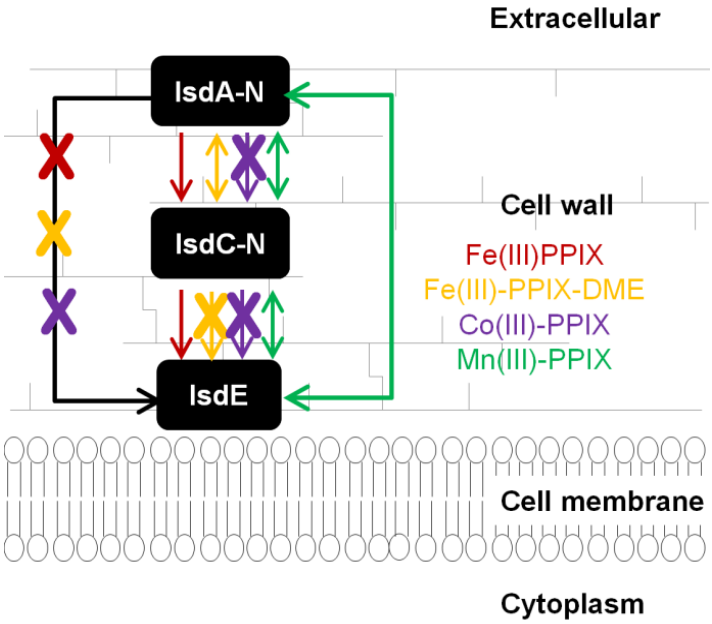

Figure 8-13 Summary of PPIX binding from this study and for heme binding from past results [18] and this study.

8.4.2 Changing the central metal of PPIX and the effect on heme transfer

Changing the central metal allows the investigation of the effects of the relative "hardness" of the central metals compared with the Fe(III) on proximal and distal donor atom binding. Co(III) is harder than Fe(III) and it was found that, although it was known that CoPPIX-DME binds to IsdA-N [11, 29], holo-IsdA-N is unable to transfer CoPPIX to IsdC-N or IsdE. The proximal

amino acid-metal bond is an important factor with the Isd heme transfer system [29] and by changing the metal there is an effect on the strength of the critical tyrosine metal bond. The hydroxide of the tyrosine is a "hard" ligand and in the Isd system, IsdA and IsdC do not bind to the "soft" ferrous heme with their ferric coordinating tyrosine ligand [16]. IsdE on the other hand, only coordinates ferric heme through an "intermediate" histidine ligand [31, 32], and this enables IsdE to be versatile in the oxidation state of heme [31]. CoPPIX binding conformationally is indistinguishable compared to heme [11]. Therefore, the tightness of binding CoPPIX may overcome the releasing factors such as the important protein-protein interactions to the point where CoPPIX transfer cannot be facilitated.

The opposite case is seen with a "softer" metal, for example, Mn(III) in MnPPIX, where MnPPIX is transferred from MnPPIX-IsdA-N to apo-IsdC-N and on to apo-IsdE. However, heme is not transferred directly from holo-IsdA-N apo-IsdE [18]. MnPPIX appears to be labile as a 619 nm peak (attributed to free MnPPIX) is found in the spectra following the reaction of MnPPIX bound holo-IsdA-N with apo-IsdC-N and apo-IsdE, Figure 8-11. From these data, it can be proposed that the Tyr ligands of IsdA-N and IsdC-N are not able to bind MnPPIX with such a high affinity as with heme. Figure 8-9C shows that signifigant amount of MnPPIX tranfers to IsdE. Therefore, since IsdE does not have a coordinating tyrosine ligand [31, 32], but instead an "intermediate" histidine, IsdE is still able to open the gated IsdA-N and IsdC-N proteins to facilitate MnPPIX transfer. Furthermore, the histidine ligand is probably able to bind more tightly to the softer MnPPIX.

8.5 Conclusion

In summary, the propionic acid chains of heme play a key role in heme transfer reactions, especially with regard to heme binding to IsdE, where the propionic acid side chains are completely buried within the heme pocket [32]. IsdA-N is able to bind FePPIX-DME and transfer it to IsdC-N. However, FePPIX-DME bound holo-IsdA-N and holo-IsdC-N are not able to transfer FePPIX-DME to IsdE. The "harder" CoPPIX on the other hand binds to IsdA-N [29], but is not transferred IsdC-N or IsdE. The "softer" MnPPIX binds to IsdA-N, which is able to transfer the ring to IsdC-N. IsdC-N is able to transfer the ring to IsdE. In a reaction unlike that found for heme, holo-Mn(III)PPIX-IsdA-N transfers the ring directly to IsdE. To overcome the protein-protein interactions shown to exist with this transfer, MnPPIX must be labile. As the

heme transfer mechanism of the Isd system in *S. aureus* becomes widely understood a new focus of using this system as a "Trojan Horse" technique to potentially kill the bacteria has emerged in recent years. This leads to the ultimate goal of potentially either utilizing metalloporphryins for cytotoxicity [28] or using photodynamic antimicrobial therapy to kill the bacteria [27]. In addition it can be proposed PPIX analogs can be used to shut down the iron-deficient regulated Isd system, which may work in either starving the bacteria or sufficiently weakening the bacteria so that other antibacterial methods can be used to kill *S. aureus*. Key to this study is that FePPIX-DME is able to transfer through to the central conduit of the Isd system, IsdC-N. It is possible that this compound would be an ideal candidate as this would affect the *S.* aureus growth as a potential antibiotic. Further studies are needed to determine the effectiveness of this compound.

8.6 References

1. Wandersman, C.; Delepelaire, P., *Annu. Rev. Microbiol.* **2004,** 58, 611-647.
2. Radtke, A. L.; O'Riordan, M. X., *Cell Microbiol.* **2006,** 8, 1720-1729.
3. Mazmanian, S. K.; Skaar, E. P.; Gaspar, A. H.; Humayun, M.; Gornicki, P.; Jelenska, J.; Joachmiak, A.; Missiakas, D. M.; Scheenwind, O., *Science.* **2003,** 299, 906-909.
4. Dryla, A.; Gelbmann, D.; Gabain, A. v.; Nagy, E., *Mol. Microbiol.* **2003,** 49, 37-53.
5. Taylor, J. M.; Heinrichs, D. E., *Mol. Microbiol.* **2002,** 43, 1603-1614.
6. Cheung, J.; Beasley, F. C.; Liu, S.; Lajoie, G. A.; Heinrichs, D. E., *Mol. Microbiol.* **2009,** 74, 594-608.
7. Mazmanian, S. K.; Ton-That, H.; Su, K.; Scheenwind, O., *PNAS.* **2002,** 99, 2293- 2298.
8. Morrissey, J. A.; Cockayne, A.; Hammacott, J.; Bishop, K.; Denman-Johnson, A.; Hill, P. J.; Williams, P., *Infect. Immun.* **2002,** 70, 2399-2298.
9. Skaar, E. P.; Gaspar, A. H.; Scheenwind, O., *J. Biol. Chem.* **2004,** 279, 436-443.
10. Reniere, M. L.; Skaar, E. P., *Mol. Microbiol.* **2008,** 69, 1304-1315.
11. Grigg, J. C.; Ukpabi, G.; Gaudin, C. F. M.; Murphy, M. E. P., *J. Inorg. Biochem.* **2010,** 104, 341-348.
12. Torres, V. J.; Pishchany, G.; Humayun, M.; Scheenwind, O.; Skaar, E. P., *J. Bacteriol.* **2006,** 188, 8421-8429.
13. Zhu, H.; Xie, G.; Liu, M.; Olson, J.; Fabian, M.; Dooley, D.; Lei, B., *J. Biol. Chem* **2008,** 283, 18450-18460.
14. Watanabe, M.; Tanaka, Y.; Suenaga, A.; Kurodo, M.; Yao, M.; Watanabe, N.; Arisaka, F.; Ohta, T.; Tanaka, I.; Tsumoto, K., *J. Biol. Chem* **2008,** 283, 28649-28659.
15. Vermeiren, C. L.; Pluym, M.; Mack, J.; Heinrichs, D. E.; Stillman, M. J., *Biochem.* **2006,** 45, 12867-12875.
16. Pluym, M.; Muryoi, N.; Heinrichs, D. E.; Stillman, M. J., *J. Inorg. Biochem.* **2008,** 102, 480-488.
17. Grigg, J. C.; Vermeiren, C. L.; Heinrichs, D. E.; Murphy, M. E., *Mol. Microbiol.* **2007,** 63, 139-149.

18. Muryoi, N.; Tiedemann, M. T.; Pluym, M.; Cheung, J.; Heinrichs, D. E.; Stillman, M. J., *J. Biol. Chem.* **2008,** 283, 28125-28136.
19. Villareal, V. A.; Pilpa, R. M.; Robson, S. A.; Fadeev, E. A.; Clubb, R. T., *J. Biol. Chem.* **2008,** 283, 31591-31600.
20. Tiedemann, M. T.; Muryoi, N.; Heinrichs, D. E.; Stillman, M. J., *Biochem. Soc. Trans* **2008,** 36, 1138-1143.
21. Tiedemann, M. T.; Muryoi, N.; Heinrichs, D. E.; Stillman, M. J., *J. Porphyrins Phthalocyanines.* **2009,** 13, 1006-1016.
22. Mack, J.; Yoshiaki, A.; Kobayashi, N.; Stillman, M. J., *J. Am. Chem. Soc* **2005,** 127, 17697-17711.
23. Pilpa, R. M.; Robson, S. A.; Villareal, V. A.; Wong, M. L.; Phillips, M.; Clubb, R. T., *J. Biol. Chem.* **2009,** 284, 1166-1176.
24. Liu, M.; Tanaka, W. N.; Zhu, H.; Xie, G.; Dooley, D. M.; Lei, B., *J. Biol. Chem.* **2008,** 283, 6668-6678.
25. Stojiljkovic, I.; Evavold, B. D.; Kumar, V., *Exp. Opin. Invest. Drugs.* **2001,** 10, 309-320.
26. Stojiljkovic, I.; Kumar, V.; Srinivasan, N., *Mol. Microbiol.* **1999,** 31, 429-442.
27. Stojiljkovic, I.; Perkins-Balding, D., *DNA Cell Biol.* **2002,** 21, 281-295.
28. Moriwaki, Y.; Caaveiro, J. M. M.; Tanaka, Y.; Tsutsumi, H.; Hamachi, I.; Tsumoto, K., *Biochem.* **2011,** 50, 7311-7320.
29. Grigg, J. C.; Mao, C. X.; Murphy, M. E. P., *J. Mol. Biol.* **2011,** 413, 684-698.
30. Adler, A. D.; Longo, F. R.; Kampas, F.; Kim, J., *J. Inorg. Nuc. Chem.* **1970,** 32, 2443-2445.
31. Pluym, M.; Vermeiren, C. L.; Mack, J.; Heinrichs, D. E.; Stillman, M. J., *Biochem.* **2007,** 46, 12777-12787.
32. Grigg, J. C.; Vermeiren, C. L.; Heinrichs, D. E.; Murphy, M. E., *J. Biol. Chem.* **2007,** 282, 28815-28822.
33. Springall, J.; Stillman, M. J.; Thomson, A. J., *Biochim. Biophys. Acta* **1976,** 453, 494-501.
34. Watson, H. C., *Prog. Stereochem.* **1969,** 4, 299-333.

8.7 Appendix

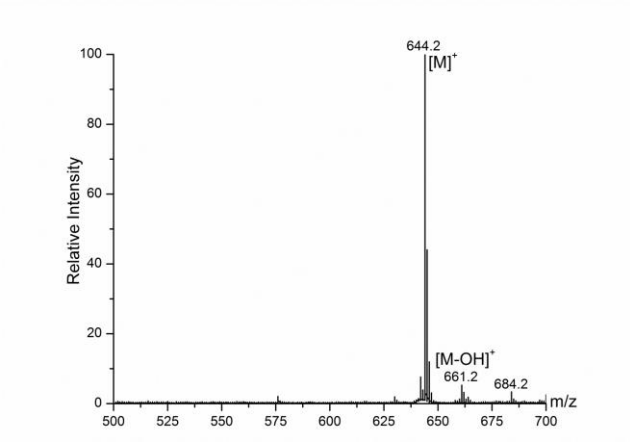

Figure 8-14 ESI-MS charge state data for FePPIX-DME. This compound matches the theoretical mass of 645.6 Da.

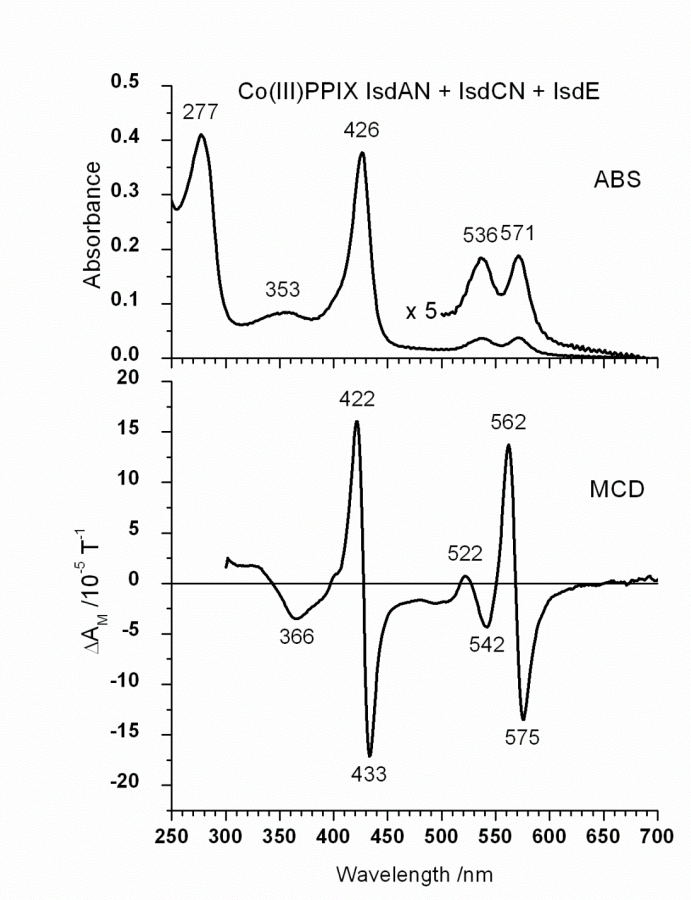

Figure 8-15 UV-visible absorption and MCD spectra of holo-Co-PPIX-IsdA-N when mixed with substoichiometric amounts of apo-IsdC-N and excess apo-IsdE. No transfer takes place; the spectra are the same as for the holo-IsdA-N.

Chapter 9. Conclusion

9.1 *Staphylococcus aureus*

The antibiotic resistant, Gram-positive bacterium, *Staphylococcus aureus* (*S. aureus*) is a significant problem in hospitals and communities worldwide where it is responsible for numerous deaths. Infections caused by this bacterium can range from superficial wound lesions to more severe infections such as pneumonia, osteomyelitis and septicemia [1]. *S. aureus* is currently the leading cause of nosocomial infections [2]. Treatment for infections is costly due to growing resistance to most antibiotics. Resistance to the 'last resort' antibiotic vancomycin is more prevalent and hence, death can still result [3]. Analysis of Canadian statistics for 2006 suggests there were over 2000 deaths in Canada attributed to *S. aureus* [4]. Understanding how *S. aureus* thrives in the host has become a major focus of research.

Iron is an essential and yet is, generally unavailable nutrient for bacteria. In the mammalian host, total free iron levels are kept to a minimum as the host binds the free iron into a number of proteins and thus, invading bacteria have difficulty obtaining iron [5]. The lack of iron inhibits the growth of invading bacteria and consequently allows the host's immune system to destroy the infection. Like most bacteria, *S. aureus* has adapted and possesses a number of iron acquisition systems. The most abundant source of iron in the human body is found in heme, which is bound by proteins such as hemoglobin and myoglobin. In 2003, Mazmanian et al. [6] reported that when grown in iron-limiting media, *S. aureus* expresses genes that are involved in iron acquisition [6]; this series of proteins were named Isd, for iron-regulated surface determinant, and comprise of a series of 9 proteins: IsdH, IsdB, IsdA, IsdC, IsdE, IsdD, IsdF, IsdG and IsdI. It was proposed that *S. aureus* could scavenge heme using the Isd protein pathway by lysing red blood cells and extracting the intact heme from the hemoglobin. An overall summary of heme flow and characterization of the Isd system is shown in Figure 9-1.

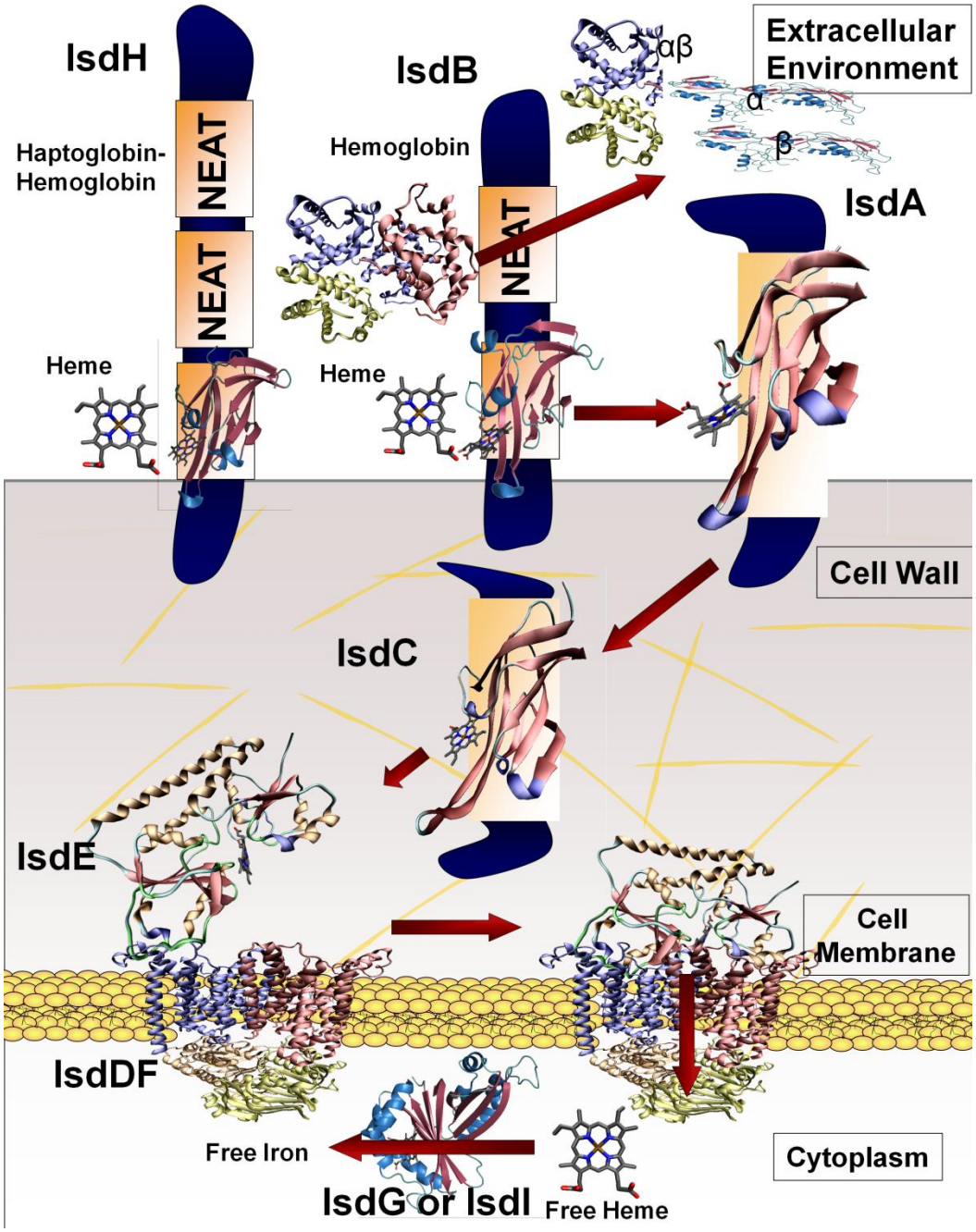

Figure 9-1 Summary cartoon schematic of heme flow through the Isd heme scavenging system in *S. aureus*. Characterization of the Isd system with the flow of heme from hemoglobin binding IsdB though IsdA, IsdC and to IsdE where heme is passed through IsdF. IsdG or IsdI finally deconstructs free heme and releases free iron. Modified from [7]. Copyright 2008 Portland Press Limited.

9.2 Heme Binding in the Isd System

Essential to heme binding in the Isd system is that all of the heme binding proteins contain a near iron transporter (NEAT) domain. These ~150 amino acid sequences are known to possess heme binding properties [8]. To date, the ferric and ferrous heme binding properties of the Isd proteins have been characterized. The NEAT domains, with the exception of IsdB-N1, IsdH-1 and IsdH-N2, of the Isd system bind ferric heme through a tyrosine amino acid binding ligand [9-11]. IsdE, which does not contain a NEAT domain, binds heme within its bilobed structure through a His ligand [12, 13].

In terms of ferrous heme binding, IsdB-N2 and IsdH-N3 bind ferrous heme through His and Met ligands [11], IsdA binds ferrous heme though a His ligand [9, 10, 14] and IsdE binds ferrous heme through 6-coordinate His and Met ligands [12, 13]. Interestingly, IsdC does not bind ferrous heme [10, 15]. Since IsdC is the central conduit of the Isd system [9, 16, 17] and can only bind ferric heme, extraction of heme from Hb must result in oxidation from biologically relevant ferrous to ferric heme before heme is passed through the cell wall of the bacteria.

Much of the spectroscopic characterization of heme binding and transfer has been elucidated using MCD spectroscopy. The value of the MCD spectral data is that although the observed MCD bands lie at the same energy and exhibit approximately the same bandwidth as the absorption bands, the MCD spectral data are sensitive to the nature of the protein axial ligands binding the heme iron, the heme-iron oxidation and the heme-iron spin state [18, 19]. These properties have such profound spectral effects that the key features in the observed MCD envelope morphology (sign, relative magnitude, and band maxima) systematically change for a range of heme proteins allowing 'fingerprinting' of novel heme binding proteins with those well-studied [19]. In this manner, the identity of the two axial ligands (the proximal 5^{th} position, and the distal 6^{th} position), the oxidation state of the iron, and its spin state, may be determined directly from dilute solutions at room temperature with considerable confidence for each of the Isd proteins. The MCD spectral data offer species identification far superior to that from the absorption spectroscopic data alone.

The heme axial ligands play important roles in stabilizing heme binding. As a result of the effects on the electronic structure of heme, each heme binding ligand significantly influence the heme spectra, Figure 9-2. Identifying the ligands of the heme scavenging system of the Isd proteins provides electronic information about how the Isd pathway is able to transfer heme from

hemoglobin. This preliminary investigation of the heme binding site environment is based on the protein backbone established by the crystal structures for IsdA, and IsdE. The orbital contributions to the B and Q bands provide initial indication of the electronic contributions by the axial ligands at the HOMO and LUMO levels, the orbitals most involved in heme binding. Molecular orbitals for many porphyrins and predicted spectra based on INDO/S and TDDFT calculations are widely available, for example, Mack et al. [20]. Figure 9-2 shows that for IsdA there is considerable involvement of the tyrosine (Tyr166) in both the ground state and excited states and that this axial ligand contributes to both the B and Q bands. IsdE with a ferrous heme was calculated with both His229 and Met78 axial ligands. Both ligands interact at the iron center for the B and Q bands, but clearly the Q band significantly involves the excited state of His229 (under the heme).

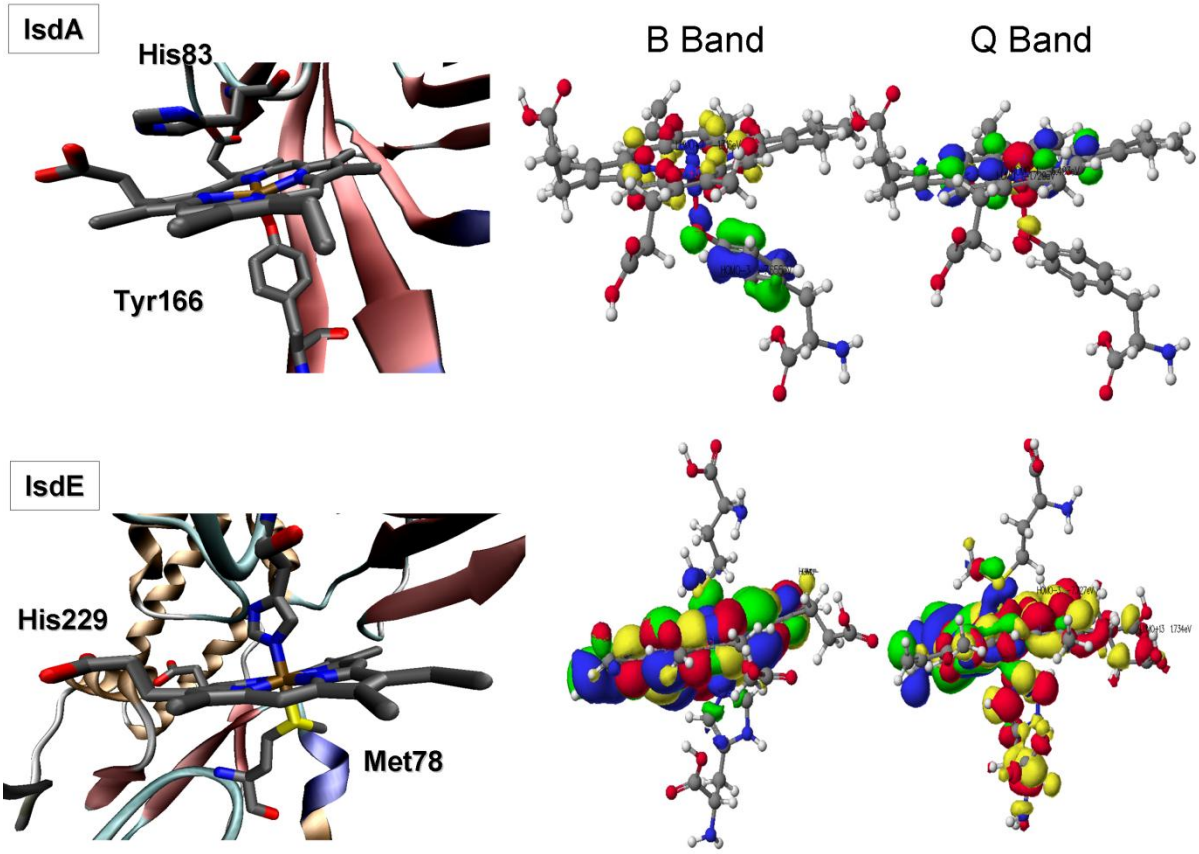

Figure 9-2 Calculations of the orbital contributions to the B and Q bands in IsdA and IsdE. IsdA binds a ferrous heme through His83 and ferric heme through Tyr166. Calculations are shown for the native ferric heme. IsdE binds ferrous heme through His229 and Met78. The calculations were carried out using ZINDO for the geometry optimizations and ZINDO/S for the

orbital calculations. Reprinted with permission from [7]. Copyright 2008 Portland Press Limited.

The spectroscopic results for the Isd heme scavenging system in *S. aureus* have allowed identification of the heme binding ligands in IsdH-N3, IsdB-N2, IsdA, IsdC and IsdE. The NEAT domains and IsdE are significant factors in heme-trafficking in *S. aureus.* The identification of the native oxidation state, spin state, and heme-binding ligands will aid in the continued effort to understand the overall mechanism of heme-trafficking in Gram-positive bacteria.

9.3 Mechanism of Heme Transfer in the Isd System

In summary, the flow of heme is from the externally-located IsdH and IsdB proteins through to the membrane-associated IsdE protein. Heme transfers unidirectionally and completely from IsdB-N2 to IsdA-N to IsdC-N then to IsdE or from IsdH-N3 to IsdA-N to IsdC-N then to IsdE. IsdB-N2 and IsdH-N3 can transfer heme to IsdC-N. Unique protein-protein interactions exist with apo-IsdB-N1N2 and Hb with regards to heme extraction and the mechanism of heme removal. Interestingly, only fully intact apo-IsdB-N1N2 is able to extract heme from metHb. Protein-protein interactions must be located in the first NEAT domain of IsdB and in the linker region between the two NEAT domains. Upon heme extraction, IsdB-N1N2 is able to denature and deconstruct metHb into subunit components that comprise of $^{ah}(\alpha\beta)$ $^{aa}(\alpha\beta)$ dimer, apo-α and apo-β strands. Addition of IsdA-N, IsdC-N and IsdE completes heme transfer from IsdB-N1N2 to IsdA-N and IsdC-N with subsequent transfer to IsdE, the end of the cell wall transfer system. Overall, when looking at heme extraction from metHb, the Isd system forms an efficient machine that is able to "shred" metHb and extract the precious iron-containing heme resource inside.

A significant component to the mechanistic analysis is that heme does not transfer from holo-IsdA-N directly to apo-IsdE; apo-IsdC-N is the required facilitator. This fact, taken together with the demonstrated unidirectionality of the transfer reactions, suggests that specific protein-protein interactions must be a necessary part of the mechanism required to drive the heme transfer towards the membrane.

IsdC-N can be considered as a catalyst that facilitates heme transfer through the cell wall anchored Isd proteins (IsdA-N, IsdC-N and IsdE). Intact IsdC-N is required to complete heme transfer from IsdA-N to IsdE. Overall, the rate of transfer from IsdA-N to IsdC-N is faster than

transfer from IsdC-N to IsdE. When IsdC-N acts as a heme shuttle between IsdA-N and IsdE, the key to fitting the transfer reaction studied is to introduce a step that slowly disables IsdC-N, by binding heme but becoming conformationally unable to transfer heme. With IsdC-N acting as a heme shuttle between IsdA and IsdE, the differential rates of heme transfer support the hypothesis that heme stockpiling would result in the cell wall. As a result, this facet of the Isd heme transfer system may impart heme cytotoxicity relief on the bacterium by throttling the heme transfer reaction into the cell interior.

When looking at the Isd protein structure, it might be thought that each Isd protein would be significantly different from each other, as each possesses slightly different heme binding spectroscopy and different heme transfer properties. Figure 9-3 shows a 3D protein structure alignment of all heme binding Isd NEAT domains (IsdB-N2, IsdH-N3, IsdA-N, IsdC-N) with secondary structure beta sheets coloured in gold and alpha helices coloured in blue. Remarkably, the structural 3D alignment and orientation of amino acids in the Isd proteins are all very similar, especially in the heme binding pocket, despite having different sequences. A major difference lies within IsdC-N, which has an extra lip in the heme pocket shown on the right of Figure 9-3. The sequence alignment is presented in Figure 9-4. The heme binding tyrosine ligands are conserved and highlighted with a red box. The extra lip of IsdC-N is highlighted in green. Interestingly, IsdA-N also has an extra sequence highlighted in green. However, this is located on the periphery of the protein away from the heme pocket. Current studies of heme transfer have found that transfer from IsdA-N to IsdC-N involves a hand clasp model, where the NEAT domains overlap each other and essential beta sheets interact in order to facilitate heme transfer [21]. Overall, the small differences in protein structure and amino acids sequences lead to a finely tuned heme transfer machine that is the Isd system.

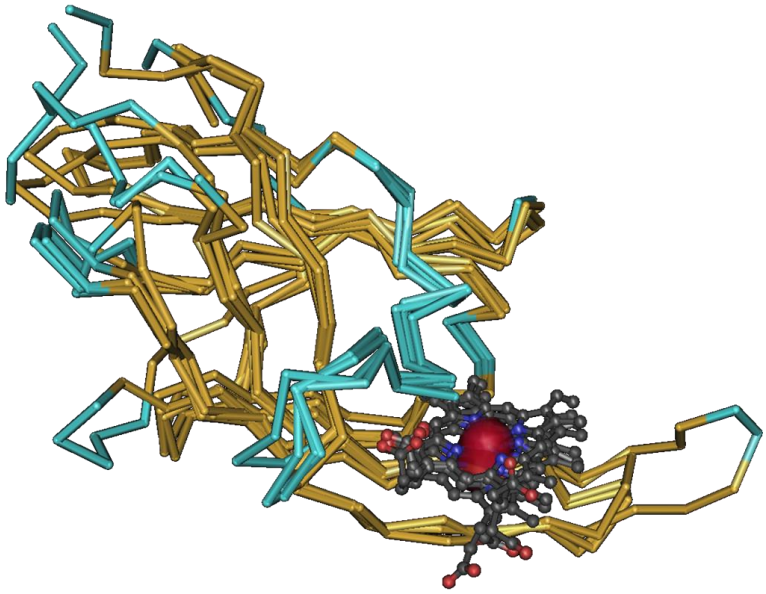

Figure 9-3 Protein alignment of all heme binding NEAT domains found in the Isd system. The Isd NEAT domains align together with amino acid positioning and similar secondary structure elements. IsdC-N contains a larger lip that can be seen at the right of the figure. The crystal structures come from the pdb with IsdC-N (2O6P), IsdA-N (2ITF), IsdH-N3 (2Z6F) and IsdB-N2 (3RTL).

```
IsdB-N2 -------GSKMTDLQDTKYVVYESVENNESMMDTFVKHPIKTGMLNGKKYMVMETTNDDYWKDFM
IsdH-N3 GSAMAPTNDQLTDLQEAHFVVFESEENSESVMDGFVEHPFYTATLNGQKYVVMKTKDDSYWKDLI
IsdA-N  -----GSHXSQATSQPINFQVQKDGSSEKSHXDDYXQHPGKVIKQNNKYYFQTVLNNASFWKEYK
IsdC-N  ----------GSDSGTLNYEVYKYNTNDTSIANDYFNKPAKYIKKNGKLYVQITVNHSHWITGMS

IsdB-N2 VEGQ-----RVRTISKDAKNNTRTIIFPYVEGKTLYDAIVKVHVKT------IDYDGQYHVRIVD
IsdH-N3 VEGK-----RVTTVSKDPKNNSRTLIFPYIPDKAVYNAIVKVVVAN------IGYEGQYHVRIIN
IsdA-N  FYNANNQELATTVVNDNKKADTRTINVAVEPGYKSLTTKVHIVVPQ------INYNHRYTTHLEF
IsdC-N  IEGH-----KENIISKNTAKDERTSEFEVSKLNGKIDGKIDVYIDEKVNGKPFKYDHHYNITYKF

IsdB-N2 KEAFTKANT--------------------------------------
IsdH-N3 QDINTKDDDTSQ-----------------------------------
IsdA-N  EKAIPTLA-----------------------------------------
IsdC-N  NGPTDVAGANAPGKDDKNSASGSDKGSDGTTTGQSESNSSNKDKVE
```

Figure 9-4 Amino acid protein alignment of all heme binding NEAT domains found in the Isd system. The heme binding Isd NEAT domains are very similar in not only residues but also structure. The ferric heme binding residues are boxed in red. IsdA-N and IsdC-N contain extra segments. IsdA-N has a sequence outside of the protein while IsdC-N has an extra string of amino acids at the lip of heme binding pocket. The crystal structure sequences come from the pdb with IsdC-N (2O6P), IsdA-N (2ITF), IsdH-N3 (2Z6F) and IsdB-N2 (3RTL).

9.4 Exploiting Heme Transfer in the Isd System

Heme transfer down the chain of proteins in the Isd system must be governed by a gate triggered by critical protein-protein interactions. The gate residues are in the heme crevice that binds the heme in place and prevents loss due to dissociation. Holo-IsdC-N does not release heme to the mutant IsdE(MH), a protein that cannot bind heme. Heme binding ligand mutations disable important heme releasing triggers. This effectively neutralizes important protein-protein interactions. Without the heme binding ligands the mutant IsdE now acts under affinity control transferring heme to apo-IsdA-N, apo-IsdC-N, and apo-IsdE. These transfers are not observed with native IsdE. Not only do the heme binding ligands play crucial roles in decreasing K_d values, from IsdA to IsdC and IsdE, but these ligands also dictate the selectivity and unidirectionality of the system.

The propionic acid chains of heme play a key role in heme transfer reactions, especially with regard to heme binding to IsdE, where the propionic acid side chains are completely buried within the heme pocket [12]. The role of the propionic side chains was tested be using FePPIX-DME heme analogue. IsdA-N was able to bind FePPIX-DME and transfer it to IsdC-N. However, FePPIX-DME bound holo-IsdA-N and holo-IsdC-N were not able to transfer FePPIX-DME to IsdE. Changing the central metal from Fe^{III} to Co^{III} and Mn^{III} tested the role of axial ligation. The "harder" CoPPIX was bound by IsdA-N [9], but was not transferred to IsdC-N or IsdE. The "softer" MnPPIX was bound by IsdA-N, which was able to transfer the ring to IsdC-N. IsdC-N was then able to transfer the ring to IsdE. In a reaction unlike that found for heme, holo-MnPPIX-IsdA-N transfered the ring directly to IsdE. In order to overcome the protein-protein interactions shown to exist with this transfer, MnPPIX must be labile. As the heme transfer mechanism of the Isd system in *S. aureus* became more widely understood, a new focus of using this system as a "Trojan Horse" technique to potentially kill the bacteria emerged in recent years. This may lead to the ultimate goal of potentially utilizing metalloporphryins for cytotoxicity [22] or using photodynamic antimicrobial therapy to kill the bacteria [23]. Critically, is that FePPIX-DME is able to transfer through to IsdC-N, the central conduit of the Isd system, but not to IsdE. It is possible that this compound would be an ideal candidate as a potential antibiotic for *S. aureus* by shutting down the Isd system and starving the bacteria of essential resources. Further studies are needed to determine the effectiveness and safety of this compound.

9.5 Final Remarks

Although utilization of Hb in *S. aureus* is mediated by the Isd heme transfer system [6, 24], this motif is also found in other Gram-positive pathogens such as *Bacillus anthracis, Chlorstridium tetani* and *Listeria monocytogenes* [2, 8, 25]. As a result of the research focus on the Isd system of *S. aureus,* the system is now almost fully characterized. With the development of techniques such as ESI-MS, MCD spectroscopy and x-ray crystal structure studies looking at heme binding and heme transfer, it is opportunistic to look at other similar systems to the Isd system of *S. aureus*. Overall, since the Isd proteins are very similar not only structurally, but also spectroscopically, it is possible that other systems may not be unique and may contain key features that are found in the Isd system. Therefore, characterization of new systems can be accelerated by technique refinement from the Isd system. Furthermore, it is possible that blocking the heme transfer system with "Trojan Horse" porphyrins may work on other bacteria.

9.6 References

1. Weems, J. J., *Post-Grad. Med.* **2001,** 110, 24-26, 29-31, 35-46.
2. Skaar, E. P.; Schneewind, O., *Microbes Infect.* **2004,** 6, (4), 390-397.
3. Rybak, M. J.; Akins, R. L., *Drugs 61* **2001,** 1, 1-7.
4. Study, C. P. H. *Canadian Nosocomial Infection Surveillance Program (CNISP) report for 2006*.
5. Weinberg, E. D., *Microbiol. Rev.* **1978,** 1, 45-66.
6. Mazmanian, S. K.; Skaar, E. P.; Gaspar, A. H.; Humayun, M.; Gornicki, P.; Jelenska, J.; Joachmiak, A.; Missiakas, D. M.; Scheenwind, O., *Science.* **2003,** 299, 906-909.
7. Tiedemann, M. T.; Muryoi, N.; Heinrichs, D. E.; Stillman, M. J., *Biochem. Soc. Trans* **2008,** 36, 1138-1143.
8. Andrade, M. A.; Ciccarelli, F. D.; Perez-Iratxeta, C.; Bork, P., *Genome Biol.* **2002,** 3, 1-5.
9. Grigg, J. C.; Mao, C. X.; Murphy, M. E. P., *J. Mol. Biol.* **2011,** 413, 684-698.
10. Pluym, M.; Muryoi, N.; Heinrichs, D. E.; Stillman, M. J., *J. Inorg. Biochem.* **2008,** 102, 480-488.
11. Tiedemann, M. T.; Muryoi, N.; Heinrichs, D. E.; Stillman, M. J., *J. Porphyrins Phthalocyanines.* **2009,** 13, 1006-1016.
12. Grigg, J. C.; Vermeiren, C. L.; Heinrichs, D. E.; Murphy, M. E., *J. Biol. Chem.* **2007,** 282, 28815-28822.
13. Pluym, M.; Vermeiren, C. L.; Mack, J.; Heinrichs, D. E.; Stillman, M. J., *Biochem.* **2007,** 46, 12777-12787.
14. Grigg, J. C.; Vermeiren, C. L.; Heinrichs, D. E.; Murphy, M. E., *Mol. Microbiol.* **2007,** 63, 139-149.
15. Pluym, M.; Vermeiren, C. L.; Mack, J.; Heinrichs, D. E.; Stillman, M. J., *J. Porphyrins*

Phthalocyanines **2007,** 11, 165-171.
16. Villareal, V. A.; Pilpa, R. M.; Robson, S. A.; Fadeev, E. A.; Clubb, R. T., *J. Biol. Chem* **2008,** 283, 31591-31600.
17. Muryoi, N.; Tiedemann, M. T.; Pluym, M.; Cheung, J.; Heinrichs, D. E.; Stillman, M. J., *J. Biol. Chem.* **2008,** 283, 28125-28136.
18. Mack, J.; Stillman, M. J.; Kobayashi, N., *Coord. Chem. Rev.* **2007,** 251, 429-453.
19. Tiedemann, M. T.; Stillman, M. J., *J. Porphyrins Phthalocyanines.* **2011,** 15, 1134-1149.
20. Mack, J.; Yoshiaki, A.; Kobayashi, N.; Stillman, M. J., *J. Am. Chem. Soc.* **2005,** 127, 17697-17711.
21. Villareal, V. A.; Spirig, T.; Robson, S. A.; Liu, M.; Lei, B.; Clubb, R. T., *J. Am. Chem. Soc.* **2011,** 133, 1417-14179.
22. Moriwaki, Y.; Caaveiro, J. M. M.; Tanaka, Y.; Tsutsumi, H.; Hamachi, I.; Tsumoto, K., *Biochem.* **2011,** 50, 7311-7320.
23. Stojiljkovic, I.; Perkins-Balding, D., *DNA Cell Biol.* **2002,** 21, 281-295.
24. Morrissey, J. A.; Cockayne, A.; Hammacott, J.; Bishop, K.; Denman-Johnson, A.; Hill, P. J.; Williams, P., *Infect. Immun.* **2002,** 70, 2399-2298.
25. Torres, V. J.; Pishchany, G.; Humayun, M.; Scheenwind, O.; Skaar, E. P., *J. Bacteriol.* **2006,** 188, 8421-8429.

Vita
Michael Thomas Tiedemann

EDUCATION

2007-2012	**Doctorate of Philosophy**, Chemistry **University of Western Ontario**
2003 - 2007	**Honors Bachelor of Science** – Chemistry, Advanced Chemistry **University of Western Ontario**

RESEARCH EXPERIENCE

Teaching Assistant – University of Western Ontario **Sep 2007 –Dec 2008**
London, ON

- Instructed students for the Department of Chemistry for courses: Chemistry 2271a, Chemistry 1024a, and Chemistry 1024b

HONOURS AND AWARDS

- **SPP Student Assistance Grant** – SPP – $ 200 Apr 2010
- **SBIC Poster Award** (ICBIC14) – Japan – $ 250 July 2009
- **NSERC Canada Graduate Scholarship** – UWO – $105,000 May 2009-Apr 2012
- **GTRF Travel Scholarship** – UWO – $ 750 Jan 2009
- **Ontario Graduate Scholarship** – UWO – $ 15,000 /year Sep 2007- May 2009
- **SPP Student Assistance Grant** – SPP – $ 200 Apr 2008
- **GTRF Travel Scholarship** – UWO – $ 900 Jan 2008
- **Graduate Tuition Scholarship** – UWO – $ 1,700 Sep 2007
- **Deans Honors List** – UWO 2003 – 2007
- **Varian Canada Prizes** – UWO – $ 250 Sep 2006
- **Chemistry Alumni Scholarship** – UWO – $ 1,600 Sep 2006
- **Western Scholarship of Excellence** – UWO – $ 2,000 Sep 2003

EXTRACURRICULAR/VOLUNTEER ACTIVITIES

- **SOGS Bylaws and Constitutions Committee –** UWO Jan 2012 – Present
- **Graduate Student Senator** – UWO Sept 2011 – Present
- **Volunteer Coordinator** - CSL – Starcraft II League – UWO Sept 2010 – Present
- **Secretary** – London Fencing Club Oct 2010 – Oct 2011
- **Epee Fencer** – London Fencing Club June 2008 – Present
- **Teacher Assistant Training Program** – UWO Sept 2007
- **Epee Fencer** – UWO Varsity Fencing Sept 2006 – Apr 2008
- **Biking** – Sudbury Bush Pigs – Sudbury Apr 2005 – Apr 2007
- **Club Member** – UWO Fencing Club Sept 2004 – Apr 2006

CONTRIBUTIONS TO RESEARCH

Articles published or accepted in refereed journals

- **Tiedemann M.T.,** Stillman M.J., (2011) *Application of Magnetic Circular Dichroism Spectroscopy to Porphyrins, Pthalocyanines and Hemes*, J Porphyrins Pthalocyanines., 15: 1134-1049. (Ph. D)
- **Tiedemann M. T.**, Naomi M., Heinrichs D. E., Stillman M. J., (2009) *Characterization of IsdH (NEAT domain 2) and IsdB (NEAT domain 2) in Staphylococcus aureus by magnetic circular dichroism spectroscopy and electrospray ionizionation mass spectrometry*, J. Porphyrins Phthalocyanines., 13: 1006-1016. (Ph. D)
- **Tiedemann M. T.**, Naomi M., Heinrichs D. E., Stillman M. J., (2008) *Iron acquisition by the heme-binding Isd proteins in Staphylococcus aureus - studies of the mechanism using magnetic circular dichroism,* Biochem. Soc. Trans., 36: 1138-1143. (Ph. D)
- Muryoi N., **Tiedemann M. T.**, Pluym M., Cheung J., Heinrichs D. E., Stillman M. J., (2008) *Demonstration of the iron-regulated surface determinant heme transfer pathway in Staphylococcus aureus***,** J. Biol. Chem., 283: 28125-28136. (Ph. D)

Other refereed contributions

- **Tiedemann M. T.**, Naomi M., Heinrichs D. E., Stillman M. J., (2008) *Iron acquisition in the pathogenic bacterium Staphylococcus aureus*, J. Porphyrins Phthalocyanines, 12: 589 (Ph. D)

Non-refereed contributions (Conference Presentation)

- **Tiedemann M. T.,** Heinrichs D. E., Stillman M. J., *"Mechanistic Studies of the Iron-Regularted Surface Determinant (Isd) Heme Transfer Pathway in Staphylococcus aureus"* 3rd Gerogian Bay International Conference on Bioinorganic Chemsitry (CANBIC-3), Parry Sound, Ontario, Canada, May 31-June 4, 2011. (Ph. D., International) Poster Presentation
- **Tiedemann M. T.,** Heinrichs D. E., Stillman M. J., *"Mechanistic studies of the Iron Regulated Surface Determinant (Isd) Heme Transfer Pathway in Staphylococcus aureus"* International Conference on Porphyrins and Pthalocyanies-6 (ICPP-6), Albuquerque, New Mexico, USA, July 4-9, 2010. (Ph. D., International) Poster Presentation
- **Tiedemann M. T.,** Heinrichs D. E., Stillman M. J., *"Demonstration of the Iron-Regularted Surface Determinant (Isd) Heme Transfer Pathway in Staphylococcus aureus"* 2nd Gerogian Bay International Conference on Bioinorganic Chemsitry (CANBIC-2), Parry Sound, Ontario, Canada, May 26-29, 2009. (Ph. D., International) Poster Presentation
- **Tiedemann M. T.,** Heinrichs D. E., Stillman M. J., *"Demonstration of the Iron-Regularted Surface Determinant (Isd) Heme Transfer Pathway in Staphylococcus aureus"* International Conference on Biological Inorganic Chemistry-14 (ICBIC-14), Nagoya, Japan, July 25-30, 2009. (Ph. D., International) Poster Presentation
- **Tiedemann M. T.,** Muryoi N., Heinrichs D. E., Stillman M. J., *"Iron Acquisition in the Pathogenic Bacterium Staphylococcus aureus: Characterization of IsdB-N2 and IsdH-N3"* International Conference on Porphyrins and Pthalocyanies-5 (ICPP-5), Russian Academy of Science, Moscow, Russia, July 6-11, 2008. (Ph. D., International) Poster Presentation
- **Tiedemann M. T.,** Muryoi N., Heinrichs D. E., Stillman M. J., *"Iron Acquisition in the Pathogenic Bacteria Staphylococcus aureus"* Engineering and Science Research Showcase, London Convention Center, London, Canada. January 25, 2008. (Ph. D., Regional) Poster Presentation
- **Tiedemann M. T**., Stillman M. J., *"Characterization of Heme Binding and Spectroscopy in Isd proteins in Staphylococcus aureus."* 40th Inorganic Discussion Weekend (IDW),

University of Toronto, Toronto, Canada. November 2-4, 2007. (Ph. D., Provincial) Poster Presentation

- **Tiedemann M. T**., Diakowski P., Ding Z. F., Workentin M. S., *"Radical Cleavage of Monolayers for Patterning using Scanning Electrochemical Microscopy (SECM)"* 35th Southern Ontario Undergraduate Student Chemistry Conference (SOUSCC), University of Ontario Institute of Technology, Oshawa, Canada. March 17 2007. (H.BSc., Provincial)